GEOMORPHOLOGY AND SEDIMENT DYNAMICS OF A HUMID TROPICAL MONTANE RIVER, RIO PACUARE, COSTA RICA

by

POLLYANNA LIND

A DISSERTATION

Presented to the Department of Geography
and the Graduate School of the University of Oregon
in partial fulfillment of the requirements
for the degree of
Doctor of Philosophy

December 2016

DISSERTATION APPROVAL PAGE

Student: Pollyanna Lind

Title: Geomorphology and Sediment Dynamics of a Humid Tropical Montane River, Rio Pacuare, Costa Rica

This dissertation has been accepted and approved in partial fulfillment of the requirements for the Doctor of Philosophy degree in the Department of Geography by:

Patricia McDowell	Chairperson
Jim O'Connor	Core Member
Mark Fonstad	Core Member
Andrew Marcus	Core Member
Josh Roering	Institutional Representative

and

Scott L. Pratt	Dean of the Graduate School

Original approval signatures are on file with the University of Oregon Graduate School.

Degree awarded December 2016.

DISSERTATION ABSTRACT

Pollyanna Lind

Doctor of Philosophy

Department of Geography

December 2016

Title: Geomorphology and Sediment Dynamics of a Humid Tropical Montane River, Rio Pacuare, Costa Rica.

Only a small body of work currently exists regarding the geomorphology of humid tropical montane rivers. The research that does exist reports rapid geomorphic processes and high sediment loads compared to other montane rivers. This research applies traditional field survey methods combined with new applications of remote sensing techniques to examine the geomorphology and sediment dynamics of the montane portions of the Rio Pacuare in Costa Rica. A suite of geomorphic components (channel slope and width, lateral contributions and planform) are examined and a model presented that illustrates the complexity of the Rio Pacuare's geomorphology and how the distribution of alluvial sediment varies in relation to geology (tectonics and lithology) and flow hydraulics (stream power). Next, average annual bedload sediment transport capacity is estimated using fifty-one years of daily discharge data at six different locations within the study area, including the temporal (monthly) variability of sediment flux due to dry versus wet season discharge regimes. Then, a time-step hydraulic model is created that simulates observed (modern) and potential future discharge scenarios based on regional climate change model results. The simulated discharge data for two locations within the study area is then integrated into the sediment transport model to examine how sediment flux, and thus channel geomorphology, is likely to change in response to changes in the river's discharge regime.

CURRICULUM VITAE

NAME OF AUTHOR: Pollyanna Lind

GRADUATE AND UNDERGRADUATE SCHOOLS ATTENDED:

University of Oregon, Eugene

DEGREES AWARDED:

Doctor of Philosophy, Geography, 2016, University of Oregon
Master of Science, Geography, 2016, University of Oregon
Bachelors of Science, General Science, 1993, University of Oregon

AREAS OF SPECIAL INTEREST:

Fluvial Geomorphology
Sediment Transport
Tropical and Montane Rivers

PROFESSIONAL EXPERIENCE:

Staff Scientist, InterFluve. Hood River, Oregon. 2010 to present

GRANTS, AWARDS, AND HONORS:

Doctoral Dissertation Research Improvement Grant, Geomorphology and sediment dynamics of a tropical montane river - Rio Pacuare, Costa Rica, National Science Foundation, 2013-2014.

Travel Award for Professional Development, International Conference on Geomorphology, University of Oregon Women in Graduate Science, 2013

Doctoral Student Research Award, Geomorphology and sediment dynamics of a tropical montane river - Rio Pacuare, Costa Rica, Geological Society of America, 2013

Research Abroad Doctoral Fellowship, Geomorphology of the Rio Pacuare, Tokyo Foundation, 2012-2013.

Student Research Award, Structure from Motion grain-size analysis, American Society of Photogrammetry and Remote Sensing, 2012.

Doctoral Student Research Award, Research development, Department of Geography (UO), 2012,

Fellowship for International Research Development, Geomorphology of Tropical Rivers, Tokyo Foundation, 2010-2011.

PUBLICATIONS:

O'Connor, J., McDowell, P., Lind, P., Massingill, C., and Keith M. 2015. Geomorphology and Flood-Plain Vegetation of the Sprague and Lower Sycan Rivers, Klamath Basin, Oregon. U.S. Geological Survey Scientific Investigation Report 2014-5223, 122 pages.

ACKNOWLEDGMENTS

Completion of this research was made possible by support and encouragement received from many. First, to my colleagues in graduate school -- it has been an honor to learn alongside of you and from you. Specific recognition to the co-graduate students that used my shoulder and offered theirs in return at critical times over the past few years, Tom Ptak, Matt Derrick, Swagata Goswami, Meche Lu, Shannon Cram, Kate Day, Chris Rasmussen, Jessica Phelps, Jenna Duffin, Suzanne Walthers, Didi Martinez, Paul Blanton, Michael Hughes, Amanda Reinhodtz, Helen Beeson, Denis Tu, James Dietrich, Jane Atha, Aaron Zettlerman, Christina Appleby, Christina Shintani, Denielle Perry, Devin Lea, and Sanon Moradi. To the River Research Group members old and new – we have a standard of comradery and support that will last a lifetime and I am proud to be a River Rat till the day I die. Thank you John Green for encouraging me to step into academia for the purpose of doing more to better the world. And, to Doug Foster, who was not only a dear friend and co-graduate student, but was and continues to be a reminder of how important the journey of Life is.

The mentorship I received from my dissertation committee members is monumental. Your vested interest in this research and in my evolution of becoming a geomorphologist has not gone unnoticed or unappreciated. Specifically, to Patricia McDowell, who has an impressive capacity to both challenge and support me at the same time – an ideal mentor, friend, and colleague. To Jim O'Connor, whom I want to be when I grow up, for the exceptional example that you are as a scientist, person, and friend. To Mark Fonstad for your inability to not help solve problems and your humble way of sharing your intelligence. You are a gift to any student or colleague that wants to learn. To Andrew Marcus who has shepherded me through my graduate school experience since day one. To Josh Roering who stepped into this complicated research project with both feet offering insightful input and ideas. I hope that my path continues to cross the paths of each of you high caliber scientists and people.

This project required a great deal of field work in wet, muddy, sometimes dangerous, breathtakingly beautiful places. Much thanks is extended to the folks that lent a hand, carried gear, offered transportation, recorded data, etc.: Octavio Arroyo Nunez, Amanda Rienholdtz, Brett Shelton, John Lind, Todd Simmler, Kurt Studt, Lua S. Solano,

Mario Achoy Vega, Neil Bjorklund, Sadie Trush. And thank you to the Costa Rican companies that supported this work by offering equipment, lodging, transportation, etc.: Serendipity Tours, Rio Pacuare River Lodge, and Costa Rica Rios. Also, I want to acknowledge the many river guides and kayakers that work every day on this river that kept an eye out for me. Also, recognition is extended to Dr. Rolando Mora Chinchilla, the director of the Central American School of Geology at the Universidad de Costa Rica for your interest in this research and for letters of support that made getting funding and access to data easier.

The friends and family that stuck with me through this process deserve special recognition. Thank you for your patience and unwavering support. I feel blessed to be part of your community and look forward to returning the many favors several of you bestowed on me these past couple of years. There are too many of you to name.

To the strong circle of women that stand next me (mother, aunts, cousins, niece, friends,). We can accomplish more each generation because of the boundaries broken by our elders and each other. May any boundaries that my generation tumbles down open more doors for the next. Thank you Meera S., Elissa P., Amy A., Julia D., Codi F., Tina A., and Marina W. – there are no words to describe the gratitude I hold for the encouragement, inspiration, friendship, and support you give.

My brother Gabby and my dad are my quiet guardian angels. Cousins Tim and Mike step in from time to time as well. I take on risks and challenges more easily because you are there and because you believe in me. Gabby, I know few people as good as you. Thank you for accepting, making light of, and living with my wackiness the past couple of years.

And, to my friend and love Todd Simmler. Thank you for giving me all the space I needed to make this happen and for believing in me wholeheartedly. Thank you for the nourishing food, laughter, compromises, inspirations, and understanding. I am grateful for how you helped hold several of my pieces together these last few months and for reminding me to look up every now and again from the books and computer to catch a glimpse of a colorful sunset, bright moonrise, or shooting star.

This research is dedicated to my parents, John and Penny, who raised me to pursue without pondering limitations that which inspires me—such as the wonder of the natural world outside my door and around the world. I have felt you in my "corner" every step of my life. I hope you know the strength you have provided me.

This work is also dedicated to the rivers and mountains of Costa Rica and people such as Kurt and Maga, that live in, off, and for them. I am deeply grateful.

TABLE OF CONTENTS

Chapter Page

LIST OF FIGURES

Figure Page

Figure Page

LIST OF TABLES

Table Page

Table Page

CHAPTER I

INTRODUCTION

Research on the geomorphology of tropical montane rivers is particularly important because of the ever-increasing demand on the resources they provide such as drinking water, irrigation, hydroelectricity, ecology, and cultural sustenance (Johnston & Kummu, 2012; Kaygusuz, 2004). Yet, numerous gaps persist in our knowledge of the geomorphology of these types of systems (Latrubesse et al., 2005; Scatena & Gupta, 2013; Wohl et al., 2012). This, in part, is because they are difficult to study due to rugged terrain, limited access, and rapidly fluctuating flow regimes. The research that does exist indicates that standard descriptions and classifications of channel processes designed for temperate systems are not adequate (Ahmad et al., 1993) and that humid tropical montane rivers express comparatively high rates of geomorphic processes and that they respond more rapidly to change (Dietrich, 1999; Garcin etal., 2005; Kuo & Brierley, 2014; Nagle et al., 1999; Restrepo et al., 2006; Wohl, 2005). This raises questions regarding our current understanding of riverine geomorphology, currently based primarily on temperate-region river research, and how it is or is not applicable to rivers in other regions of the world where climate patterns, weathering rates, and geologic histories are different.

Humid tropical montane regions receive 2000mm or more annual precipitation, including intense rain events that fall on steep montane surfaces (Restrepo & Kjerfve, 2000; Waylen et al., 1996). The frequent and intensity of storm events typically generate large-magnitude flows multiple times each year (García-Martinó et al., 1996; Garcin et al., 2005; Restrepo et al., 2006). Consequently, both fluvial channel processes and landscape erosion rates are often exaggerated high compared to other montane river systems (Aalto et al., 2006; Dietrich, 1999; Gupta, 2011; Thomas, 1996; Ziegler et al., 2014a). Considering these factors, humid tropical montane watersheds not surprisingly produce a disproportionate amount of the sediment and nutrients delivered to the world's seas and coastal regions (Kao & Milliman, 2008; Milliman & Syvitski, 1992).

This research examines the geomorphology and sediment dynamics of the montane portions of the Rio Pacuare in Costa Rica. The Rio Pacuare is located on the

northeast side of the Talamanca Mountains and flows from the crest of the range to the Caribbean Sea. The Rio Pacuare was selected for this study because it is currently free flowing, is relatively accessible in a few locations yet minimally impacted by anthropogenic influences, and contains a variety of geologic and hydrologic characteristics common in the montane regions of Central America (Marshall, 2007; Sitchler et la., 2007). As such, the Rio Pacuare is considered an analog for others rivers in the region, making the results of this research relevant beyond the boundaries of the study area.

A river's geomorphic capabilities, as a function of its discharge, are characterized by the quantity and size of the sediment it manages and transports (Julien, 2015). In mountain rivers, the caliber and quantity of bedload, combined with the related discharge regimes (magnitude, frequency, and power), control channel form and adjustments (Emmett & Wolman, 2001; Lenzi et la., 2006; McLean et la., 1999; Wohl, 2010). Bed morphology in turn influences local hydraulics (Recking et al., 2015) and can define the aquatic habitat that a channel provides (Bertoldi et al., 2010; Bravard et la., 1999; Habersack, 2000; Hassan et al., 2008). By providing information on the interconnected components responsible for the Rio Pacuare's geomorphology, estimating bedload sediment transport capacity, and examining how the river's sediment transport capacity may respond to predicted climate change this body of research aims to fill a few of the existing gaps in our knowledge about the geomorphology of humid tropical montane rivers. To accomplish this, the following questions are addressed:

1. *How does channel geomorphology vary downstream in relation to geology, available sediment, and flow hydraulics?*
2. *What is the bedload sediment transport capacity and how does it vary spatially and temporally along the study area?*
3. *How will sediment transport capacity change in response to changes to of predicted future climate change scenarios?*

Chapter II addresses research question 1 by examining how geology (tectonics and lithology), climate (as the driver of discharge and weathering), and hydraulics (represented by stream power) interact and/or influence the distribution of alluvial

sediment and thus channel geomorphology. A conceptual model is presented to illustrate the interactions between the primary forcing elements (geology, climate, and hydraulics) and intermediate geomorphic components (channel planform, active channel width, valley width, lateral contributions (tributaries, landslides, and debris torrents), and channel slope) to determine how each influence the distribution of alluvial sediment in the study area. The results of this chapter indicate that the geomorphology of the Rio Pacuare is driven by the precipitation-generated discharge regime, channel slope, and its plentiful available sediment. Flow hydraulics governs sediment distribution and exerts some influence on reach-scale slope. However, lithology and active tectonics affect channel geomorphology via influencing channel form, width, watershed slope, and lateral sediment contributions. This study not only provides more information on the geomorphic interactions and processes of this tropical montane river, it also sets a foundation for future examination of potential channel response to changes in climate (discharge) in this and other rivers of the Talamanaca Mountains.

Chapter III addresses research question 2 by estimating bedload transport capacity at six field sites distributed within the study area. The results indicate the Rio Pacuare has high sediment flux capacity, ranging from hundreds of thousands to over millions of tons per year. The Rio Pacuare experiences high magnitude flows that have the ability to mobilize its boulder-dominated bedload multiple times a year at all six field sites. Differences in the magnitude, as well as the temporal variations, of the calculated sediment transport capacities are discussed in relation to stream power, and seasonal discharge patterns. Over 50 percent of the annual sediment transport occurs during the rainy season months of October – December. This study provides a first attempt to estimate bedload transport capacity and potential sediment flux in the rivers of the Talamanca Mountains. The results of this analysis indicate that additional research on the manner and timing in which sediment is convened through the system is needed. The development of segment-scale sediment budgets is recommended.

Chapter IV addresses research question 3 by examining how bedload transport capacity changes at two locations on the Rio Pacuare in response to a set of climate change scenarios. The results from two regional climate change models that predict future precipitation changes specific to the region and one global model that predicts

changes in extreme events for the time period 2070-2100 were used to develop the potential future discharge scenarios. Fifty-one years of observed daily discharge data from a gage on the Rio Pacuare was statistically decomposed to create a time-series hydrological model comprised of trend, seasonal, and irregular components. The model is used to simulate twenty years of daily discharge that is representative of modern observed discharge and, through model component manipulation, future climate scenarios. In total eight discharge scenarios were simulated based on climate change predictions – including a no-change scenario. Changes in bedload sediment transport capacity decrease slightly with reduced dry season discharge scenarios yet increase notably with even small increases to the wet season discharge scenario. The likely geomorphic response to the changes in transport capacity at each site are discussed based on the geomorphic assessment provided in Chapter II. The goal of this work is to not only examine how sediment transport capacity may change in response to changes in the river's seasonal discharge regime. This research exposes the need for better climate change predictions and the need for research on other factors, such as dam impoundment, that alter discharge quantity and timing on this and other humid tropical montane rivers.

An innovative mix of field, remote sensing techniques, and modeling were implemented to answer the questions presented in this dissertation. Some methods were designed specifically to overcome some of the noted challenges of tropical river research (e.g., access, high sediment flux, rapidly fluctuating flows, large-grain mobilization). Traditional field mapping and surveys (grain size, topographic channel cross sections, etc.) were done. The application of Structure from Motion (SfM) in repeat photogrammetric topographic surveys to identify grain mobilization after a flood event is implemented for the first time in this study. Grain mobilization was identified through change analysis of the SfM produced digital elevation models (DEMs) and high-resolution ortho-photos of the study sites. SfM is also used to produce ortho-photographs and a DEM to map and measure channel features of 78 river kilometers within the study area from helicopter-collected imagery. The relatively new bedload transport model developed by Recking (2013) for mountain streams is used to calculate transport capacity. A time-step (daily) hydrologic model was created using observed daily discharge data from the one long term gage site on the Rio Pacuare.

Beyond expanding the science of fluvial geomorphology, specifically tropical river morphology, this body of work provides a foundation for future research to expand upon. Ideally, this research and future work will aid in the sustainable development, management, and conservation of tropical rivers by offering fundamental information to scientists and resource managers of the region about how these systems work.

Research contributions

Chapter II:

James Dietrich, PhD aided in creating the camera box that was mounted on the helicopter and the photo-capture technique used for the aerial imagery collection.

Chapter III:

Mark Fonstad, PhD developed the spreadsheet with calculations used for estimating the topographic shape and maximum depth of the incomplete cross sections (described in Section 3.2.1)

Mark Fonstad, PhD created the method for developing a discharge to upstream area relationship to produce daily discharge values (described in Section 3.2.2)

Chapter IV:

Patrick Bartlien, PhD created the time-series hydrologic model used to simulate daily discharge values and aided in the written description of the model (described in Section 4.2.1).

CHAPTER II

GEOMORPHOLOGY, GEOLOGY, AND ALLUVIAL SEDIMENT DISTRIBUTION OF A HUMID TROPICAL MONTANE RIVER, RIO PACUARE, COSTA RICA

2.1 INTRODUCTION

Montane river geomorphology is the result of a complex set of interactions and responses to the geology (tectonics and lithology), climate (discharge and weathering), and fluvial processes of erosion (channel and landscape) occurring in the watershed. These characteristics interact to define the channel's slope and how water and sediment transfer through a system (Golden & Springer, 2006; Shumm, 2005; Wang et al., 2015; Wohl, 2010). In humid tropical montane regions, climate patterns deliver 2000mm or more annual precipitation, including intense rain events that fall on the high-gradient montane surfaces (Restrepo & Kjerfve, 2000; Waylen et al., 1996). The frequency and intensity of storm events typically generate large-magnitude flows multiple times each year (García-Martinó et al., 1996; Garcin et al., 2005; Restrepo et al., 2006). Consequently, both reported fluvial channel processes and landscape erosion rates are often exaggerated compared to other montane river systems (Aalto et al., 2006; Dietrich, 1999; Gupta, 2011; Thomas, 1996; Ziegler et al., 2014a). Large quantities of hillslope sediment inputs (landslides and debris flows torrents) are regularly contributed from weathered, frequently-saturated hillslopes, especially in seismically active regions where earthquakes can trigger mass movements (Benda et al., 2005; Ohl & Bussmann, 2004). Considering these factors, humid tropical montane watersheds not surprisingly produce a disproportionate amount of the sediment and nutrients delivered to the world's seas and coastal regions (Kao & Milliman, 2008; Milliman & Syvitski, 1992; Warrick et al., 2013).

Demands on tropical montane rivers' resources (e.g., water supply for cities and agriculture, hydroelectricity, ecology, and agriculture) continue to increase steadily (Johnston & Kummu, 2012; Kaygusuz, 2004), yet numerous gaps persist in our knowledge of the geomorphology of these systems (Latrubesse et al., 2005; Scatena &

Gupta, 2013; Wohl et al., 2012). The research that does exist on humid tropical montane rivers has found, even early on, that standard descriptions and classifications of channel processes designed for temperate or arid systems are not adequate (Ahmad et al., 1993). The studies that have been done report comparatively high rates of geomorphic processes on rivers such as the Remparts River on Reunion Island (Garcin et al., 2005), the Fly River of Papua New Guinea (Dietrich, 1999), the Nizao of the Dominican Republic (Nagle et al., 1999), the Liwu in Taiwan (Kuo & Brierley, 2014), and Andean rivers in Columbia (Restrepo et al., 2006). Two studies were found that examined the influence of geology (lithic resistance and tectonics) on channel geomorphology. Both reported that the abundant sediment supply which is organized by frequent strong flow hydraulics in the upper Rio Chagres in Panama (Wohl, 2005) and streams of the Luquillo Mountains in Puerto Rico (Pike et al., 2010) exert more control on watershed slope than local geology does. Also on the Rio Chagres, sediment supply and channel width were reported to exert more control on sediment distribution and grain size than a normal downstream-fining pattern (Rengers & Wohl, 2007). This may be because in tropical montane watersheds sediment delivery is exaggerated compared to other montane rivers, which has been attributed to sediment generation from upslope channel extension, and the density of tributary networks (Lisenby et al., 2014; Plink-Björklund, 2015). The few available studies to date conclude that more research on the geomorphology of additional humid tropical montane rivers is needed to fill the numerous gaps in knowledge that remain regarding these hydrologically and geomorphically dynamic, significant river systems.

This study provides a greater understanding of the geomorphology of the montane portion of the Rio Pacuare in Costa Rica by examining how channel geomorphology varies downstream in relation to bedrock lithology, fault intersections, and alluvial sediment distribution. This study builds on past work by expanding the number of geomorphic components examined within a tectonically active watershed. The primary goal is to show how geology (tectonics and lithology), climate (as the driver of discharge and weathering), and hydraulics (flow competence) interact and/or influence the distribution of alluvial sediment and thus channel geomorphology. It is important to clarify that discharge and weathering produced by the area's tropical climate conditions are not evaluated or modeled in this study. Instead, they are simply considered driving

mechanisms in channel and landscape development. Figure 0-1 presents the framework of the conceptual model developed to map the interactions between the external forcing components (geology and climate)) which combine to drive flow hydraulics, and a set of internal geomorphic components evaluated in this study. Those geomorphic components include channel form, active channel width, valley width, lateral contributions (tributaries, landslides, and debris torrents), and alluvial sediment distribution.

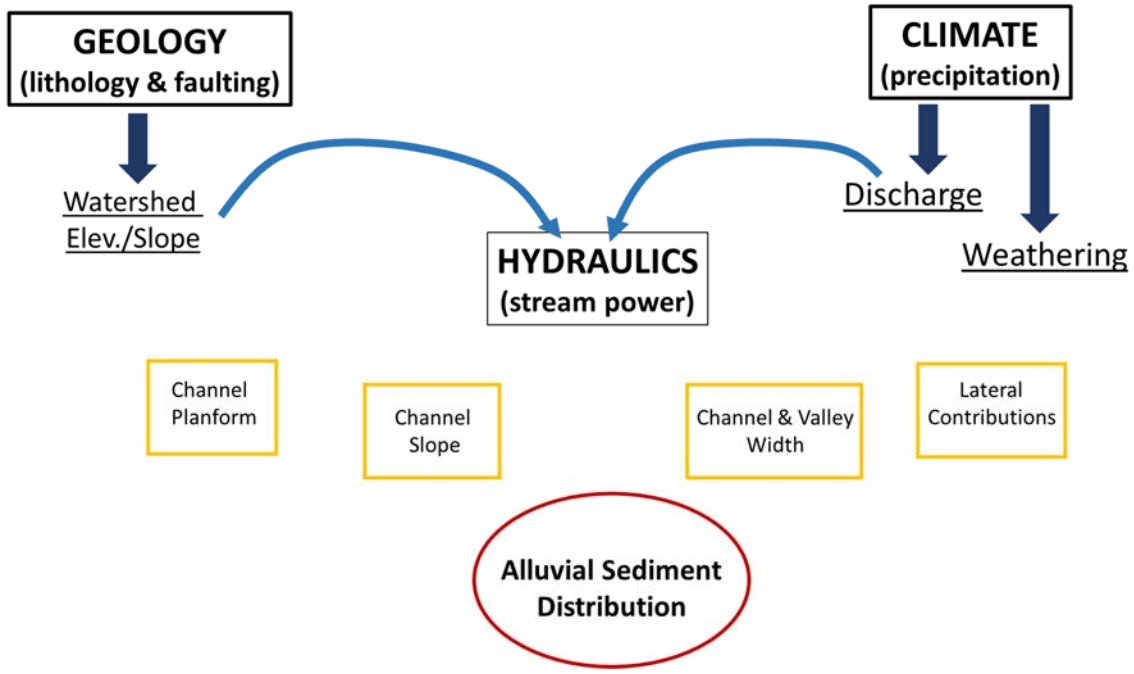

Figure 0-1. Framework for the geomorphic model of the Rio Pacuare.

Beyond the process of channel development in montane environments via fluvial incision, this study evaluates the complex and interconnected relationships between the geomorphic components included in Figure 0-1 to determine how each component influences the distribution of alluvial sediment in the Rio Pacuare. The primary external components of geology and climate control the watershed elevation and channel discharge regime, respectively. Combined, these two external controls produce the channel's hydraulics or flow competence as measured via stream power. Through this research, the relationships between the primary components (geology, climate, and flow hydraulics) and the intermediate components (channel form, active channel width, valley width, lateral contributions, and alluvial sediment distribution) will be identified. The

model is used as a tool for mapping the complex manner in which primary components influence intermediate component and how primary and intermediate components combine to influence alluvial sediment distribution.

This study provides information on the geomorphic processes of tropical montane rivers. Identifying the relative influence the primary and intermediate geomorphic components have on one another also allows for prediction of the response the channel is likely to have in the face of climate change, dam impoundment, land use, or otherwise.

2.1.1 Regional Setting

This research examines the montane portion of the Rio Pacuare, located in Costa Rica's Talamanca Mountains in the central portion of the Chorotega volcanic front of Central America (Figure 0-2). In total, the channel is approximately 132 river kilometers (Rkm) long from headwaters to sea, flowing north-northeast through the Talamanca Mountains, exiting the confinement of the mountains across a prominent alluvial fan onto a low-gradient alluvial plain, and eventually flowing into the Caribbean Sea. The entire watershed is 890km^2, and the mainstem channel falls approximately 3018 meters in elevation with almost the entire fall (2068m) occurring in the upper 88 Rkm contained within the mountains. The overall slope (m/m) of the channel within the study area is 0.02 with local-scale (500m) slopes ranging from 0.001 to 0.2.

The montane portion of the Rio Pacuare (Rkm 44.2-to-132) was selected for study because it is currently free flowing, is relatively accessible in a few locations yet minimally impacted by anthropogenic influences, and contains a variety of geologic and hydrologic characteristics common in the montane tropics of Central America (Marshall, 2007; Sitchler et al., 2007). Dense tropical mid-elevation forests dominate the vegetation cover. Only small-scale farming plots, a few unincorporated villages, and a handful of rafting camps accessed by dirt roads, trails, or river are found in the montane Rio Pacuare watershed. The river is bordered on both sides by the Talamanca Cabecar Indigenous Reserve upstream of Rkm 85.From Rkm 44.5 to 72 the east side of the river is bordered by the Pacuare Bio-Reserve. Within these reserves, anthropogenic land-use impacts are minimal.

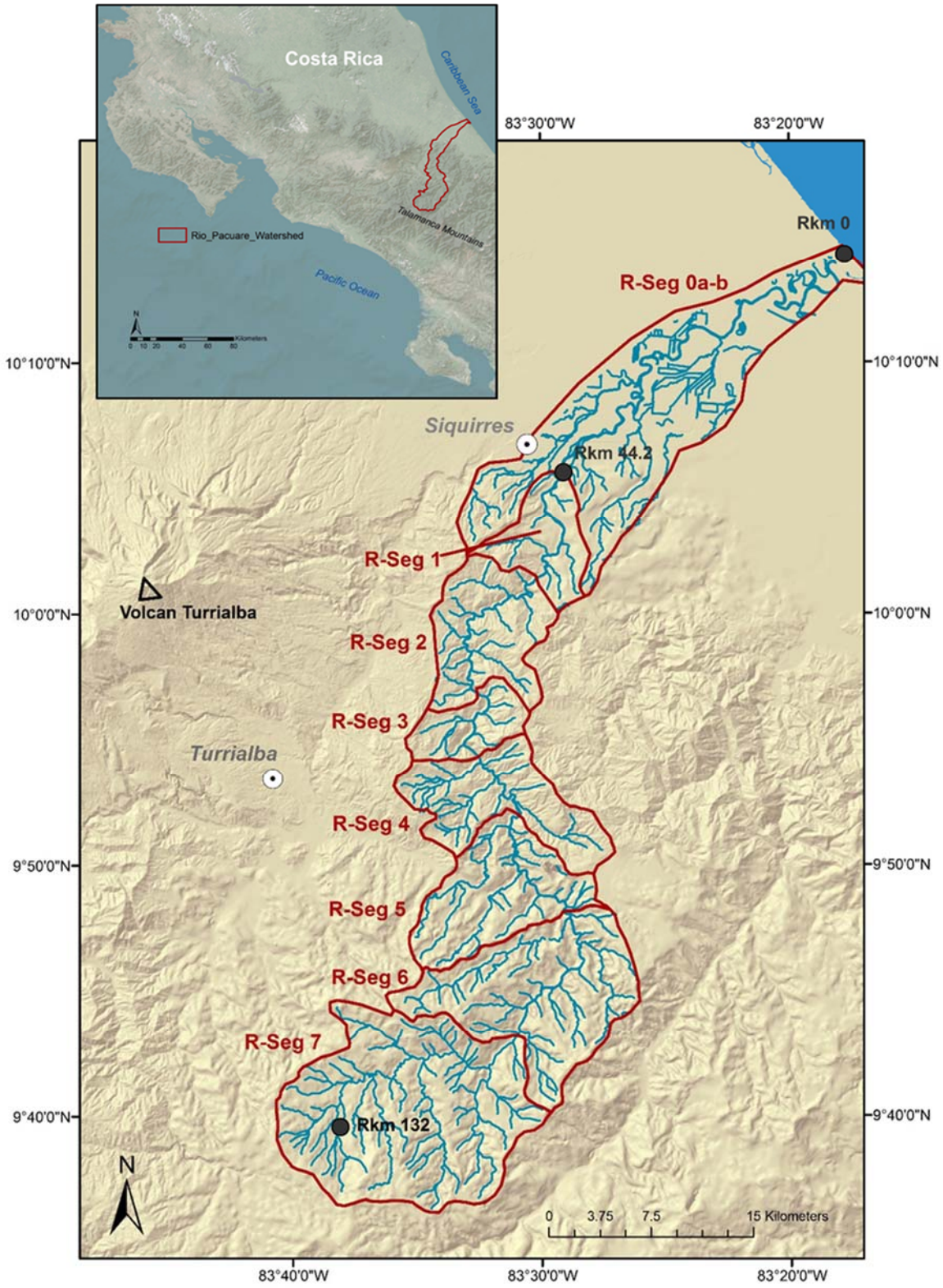

Figure 0-2. Map of the Rio Pacuare and the study area defined by geomorphic River Segments (R-Seg). Basemaps: Esri GeoEye, 30m DEM (ASTER, 1999).

For this study the Rio Pacuare is subdivided (Figure 0-2) into eight river segments (R-Seg 0-7) delineated by channel form, channel slope, confinement, and sediment distribution patterns (exposed bars and floodplain or low terrace surfaces). The study area includes the montane segments 1-7 (Rkm 44.2-132). Segment 0 (Rkm 0-44.2), not included in this study, is the meandering segment of the river that traverses the alluvial lowland coastal plain (at RKM 0-44) and the partially braided segment that crosses the alluvial fan at the foot of the mountains (0b at RKM 44-44.2).

River confinement for this study is characterized as either "confined" or "semi-confined." Semi-confined reaches or segments include discontinuous pockets of floodplain or low terrace surfaces. In these sections the active channel occupies 80-50% of the valley width and the banks of the channel usually alternate between bedrock and coarse alluvium or colluvium (Figure 0-3 - A). Confined sections are 100-80% occupied by the active channel, with basically no floodplain accumulations (Figure 0-3 - B). River segment (R-Seg) 1 is semi-confined with two confined reaches, and R-Seg 2 is confined with multiple semi-confined reaches. R-Segs 4, 5 and 6 are semi-confined by bedrock and/or hillslopes with small pockets of floodplains and terraces. R-Segs 3 and 7 are bedrock-confined with relatively minimal floodplain development. Large active bars composed of imbricated boulders influence channel form at low flow in much of the study area, included some confined reaches.

Throughout almost all of the study area, the channel's bed has a layer of coarse bedload (cobble and boulder) of unknown depths, even in the bedrock-confined sections such as R-Seg 3 and 7. At locations of cascade steps very large rounded boulders impose local grade control on the channel bed. In some locations, massive (usually >3m diameter) stable boulders sourced from colluvium as rock fall or in landslides, or debris torrents impose in-channel obstacles to mainstem flow pattern.

Figure 0-3. A) Alternating boulder bars in semi-confined section, at Rkm 104.4 – R-Seg 6; and B) confined section at Rkm 74.7 – R-Seg 3. Photos by P. Lind.

With no snow storage, precipitation events drive the Rio Pacuare's hydrologic flow regime, and thus the frequency of flows that are competent to mobilize its bedload. In general, the region experience two rainy seasons and two dry seasons annually (Giannini et la., 2000; Vargas & Trejos, 1994; Waylen et la., 1996). However, in the Talamanca Mountains the Rio Pacuare watershed is typically wet year around with a drier season that occurs January to April (and occasionally in September), and a wetter period from May to December (Figure 0-4).

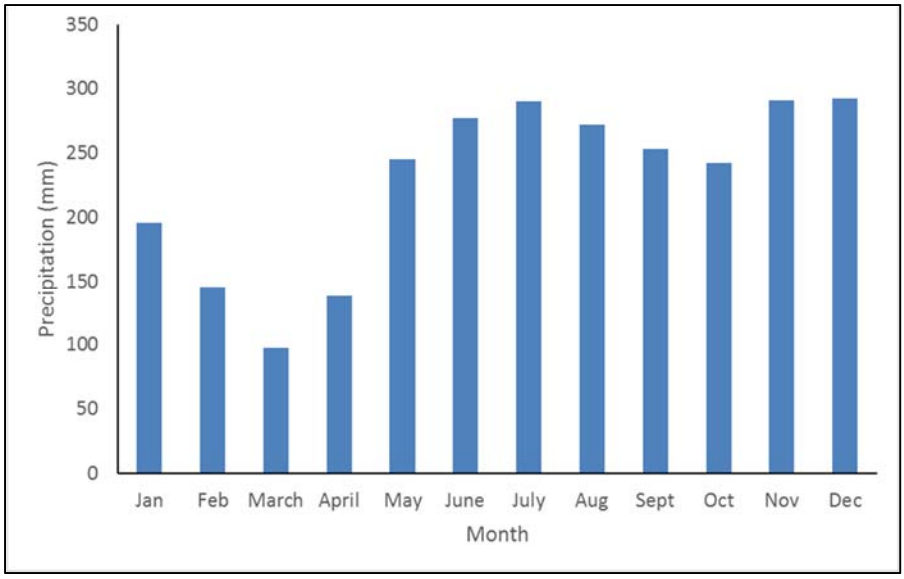

Figure 0-4. Monthly average precipitation (mm) at Turrialba (1959-2012) (see Figure 2 for location of climate stations). Source: (CATIE - Centro Agronómico Tropical de Investigación y Enseñanza, 2016)

During intense precipitation events, the Rio Pacuare experiences rapid increases in discharge. Daily discharge data acquired from the Instituto Costarricense de Electricidad (ICE) for two gages (8-01, Bajo Pacuare at Rkm 90.5 [1958-2013]; and 8-03, Dos Montañas at Rkm 47 [1970-2000]) indicates that high magnitude flow events occur most commonly in November and December, and also often in July. As an example, the reported daily discharge values for 2012 at Bajo Pacuare (ICE gage 8-01) are provided in Figure 0-5, exposing the flashiness of the river's annual hydrograph.

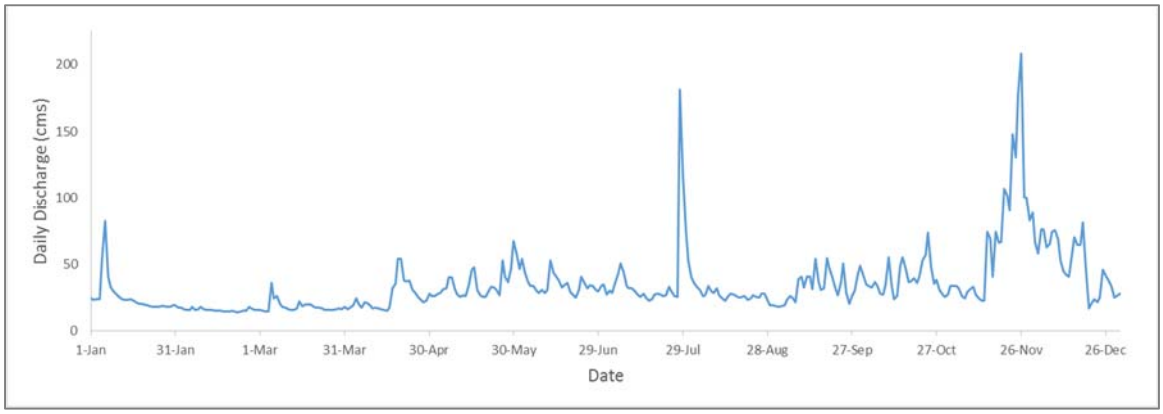

Figure 0-5. Annual hydrograph of daily discharge (cms) at Bajo Pacuare (ICE gage 8-01) for the year 2012.

2.1.2 Geology

Geomorphology of rivers across the world is influenced, in large part, by the geology and related landscape evolution of their watersheds (Gupta, 1995; Wang et al., 2015; Wohl & Merritt, 2001; Wohl, 2010). The term "geology" in this paper refers to lithology as well as tectonic processes and the related faulting. The watershed of the Rio Pacuare contains a mix of metamorphic conglomerates and resistant limestones as well as intrusive granodiorites, extrusive andesites, and basalts. The history that created this geologically complex watershed is summarized below.

Formation of the Talamanca Mountains

The Talamanca Mountains, in which the Rio Pacuare flows (see Figure 0-2), are the highest portion of the Chorotega volcanic front of Central America. The formation of the Chorotega volcanic front, including the Talamanca Mountains, resulted from tectonic subduction that began as early as the Paleocene/Eocene along what is now referred to as the Middle America Trench (Figure 0-6). The initiation and continued subduction of the Farallon plate of the Pacific Ocean under the Caribbean plate at the trench resulted in the emergence of an arc of volcanic islands, the Chorotega volcanic front. By the mid-Oligocene, the Farallon had subdivided into the Cocos and Nazca plates, which continued to provide subducting mantle-derived material to the developing volcanic arc (de Boer et al., 1995). Extensive oceanic reefs and sediment, derived around and from the developing volcanism, accumulated around the evolving islands. The ocean reefs and sediment, layered and diked by igneous material, now constitute the primary geologic composition of the eastern side of the Talamanca Mountains where the Rio Pacuare is located.

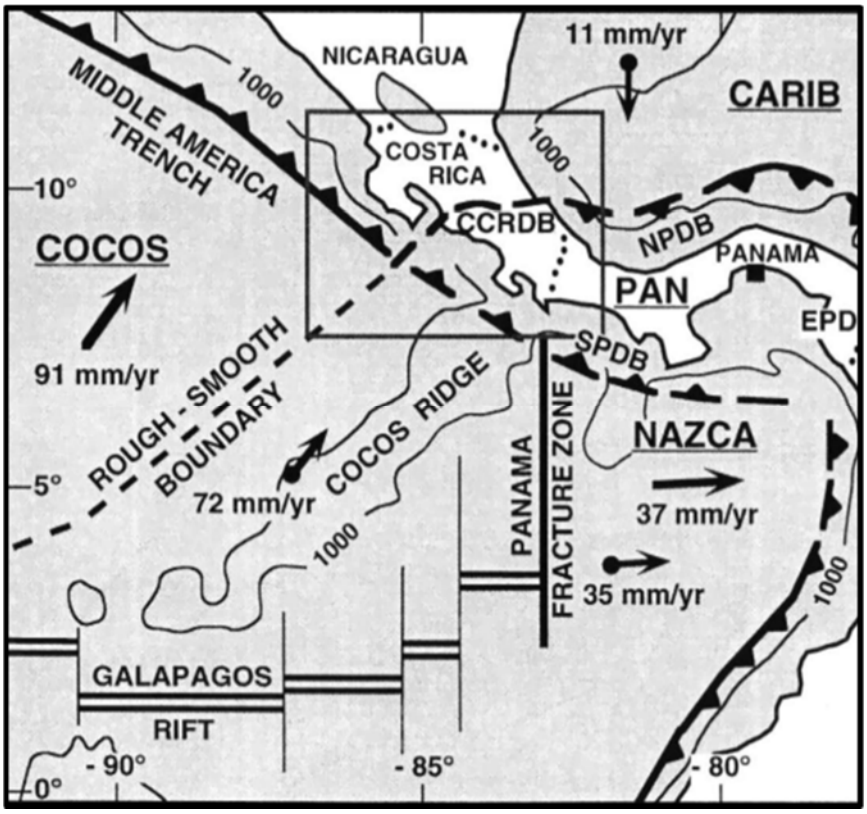

Figure 0-6. Map of major tectonic features of southern Central America. CCRDB=Central Costa Rican Deformation Belt; NPDB=Northern Panama Deformation Belt; SPDB=Southern Panama Deformation Belt; CARIB=Caribbean plate; PAN=Panama fracture zone. Extracted from Figure 1 from Marshall, et al. (2000).

In the late Miocene subduction of the Cocos Ridge (Figure 0-6), as part of the Cocos Plate, altered the composition and thickness of the material subducting below a portion of the Caribbean plate. Cocos Ridge is a chain of volcanic seamounts that originated over the Galapagos hotspot and stands approximately 2km above the sea floor. The Cocos Ridge is relatively young and buoyant compared to the mid-ocean ridge basalts beneath it, resulting in shallower subduction. The shallow subduction of Cocos Ridge is recognized as the cause of reduced volcanic magma production in and relatively rapid uplift of what are now the Talamanca Mountains portion of the Chorotegas, raising the Talamancas from an estimated elevation of 400-900m to over 3,000m (Abratis & Wörner, 2001; Kolarsky et al., 1995; MacMillan et al., 2004). The modern Talamancas contain no active volcanoes but, they are located between active Volcan Turrialba (25 km north of the Rio Pacuare) and Volcan Baru in Panama, 175 km to the south.

Also related to the Cocos Ridge subduction is the development of the North Panama Deformation Belt (NPDB) which is located between the southward-moving Caribbean Plate and the relatively stationary Panama plate (Escalante & Astorga, 1994; MacMillan et al., 2004; Jeffrey S. Marshall et al., 2000). The NPDB extends across southern Costa Rica to the Middle America Trench (Figure 0-6). The portion that extends across Costa Rica is referred to as the Central Costa Rican Deformation Belt (CCRDB). The CCRDB includes most of the montane portions of the Rio Pacuare (Marshall et al., 2000; Montero & Linkimer, 2005). The NPDB/CCRDB is a relatively stationary plate that accommodates tectonic shortening caused by subduction of the Cocos and the Nazca plates to the southwest and subduction and slip of the Caribbean Plate to the northeast.

Lithology and Faulting

Located on the back-arc side of the Chorotega volcanic front, the Rio Pacuare traverses a complex set of sedimentary, metamorphic, and magmatic lithologies along its pathway to the Caribbean. The primary lithologies (Figure 0-7) include fossiliferous-limestone, calcareous sandstones to mudstones, and conglomerates. The volcanic materials are of both intrusive and extrusive igneous rocks, including but not limited to andesite, basalt, granodiorite, dacite, and ash (de Boer et al., 1995; Escalante & Astorga, 1994; Fernandez et al., 1994; MacMillan et al., 2004; Marshall, 2007; Sitchler et al., 2007).

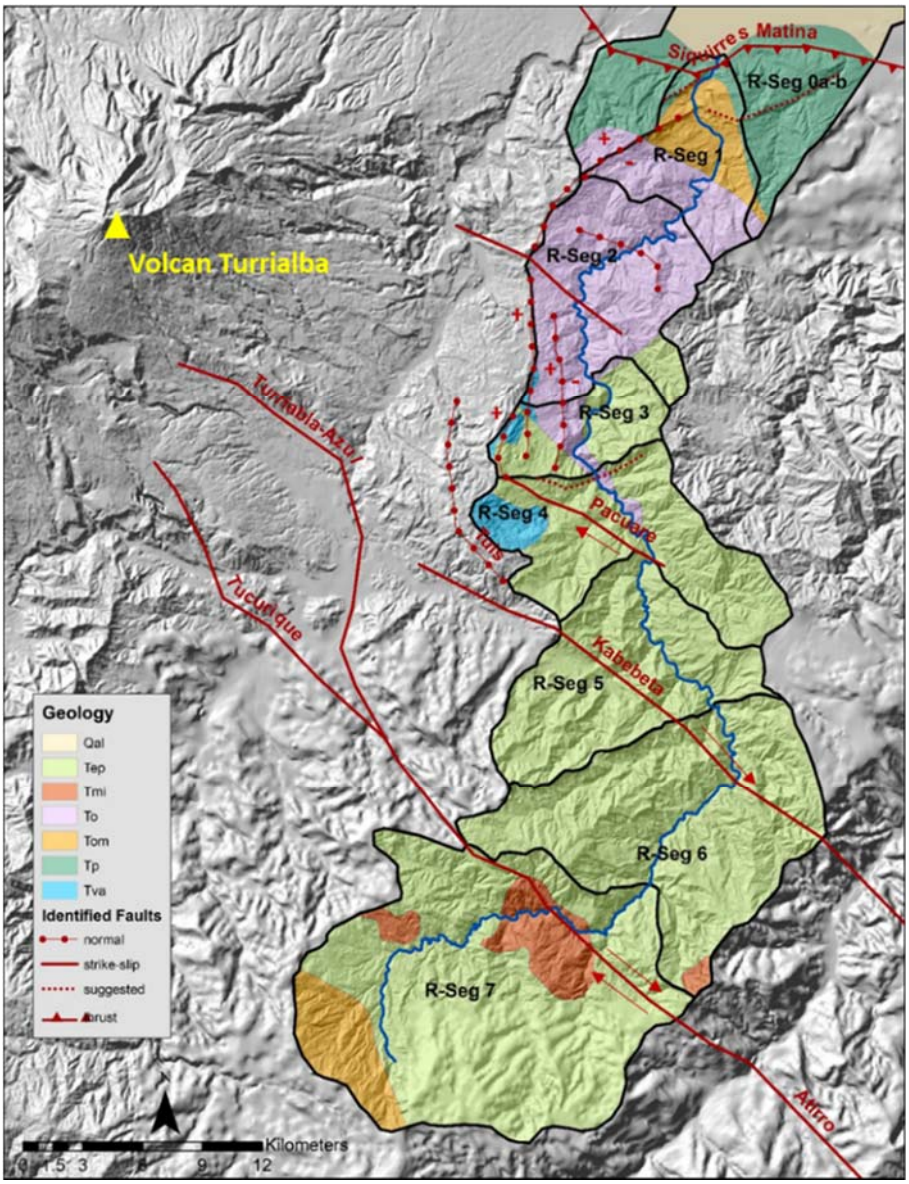

Geol Unit	Description
Qal	Fluvial deposits
Tp	blue-green shales; conglomerate of basalt, andesite with quartz-clay matrix,sandstones inter-beds; lahars-dominated with fragments of basalts and rich in bauxite
Tom	silty shales and calcareous sandstone, reefal limestone
To	sandstones, shales and calcareous fossiliferous sandy clays; brecciated limestones with ; calcic sandstone
Tep	well stratified sedimentary conglomerates (sandstone & siltstones) of volcanoclastics and resistant reef limestone & marl (calcite or lime-rich mudstone) and calcareous conglomerates;
Tva	conglomerates of andesite and basalt; shales, siltstones and fine-grained conglomerates
Tom	black dark shales, siltstones, tuffaceous sandstones, conglomerates and turbidites
Tmi	instrusives: granodiorites, diorites and granite

Figure 0-7. Map of generalized geology and faults of the Rio Pacuare watershed. Geology unit boundaries and descriptions from Sandoval (1982). Major fault types and locations compiled from Fernández-Arce(2009), Fernández-Arce (2013), Marshall et al. (2000), and Montero et al., (2013). *"Suggested" faults identified in this research but not confirmed. Basemap: 30m DEM (ASTER, 1999) and 5m DEM (Sigma, 1998).*

Ongoing deformation and uplift of the CCRDB and NPDB has produced extensive tilting (northeast), low-angle thrust faults, strike-slip faults, and broad folding (Figure 0-7) throughout much of the Talamanca Mountains, including the Rio Pacuare watershed (Fernandez et al., 1994; Fernandez et al., 2007; Fernández-Arce, 2009; Fernández-Arce, 2013; Montero & Linkimer, 2005). The Rio Pacuare crosses the northern border of the CCRDB, named the Siquirres-Matina thrust fault, at Rkm 47, within R-Seg 1 (Figure 0-7). At this fault the Rio Pacuare flows through the sheer canyon walls of Dos Montañas for approximately 200m, a topographic feature produced by uplift (thrusting), deformation, and subsequent channel incision (Figure 0-8).

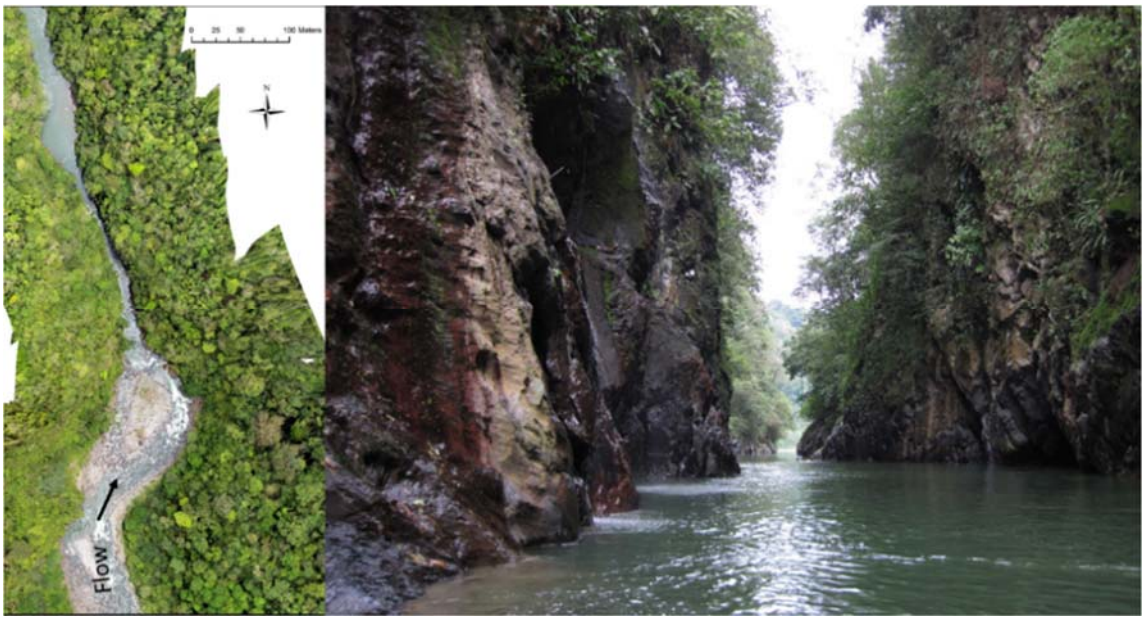

Figure 0-8. Dos Montañas Canyon at Rkm 47 – R-Seg 1. Photos by P. Lind - 2014.

The Siquirres-Matina thrust fault and almost all the faults within the Rio Pacuare watershed, are reported to be currently active (Marshall et al., 2000). Major earthquakes in this region have occurred in 1910, 1973, 1983, and 1991 (Lindholm et al., 2007; Tajima & Kikuchi, 1995). Coastal uplift of 0.5-1.9 meters along sections of the Caribbean coastline was associated with the 1991 earthquake along the Siquirres-Matina fault (Fernandez et al., 1994). Between 1992 and 2002 alone, 359 low magnitude (1.0-4.1 M_L) earthquakes were reported within the CCRDB, including along three of the major faults that bisect the Rio Pacuare watershed (Kabebeta, Pacuare, and Siquirres-Matina

faults) (Montero and Linkimer, 2005). Additional review of seismic activity between 1992 and 2009 shows the region of the Rio Pacuare watershed as an important seismic zone with dense clusters of recorded activity throughout (Fernández-Arce, 2013).

The uplift and faulting, combined with resulting channel incision into the bedrock, accentuates the topographic relief of the Talamanca landscape (Marshall et al., 2003). An average rate of Quaternary uplift for the high central Talamanca Mountains, based on paleosol analysis, has been reported as 1km/Ma (1mm/yr) (Driese et al., 2007). No reported uplift or landscape denudation rates have been found specifically for the Rio Pacuare.

Field observations during this study confirm that the Rio Pacuare has a complicated and mixed geology. As a result of historical uplift and efficient channel incision, in much of the study area the channel is flowing through the mountain's basement stratigraphy, primarily composed of calcareous sandstones/mudstones, conglomerates, and some resistant limestone (Tep in Figure 0-7). Bedrock stratigraphy of the basement lithics, where exposed along the banks, often display moderate to extreme degrees of tilting (10-90º from horizontal) from the orogenic folding that has occurred (Figure 0-9- A). Marine fossils such as pieces of coral and anemone rings were observed in the limestone and calcareous mudstones (Figure 0-9– B). Dikes or interbedded layers of igneous material (basalt and andesite) not included in the generalized geology map (Figure 0-7) were observed occasionally in the exposed banks of the channel.

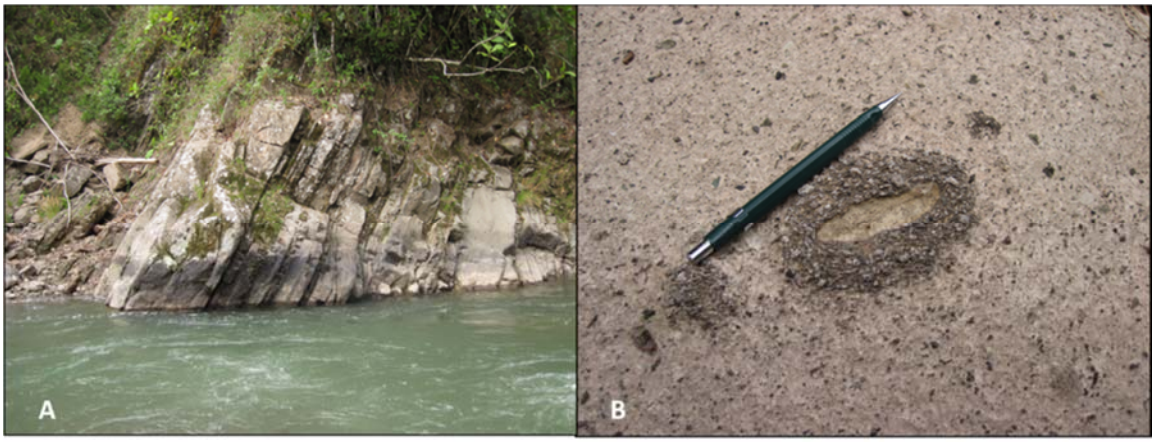

Figure 0-9. A) an example of tilted stratigraphic layers at Rkm 87.5 and B) anemone fossil ring in calcified sand-sandstone at Rkm 75. Photos by P.Lind.

2.2 MATERIALS AND METHODS

To characterize the geomorphology of the mainstem Rio Pacuare, this study combines field observations and feature mapping with analysis and interpretation of remotely sensed and other digital data. Remotely sensed data has proven useful for collecting and analyzing detailed geomorphic information. This includes small-scale applications as well as over very large study areas, and where terrestrial access is limited or difficult (Carbonneau et al., 2012; Gilvear & Bryant, 2003; Hamilton et al., 2007; Javernick et al., 2014; Lisenby et al., 2014). In this study, remotely sensed data (imagery) is used to map and measure features along approximately 88 kilometers of river that has fairly limited access otherwise. The remotely sensed data this study utilizes includes high-resolution aerial imagery and Digital Elevation Models (DEM) collected and created as part of this study, as well as acquired digital imagery and DEMs (5m and 30m) from Costa Rican organizations and the agencies described below.

Fieldwork was conducted November 2012 – April 2013, October– December 2013, and April 2014. The study area's relatively large size combined with difficult access limited the extent of field-based feature mapping. Geomorphic features observed from nearby (trails and roads), at river's edge, or from within the channel (by raft) were noted where possible. Rkm 95 to 80 and Rkm 73.5 to 44 were accessed by raft. The area upstream of Rkm 107 to Rkm 120 was viewed aerially via helicopter, but not visited on the ground. Difficult access also denied field observations in the upper portion of Mollejones Cañon from Rkm 75.5 to 77. The primary features noted in the field include bars, islands and floodplains, low terraces, major landslides, bedrock outcrops, and debris flow/torrent inputs from tributaries. Grain-size was measured (Figure 0-10) using methods described by Bunte and Abt (2001) at eight large, active cobble-boulder bar deposits located at Rkm 62.5 and 66.25 in R-Seg 2, Rkm 74.9 in R-Seg 3, Rkm 82.6 in R-Seg 4, Rkm 90.35, 90.5, and 93.75 in R-Seg 5, and Rkm 106.4 (Figure 0-11). Visual observations of bedload distribution, size, and lithology were otherwise periodically qualitatively noted in the field.

Figure 0-10. Conducting grain-size surveys at depositional bars along the Rio Pacuare (Rkm 62.5, 82.6, and 74.9). Photos by P. Lind.

To examine the possibility of using distinct lithologies for tracing sediment movement in the river from source layers to deposition points, composition of the sediment was recorded as part of the gravel count surveys (see Figure 0-11). This survey revealed a mixed lithology to the bedload throughout much of the study area. For example, a unit of intrusive granodiorite is mapped only in the upper watershed within R-Seg 7 (Figure 0-7), and a unit of andesite is mapped in the hillslopes of R-Seg 2. But, the prevalence of andesite, basalt and granodiorite clasts observed in the bed material throughout the mainstem channel suggest highly competent sediment transfer from upstream sources and/or that the coarsely-scaled geology map may not reveal the only source for these lithologies in the watershed. Also, sedimentary conglomerates within the watershed, often contain clasts of mixed lithics, including volcanoclastic material. Perhaps the presence of well-rounded clasts of basalt, andesite, and even granodiorite in the modern bedload throughout the study area is the result of weathered conglomerates releasing the clasts. Or, perhaps they were exhumed by historical channel development into igneous strata that has since been eroded. Whatever the case may be, it was not possible to trace alluvial sediment to source layers based on lithology of the bedload material.

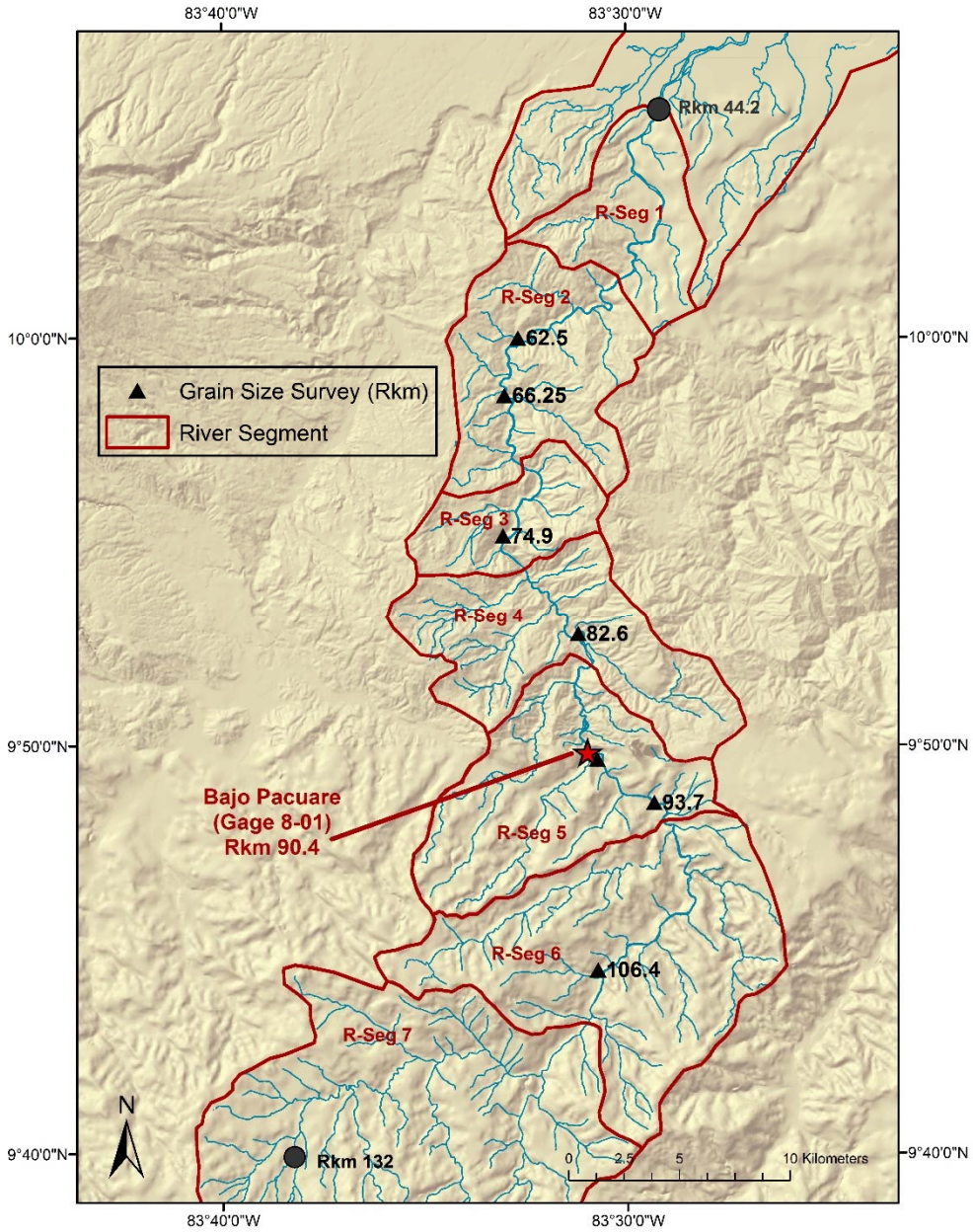

Figure 0-11. Map of grain size survey locations, with river kilometer.

2.2.1 Remotely Sensed Data

As part of this research, low-elevation aerial photos and video were collected during April 2014 with a helicopter-mounted camera. Photos were taken during the dry season and in the morning to decrease potential cloud cover, increase the quantity of exposed bedload deposits, and reveal low-flow channel form. Imagery was collected in a swath approximately 100-300 meters wide, over Rkm 44 – 122 (R-Seg1 to mid-section of

R-Seg 7) of the mainstem Rio Pacuare. An almost continuous 0.1m DEM with corresponding high-resolution orthophotos was created from this imagery utilizing Structure-from-Motion (SfM) photogrammetry (Koch, 2003). To collect this imagery, this study further developed methods of aerial photo collection and SfM model development used by Dietrich (2016). Only one small data gap at Rkm 57.7 – 61.2 occurred due to wind-gusts that increased helicopter speed enough to disrupt photo-overlap, hindering accurate model production.

The ground control points (GCP) used for photo and model rectification in SfM were established and surveyed prior to the helicopter flight. GCP were collected along both sides of the channel at intervals of 0.2-3.0 kilometers. All control points were located on hard points, such as bridge supports, or as spray-painted 'X'es on large boulders or bedrock (Figure 0-12). The control points' geographic coordinates were collected using a handheld Trimble GPS unit (GeoXS - Trimble, 2009). After post-processing, a vertical precision of 0.3 to 13.8 meters (average vertical precision of 1.1m) and horizontal precision of 0.2 to 1.5 meters (average horizontal precision of 0.5m) accuracy was obtained. The use of an external Trimble Zephyr antenna added to the GPS unit when collecting GCPs from land at bridge crossings did not significantly increase accuracy. Post-processing was accomplished using GPS Pathfinder Office software. A pixel-resolution of 0.1m was obtained for the SfM-produced DEM and orthophotos, similar to other high-resolution data obtained in this manner (Dietrich, 2016; Fonstad et al., 2013; Javernick et al., 2014).

To examine the accuracy and utility of the SfM DEM and orthophotos, horizontal alignment was compared to available ESRI imagery in ArcMap (GeoEye 2011 and 2002), resulting in very good overlap. Vertical alignment of the SfM 0.1m DEM compared to an acquired 5m DEM was also good. Longitudinal profiles extracted from the 0.1m DEM and the 5m DEM (SIGMA, 1998) showed very similar elevations throughout the study area.

Figure 0-12. Photos of collecting ground control points for SfM model development with Trimble GeoXS and Zephyr antenna on the Rio Pacuare. Photos by P. Lind.

The high-resolution SfM orthophotos were used for identification and digitization in ArcMap of the active channel boundary, active channel center line, low-flow channel centerline, river-valley boundary, active exposed bar surface area, floodplains or terrace surfaces, and the location of modern (visible in 2014 imagery) contributing landslides and debris torrents along the mainstem channel. The 0.1m DEM was used to extract channel surface elevations and calculate channel slope. Familiarity with the study area proved very useful in identifying and digitizing features.

The SfM-created DEM and imagery captured the channel and a band 50-300 meters wide on the hillslopes along the channel. However, it did not capture elevation data for the channel's submerged bed or ground elevation below the tall, dense vegetation of the tropical forest that covers most of the river's banks and hillslopes. Therefore, additional photo imagery and digital elevation models were used to characterize the adjoining hillslopes and contributing tributaries. The additional DEMs and aerial imagery utilized in this study were acquired from multiple sources including a 5m DEM (SIGMA, 1998) and a 30m DEM (ASTER, 1999). The 30m DEM was used for regional topographic analysis and map creation. The 5m DEM was used to characterize hillslope gradient and tributary slopes throughout the Rio Pacuare watershed. Additional digital data used for mapping and analysis in this study include the generalized geologic units and the drainage network of primary tributaries provided by the Costa Rican Ministerio de Ambiente y Energia (MINAE).

Google Earth images provided affordable review of historical aerial imagery of the Rio Pacuare (1969, 2002, 2008, and 2011). However, coverage of 75% or more of the study area is available only for 2002 (acceptable resolution to identify bar features) and 1969 (very poor resolution). The other year sets of Google Earth photos are discontinuous and patchy. The channel centerline and visible depositional bars were digitized from the 2002 Google Earth imagery (DigitalGlobe) and then transferred to ArcMap. This data was used for a qualitative comparison of bar and channel locations between 2002 and 2014. The comparison was qualitative because the 2002 imagery is incomplete, clouds visually block sections of the channel, and the images are from three different days in 2002 (Feb. 4, Mar. 9, and Dec. 22). Day-to-day differences in discharge changes the exposed bar area.

2.2.2 Geomorphic Feature Mapping and Measurement

The geomorphic features digitally mapped and/or measured are described in Table 0-1. Features include active channel boundary, active channel width, exposed bars, floodplains and low terraces, valley floor boundary, valley floor width, active channel centerline, low-flow channel centerline, tributary length and slope, and location of modern landslides and debris torrent inputs. The scale used for digitizing depended on the general size of the feature. For example, a scale of approximately 1:500-800 was used to digitize bars, while a scale of approximately 1:1500-2000 was used to digitize terraces.

To analyze how flow competence influences modern distributions of exposed bars, unit stream power was calculated for the 0.2% exceedance flow, every 100 meters between Rkm 44.2 to 118 (R-Seg 1 through R-Seg 6). The 0.2% exceedance flow (average daily discharge with a recurrence interval of one-year) was selected because it represents a high-flow event capable of inundating bar features and filling the active channel, based on hydraulic modeling explained in Chapter III (this dissertation). Unit stream power (ω) in Watts/m^2 was calculated using the equation:

$$\omega = \rho g Q S / w$$

where ρ is density of fluid, g is acceleration due to gravity, Q is discharge, S is slope, and w is active channel width. Discharge (Q) for each 100m increment was estimated using data from ICE gaging station 8-01 (Figure 0-11), and a discharge to upstream drainage

area relationship established for the Rio Pacuare (Chapter III, this dissertation). Slope and active channel width were extracted from the data generated in this study.

Table 0-1. Geomorphic features mapped, a brief description of each feature, and the data source the feature was mapped from.

Feature	Description	Data source and year created
Active Channel	includes wetted channel, active bar surfaces, and bare bedrock. Area visibly inundated by high flow	0.1m DEM and Orthophoto--2014
Active Channel Centerline	midline between Active Channel boundary; represents estimated center of channel when flow inundates active channel area	0.1m DEM and Orthophoto--2014
Low-Flow Channel Centerline	midline of low-flow wetted channel at time of photo collection (April 2014)	0.1m Orthophoto--2014 and GoogleEarth--2002
Bars	all exposed active alluvial surfaces composed of consolidated bedload material within the Active Channel; unvegetated or marginally vegetated with non-woody species;	0.1m DEM and Orthophoto--2014; GoogleEarth--2002
Valley	the floor of the valley between confing hillslopes; Valley boundary includes Active Channel, Bars,and Floodplain and Low Terraces	0.1m DEM and Orthophoto--2014; 5m DEM--1998
Floodplain and Low Terraces	alluvial surfaces on the valley floor with established mature vegetation and/or human occupation; includes islands with high potential for activation during high-flow events	0.1m DEM and Orthophoto--2014; 5m DEM--1998
Active Channel Width	width of Active Channel; measured at 100 m increments perpendicular to Active Channel Centerline	0.1m Orthophoto--2014
Valley Width	width of valley; measured at 100 m increments perpendicular to Active Channel Centerline	0.1m Orthophoto--2014
Landslide	modern direct hillslope sediment contributions to the channel; bare and/or partially/sparsely-vegetated	0.1m Orthophoto--2014; GeoEye 2011
Debris Torrent	modern direct fluvially-mobilized sediment contributed to the channel via a tributary and/or its valley	0.1m Orthophoto--2014; GeoEye--2011
Channel Slope	Slope of low-flow channel surface (2014); calculated at 100 meter increments using elevations from points 100 m up and downstream from the point of interest; water surface elevations extracted from the Low Flow Channel Centerline	0.1m DEM--2014
Tributary Length and Stream Order	length calculated in ArcGIS from aquired line data -- with some minimal corrections and additions done; Stream Order defined by upstream contributing tributary network (1-4)	ICE--no year specified
Tributary Slope	slope of each contributing tributary using only the upstream-most and downstream-most elevation values divided by the Tributary Length	5m DEM--1998
Hillslope Gradient	mapped using slope analysis tools available in ArcMap	5m DEM--1998

2.3 RESULTS

The results from this analysis provide the data necessary to evaluate the relationships and identify the influences of the primary and intermediate geomorphic components presented in the conceptual model in Figure 0-1. The geomorphic components and their relationships to each other are used to understand how channel geomorphology varies downstream in relation to geology and sediment sources.

Observations and results at the watershed, river segment, and within segment scales are provided, with selected reach-scale examples used where appropriate. First, watershed-scale observations are presented to establish a qualitative context to some of the landscape processes that influence the geomorphology and sediment distribution within the Rio Pacuare. Then, downstream patterns of active channel width, valley width, slope, and unit stream power are compared between, and also within, each river segment. The surface areas of depositional features (exposed active bars, and floodplain or low terraces) are examined as a percent of the active channel area and valley area within each segment.

2.3.1 Observed Watershed and Channel Characteristics

Watershed Topography

An exaggerated topography of sharp ridge-lines and steep V-shaped valley troughs created through processes of hillslope erosion and channel incision define the Rio Pacuare's watershed, similar to other humid tropical montane basins (Ahmad et al., 1993; Kirby & Whipple, 2012; Marshall et al., 2003). The steep hillslopes (6-84% gradient) are topped with ridges that are usually scalloped with concave head scarps resulting in essentially no interfluve area between tributaries considered as low or moderately sloped (Figure 0-13). The troughs that house the channel and its dense network of tributaries are narrow and steep-walled. The head-scarp scars along the ridges are the initiation points of historical and active landslides and debris torrents. Debris torrents, comparable to channelized debris flows, are the delivery of material (including fines, but dominated by coarse-grained material) via fluvial and gravitational processes that initiate in steep (gradient 10-25%) upslope areas and flow down a valley trough or channel (Galia & Hradecký, 2012; Slaymaker, 1988; Sterling & Slaymaker, 2007). Although the dense vegetation cover on most of the hillslopes makes it difficult to see all tributary initiation points, the headwaters of many tributaries were observed extending upslope into concave scarps. This process of upslope extension expands the rectangular-shaped tributary networks that radiate off the mainstem channel. The narrow rectangular shape and dendritic pattern of the tributary networks also reflect the rectangular drainage pattern of the Rio Pacuare watershed (Figure 0-13). .

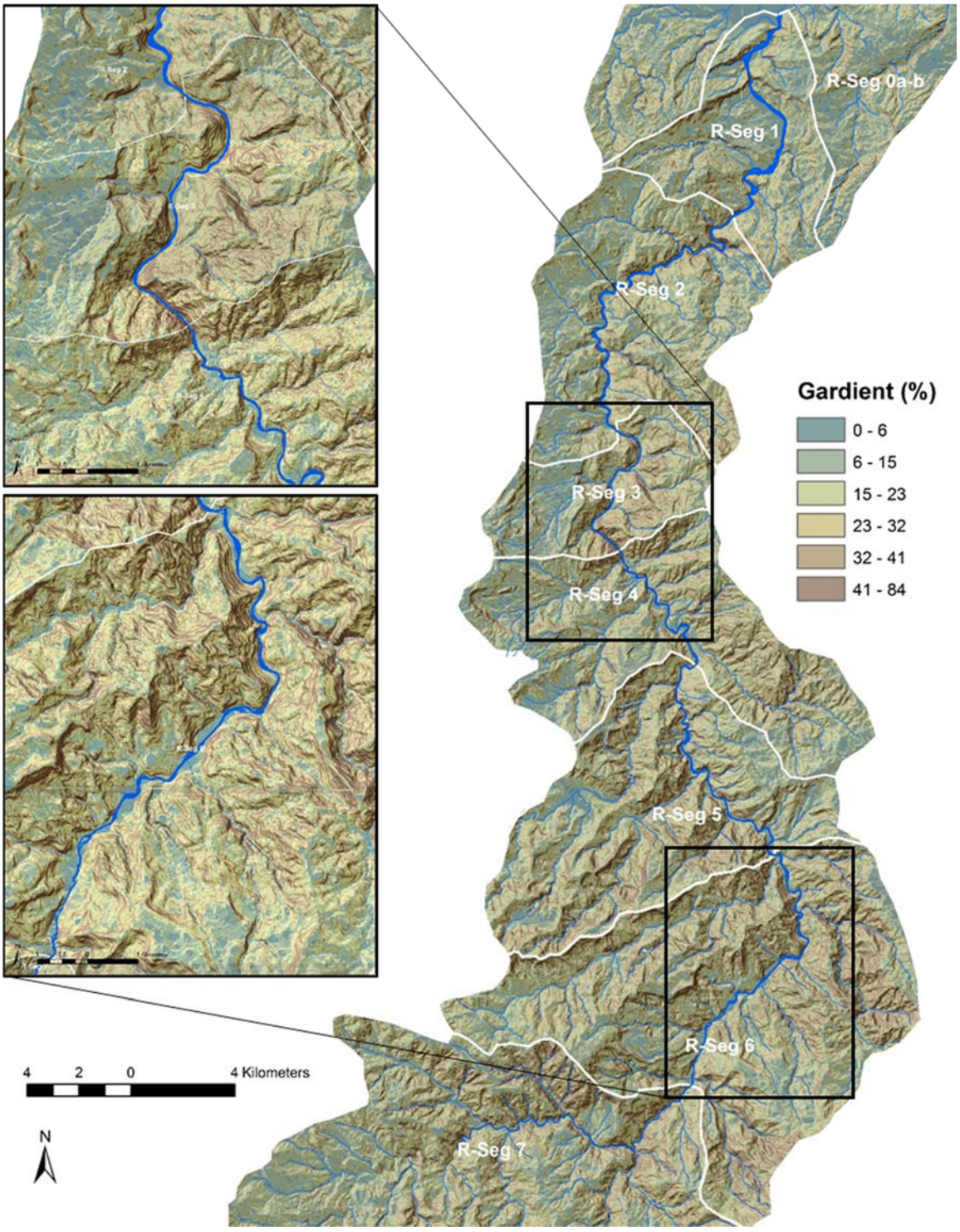

Figure 0-13. Map of hillslope gradient and river segments (R-Seg) of the Rio Pacuare. Basemap: 5m DEM (SIGMA, 1998)

When compared across the watershed, the ridge and trough topography is most prominent upstream of Rkm 77, at the border between R-Seg 3 and R-Seg 4 (Figure 0-13). Based on studies done elsewhere (Goldsworthy & Jackson, 2000; Schlunegger, Melzer, & Tucker, 2001; Sterling & Slaymaker, 2007; von Blanckenburg, 2005) this likely occurs due to differences in the types of faults (strike-slip horizontal displacement versus thrust-fault vertical displacement) and the lithology of the underlying bedrock (weathering rates). More resistant lithologies can impede the development of a pure ridge and trough topography. This is occurring in R-Seg 3 on river left where steep valley walls are composed of resistant fossiliferous limestone and calcareous silt- and mudstones (To in Figure 0-7). These very steep slopes contain a stair-step set of normal faults (vertical off-set) on the west side (river left) of the channel. Tributary extension and trough development here is relatively minimal, except along the top of the slope, which is composed of less resistant sedimentary conglomerate (Tep in Figure 0-7). Figure 0-14-A shows hillslope gradients and the location of the normal faults in R-Seg 3. The uplifting limestone in R-Seg 3 is more resistant to tributary trough development so it maintains steeper hillslopes (Goldsworthy & Jackson, 2000). Landslides here are shallow, long, and narrow due to marginal soil development over the steep uplifting bedrock.

In comparison, the major fault types upstream of Rkm 77 are strike-slip with primarily horizontal offset and a lithology of predominantly conglomerate-sedimentary and igneous materials. Figure 0-14 – B provides an example of ridge and trough from Rkm 88-103. Landslide scarps in the conglomerate-sedimentary and igneous material often reveal deeper saprolitic soils. Here, hillslopes and tributaries are slightly less steep overall, and a more developed ridge-trough topography occurs. The inset maps in Figure 0-13 of R-Seg 3 and R-Seg 6 also provide images of the difference between the steep resistant limestone slopes within R-Seg 3 compared to the ridge and trough topography upstream. Therefore, geology (lithology and faulting) influences hillslope gradient and tributary development within the watershed. Based solely on observation, this may also influence the quantity of material produced in landslides and debris torrents – but further research beyond the scope of this research is needed to confirm that hypothesis.

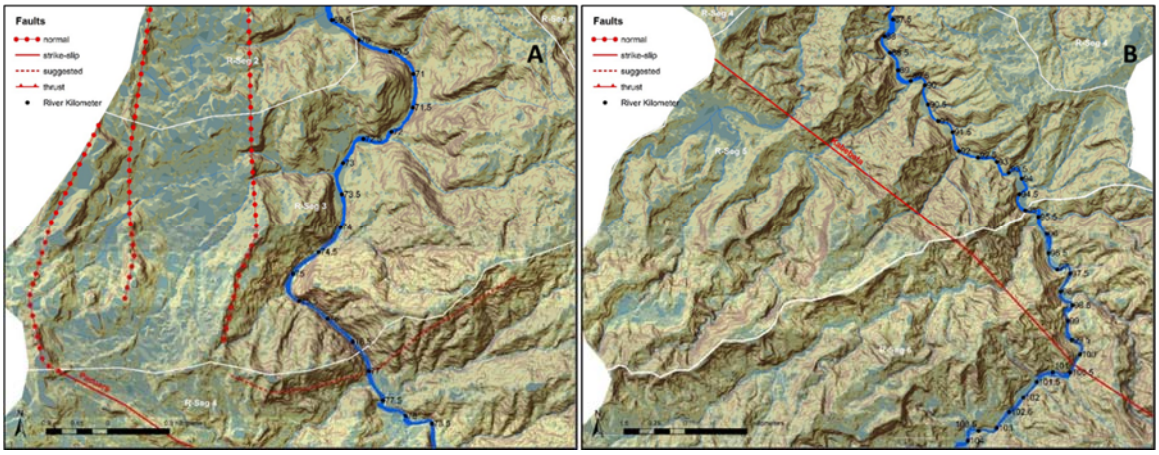

Figure 0-14. Map of faults and local topography at (A) Rkm 70-78 and (B) Rkm 88-103. Background map same as in Figure 0-12.

Another example of geologic control on watershed topography is the Siquirres-Matina thrust faulting at the downstream end of the study area (Rkm 44.2-47.5 in R-Seg 1). Here, the set of hanging walls of the Siquirres-Matina thrust fault dip northeastward below the alluvial deposits that comprise the Caribbean coastal plain (Figure 0-15). The Rio Pacuare cuts perpendicularly through the set of thrust-fault walls that create a set of SE-NW trending ridges that gently slope downward on the east side, but have near-vertical west-side faces. The southern-most set of these faults has been characterized as a normal type fault but it is an extension of the deformation and thrusting of the Siquirres-Matina fault. These faults force tributary development and drainage patterns to evolve between and off the ridges of the hanging walls, resulting in a slightly more angular tributary network pattern that is less dense than in the rest of the watershed (see Figure 0-2 R-Seg 1). In addition, the much steeper west side of the fault ridges have visible evidence of extensive mass wasting (landslides and debris torrents). A well-developed depositional fan at Rkm 47.5 to 52 indicates that mass-wasting processes here have contributed large quantities of material to the channel, likely for a long period of time. This is another example of how geology combined with weathering is controlling channel form, tributary development, and the character of lateral contributions to the mainstem channel.

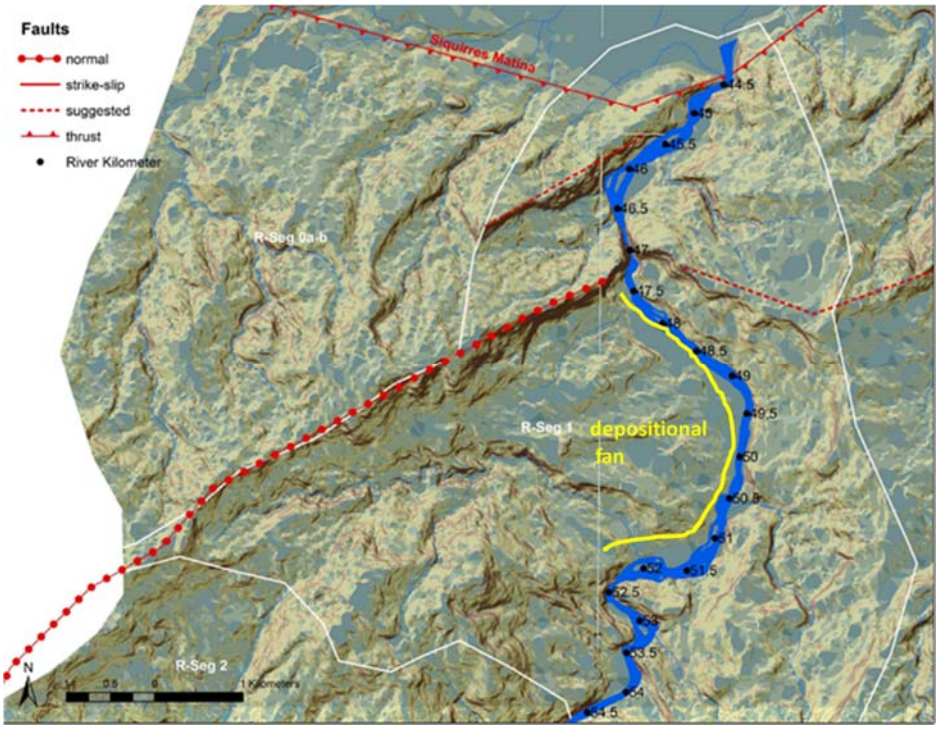

Figure 0-15. Map of the Rio Pacuare intersecting with the Siquirres-Matina faults and the depositional fan upstream (Rkm 44.2-54). Background map same as in Figure 0-13.

Historical and active tectonic uplift and faulting instigate channel incision, which, when combined with heavy precipitation and hillslope weathering, destabilizes hillslopes and promotes landslides and debris torrents. (Montgomery & Brandon, 2002; Roering et al., 2007; J. Roering, 2012). In the steep montane humid tropics, where regolith and bedrock weathering rates (chemical and physical) are rapid, saprolite soils can be deep and large storm events occur regularly. In these environments, landslides and debris torrents often play key roles in landscape evolution and the delivery of sediment to the mainstem channel. This appears to be especially true in seismically active regions in the humid tropics (Dadson et al., 2004; Golden & Springer, 2006; Kuo & Brierley, 2014; Ohl & Bussmann, 2004). Repeated sequencing of these processes places a river and its tributaries, though geographically the smallest components of the landscape, as primary controls of denudation, landscape evolution, and thus sediment flux downstream (Benda et al., 2005; Stock & Dietrich, 2006; Whipple, 2004). Soil creep and surface wash on saturated slopes were observed contributing to hillslope erosion in the watershed of the Rio Pacuare, but this produced relatively minor contributions of bedload sediment to the

channel compared to landslides and debris torrents. In addition, massive boulders contributed via rock fall from adjacent hillslopes divert flow, add roughness, and influence local channel features such as steps where they sporadically occur, primarily in confined reaches.

Tributary Characteristics

Examination of the length, slope and stream order of tributaries is used to better understand the spatial distribution and processes of sediment transfer from the watershed to the mainstem. The tributaries of the Rio Pacuare have either extremely coarse bedload and/or scoured bedrock channel beds, as observed in the field. This implies sequences of debris torrents as a dominant process in these tributaries, and likely a major source of lateral sediment contribution from the uplands to the mainstem channel (Benda & Dunne, 1997; Lisenby et al., 2014). Although tributary drainage density in the Pacuare is high, most are only second- or first-order streams when they join the mainstem. A few tributaries are third-order, and only one is a fourth-order stream (at Rkm 79.3 in R-Seg 4). Figure 0-16 displays length, slope, and stream order of the tributary streams that join the mainstem channel, in order of confluence occurrence. Sixty-four percent of the tributaries joining the mainstem Pacuare are first-order tributaries, with an average slope (m/m) of 0.23 (gradient of 23%). Second-order tributaries comprise twenty-five percent of the tributaries with an average slope of 0.15 (gradient of 15%). Third-order and fourth-order each have an average tributary slope of 0.11 (gradient of 11%). The average length for first, second, and third order tributaries is 2 kilometers and for the fourth order tributary it is 2.1 kilometers. This is indicative of the narrow rectangular shape of the drainage area. Tributaries of this scale, shape, and slope fit the characteristics of channels that deliver debris torrents (Galia & Hradecký, 2012). When examined individually, the shorter first-order streams draining steep hillslopes adjacent to the channel have the greatest slopes, as expected.

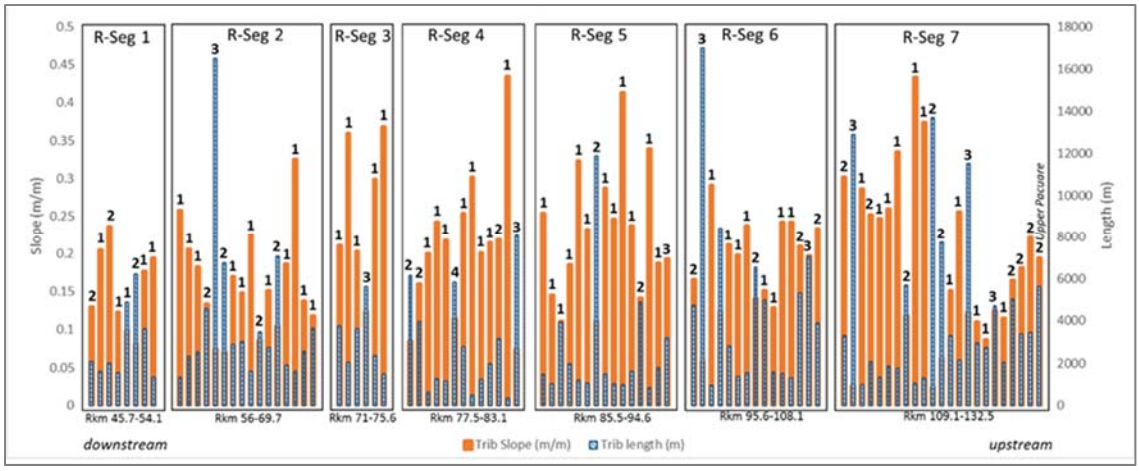

Figure 0-16. Graph of tributary slope, length, and stream order--in order of confluence location along the mainstem channel. Source: river layer from MINEA (undated) modified for this study.

Lateral Sediment Contributions

Materials delivered to the channel via lateral contributions (debris torrents, landslides, and tributaries) are important sources of sediment to the channel. It is assumed that the quantity and location of these contributions fluctuate over time, depending on upslope erosion processes, storm events, and local seismic activity (Benda et al., 2005; Restrepo et al., 2006). Gonzalez et al. (2016) showed that, on rivers in Panama, lateral contributions from landslides or debris torrents contribute a substantial quantity of the river's load, though inputs are likely temporally and spatially dispersed. This same study reported that for landslides alone, 78% of the coarse-size fraction and 11% of the fine-grain fraction of bed material in the mainstem channel downstream from the input locations were sourced from the slide areas. This further suggests the importance of lateral contributions to the quantity of bedload available in the channel and the channel's capacity to integrate those contributions into its active bedload.

The locations of recent debris torrent and landslide contributions observed on the Rio Pacuare in the field in 2013-2014 and in 2014 aerial imagery are shown in Figure 0-17. The density of contribution locations indicates the important role that lateral sources likely have on the available sediment in the mainstem channel. Tributaries occur at 0.7 to 1.8 per river kilometer. The mapped landslides and debris torrent (visible in 2013-2014 imagery) occur at 0.5 to 2.1 per river kilometer and 0.1 to 0.5 per river kilometer, respectively.

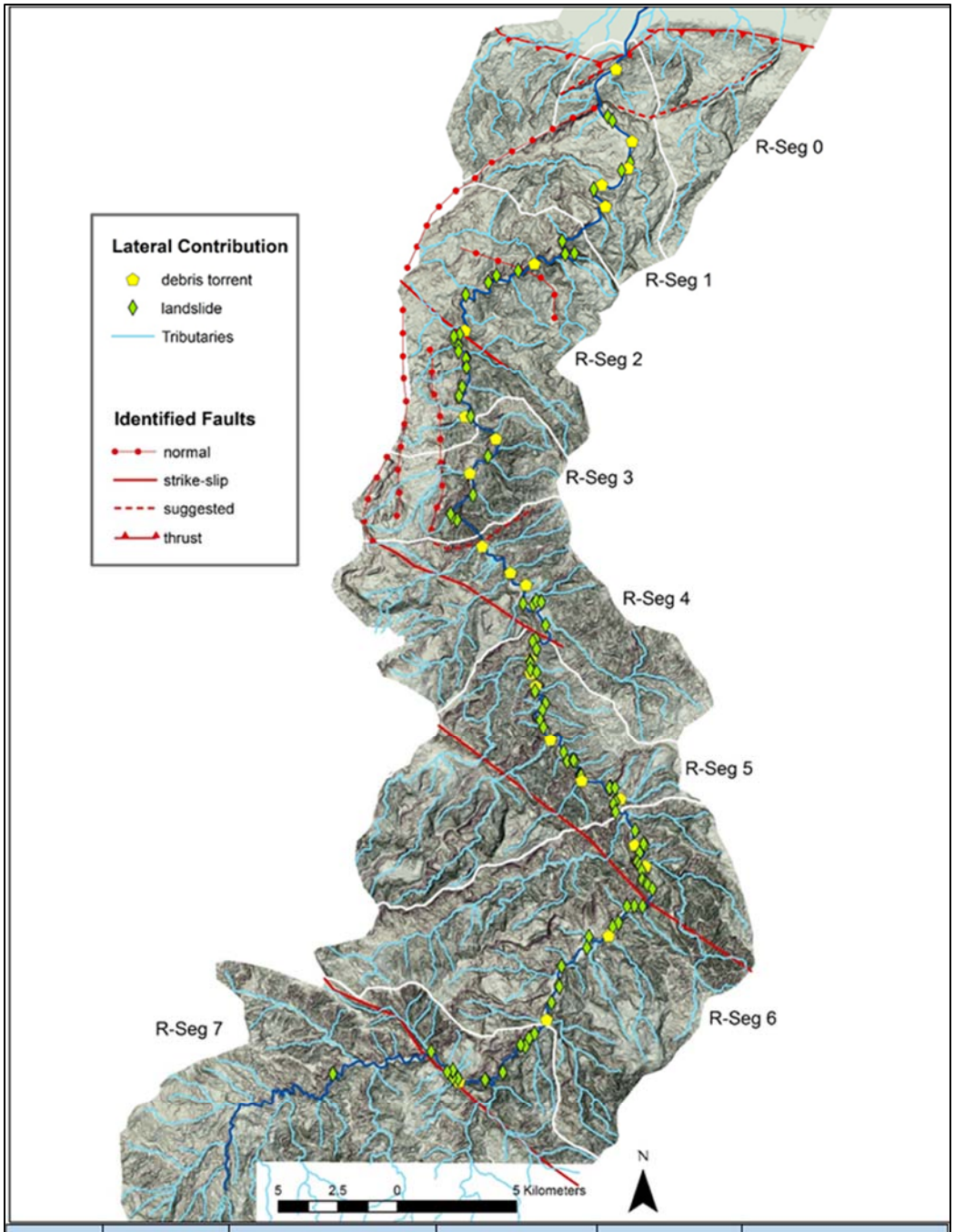

River Segment	Rkm	Channel Slope (R-Seg Mean) (m/m)	Tributaries per Rkm	Landslides per Rkm	Debris Torrents per Rkm
1	44.2-54.9	0.008	0.7	0.5	0.5
2	54.9-70.1	0.007	1.0	1.2	0.2
3	70.1-76.9	0.010	0.9	0.7	0.3
4	76.9-84.1	0.022	1.8	0.7	0.4
5	84.1-95.25	0.011	1.5	2.0	0.4
6	95.25-108.3	0.013	1.1	2.1	0.5
7	108.3-132	0.031	1.6	1.0	0.1

Figure 0-17. Map and table of modern (visible in 2013-2014 imagery) landslides and debris torrents with tributaries and their spatial frequency.

Mapped throughout the watershed, debris torrents and landslides for this time period had a slightly greater occurrence in R-Segs 5 and 6 (Rkm 84-108). Density of landslides in both of these segments was highest near prominent faults. There is no historical information regarding past occurrences of debris torrents or landslides in the Rio Pacuare, thus the frequency and distribution of lateral contributions over time within the watershed are not included in this study. However, it would be a worthwhile undertaking to utilize this data and compare it to future distributions of these features for a better understanding of the spatial and temporal patterns of mass-wasting, landscape denudation rates, and lateral contributions to the mainstem channel.

Although debris torrents, landslides, and tributaries are common sources of sediment to the channel, no or only minor accumulation of sediment (fines to boulders) was observed in the Rio Pacuare at most of the lateral contribution input locations. Instead, lateral inputs appear to be rapidly mobilized downstream and integrated into the bedload or suspended load of the channel. This indicates that the Rio Pacuare, similar to the upper Rio Chagres in Panama (Wohl, 2005), frequently produces highly competent flows capable of regularly transporting incoming lateral coarse material.

An example that illustrates flow competence and the integration of lateral sediment contributions into the bedload of the Rio Pacuare is at the largest modern debris torrent that enters the channel at Rkm 70 in the upstream reach of R-Seg 2 (Figure 0-18). A large-volume debris torrent occurred in late November 2008 during a high-magnitude storm/discharge event. The debris torrent was approximately 300 meters wide and at least 10 meters deep where it entered the Rio Pacuare at the mouth of a tributary. Today, material from the 2008 torrent still exists on the opposite bank of the channel, indicating that torrent material filled the channel and rolled up the wall on the other side of the valley. When the storm subsided the following day, however, rafters and kayakers reported freely passing through the section with only minor changes to bar development downstream (Studt, 2014). Figure 0-18 shows the modern active channel of the Rio Pacuare cutting through where a debris fan would have otherwise accumulated. Since 2008, this tributary has periodically contributed additional debris torrent material, but at a smaller scale than in 2008. Those contributions continue to be integrated into the mainstem channel's bedload material and to supply material for downstream bar

development. The remaining torrent deposits that currently fill the tributary valley remain a viable source of additional lateral sediment contributions, when weather permits.

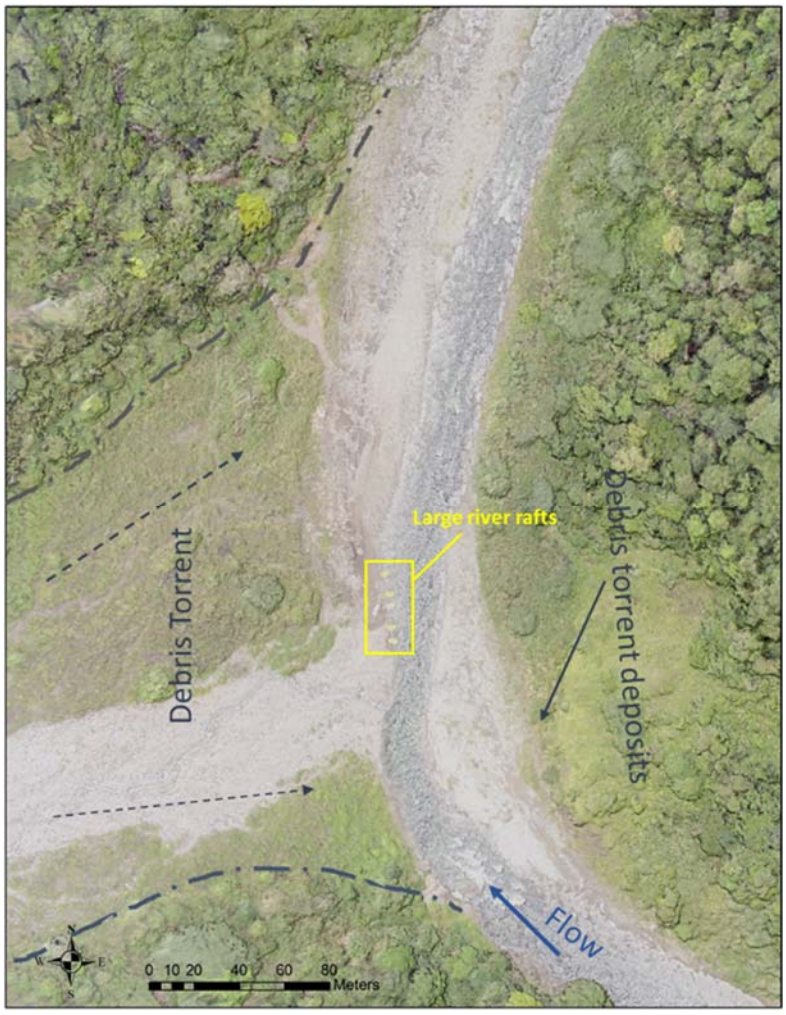

Figure 0-18. Debris torrent tributary entering the Rio Pacuare at Rkm –70. 2008 debris torrent boundary outlined. Photo by P. Lind, 2014.

Bedload

Bedrock channel units occur in only a few places while coarse bedload of varying but unknown depths forms the channel bed throughout most of the mainstem Rio Pacuare. However, bedrock walls confine the width of the active channel on one or both sides throughout most of the study area.. Large boulder bars that can reach more than 500m length define channel form during periods of low-to-normal flow. The active bar

deposits are mostly unvegetated and composed primarily of strongly imbricated cobbles and boulders (Figure 0-19), indicating relatively frequent bedload mobilization.

Figure 0-19. Boulder bar at Rkm 62.5 in R-Seg 2 – man in background for scale. Photo by P.Lind – 2014.

The eight grain-size surveys conducted on large depositional bars throughout the study area (see Figure 0-11) indicate that the typical median bed material size is large cobble to boulder, and grain size ranges from coarse gravels to very large boulders (Table 0-2). Based on the grain-size surveys and field observations, grain size does not appear to express a normal downstream-fining trend, though more complete grain-size surveys should be done before this is definitive. However, similar non-downstream-fining grain-size trends were also reported on the upper Rio Chagres in Panama (Rengers & Wohl, 2007) and the Liwu River basin in Taiwan (Kuo & Brierley, 2014). This further suggests that, in addition to upstream-to-downstream in-channel sediment flux, lateral inputs are an important component of sediment supply, contributing material along the length of the

channel. When combined with local flow competence, lateral inputs likely play a role in grain size distributions in this and other humid tropical montane river systems.

Table 0-2. Grain-size distribution at eight representative boulder bar deposits within the study area.

		B-axis Diameter (mm)							
Site	River km	D16	D50	D84	% sand	% gravel	% cobble	% boulder	# of samples
Bajo Tigre	62.5	68	190	450	0	15	45	41	218
Tres Equis	66.25	3.2	62	400	0	51	27	23	229
Mollejones Cañon - *shelf deposit*	74.9	44	290	900	0	25	21	54	141
Bajo Pacuare por San Juaquin	82.6	48	130	360	0	23	49	28	205
Bajo Pacuare 01	90.35	73	310	780	0	13	32	56	183
Bajo Pacuare 02	90.5	3.1	150	530	0	34	23	43	136
Paso Marcos	93.75	3.1	51	430	0	55	25	19	251
Arriba Pacuare	106.4	17	140	590	0	32	33	35	222

Large Wood

Large wood, often considered an important agent of geomorphic processes and ecologic complexity in mountain rivers (Benda & Bigelow, 2014; Gurnell et al., 2002; Mao et al., 2013; Montgomery & Buffington, 1997; Ryan et al., 2014; Vera et al., 2014), appears to assert very little influence on the Rio Pacuare's geomorphology. Abundant large wood source material exists along most of the study area as thick, mature tropical forests on steep adjacent hillslopes, including massive hardwood trees that can grow over 50 meters tall. Evidence of direct inputs of wood was observed in the field as single-tree infall or in conjunction with soil and rock in landslide and debris torrent deposits. However, large wood is neither retained in the system nor observed influencing bar or bedform development. Instead, the observed sparsely distributed large wood was either single log, or sometimes a few logs, located along the margin of the channel or on top of a large bar. Often these pieces are removed, unless lodged between large boulders, by subsequent high flow events. Some studies on the role of large wood in a few headwater streams in Costa Rica also found that large wood plays either no role or only a minor, short-term role in geomorphic channel processes (Cadol & Wohl, 2010, 2013; Lisenby et al., 2014). Large wood is not retained in these systems, because decay is rapid from decomposition in the tropics and physical breakdown of the pieces is rapid due to high-stream power and impact by coarse-grained bedload in transport.

2.3.2 Mainstem Channel Analysis

For this analysis the Rio Pacuare watershed has been subdivided into separate geomorphic river segments delineated by channel form and type, channel slope, and sediment distribution (bars and floodplain or low terraces) (Table 0-3). Overall, the Rio Pacuare's montane portion is laterally bedrock-confined with a plentiful quantity of bedload material. Channel plan form (straight or bedrock-controlled meandering) is the result of the river incising, over time, into the least-resistant pathway through the watershed's geology. Small pockets of floodplains and occasional low terraces subtly influence channel planform where they exist. Bars of cobble-boulder bed material are common and are important in defining channel form at low and normal flow. The dominant channel type in each segment was defined following Montgomery and Buffington (1997). One new classification type is added in this study: cascading riffle-pool. A cascading riffle-pool reach has a higher gradient than a typical riffle-pool reach (> 0.015) and it contains large boulders that create hydraulic drops and jumps within the riffle-like feature. A cascading riffle is usually followed by an elongate scour pool that often has additional large boulders below the water surface. The confined segments of R-Seg 3 and 7 are dominated by step-pool. The other semi-confined to confined segments are dominated by riffle-pool or cascading riffle-pool channel types.

Due to the extent of the high-resolution imagery, most analyses and results presented in this section are for Rkm 44.2 to 122 (R-Seg 1 through mid-section of R-Seg7). Upstream of Rkm 122 to Rkm 132 in R-Seg 7, the mainstem channel is a steep, completely confined single-thread, cascading to a step-pool channel with large boulders lining the channel bed. The limited extent of the high-resolution DEM also restricts calculations of channel slope and unit stream power to within Rkm 44.2 to 118. Thus, the results presented here for R-Seg 7 (Rkm 108.3 to 132) underrepresent the confinement and increased slope that actually occurs in the segment's upper reaches.

Table 0-3. River segment and length (river kilometers), upstream drainage area, dominant channel forms, and dominant channel types.

River Segment	Rkm	Upstream Drainage Area (km^2)	Channel Form	Channel Type
1	44.2-54.9	660.7	confined / semi-confined bedrock meander / straight single thread / braided	riffle-pool
2	54.9-70.1	616.4	confined / semi-confined bedrock meander single thread	cascading riffle-pool
3	70.1-76.9	542.8	confined straight single thread	step-pool / cascading riffle-pool
4	76.9-84.1	510.0	semi-confined bedrock meander single thread / minor braiding	cascading riffle-pool / riffle-pool
5	84.1-95.25	432.4	semi-confined bedrock meander single thread / minor braiding	riffle-pool / cascading riffle-pool
6	95.25-108.3	347.5	semi-confined bedrock meander / straight single thread / minor braiding	riffle-pool / minor cascading riffle-pool
7	108.3-132	213.3	confined straight / bedrock meander single thread	step-pool / cascading riffle-pool / minor riffle-pool

Geometry and Confinement

Mountain rivers often express variation in downstream channel geometry (width and depth) that reflects bedrock or hillslope confinement, rather than a normal power-function relationship that consistently accommodates increasing downstream discharge in purely alluvial systems (Montgomery & Gran, 2001; Wang et al., 2015; Wohl, 2010; Yanites & Tucker, 2010). This study uses the width of the active channel to examine downstream changes in channel geometry. Variations in the width of the channel and the valley floor are used to identify areas of hillslope confinement.

Figure 0-20 presents the distribution of active channel widths and valley widths measured at 100m increments (Rkm 44 to 122) organized by river segment. While the active channel width and valley width increase from the upstream-most segment to the downstream-most river segment, the overall pattern is irregular. Mean channel width increases from segment 7 to 6, then width is relatively constant for segments 6 to 4,

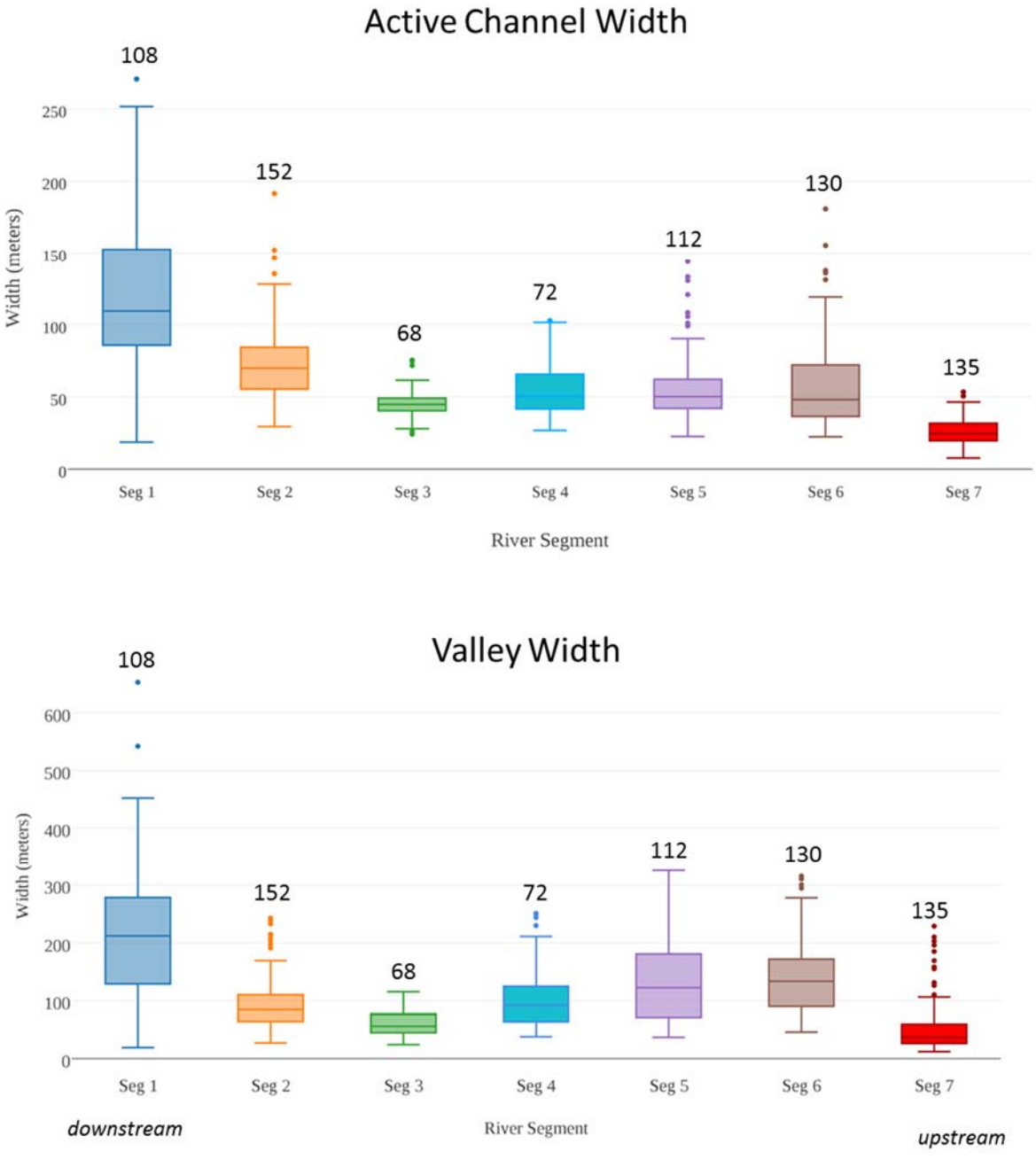

Figure 0-20. Distribution of active channel widths (100m increments) and valley widths (500m increments) by river segment. Number of measurements in each segment posted above each box. Range in active channel and valley widths represented by the extended whiskers and outlying points

decreasing slightly in 3. From segments 3 to 1, channel width increases going downstream as expected. The pattern of downstream active channel width and valley width is very similar, indicating the strong control of valley width on channel width.

The range of widths (Figure 0-20) in each river segment represents changes in confinement. For example, the range in width measured in semi-confined R-Seg 6 increases significantly from the narrowly confined upstream R-Seg 7. The overall trend in widths (channel and valley) in the study area increases downstream as drainage area increases, except for at bedrock confined R-Seg 3. Bedrock incision here, likely enhanced by vertical uplift, results in a more narrow channel than up and downstream segments composed primarily of conglomerates and sandstone. This implies an increase in depth and/or slope in R-Seg 3 to accommodate hydraulic geometry requirements. In the semi-confined R-Segs 1, 4, 5, and 6, the mean valley widths are greater than or equal to twice the mean active channel width. At the downstream end of the study area, R-Seg 1 has the greatest range of widths because the river travels over the foot of the Siquirres-Matina thrust fault, and cuts through the very narrow Dos Montañas Canyon. At Dos Montañas, channel and valley width are equal at a mere 18m as the channel continues to incise into the hanging wall of the fault (Figure 0-8). As expected, the almost completely bedrock-wall confined segments (R-Segs 3 and 7) have a more limited range of widths.

Figure 0-21 presents active channel and valley widths measured at 100m increments to examine, in more detail, the relationship between valley confinement and channel width. When valley width is equal to active channel width, the river is completely confined and when the valley is wider than the active channel, pockets of floodplain and low terraces exist on the valley floor. Where pockets of floodplain or low terraces exist, the channel has an alluvial, less-resistant boundary (usually on one side) and channel width is expected to self-adjust its geometry for the discharge and slope of the reach. The irregular but general downstream increase in active channel width is visible in this data. However, the consistently fluctuating pattern in channel width clearly depicts the local control that confinement plays in channel geometry throughout the study area. Even in areas where floodplain or low terraces exist, partial confinement (one side of the valley) or the grain-size of the floodplain material likely exert partial control on active channel width. Nonetheless, while hillslopes and bedrock exert control on channel

width in confined reaches, in the semi-confined reaches the channel does adjusts its width to accommodate hydraulic geometry where possible. The irregular patterns in both valley and active channel width illustrate the amount of control that confinement exerts on the geometry of the channel throughout the study area.

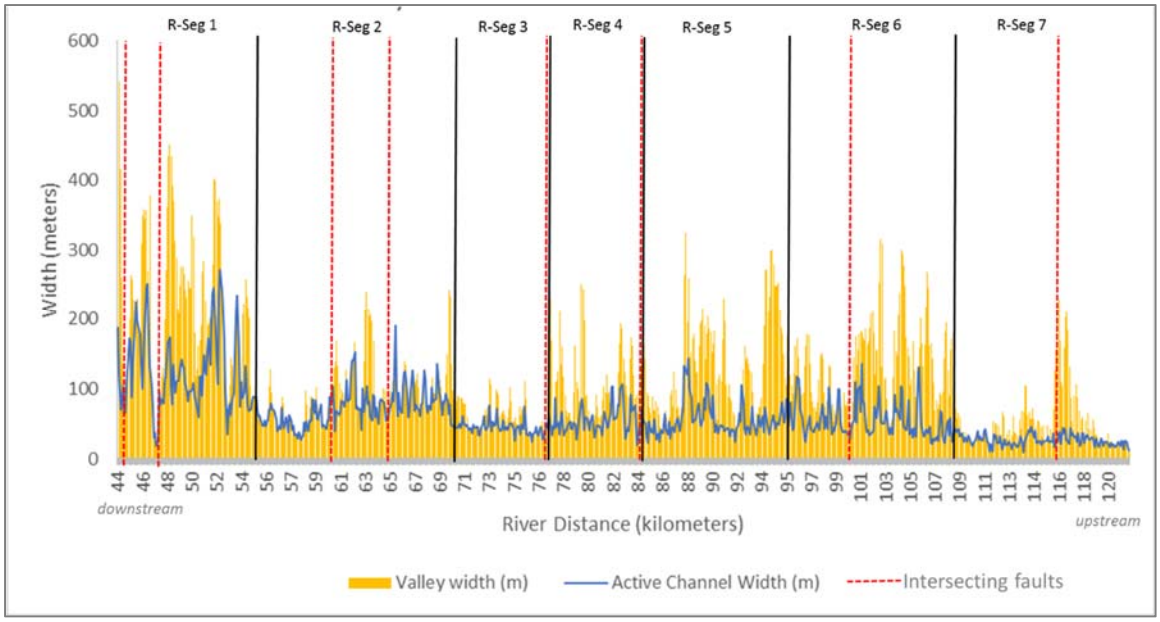

Figure 0-21. Valley width and active channel width, at 100 meter increments along the study area.

Usually channel intersections with faults result in changes, often abrupt, in valley and sometimes channel widths (Holbrook & Schumm, 1999; Ouchi, 1985; Schumm et al., 2000). On the Rio Pacuare this was observed to be the case at most channel-fault intersections (Figure 0-21). At most fault intersections, valley width is larger on the fault's upstream side with more confinement occurring on the downstream side. The degree to which this occurs is not constant, likely reflecting the relative uplift (vertical) or off-set (horizontal) rates of each fault and how that compares to the channel's local capacity to adjust (incise). For example, at the strike-slip faults that intersect the channel near Rkm 116 and at Rkm 100, obvious valley widening occurs upstream for at least two kilometers. However, at the intersecting faults at Rkm 60 (normal), 65 (strike-slip) and 84 (strike-slip), only slight upstream widening occurs. Figure 0-21shows that active channel

width is less influenced by the location of intersecting faults than it is by degree of valley confinement.

Although the set of normal faults in R-Seg 3 (see Figure 0-14) do not intersect the river and thus are not included in Figure 0-21, they do produce horizontal uplift on the west side of the river. The uplift appears to have instigated incision into the resistant limestone and calcareous sand and mudstones, resulting in a narrow bedrock confined river segment. Studies report that rapid uplift rates correlate to rapid incision rates (Humphrey & Konrad, 2000; Kirby & Whipple, 2012; Whipple, 2004).

However, faulting does not explain all the variability of valley width and active channel width that occurs on the Rio Pacuare. Resistant bedrock appears to deflect the channel into more easily eroded material, creating a bedrock-controlled meander form. This was observed in the field where the channel deflects around bedrock walls composed of more resistant material. For example, large bedrock-controlled channel deflection meanders are visible at Rkm 52.5, 57, 82, and 121 (Figure 0-22). In addition, incision into certain lithologies, such as limestone, has been found to be two-to-twenty times faster in the tropics than elsewhere (Thomas, 1996; Wang et al., 2015). Thus, the narrow, incised, relatively straight channel of R-Seg 3, which is contained within limestone or other calcareous bedrock, is likely the result of both faulting and uplift (as described in the paragraph above), combined with lithic-specific incision (see Figure 0-14-A).

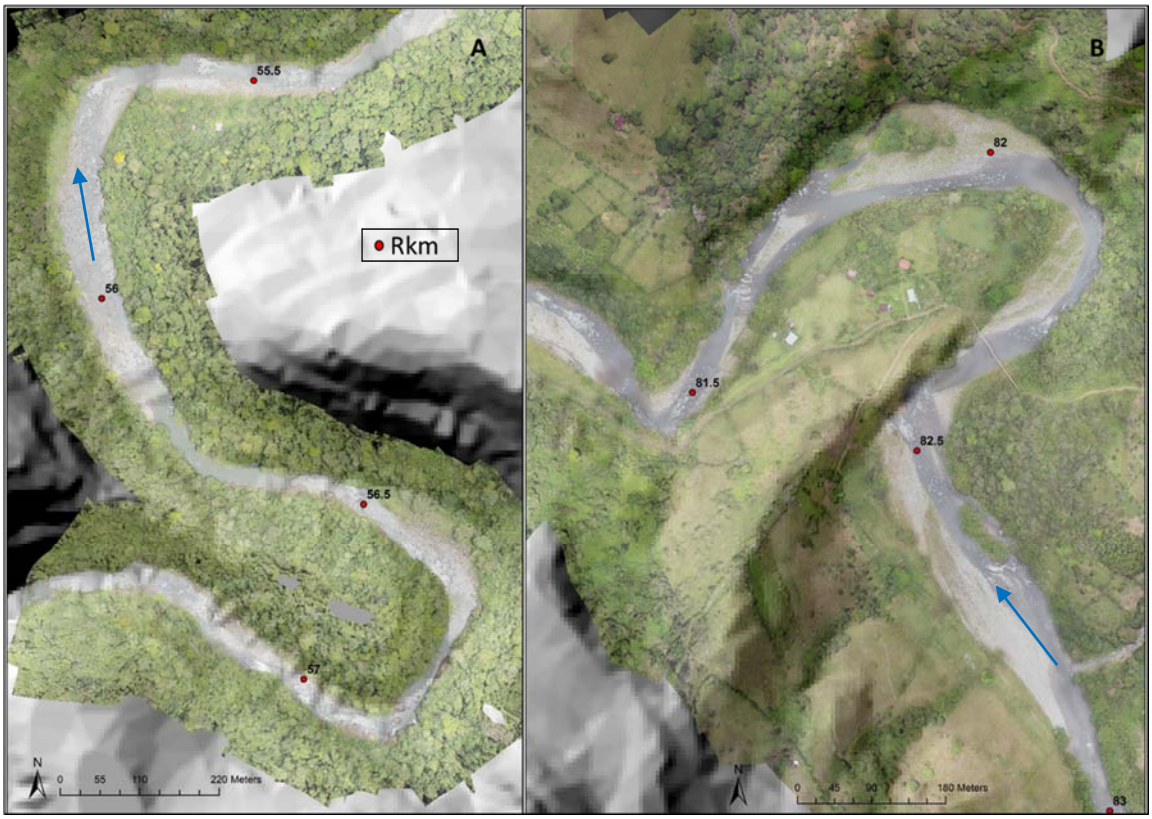

Figure 0-22. Aerial images of channel deflection (bedrock controlled meandering) at (A) Rkm 57 and (B) Rkm 82.

Channel Slope and Unit Stream Power

Stream power is used for characterizing flow competence, or the ability of a channel's discharge to transfer sediment. Unit stream power, as a product of discharge, slope, and channel width at a particular cross section, offers a way to examine relative changes in flow competence between and within river segments. Unit stream power is expected to be greatest at mid-basin where relatively moderate channel width, slope, and discharge often combine to create the most competent flows (Knighton, 1999). For mountain rivers, however, downstream patterns of stream power often vary due to the geologic constraints on channel width and slope (Fonstad, 2003; Wohl, 2010). In this section, I examine how unit stream power and slope vary going downstream and determine if local slope or channel width (geometry) exert more influence on unit stream power and thus the channel's competency to transfer sediment.

Slope influences the flow velocity and discharge rate through a given cross section (Leopold & Maddock, 1953). Normal downstream channel-slope trends are expected to display a concave-up shape where the steepest river reaches are in the channel's upstream portions and the least steep are in the downstream reaches (Flint, 1974). However, the downstream trend of channel slope for montane rivers is often irregular due to geologic controls such as knick-points created by differences in bedrock resistance or uplift rates (Kirby & Whipple, 2012; Whipple, 2004; Wohl, 2010).

Figure 0-23 provides the distribution of channel surface slope and unit stream power (estimated for the 0.2% exceedance flow or 1 year recurrence discharge – see Section 2.2.2), by river segment, for the montane portion of the Rio Pacuare. The downstream patterns of mean slope and mean unit stream power are similar with a general trend of downstream-decreasing unit stream power with decreasing slope. The range in slope depicts the local-scale differences in channel units captured in the 100m incremental measurements. For example, the high range in slope and stream power in R-Seg 7 is the result of steps and pool existing in the same segment. Then, in R-Seg 6, dominated by riffle-pool units, slope is decreased and so is unit stream power. A subtle mid-basin unit stream power maximum is apparent at R-Seg 4.

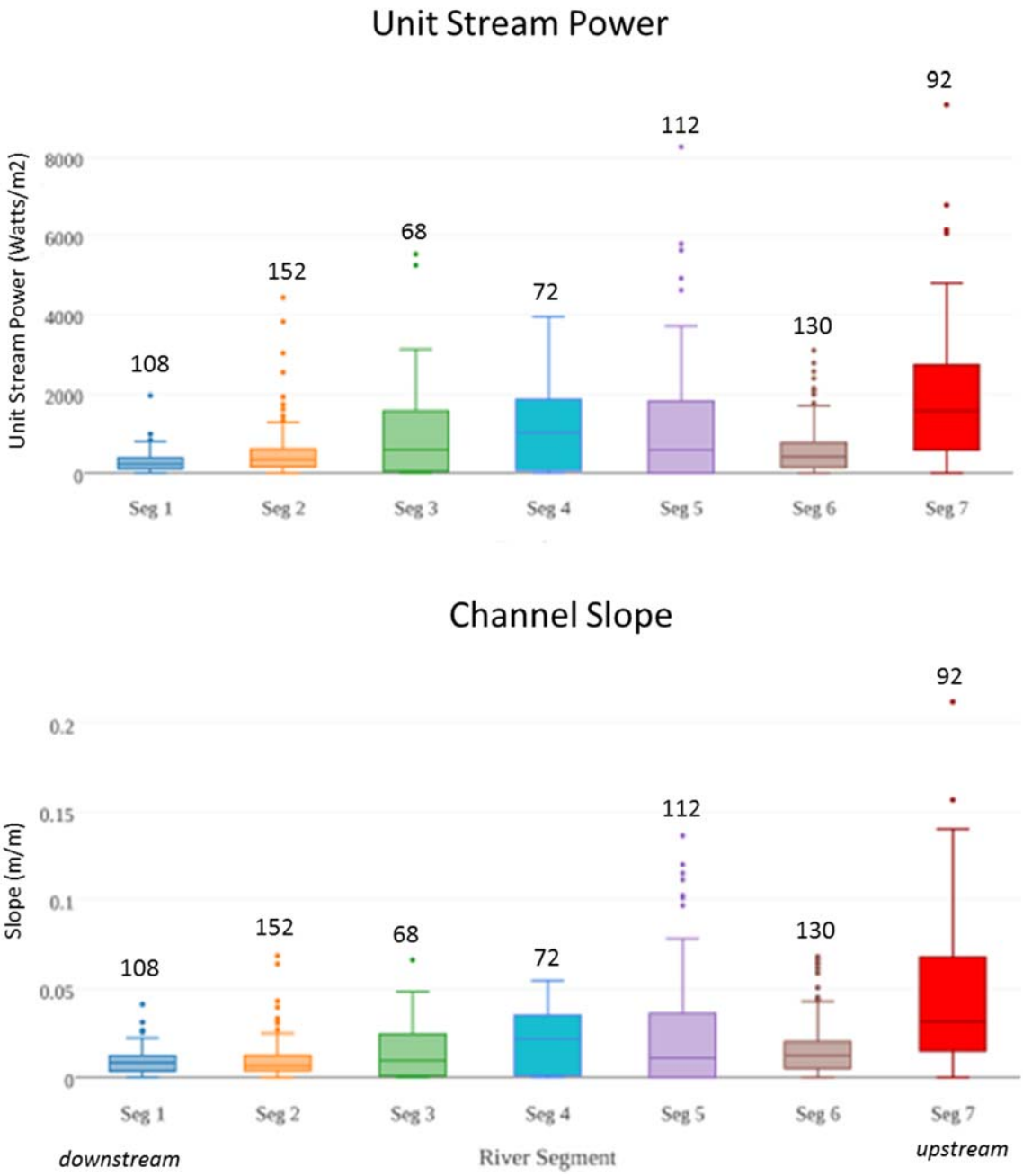

Figure 0-23. Distribution of channel slope and unit stream power by river segment. Number of measurements in each segment posted above each box.

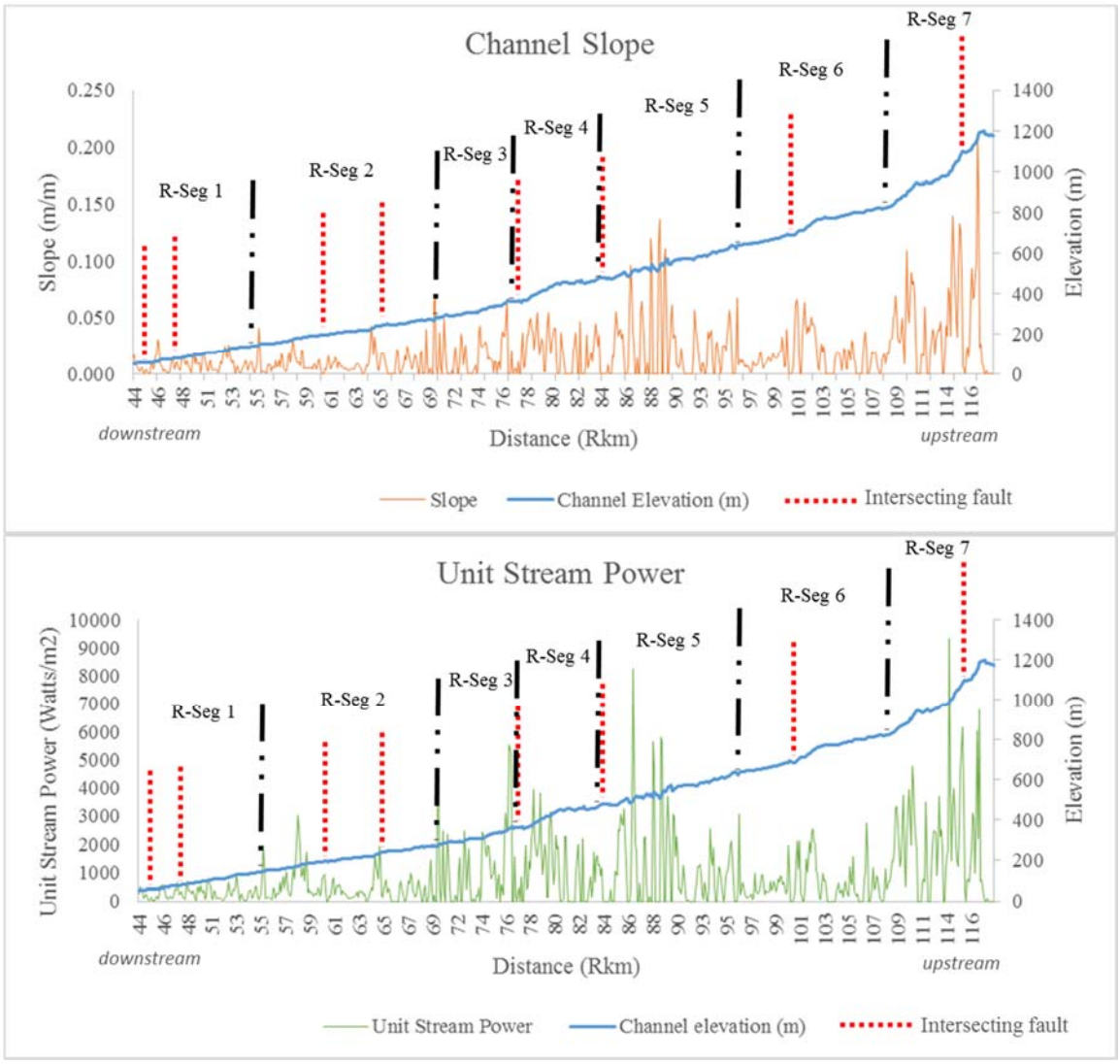

Figure 0-24. Downstream plot of longitudinal profile, channel slope and unit stream power at a discharge equivalent to 0.2% exceedance flow.

Figure 0-24 presents channel slope and unit stream power plotted at 100m increments with the channel's longitudinal profile. The irregularities in the detailed longitudinal profile are partially a product of extracting the elevations from the SfM 0.1 DEM. The SfM DEM has some inevitable imperfections itself but the active channel centerline used to extract the elevations for the longitudinal profile traverses over low-flow channel surfaces, and exposed higher bar tops. In general, the profile expresses a fairly constant linear shape from Rkm 44 to 108, and then upstream of Rkm 108 it has a concave-up shape. No significant vertical knick-points or waterfalls exist on the mainstem channel. However, there are a number of relatively steeper sections associated

with sets of steps or cascading steps in R-Seg 3 downstream from the suggested secondary fault at Rkm 77 for about 1 km, in R-Seg 7 downstream of the Atirro fault (Rkm 116) for about 2.5 km, and in the headwaters upstream of Rkm 122.

Unit stream power varies irregularly going downstream but expresses an overall downstream decrease in stream power across the study area. High variability in slope and unit stream power (Figure 0-24), such as in R-Seg 7, 5, and 3, reflect step-pool and cascading riffle-pool channel-unit sequences where the steps and cascading riffles have a much greater slope than do the pool units. In R-Seg 5 at Rkm 87, a set of cascading step-pools formed from very large boulders (Figure 0-25), supplied from the steep adjacent hillslope in a bedrock confined reach, produce some of the highest unit stream power estimates within the study area.

Figure 0-25. Photo of cascading step-pool at Rkm 87 in R-Seg 5.

Other locations of high unit stream power occur at channel constrictions at Rkm 52.5, 57, 82, and 121where the channel is diverted into less-resistant bedrock or is forced around tight, confined bedrock meander bends. When the two charts in Figure 0-24 are examined together, it is possible to see that unit stream power values deviate from slope in some locations. The most obvious examples are at Rkm 58, 86, and 113 where increases in unit stream power are relatively much greater than for slope. At such locations, it is assumed that decreases in channel width influence unit stream power to a greater extent than does slope.

To discover the relative influence of channel width and slope on unit stream power across the study area, the relationship between these variables is plotted (Figure 0-26). Although channel width shows some influence on unit stream power at the local or perhaps even reach scale, Figure 0-26 illustrates that overall channel slope exerts a more direct control on unit stream power on the Rio Pacuare.

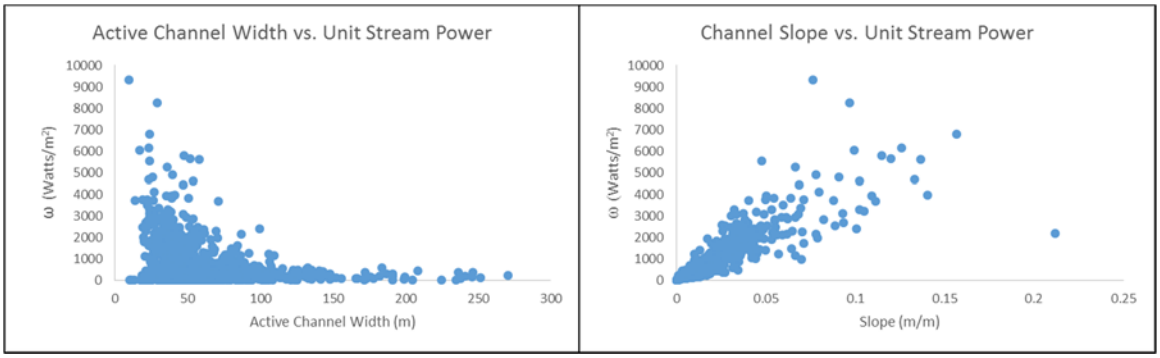

Figure 0-26. Plots of active channel width vs unit stream power and channel slope vs unit stream power.

Next, we examine if slope controls unit stream or if unit stream power (as a measure of flow competence and sediment transfer) influences channel slope. Figure 0-24 displays the locations where identified faults intersect the channel's path along the longitudinal profile. Unlike the amplified variation that occurs at several of the fault-intersection locations for valley widths, the variation in channel slope at most fault intersections is relatively average compared to other slope variations that occur within the same river segment. This suggests that hydraulic forcing exceeds or masks vertical tectonic forcing, either by efficient processes of vertical incision or by arranging the

plentifully available coarse bedload material into channel units (riffle-pool, etc) that adjust and minimize channel slope within a reach. This is significant, considering the prominence of major active faults on the landscape, and the historical and modern seismic uplift responsible for building the Talamanca Mountains since the early Miocene.

Minimal change in the variation of unit stream power occurs immediately upstream of faults but it increases on the downstream side. This indicates some geologic control on local-scale unit stream power via increased slope and/or decreased channel width (see Figure 0-21). However, the amount that unit stream power increases downstream of fault intersections is not consistent at every fault. This likely reflects inconsistent rates of uplift (vertical) occurring at each fault and the channel's local capacity at the fault intersection point to adjust (incision). Unit stream power is mapped for each river segment and available in Appendix A.

Alluvial Sediment Distribution

Alluvial sediment is a critical component of a channel's geomorphology. If it exists, its quantity, location, and grain size reveal a great deal about a channel's capacity to manage local, upstream, and upslope sediment contributions. When in transport, alluvial sediment aids in incision through processes of abrasion and impact in bedrock channels (Sklar & Dietrich, 2012). Distribution and accumulations of alluvial sediment can influence channel form (plan and longitudinally) in montane systems and thus influence the aquatic habitat a channel provides (Carey, 1994; Castellarin et al., 2004). Fine sediment (silts and fine sands) can accumulate where reduced stream energy allows, but in high-gradient montane systems, such as the Rio Pacuare, they are often flushed through the system as wash load. In these rivers, the coarser grain fractions (gravel, cobble, boulder) constitute the bedload that often comprise bedforms and floodplains. At normal or low-flow periods on the Rio Pacuare, large alluvial cobble-boulder bars, boulder riffles and steps, and cascades define the channel bed's topography and characterize channel types. The goal of this section is to determine where active alluvial sediment, in the form of deposited bedload material in active bars or as floodplain and low terrace surfaces, is located and how it is distributed in the mainstem Rio Pacuare.

Discussion is provided on what controls the patterns of distribution and how alluvial sediment influences channel morphology.

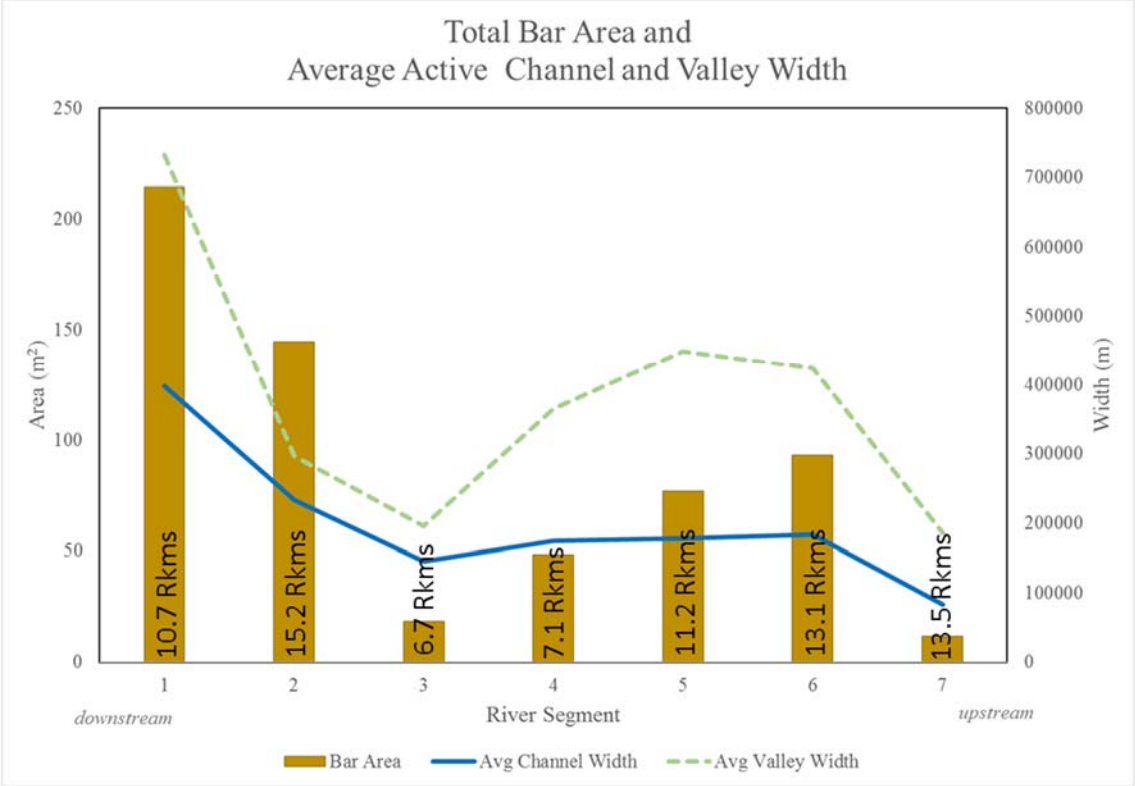

River Segment	Channel Length (m)	Exposed Bar Area (m^2)	Bar Area per Channel Length (m^2/m)
1	10,705	686,387	64
2	15,233	463,506	30
3	6,735	59,130	9
4	7,162	154,834	22
5	11,190	246,224	22
6	13,126	297,725	23
7	13,507	37,363	3

Figure 0-27. Total exposed bar surface area, average channel width, and valley width, and bar area per channel length by river segment.

Coarse bedload material observed throughout almost all of the study area occurs as a veneer over the bedrock or as active accumulations of unknown depths. Bedrock is common as confining channel banks but within the study area is only exposed in a few locations on the bed of the channel. To characterize the distribution of bedload accumulations, exposed bar surfaces at low flow were mapped using the 2014 aerial imagery. See Appendix A for segment maps of exposed active bar surfaces and

floodplain or low terraces surfaces. Accumulated bedload sediment is plentiful within the study area but unevenly distributed. Figure 0-27 presents the total exposed bar surface area in each river segment during low-flow dry season (April 23, 2014). Basically, more bar material is located in the segments with more available valley and channel width. For example, more than half of the total exposed bar surfaces in the study area occurs in the downstream river segments where the channel is widest and unit stream power is smallest (see Figure 0-23 and Figure 0-20). Segments 3 and 7 are markedly narrower, and they have the lowest bar area per unit channel length. Segments 2, 4, 5, and 6 are intermediate in width and in bar area per unit channel length. Segment 6 has a similar average width as segments 4 and 5 but its slightly lower mean slope and unit stream power were expected to produce higher bar area per river length than they do. Perhaps bedload depths instead of surface area are greater here. According to the data (Figure 0-28), at 56% R-Seg 1 has the greatest percent of channel as bar surface area at low-flow compared to the other river segments. Segments 2, 4, 5, and 6 have 40-43% of their channel area occupied with active bar surfaces at low flow. R-Seg 2, a confined segment, has more bar area than the other confined segments (3 and 7).

Figure 0-28 also provides the percent of total bar area by bar type. Bar types for this analysis include mid-channel bars, point bars, and side-channel bars. The term side-channel bar is used to describe the location of the bar feature. Unlike lateral bars, side-channel bars are bedforms exposed at low flow. Although a point bar is also technically a side bar, the location of a point bar at the inside of a meander bend differentiates it as a hydraulic drop point due to channel form change. An additional bar type classified as "combination bar" (combo) is used and refers to side bars that extend downstream and evolve into a point bar, or vice-versa. Combo bars represent the system's most elongate bar forms.

Although all river segments contain every bar type, the dominant bar type is side-channel bars throughout. Point bars and mid-channel bars are in the minority. The distribution of bar type within each reach corresponds to low-flow channel form. For example, where confined straight channel reaches occur (i.e. R-Seg 3) bar distribution is dominated by side-channel bars. Bedrock controlled meandering produces more point bar

areas than in straight segments, and unconfined segments have a greater proportion of mid-channel bars (related to low-flow braided form).

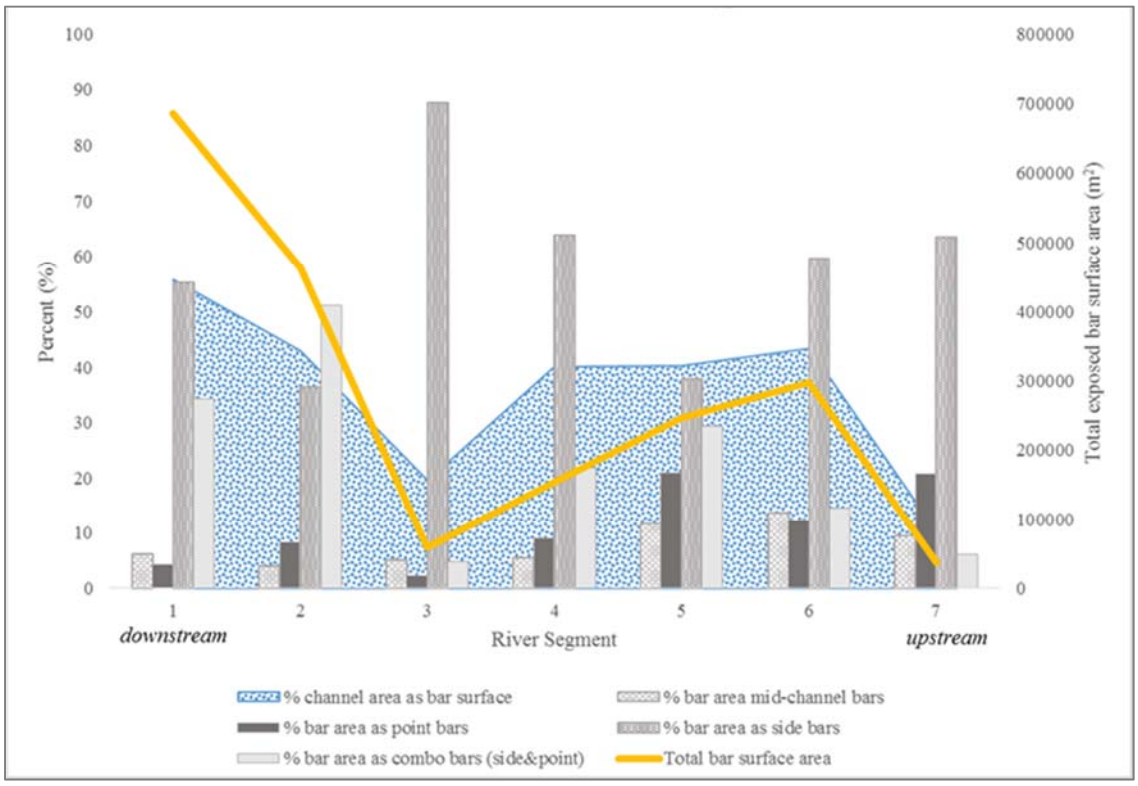

Figure 0-28. Percent of active channel area as exposed bar surface area. Total bar surface area and percent active channel area as bar surface and percent of bar surface area as bar types, organized by river segment.

Floodplain and low terrace surfaces represent additional stored sediment available for reactivation by lateral channel migration or during large-scale flood events. To better understand the distribution of stored alluvial sediment, Figure 0-29 presents the total valley surface area in each river segment along with the percent of the valley occupied by floodplain or terraces, bars, or wetted channel at low flow. Valley area is defined as the space between confining hillslopes and is the sum of floodplain or low terrace surfaces, wetted channel area, and exposed bar surface area. The greatest percent of valley area occupied by floodplain or low terrace occurs in the semi-confined segments (1, 4, 5, and 6). In segments 4, 5, and 6 half or more of the valley area is occupied by sediment stored in floodplain or low terrace surfaces. In R-Seg 1, the widest river segment (Figure 0-21), less than half of the valley area is occupied by floodplain or low terraces. This is because

the channel is wider here and approximately 30 percent of the valley is occupied by bars. Interestingly, in the confined reach of R-Seg 7 over 40% of the valley area in the lower portion of this segment is occupied by floodplain or low terraces. This occurs here because of the 2.5 kilometer section upstream of the Atirro strike-slip fault where the valley widens. The remainder of this river segment, especially the upstream section, is very confined with minimal bar development.

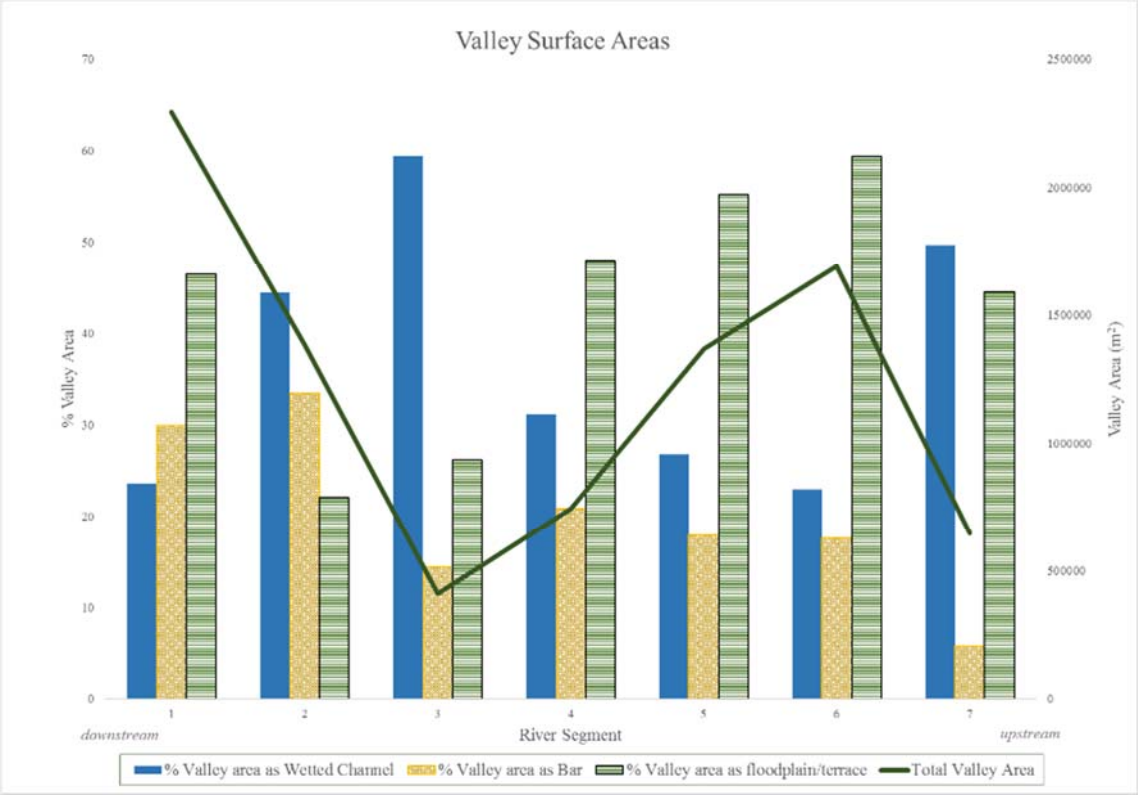

Figure 0-29. Total valley surface area for each river segment and percent area of the valley as wetted channel, exposed bar, and floodplain or low terrace surfaces (mapped at low-flow, April 2014).

When the percent of the valley width that is occupied by active channel is examined in more detail (Figure 0-30), at 500m increments along the channel, it is clear that floodplain and low terraces are not continuously distributed surfaces throughout the study area or within each river segment. In Figure 0-30, where active channel occupies 100% of the valley width the channel is completely confined and no floodplain or low terrace exist. Where the active channel occupies less than 100% of the valley width,

pockets of floodplain or low terrace surfaces occur. Even in the confined R-Seg 3, floodplain or low terrace sediment stores occur but are discontinuous and distributed throughout much of the segment. R-Seg 1 has the greatest total surface area as floodplain or terraces (Figure 0-30) however, based on this data R-Seg 6 has the most continuous alluvial sediment storage as floodplain or low terrace surfaces in the study area. In R-Seg 6 the channel never occupies more than 90% of the valley at this scale, meaning that at least 10% or more of the valley is occupied by floodplain or low terrace surfaces. However, even in R-Seg 6 the proportion of the valley floor occupied by stored sediment vs active channel varies dramatically. This varied pattern shows that geologic confinement of valley width, relative to channel width, defines where alluvial sediment stores as floodplain or low terraces occurs.

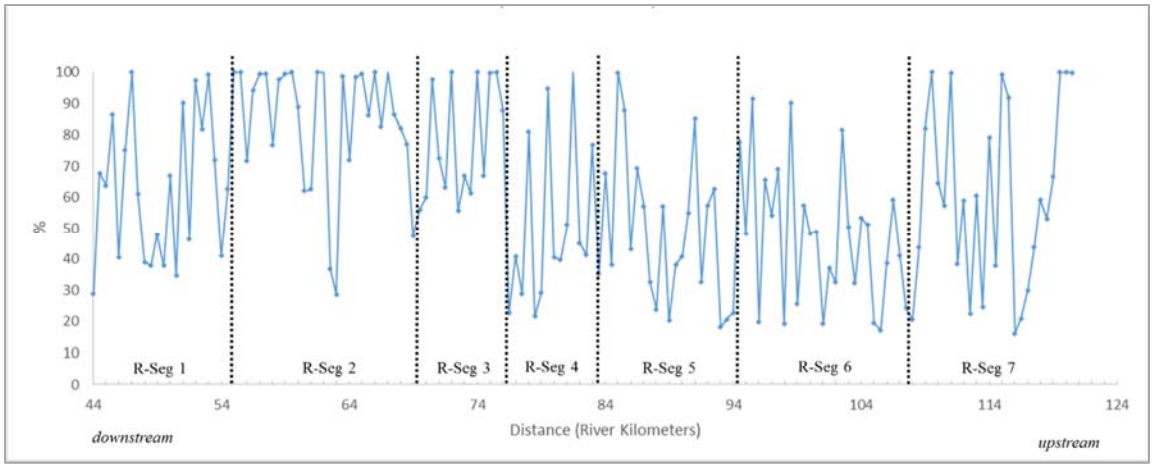

Figure 0-30. Chart of percent valley width occupied by active channel in 500 meter increments.

A summary description of alluvial sediment distribution and the influencing components within each river segment is provided in Appendix A. The appendix provides discussion on the how evaluated components combine to produce the geomorphology of each river segment. Maps for each river segment with the major identified faults that intersect the channel, as well as the digitized channel, bars, floodplain and low terrace surfaces, plus the locations of modern landslides and debris torrents either identified in the field and/or in the high-resolution aerial imagery collected April 2014, are also included in the appendix. In addition, channel slope and estimated unit stream power (for the 0.2% exceedance flow) at 100m increments along the channel

pathway are also provided as parallel maps for each river segment. These combined variables are intended to visually illustrate the primary sediment sources (upstream and laterally) and alluvial sediment distribution (bars and floodplain or low terraces) in each river segment, and how alluvial sediment distribution correlates to measurements of flow competence along the channel.

Channel Change and Sediment Mobilization

For most mountain rivers, the pathway of a channel is relatively established by the confining hillslopes that it has incised into. Where valley width has accommodated floodplain or terrace development, lateral channel movement into these surfaces reactivates stored alluvium. Likewise, slight deviations in the channel's pathway or even thalweg can deconstruct or deform established bedforms and construct new bedforms as sediment is moved downstream (Wohl, 2010). In this section channel and bar locations are compared between aerial imagery collected as part of this study in 2014 and the 2002 GoogleEarth GeoEye imagery. This is done to identify where changes in channel location and bar distribution have occurred during this particular time period.

The locations of notable lateral channel movement between the 2002 and 2014 wetted channel centerline are presented in Figure 0-31. As is illustrated in Figure 0-31, the type of lateral channel movement varies from neck cut-offs to meander extensions, and avulsions. However, due to valley confinement none of the lateral shifts are grandiose but all are expected to have activated the available sediment stored in a floodplain or low terrace surface.

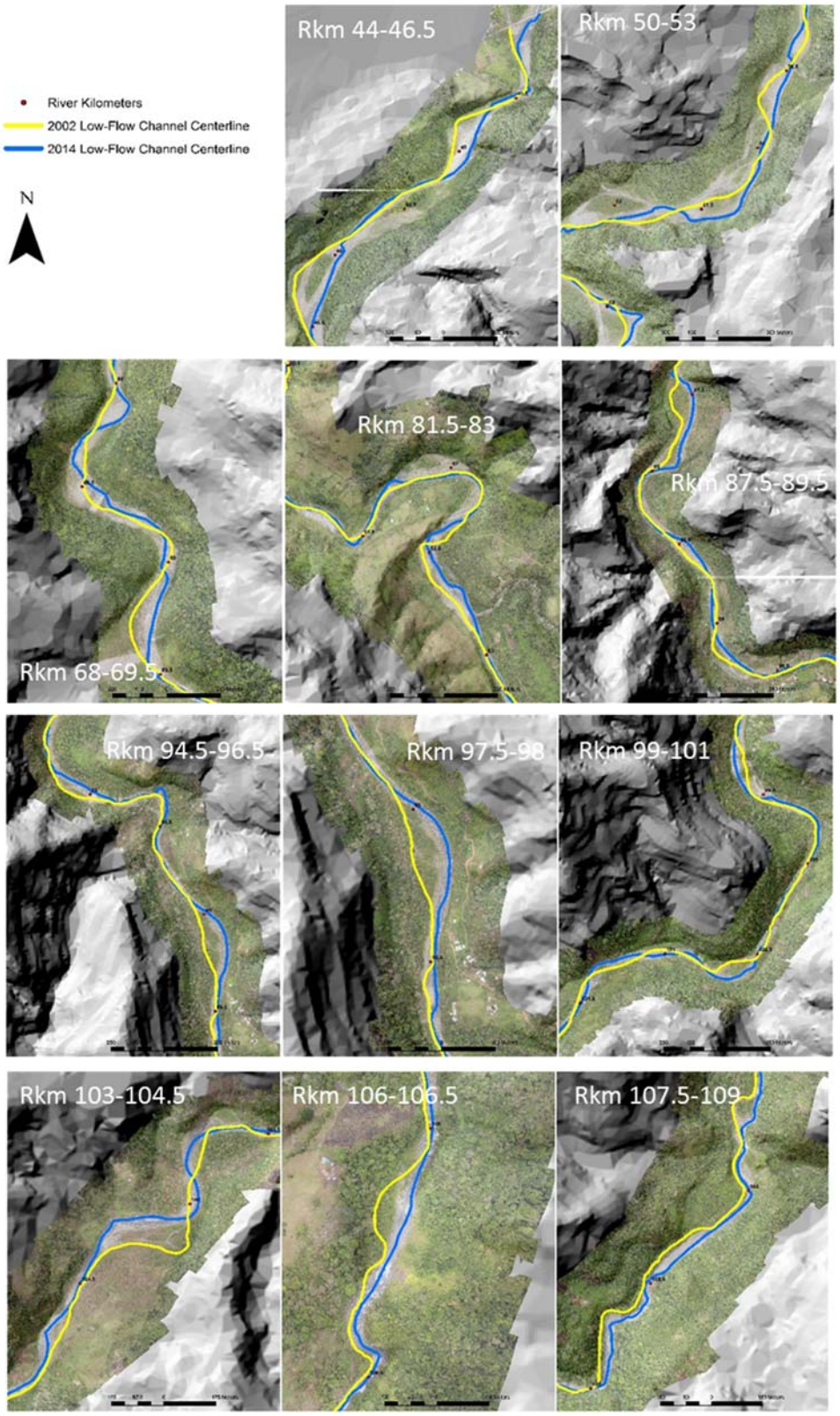

Figure 0-31. Locations of lateral channel movement (2002 and 2014) from wetted channel centerline. Channel flow is from south to north in all images. Basemap: (Lind, 2016; SIGMA, 1998)

According to this analysis, only 19.5 of the 88 river kilometers included in the study area displayed any degree of lateral movement in the time period analyzed (2002 and 2014). Channel sinuosity and length appear to remain generally the same between year sets. All lateral movement, as expected, occurred in semi-confined reaches rather than confined reaches, though several semi-confined reaches showed no change. The greatest lateral changes occurred in R-Seg 1 between Rkm 44-46.5 and Rkm 50-53, constituting most of the channel that contains mid-channel bars in that segment. At a few places (Rkm 45, 51, 68.5, 82.6, 88, and 105.5), there is evidence that the change may have been gradual lateral migration (as indicated by lack of vegetation within the change area), but otherwise it is likely that changes occurred as avulsions during high-flow events. The distribution of change indicates that the channel is capable and does activate the available alluvium at points throughout the study area.

In most cases, it is not possible to determine whether the observed channel location changes occurred incrementally over the 14-year period, or during a single high flow event. Table 0-4 provides the dates of the larger floods that occurred between 2002 and 2014. Identifying the exact dates of change with only two year-sets of photo imagery is not possible but it is assumed that most change occurs during peak flow events. At Rkm 69.5, the channel shift from valley left to valley right was likely caused by the debris torrent that occurred during the November 2008 flood event (Figure 0-18) that pushed the channel to the other side of the relatively narrow valley.

Table 0-4. Large flood events between 2002 and 2014. Based on daily discharge data reported at ICE 8-01 located at Rkm 90.2. Flood Rank relevant to this list only. % Exceedence flow based on full discharge record (1959-2012).

Date	Q (cms)	flood rank	% Exc	RI (years)
11/24/2002	175	11	0.29	0.93
11/29/2003	166	14	0.34	0.81
12/11/2003	194	8	0.24	1.16
12/12/2003	162	15	0.35	0.78
11/8/2004	273	3	0.1	2.69
11/9/2004	275	2	0.1	2.84
11/10/2004	150	17	0.42	0.65
1/10/2005	144	20	0.46	0.59
1/16/2006	170	13	0.33	0.84
11/9/2007	200	7	0.23	1.22
11/19/2008	174	12	0.3	0.9
11/20/2008	149	18	0.43	0.64
11/22/2008	254	4	0.12	2.32
11/23/2008	245	5	0.13	2.04
11/24/2008	334	1	0.05	6.38
2/7/2009	153	16	0.41	0.68
7/28/2012	181	9	0.26	1.03
11/23/2012	148	19	0.43	0.62
11/25/2012	177	10	0.28	0.96
11/26/2012	208	6	0.18	1.5

Along with lateral channel pathway changes are expected changes in bar type and location between 2002 and 2014. It is not possible to compare bar area change with these data sets because the 2002 photo set is incomplete and is a compilation of three different photo set dates (Feb. 4, Mar. 9, and Dec. 22) with different discharge rates, which can greatly influence the amount of bar exposure. Nevertheless, review of the images show that bar type at a location can change (i.e. mid-channel bar changed to a side bar) in response to inundation and channel pathway change (see Figure 0-31). Although bar type and shape may change, the reaches where bars occurred in 2002 are the same in 2014. This further indicates that channel form (via geologic forcing) and flow hydraulics influence where alluvial sediment is distributed. This also suggests that within the confined reaches where little channel pathway change was detected but active bars exist

(i.e., R-Seg 2 and 3), the bedload and bar material is replaced with incoming material during flow events of relatively moderate size.

No particularly large flood events occurred between 2002 and 2014; the largest event had a recurrence interval of about 6 years (Table 0-4). Despite the moderate flood events, lateral channel shift was observed at several places where confinement allowed. Changes in bar form occurred even in confined reaches where lateral channel shift was not possible. This indicates that boulders are mobilized and bedforms are reshaped during flow events with a 6-year recurrence interval and likely smaller. For example, bedform deformation and bar material replacement were observed in the field at Rkm 62.5 and 66.25 in R-Seg 2 as the result of a high-flow event (77.4 cfs at gage 8-01) on November 28, 2013. This flow has a recurrence interval of about every 152 days (or approximately twice a year).

2.4 DISCUSSION

The geomorphology of the Rio Pacuare has proven to be the result of interactions between the external controls of geology (tectonics and lithic resistance) and climate (as a generator of discharge and weathering) which combine to control flow hydraulics in the channel. The internal geomorphic component of flow hydraulics, in turn, exerts influence on channel geomorphology through incision and sediment mobilization. For example, the watershed elevation and slope are the result of on-going tectonic uplift, counteracted by hillslope and channel-bed erosion, which is driven by the rapid weathering processes of humid tropical climates and hydraulic incision. Likewise, the planform of the channel is directly controlled by tectonic uplift and/or off-sets and lithologic resistance of the bedrock, which is carved by the channel's hydraulic capacity to incise a pathway into it. As described by Shumm and Lichty (1965) and Knighton (1998) these watershed-scale processes occur over geologic timescales.

Figure 0-32 synthesizes the results of this study to illustrate how each of the external forcing elements (geology, climate) combine to control hydraulics (stream power), as well as influence the other geomorphic components examined in this study (valley width, channel width, lateral contributions, channel slope, and alluvial sediment

distribution). The thickness of the arrows depicts the relative influence one component has on another. Red depicts a direct influence on alluvial sediment distribution.

This model (Figure 0-32) displays the role and influence that the different components have on each other as well as their relationship to alluvial sediment distribution, and thus the geomorphology of the Rio Pacuare. The components identified as direct influences on alluvial sediment distribution include channel and valley width, lateral sediment sources, flow hydraulics, and channel slope. Channel slope at the local, reach and segment scales however have an interdependent relationship with the distribution of alluvial sediment. The directly influential components identified in the model are discussed in more detail below.

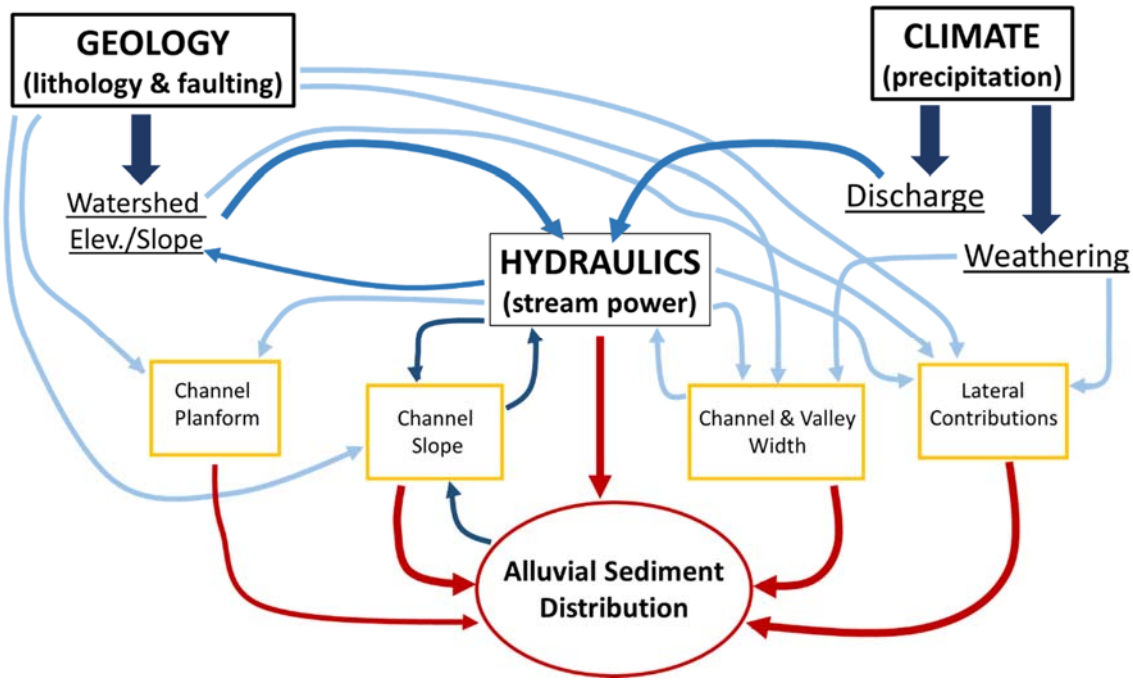

Figure 0-32. Conceptual model of the geomorphic components that exert control on alluvial sediment distribution (bedload, bars, and floodplain or low terrace surfaces) of the Rio Pacuare. The model includes the process of incision. The relative importance of the influence is depicted by the thickness of the connecting line. Red lines indicate direct influence on alluvial sediment distribution. Blue lines depict indirect influences on alluvial sediment distribution.

Channel and Valley Width

Valley and active channel widths on the Rio Pacuare are the product of geology (tectonics and lithologic resistance), climate (hillslope weathering), and hydraulics– see

Figure 0-32. However, results from this study indicate that the influence of lithology and faulting on valley and channel width exceeds the influence of hydraulics (stream power) throughout most of the Rio Pacuare. Changes in valley and active channel widths at the reach-scale occur throughout the study area, including at fault intersection locations or where the channel is confined in bedrock of varied resistance. Valley confinement therefore is controlled mainly by geology, and it in turn influences the distribution of alluvial sediment by limiting the space available to accommodate pockets or strips of floodplain or low terraces alongside the channel, similar to findings on the Liwu River in Taiwan (Kuo & Brierley, 2014). At or immediately upstream of most all fault intersections on the Rio Pacuare small pockets of floodplain or low terraces surfaces occur more frequently while downstream of fault intersections is usually more confined with minimal or no floodplain or low terrace accumulations.

Confinement also controls alluvial sediment distribution as bars and bedload within the channel by controlling available space for sediment accumulation. Alluvial sediment, as exposed cobble-boulder bars at low flow within the active channel, is less abundant where channel width is narrow due to bedrock confinement at all scales examined in this study, the segment, reach, and local scales. These results reveal that channel width can influence bar distribution by influencing relative flow competence (unit stream power). When the channel narrows and/or steepens, flow competence increases and the channel's capacity to transfer or reorganize alluvial sediment increases. Although slope has a more direct relationship with unit stream power in the Rio Pacuare, variations in channel width have also proven influential at controlling local scale unit stream power.

The least exposed bar area per unit channel length occurs in the confined segments, R-Seg 3 and 7. In contrast, the confined R-Seg 2 has a relatively large active channel width and a relatively moderate slope, which accommodates the development and maintenance of large boulder bars. The difference in the quantity of exposed bar area up and downstream of fault intersection locations is far less than the difference in floodplain or terrace surface area. Overall, channel and valley width or confinement control the distribution of alluvial sediment by limiting the space available for

accumulation, controlling channel form, and influencing local sediment transfer via flow competence.

Lateral Contributions

Lateral contributions (tributaries, landslides, debris torrents) are a product of tectonics and lithologic resistance, hillslope weathering, and incision. However, geologic forcing (uplift rates and lithologic resistance to weathering) appears to be responsible for the subtle variations in the distribution of lateral contributions along the study area. Nonetheless, a relatively dense distribution of lateral contribution points occur along the mainstem channel throughout the study area. The highest density of tributary confluence points is associated with less resistant sedimentary conglomerates, and the lowest density of tributaries is associated with faulting and high local uplift that limits tributary extension. Like tributary confluences, modern (2014) landslides that enter the mainstem channel are also fairly evenly distributed. Slightly higher-density clusters of landslides were observed near fault intersections. This suggests steeper and/or less stable hillslopes near seismically active areas or that seismic events can trigger local mass wasting. Modern (2014) evidence of debris torrent inputs to the mainstem channel are distributed throughout the study area. This implies that all lithologies present in the Rio Pacuare produce debris torrents. The volume and frequency of material delivered by debris torrents from the different lithologies in the watershed were not explored in this research, but based on visual observations, a hypothesis of high quantities of material being produced from hillslopes with less resistant conglomerate and sandstone dominated parent material.

Since a relatively small amount of alluvial sediment is stored along the channel as floodplain or low terraces, lateral contributions are considered a primary source of sediment to the Rio Pacuare, similar to other humid tropical montane systems (Garcin et al., 2005; Gonzalez et al., 2016; Rengers & Wohl, 2007; Wohl, 2005). The relatively even density of lateral contribution locations indicates that the Rio Pacuare receives incoming sediment along the length of the study area. The narrow, elongate, rectangular shape of the watershed and its ridge and trough topography have developed tributaries of generally the same length and drainage areas throughout the watershed. This suggests

similar input potential from tributaries throughout the study area, unless otherwise subtly influenced by lithologic resistance and/or seismic instability.

Lateral contributions renew local sediment supply to the channel throughout the study area. However, lateral sediment contributions to the Rio Pacuare are quickly mobilized downstream and integrated into the bedload of the channel instead of accumulating at input points. This indicates that the Rio Pacuare frequently generates flows capable of mobilizing lateral sediment inputs, including coarse-grained (cobble-boulder) bed material. However, bedload material is plentiful and active bedload material exists at varied unknown depths throughout almost all of the study area. These results show that the lateral contributions received by the mainstem channel (though spatially and likely temporally varied across the watershed) are significant to the quantity of alluvial sediment in the system.

Flow Competence

Hydraulic flow competence, represented by unit stream power, is controlled by discharge combined with slope and channel width. It is presumed that flow competence is responsible for incision into the underlying bedrock (Sklar & Dietrich, 2012) and, as described above, the flux of alluvial sediment from upstream to downstream. The longitudinal profile and organized bedload of this channel indicate that flow competence on the Rio Pacuare is adequate to incise geologic constriction points and/or re-distribute its plentiful bedload material such that basin, segment, and reach-scale channel slope is normalized to be relatively linear. The redistribution or arrangement of sediment into relatively evenly-spaced channel units (i.e. riffle-pool, step-pool) at the reach scale via flow hydraulics adjusts the channel slope at the reach and unit scale. The variation in unit stream power when measured at 100m increments along the channel reveals channel unit development, where steps, cascading-riffles, and riffles have greater slopes and stream powers than do pools. Since bedload material is frequently replenished by lateral contributions, channel adjustment via bedload arrangement in response to a seismic uplift event would likely be rapid with the river's modern discharge regime.

Bedform types and grain size appear to correlate to relative flow competence (unit stream power). Where flow competence is greatest, large boulders were observed as a

veneer on the bedrock while the less-coarse bedload (gravels, cobbles, boulders) is transferred downstream into active bedforms (bars, riffles, etc.) of unknown depths. Field observation before and after high-flow events and the qualitative analysis of exposed bar distribution and channel thalweg change between 2002 and 2014 suggests that the mobilization of bedload material results in the maintenance of active bars and bedforms via replacement as sediment is regularly transported through the system.

Channel Slope

The linear shape of the channel's longitudinal profile and the slope of the channel at the watershed-scale is dependent on the long-term interactions of geology and climate. On shorter time-scales (days-decades) at the reach and channel unit scales, an interdependence of channel slope and flow hydraulics (stream power) occurs on the Rio Pacuare (Schumm & Lichty, 1965). In this manner, channel slope is both a driver and a product (through incision and sediment arrangement) of flow hydraulics (stream power). It influences alluvial sediment distribution but is also partially controlled by it. This does not, however, remove the influence of geology and climate (discharge and weathering) at segment, reach and local scales. At the reach-scale, in at least two places (in Seg 7 and 3), tectonic uplift has produced reaches with channel slopes relatively higher than surrounding reaches. This suggests either a rate of tectonic offset at these faults that is higher than the local incision rate or a more resistant bedrock. Otherwise, the longitudinal profile of the mainstem Rio Pacuare is fairly linear and absent of any significant vertical knickpoints or waterfalls. Only in the upper-most 25 kilometers of the 90 kilometer study area does a concave-up pattern occur. The shape of the longitudinal profile and lack of major knickpoints throughout is significant, considering the active tectonic processes of uplift, localized faulting, and the varied lithologies that the channel traverses. This reveals hydraulic processes of incision as a major basin-scale control on channel slope.

Alluvial sediment distribution and arrangement into channel unit types (riffle, pool, step, etc.) occurs as a result of hydraulics (unit stream power) as a produce of slope. At the segment-scale, the downstream trend in mean channel slope reveals an increase in gradient within R-Seg 4 and a decrease in slope variability in R-Seg 6. R-Seg 4 has plentiful cascading riffle-pool sequences that are relatively close together and R-Seg 6 is

dominated by extended units of riffle-pool. Interestingly, in the upstream portion of R-Seg 3 where the channel width decreases from geologic confinement and the channel slope increases step-pool and cascading channel types dominate. In the downstream portion of R-Seg 3 where slope is reduced a cascading riffle-pool channel type dominates.

The model presented in Figure 0-32 provides a framework for understanding the complex interactions responsible for the geomorphology of the Rio Pacuare. Similar to results found for a humid tropical montane river in Panama and a watershed in Puerto Rico (Pike et al., 2010; Rengers & Wohl, 2007), the Rio Pacuare is hydraulically competent so that it rapidly integrates and redistributes lateral sediment contributions and adjusts to geologic influences on slope and channel width. However, lithology and the historical and modern tectonic processes underway in the Talamanca Mountains, including the multiple active faults that intersect the river, exceed hydraulic forcing when it comes to valley width and, in areas of bedrock confinement, channel width. Thus, alluvial sediment distribution is the product of hydraulic forcing and geologic forcing combined.

2.5 CONCLUSIONS

The geomorphic components examined in this study are all, to some degree, influenced and/or controlled by the external forcing elements of geology (tectonics and lithology) and climate (as a generator of discharge and weathering) which combine to define flow hydraulics (stream power). On the Rio Pacuare geologic forcing exceeds climate and hydraulics in controlling valley width, channel width, and lateral contributions. Hydraulic competence exceeds geology at influencing downstream sediment flux and channel slope through processes of bedrock incision (long-term processes) and/or arrangement of the available sediment (short-term processes). Localized slope increases downstream of two of the faults indicating a lag in the hydraulic adjustment to tectonic forcing at these locations. At other faults on the mainstem channel, there is no tectonic signature on channel slope.

Tectonic uplift and lithology combined with rapid humid tropical weathering processes are responsible for watershed hillslope evolution and thus upslope sediment

production and delivery to the channel. The abundance of alluvial coarse-grained sediment throughout the study area is related to the high density of lateral contributions, including landslides, debris torrents, and other tributary contributions. This study demonstrates, however, that the spatial distribution of alluvial sediment along the mainstem channel is organized by relatively frequent competent flows that integrate and arrange incoming sediment into the active bedload of the channel. In this manner flow competence defines channel unit types (riffle, pool, step) within the otherwise geologically controlled planform (bedrock defined meandering) of the channel. For example, riffle-pool channel types occur where unit stream power (the measurement of flow competence used in this study) is relatively lower than where step-pool or cascading riffle pool types occur. Unit stream power is dependent on variations in both channel width and slope. However, results conclude that slope has a more direct relationship with unit stream power overall. The local-scale distribution of bedload into bedforms that reflect reach-scale slope, similar to an alluvial channel, creates a positive feedback relationship between slope and unit stream power on the Rio Pacuare.

The river's longitudinal profile is fairly linear except in the uppermost 20 river kilometers where the highest gradients and a concave-up shape in the river profile occurs. This is somewhat unique in tectonically active bedrock confined montane rivers. It indicates that flow hydraulics are, and have been, competent enough to over-come geologic forcing such that the longitudinal profile of the channel is consistent. The downstream trend in mean unit stream power at the river-segment scale is similar to mean channel slope with the highest values occurring in the steep upstream segment, an increase in unit stream power at mid-basin, and then a normal downstream decrease. However, slope has a greater influence on flow competence than width, except at local- and a few reach-scale confinements. In this manner, slope is an important influence on the distribution of alluvial sediment.

Irregular downstream trends at the river segment scale in channel and valley width as a result of geologic confinement occur in the middle of the study area (R-Seg 3). Variations in confinement at the reach and local scale occur throughout the study area. Valley width, and thus the presence of floodplain or low terrace surfaces, increase upstream of fault intersections and decrease downstream of fault intersections, revealing

an additional geologic control on valley width. Alluvial sediment as exposed bar surfaces at low flow is greater where the channel is unconfined and slope is reduced. However, bedload material of varied unknown depths occurs throughout almost all of the study area even though the Rio Pacuare is a bedrock defined montane system, indicating plentiful upstream and lateral sediment supplies.

This study provides a conceptual model that illustrates the interconnected processes that shape the geomorphology of the Rio Pacuare. Based on these relationships it is concluded that the river's geomorphology will likely respond rapidly to changes in discharge, slope, or confinement. I recommend additional research to estimate the rate at which the channel currently transports its alluvial sediment.

CHAPTER III

SEDIMENT TRANSPORT IN A HUMID TROPICAL MONTANE RIVER, RIO PACUARE, COSTA RICA

3.1 INTRODUCTION

The morphology and stability of a river is a direct result of the caliber and quantity of available sediment and the river's ability to transport it. Therefore, investigating transport capacity as well as the spatial and temporal variations of sediment flux is a critical component of river research, especially for applications in resource management and conservation, hazards assessment and planning, and riverine ecology. In mountain rivers, the caliber and quantity of bedload, combined with the related discharge regimes (magnitude, frequency, and power), control channel form and deformation (Emmett & Wolman, 2001; Lenzi et al., 2006; McLean et al., 1999; Wohl, 2010). Bed morphology also influences local hydraulics (Recking et al., 2015) and can define the aquatic habitat that a channel provides (Bertoldi et al., 2010; Bravard et al., 1999; Habersack, 2000; Hassan et al., 2008). Bedload in mountain rivers is composed of a wide range of sediment sizes, from coarse sand to large boulders (Pitlick, etal, 2008; Rickenmann, 2001). This study estimates bedload transport rates at six locations within the montane portion of the Rio Pacuare, Costa Rica to better understand sediment flux and thus channel geomorphology in humid tropical montane rivers.

Humid montane tropical rivers are capable of producing some of the largest quantities of sediment and nutrients per unit drainage area (Scatena & Gupta, 2013). Bedload flux results reported by Bidorn et al. (2015), Ziegler et al. (2014), Turowski et al. (2010), and Dodson (2003) on Southeast Asian humid tropical montane rivers show that bedload constitutes 16- 75% of the total sediment delivered (i.e., more than double the generally accepted 10% of a channel's sediment load (Milliman & Farnsworth, 2013). However, the relatively small body of research done on sediment transport in humid tropical systems, including in Costa Rica, has almost entirely focused on suspended load (Brandt & Swenning, 1999; Jansson, 1996, 2002; Kesel & Lowe, 1987; Krishnaswamy et al., 2001; Restrepo et al., 2006). Jansson (2002) found a suspended load in the Rio

Pijibaye and the Rio Oriente, neighboring montane rivers to the Rio Pacuare, of up to 2785 tonnes and 10,000 tonnes, respectively, in response to a single gaged storm event (24 hours). These valuable studies confirm the dynamic hydrology as well as the high sediment availability and transport potential of humid tropical montane systems, yet only a few published articles have included bedload transport (Asfaha et al., 2015; Bidorn et al., 2015; Ziegler et al., 2014a) or characterized the size and distribution of coarse bed material in these dynamic systems (Pike et al., 2010; Rengers & Wohl, 2007). Only one non peer-reviewed report on bedload transport rates from Costa Rican rivers was found, produced by the Costa Rican Institute of Electricity (Instituto Costarricense de Electricidad —ICE) to justify gravel extraction from the Rio Reventazon for an ICE dam construction project (Vargas, 2007).

This study presents bedload transport capacity estimates from six field sites established within 45 river kilometers (Rkm) of the montane portion of the Rio Pacuare. Differences in the magnitude, as well as the spatial and temporal variations, of sediment transport capacity are discussed in relation to stream power, and annual/inter-annual climate patterns. Based on field assessments and bedload distribution (Chapter II, this dissertation), the Rio Pacuare has a plentiful supply of bedload throughout the study area and high flow competency to frequently mobilize the bedload.

The frequency of bedload transport characterizes the dynamics of sediment flux in a system. In humid tropical river systems mobilization of the bedload is caused by precipitation-generated discharge. Tropical low pressure systems coupled with orographic uplift produce intense rains on the high-gradient landscape (Giannini et la., 2001; Giannini et al., 2000; Thomas, 1996). This study also examines the frequency at which flows capable of mobilizing a bedload dominated by cobbles and boulders occur in the montane section of the Rio Pacuare.

To addresses these questions, this study uses a unique mix of field and remote sensing techniques to overcome some of the challenges of tropical river research (e.g., difficult access, high sediment flux, rapidly fluctuating flows, large-grain mobilization, etc.). A relatively modern bedload transport model developed for high gradient systems by Recking (2013) is used to estimate transport rates at the field sites. Similar to the protocol followed by the U.S. Geological Survey for quantifying annual sediment

transported and channel change in the coarse-bedded Chetco River, Oregon (Wallick et al., 2012), this study inputs the data collected in the field into the HEC-RAS hydraulic model to calculate hydraulic parameters (slope, hydraulic radius and channel width) for the sediment transport model. Unlike in the Chetco study however, sediment traps were not used to validate modeled transport, due to the fact that grain size and stream energy on the Rio Pacuare would destroy the equipment. On the Rio Pacuare, identification of grain mobilization and validation of modeled shear stress requirements for an observed flood event is made for the first time through repeat photogrammetric surveys. As some of the first research of this type on a tropical montane system, this study expands our knowledge of tropical rivers and sediment transport by providing a broad view of bedload sediment flux in a hydrologically dynamic humid tropical montane system.

3.1.1 Regional Setting

This research is conducted on the Rio Pacuare, located in Costa Rica's Talamanca Mountains in the central portion of the Chorotega volcanic front of Central America (Figure 0-1). In total, the channel is approximately 132 river kilometers (Rkm) long from headwaters to sea. It flows north-northeast through the Talamanca mountains, exits the confinement of the mountains across a prominent alluvial fan onto a low-gradient alluvial plain, and eventually flows into the Caribbean Sea. The entire watershed is 890km^2, and the mainstem channel falls approximately 2160m in elevation with almost the entire fall (2098m) occurring in the upper 88 Rkm contained within the mountains. The montane portion of the Rio Pacuare (44.2 to 132 Rkm) was selected as the study area because it is currently free flowing, accessible in a few locations yet minimally impacted by anthropogenic influences, and contains a variety of geologic and hydrologic characteristics common in the montane tropics of Central America (Marshall, 2007; Sitchler et al., 2007). Dense tropical mid-elevation forests dominate the vegetation cover. Only small-scale farming plots and a few unincorporated villages accessed by dirt roads and trails are found along the montane portions of this river system. The Talamanca Cabecar Indigenous Reserve and Pacuare Bio-Reserve border the Rio Pacuare along channel right from Rkm 44-72. Upstream of Rkm 85 the river is bordered on both sides by the reserves.

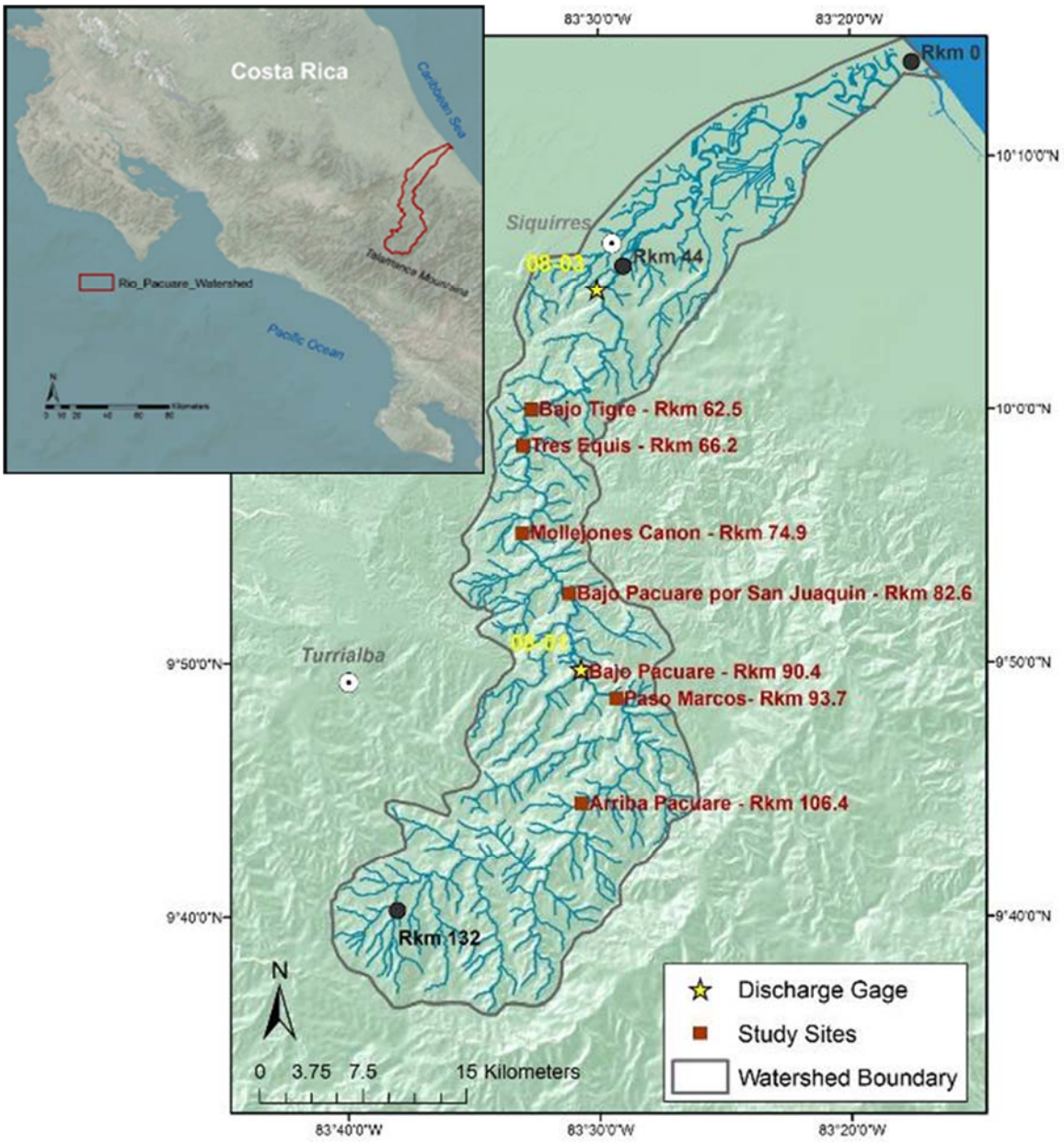

Figure 0-1. Study area and field sites. Basemaps: Esri GeoEye, 30m DEM (ASTER, 1999).

The Rio Pacuare drains the tectonically active and steep Talamanca Mountains. Geologic constraints and faults influence the channel's current and historical pathway. However, the lack of large grade-breaking knickpoints (waterfalls) along the mainstem channel, even at fault intersections, suggests that the flow competence (stream power) of the Rio Pacuare is strong enough to erode tectonically uplifting bedrock and/or arrange

its available sediment to adjust channel slope (Chapter II, this dissertation). Channel gradient at the field sites range from 1-4% (Figure 0-2).

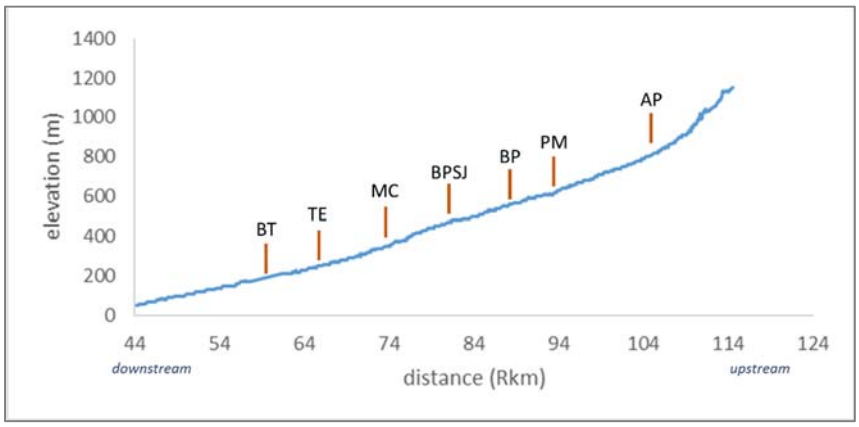

Figure 0-2. Longitudinal profile of the montane portion of the Rio Pacuare and the locations of the field sites.

The discharge regime of the Rio Pacuare is governed by regional and localized precipitation patterns. Although the river's headwaters are at relatively high elevations, no precipitation falls or is stored as snow due to its tropical location. The Talamanca Mountains experience two rainy and two dry seasons annually (Giannini et al., 2000; Vargas & Trejos, 1994; Waylen et al., 1996). However, given the combination of local orographic uplift and incoming lowland climate patterns from the Caribbean, the Rio Pacuare watershed is typically wet with a drier season that occurs January to April (and occasionally in September), and a wetter period from May to December (Figure 0-3). High discharge most commonly occurs in November and December and often July. During intense rains, flows on the Rio Pacuare rise rapidly. This is most evident May to December when the watershed is more likely to be saturated and storm runoff is immediate.

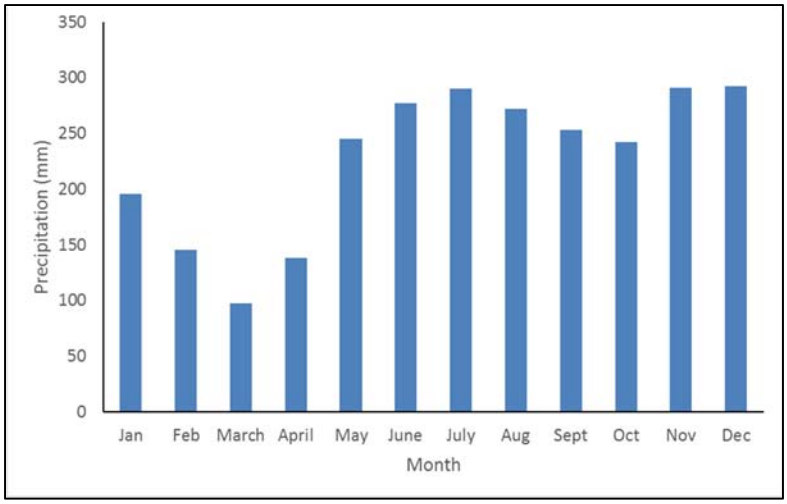

Figure 0-3. Monthly average precipitation at Turrialba, CR (1959 – 2012). See Figure 0-1 for location of Turrialba. Source: CATIE 2016.

The montane section of the Rio Pacuare flows through confining bedrock and/or steep hillslopes. Narrow inset pockets of floodplain terraces exist in areas of semi-confinement, but in these reaches the banks of the channel usually alternate between bedrock and coarse alluvium or colluvium. The channel's bed is covered with a coarse boulder-dominated bedload of unknown depths throughout most of the study area – even in many of the bedrock-wall confined sections. It is assumed that when mobilized, the bedload aids in bedrock incision processes.

Seven field sites were selected at representative depositional features along the channel (see Figure 0-1 for site locations). Six of the sites are located on active bars, 50 – 300m in length, composed of imbricated boulders. Cobble-boulder bars define channel form at low to moderate flow within much of the study area (Example: Figure 0-4-A). One field site is a cobble and boulder deposits located on a bedrock shelf in Mollejones Cañon, similar to other depositional features found at a few locations in the canyon. Site selection was based on representative characteristics of the depositional features within the river segment and ease of accessibility by dirt roads and trails for conducting repeat surveys (See Appendices B for site photos). Bars located on relatively straight sections of the channel were selected to reduce hydraulic variability in the modeling. The active surfaces of the bars indicate frequent mobilization of coarse bedload fractions and abundant bedload sediment availability.

From Rkm 73-77 (Mollejones Cañon -- MC) the channel is confined within narrow, relatively straight bedrock walls that extend upslope into steep gradient hillsides (Figure 0-4-B). The bed of the channel in the canyon is mantled with plentiful bedload, but due to the relatively narrow and deep channel, few bars and bedforms are exposed except during very low flow periods. The uppermost field site (Arriba Pacuare, at Rkm 106.4) required a twenty-five-kilometer hike, and was therefore accessed only during the dry season. Approximately 3 Rkm above the uppermost field site at Arriba Pacuare, the channel shifts to a very confined cascading and step-pool stream dominated by large boulders and minimal boulder-cobble bar accumulations. This steep headwaters portion of the mainstem Rio Pacuare is considered more similar to other contributing tributaries than the mainstem channel, and thus does not have a study site located within it.

Figure 0-4. A) Alternating boulder bars in semi-confined section, at Rkm 104.4; B) Bedrock confined channel in Mollejones Cañon, at Rkm 74.7. Photos by P.Lind - 2013.

3.2 MATERIAL AND METHODS

This research combines traditional field-based data collection, a new application of remote sensing techniques, daily discharge data, and 1-D HEC-RAS hydraulic

modeling to generate channel and flow parameters necessary to estimate sediment transport capacity at six (BT, TE, BPSJ, BP, PM and AP) of the seven field sites. Table 0-1 is a list of the field site names and their river kilometer (Rkm) measured from the river's downstream mouth at the Caribbean Sea.

Table 0-1. List of field sites and their river kilometer (Rkm) location from downstream to upstream.

Field Site	Code	Rkm
Arriba Pacuare	AP	106.4
Paso Marcos	PM	93.7
Bajo Pacuare	BP	90.4
Bajo Pacuare por San Juaquin	BPSJ	82.6
Mollejones Cañon	MC	74.9
Tres Equis	TE	66.2
Bajo Tigre	BT	62.5

Sediment transport capacity is calculated from the channel's hydraulic variables, grain size, and channel geometry (Julien, 2010). Field data on sediment size, channel cross section geometry, and roughness, along with gaged and estimated discharge data were used to determine the sediment transport capacity at each of the field sites following methods similar to Emmett and Wolman (2001), Yager et al. (2007), Wallick et al. (2012), and Hicks and Gomez (2003). The HEC-RAS 4.1.0 model (Brunner, 2010) was used to predict hydraulic variables for a range of discharges. Digital photogrammetry using Structure from Motion (SfM) pre- and post-flood events is used for the first time to validate grain mobilization and flow inundation after a flood event. A sediment transport model developed by Recking (2013) for steep mountain streams is used to estimate sedimenttransport capacity at the field sites. A summary list of the data collected is provided in Table 0-2.

Table 0-2. Summary list of data collected, method used for collection, output data, and application of that data in this study.

Data Collected	Method / Process	Output	Application/Use
cross-section topography	Field GPS and Laser range finder (LSF)	multiple cross sections at each site	HecRas hydraulic model
			Stream power
surface roughness	Field notes & reference photo-book comparison	Mannings n at each cross section	HecRas hydraulic model
flow characteristics	Field float method	flow velocity	combined with cross section to find discharge
bed material chracterization	Field grid-pattern grain counts (gravelometer & boulder caliper)	Grain size-fraction distribution at each site	HecRas hydraulic model
			Recking bedload transport model
			Critical shear stress - grain mobilization
Pre and post-flood bar surface model	Field repeat photogrammetric surveys (Sfm)	high-resolution DEMs and orthophotos	validate grain mobilization - GIS DEM of difference
			validate flood-event min. bar inundation -- GIS orthophoto analysis
Flow regime	Aquired	Daily Discharge (1959-2012)	estimate daily discharge at ungaged sites
			Flow duration curves
			Synthesized sub-daily 8hr hydrograph - all sites
			Stream power

3.2.1 Data Collection

At each field site, survey control points were established to tie all surveys to a set of established coordinates. Permanent control points meant to last over two years were secured into bedrock or extremely large boulders with a rock-hammer drill and mason bolts. Temporary control points were established with a grease pencil on additional large boulders where needed (Figure 0-5). The location of all the control points was collected on a hand-held Trimble GPS unit (GeoXH). After post-processing, a vertical precision of 0.18 to 4.36 meters (average vertical precision of 0.65m) and horizontal precision of 0.12 to 2.02 meters (average horizontal precision of 0.35m) accuracy was obtained. A Laser Technologies laser range finder (LRF) (Impulse-Series) with a typical range accuracy of 0.01 meters and inclination accuracy of 0.1 degree was attached to a stabilizing pole and used to establish elevation of the control points at each site for a higher degree of vertical accuracy than the GeoXH can consistently produce. It is unknown what the actual vertical accuracy of this technique produced. However, an evaluation of the difference in elevations for a set of the control points measured from different distances produced an error of 0m at distances less than thirteen meters apart and an error up to 1.62 meters at a distance between points of more than 55 meters. This prompted field measurement with the LRF of less than 25m distances when possible.

Figure 0-5. Examples of survey control points at field sites. Photos by P.Lind & O. Arroy Nunez.

Cross Sections and Roughness

At each field site, channel geometry was collected with a series of cross section surveys, using the LRF and established control points. The surveys captured active channel topography as well as flow velocity, depth of flow, channel width, site slope, recent high-water marks, and Manning's roughness estimates. A minimum of two control points fixed the location of each cross section, and a tape was stretched along the cross section for field checking LRF distances and to ensure that the survey path was straight (Figure 0-6). The number of cross sections at each site depended on site size, bar and channel topography, and access. Spacing between cross sections ranged from 11 to 445 meters. Figure 0-7 provides maps of the cross sections surveyed at each field site.

The cross sections were surveyed during dry season months (late February to early April) to maximize exposed bar and bed surfaces. However, even at dry season flows in 2013, not all cross sections at each site were completely wadable because of flow depth and energy. However, at least one cross section was fully surveyed at every site. This allowed calculation of discharge at the time of survey, and documentation of thalweg topography for extension to other incomplete cross-sections at the site.

To construct the topographic shape and maximum depth (d_{max}) of the incomplete cross sections, a set of flow and geometry equations were combined. First, the area of the complete cross sections was calculated by inputting the survey data (topography and

Figure 0-6. Cross section surveys at field sites Bajo Pacuare for San Juaquin, Arriba Pacuare, Tres Equis, and Bajo Pacuare - Laser range finder on stabilizing pole shot at mounted target placard.

water elevation) into Grapher software. Discharge was then calculated from the field data for those sites. Using site discharge and cross-section velocity, the area of the incomplete cross sections was determined. The channel cross-section shape equations for general geometric relations (triangle, rectangle, and parabola) derived by Conrad and Fonstad (Conyers, Fonstad, Lovell, & Marcos, 2005) were combined with a set of geomorphically appropriate flow equations that included:

Manning's (1891) equation: $v = R^{0.67} S^{0.5} / n$

Jarrett's equation (1984) for high-gradient streams: $n = a * S^{-0.12} * R^{0.83}$

Grant's equation (1997) for critical flow channels: $v = (gd)^{0.05}$

where v is velocity, R is hydraulic radius, S is slope, n is average channel roughness, g is gravitational acceleration, and d is flow depth. The flow equations were rearranged to solve for d_{max} of each potential geometric shape (triangular, rectangular, and parabolic) for the known site discharge (Q). The d_{max} was then used to calculate the wetted perimeter and area of the known cross sections to determine which shape and flow equation best represented channel shape at each field site. Iterations of shape and d_{max} were then applied to the incomplete cross sections for shape selection and adjustment until an approximated topography with the necessary area and wetted perimeter to convey the field-measured discharge was discovered.

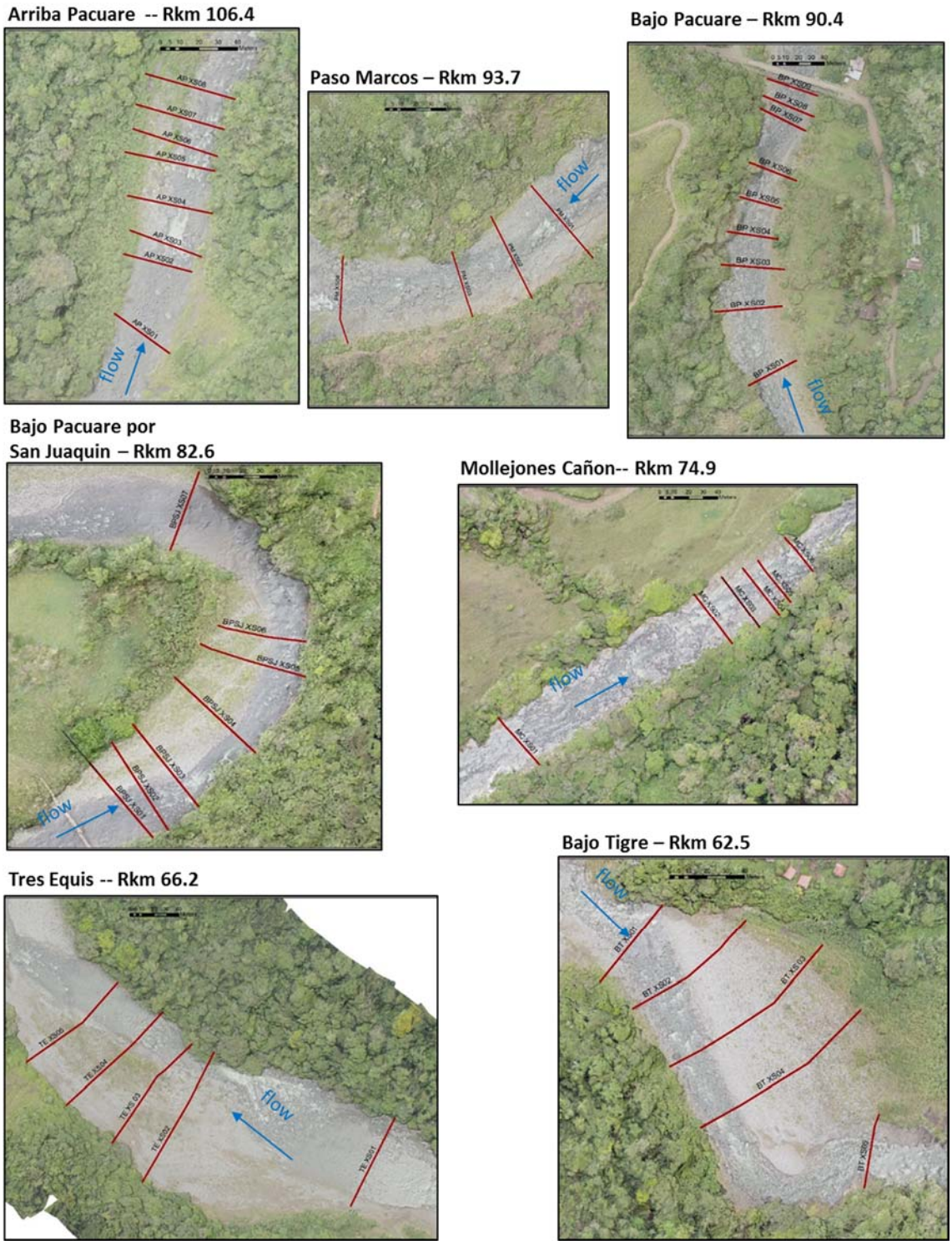

Figure 0-7. Cross section locations at each field site. Aerial imagery collected for this study, April 2014.

Site-averaged and cross-section specific roughness (Manning's n) values were estimated from field observations (Arcement & Schneider, 1989) and then field photos were compared to roughness values offered in Hicks and Mason (1998). Above the high-water marks floodplain roughness values were determined using the table provided in the HEC-RAS modeling manual (Brunner, 2010). Above the high-water scour line the highest n values offered in the manual for forested and agricultural floodplains were used because of the density of tropical vegetation in the watershed.

Velocity

Flow velocity was measured at every cross section to combine with cross sectional area to calculate location-specific discharge. Velocity was measured using the "drift" (aka "float") method (Burton & Pitt, 2002; SWAP, 2011; USBR, 1997) over a distance of 10 to 50m at each surveyed cross section and time was recorded to the tenth of a second. This was done three to six times at each cross section to establish an average travel time. As recommended (Burton & Pitt, 2002; SWAP, 2011; USBR, 1997), correction factors were applied to the calculated flow velocity to adjust for the fact that surface flow velocity is faster than the velocity of flow below the surface and near the bottom of the channel. Based on evaluation of applied correction factors established by others (Burton & Pitt, 2002; Kra & Merkley, 2004; SWAP, 2011), a factor of 0.8 was applied to irregularly shaped cross sections located at riffle crests, or within riffles or cascades that had a relatively higher slope and protruding boulders and a correction factor of 0.6 was applied to cross sections located within fast-moving glides with relatively lower slope and less relative bed roughness.

Gravel Counts

Grain size fractions across the surface of the exposed bar at each field site were determined by gridded sampling laid out with 100m tapes (Bunte & Abt 2001) to eliminate bias of grain selection. Grain size was measured with a gravelometer and boulder calipers (Figure 0-8). A single gravel (cobble-boulder) count was done at each site. At Bajo Pacuare, there is a bar on both sides of the river and thus a count was done

on each. Gravel counts extended across the exposed bar surface but less than a meter into the wetted channel. A total of 136 to 251 grain samples were measured at each site.

Figure 0-8. Gravel count completed with calipers and gravelometer at field site Tres Equis, Bajo Pacuare por San Juaquin, and Paso Marcos. Photo by P.Lind.

Repeat Photogrammetric Surveys – Structure from Motion (SfM)

The modern remote sensing method called Structure for Motion (SfM) offers a low-tech, high-resolution tool for capturing detailed topographic surveys (Carbonneau et al., 2012; Micheletti et al., 2015). For this research, repeat photogrammetric SfM surveys were completed before and after a high-flow event (referred to as the T-day flood: 11/28/2013) to verify grain size mobilization and bar inundation for a gaged discharge event. The SfM surveys were used to create high-resolution, rectified, digital elevation maps (DEM) and orthophotos of the bar surfaces for overlays and change analysis. Time consuming point-surveys done with an RTK, GPS, or Total Station could not have captured the topographic detail necessary to detect change on these bar surfaces, because the coarse scale of the material creates irregular surface topography. SfM surveys were conducted following methods by Dietrich et al., (2012) developed further by Dietrich and Lind (2013), which entail attaching a waterproof Canon PowerShot D10 camera mounted on a three-meter extension pole. The camera was used to take photos of the bar surface in an overlapping grid pattern that included capturing the established control points, which were used to rectify and overlay the SfM products.

Photogrammetric SfM data processing and digital model creation was accomplished using AgiSoft Photoscan software similar to application by (James & Robson, 2012; Javernick et al., 2015). The high resolution digital elevation models and orthophotos were then input into GIS for analysis including DEM change detection and visual comparison analysis (Wheaton et al. , 2010). The resulting pixel resolution of the DEMs and orthophotos is 1cm. Accuracy of the models is based on the precision of the established control points, discussed in Section 3.2.1.

3.2.2 Data Processing

Some collected and acquired data for this study required additional processing prior to application in the hydraulic and sediment transport models. Daily discharge was derived for the ungaged sites by establishing the region's discharge-to-area relationship(s). Sub-daily discharge for each field site was then synthesized from the daily values to better represent the flashy character of flood events in the system. The data processing methods are described below.

Discharge Data

To estimate annual sediment transport rates at each site and to explore temporal variation in daily sediment transport capacity, it was necessary to have daily discharge data for each field site in the study. The available daily discharge data for the two gages on the Rio Pacuare (see Figure 0-1 for locations) were obtained from the Instituto Costarricense de Electricidad (ICE). At the time of this research, instantaneous and peak-flow discharge data were not available for the Rio Pacuare. On the Rio Pacuare, ICE gage 8-03 (Dos Montañas, located at Rkm 46.3 had data from 1971 to 1999; and ICE gage 8-01 (Bajo Pacuare) located at Rkm 90.4 at the BP field site had data from 1958 to 2013. For calculating annual sediment transport capacity, only years with complete data records at gage 8-01 were used (1959-1990, 1993-1994, 1996-2012).

Because only the Bajo Pacuare (BP) field site located near the gage had discharge data, the daily discharge for the other six sites was estimated by developing a discharge (Q) to drainage area (DA) relationship ($Q \propto DA^{\beta}$). This was done using gaged daily discharge data from other rivers in the region. Daily discharge data from nine montane

rivers on the eastern side of the Talamanca Mountains of Costa Rica and northern Panama (Figure 0-9) were obtained from the Global Runoff Data Centre (GRDC) at the research institute of Bundesanstalt fur Gewasserkunde (2014). Discharge data overlap occurred for the other gaged rivers during a span of twenty years (1973-1993), though not every year's set of data was complete for every gage.

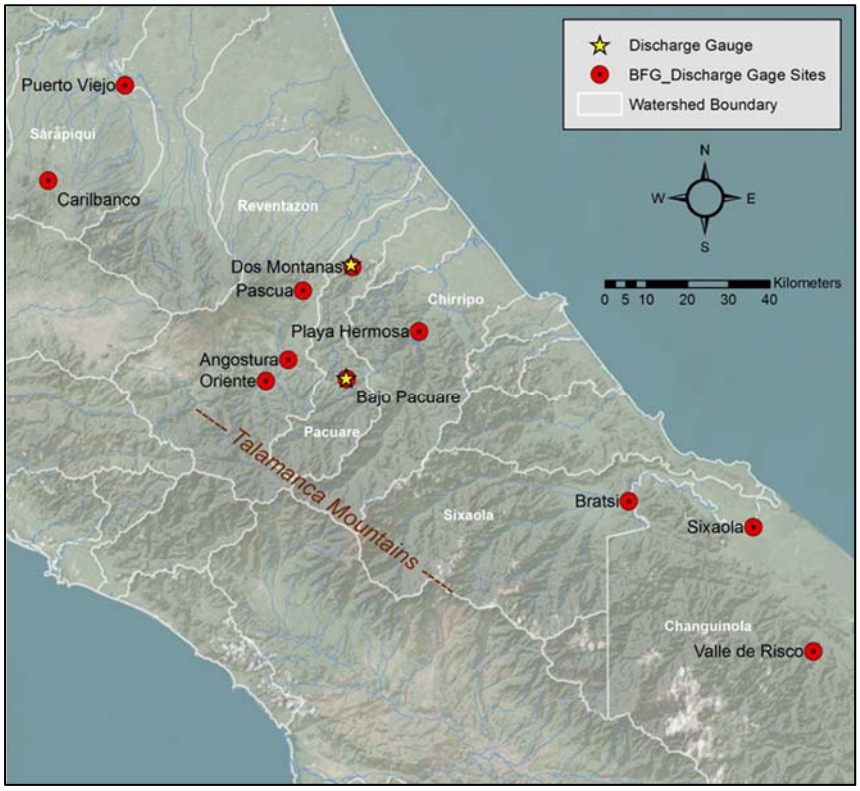

Figure 0-9. Map of Costa Rican watersheds with gage locations identified were daily discharge data was obtained from the GRDC. Basemap source: ESRI Earthstar TerraColor 1999; MINEA watershed boundaries.

Based on the conventional expression $Q = aDA^b$ (Jennings et al. 1994), a and b were calculated through logarithmic regression between daily discharge (Q) and its recurrence interval (RI) over the period of record for each river gage. Better-fitting regression models were found by splitting the record at each gage into low flows ($RI \leq 100$ days) and medium to high flows ($RI > 100$ days). The resulting area to discharge regression equations for the Talamanca gages are provided in Table 0-3.

Table 0-3. River name, gage, upstream drainage area, and elevation of sites used to establish discharge to area relationship for the region.

River	gage name	Drainage Area (km^2)	Elevation (m)	R^2 (RI>100)	y=aln(x)-b (>100)	R^2 (RI<100)	y=aln(x)-b (<100)
Pacuare	Bajo Pacuare	367	582	0.948	y=55.368ln(x) - 170.65	0.99	y=19.521ln(x) + 10.478
Pacuare	Dos Montanas	652	69	0.935	y=118.66ln(x) - 387.38	0.987	y=33.628ln(x) + 18.868
Reventazon	Pascua	1673	247	0.934	y=283.73ln(x) - 970.54	0.986	y=73.588ln(x) + 53.716
Reventazon	Angostura	1337	532	0.933	y=137.26ln(x) - 411.21	0.977	y=49.441ln(x) + 44.086
Pejibaye	Oriente	227	619	0.94	y=60.981ln(x) - 192.93	0.992	y=19.498ln(x) + 9.2618
Chirripo	Playa Hermosa	821	140	0.94	y=157.63ln(x) - 488.65	0.97	y=38.044ln(x) + 23.317
Changuinola	Valle de Risco	1680	47	0.826	y=307.89ln(x) - 930.92	0.989	y=90.671ln(x) + 65.388
Sarapiqi	Cara Blanca	73	752	0.972	y=51.649ln(x) - 207.8	0.917	y=5.6832ln(x) + 1.6391
Sarapiqi	Puerto Viejo	821	22	0.974	y=276.72ln(x) - 819.65	0.979	y=80.328ln(x) + 35.09
Sixaola	Brasti	2121	35	0.865	y=489.71ln(x) - 1778.7	0.982	y=94.45ln(x) + 69.672
Sixaola	Sixaola	2716	2	0.778	y=468.79ln(x) - 988.09	0.959	y=157.65ln(x) + 69.27

From these a regional RI was established by averaging all of the recurrence intervals for all the gaged sites. To do so, the daily discharge values for the six ungaged sites were estimated by identifying a daily multiplier rather than a particular RI discharge – because daily values instead of single peak flows are desired for calculating annual sediment transport. To achieve this, the equation $Q = aDA^b$ was recast in terms of a set of non-dimensional ratios:

$$(Q_u/Q_{REF}) = a\,(DA_u/DA_{REF})^b \qquad (1)$$

where u is the ungaged location and REF is the reference gage location (ICE 8-01 at Bajo Pacuare). The natural log of the ratios for each RI for all sites was then averaged and plotted against the RI to find the constant value of a and b – as shown in Table 0-4.

Table 0-4. The resulting equations and R^2 values for the constants a and b.

constant		R^2
a	y=0.0259ln(x)-0.456	0.9213
b	$y=0.992x^{-0.039}$	0.943

The log natural of the ratios equation is then:

$$\mathrm{Ln}\,(Q_u/Q_{REF}) = b*\mathrm{Ln}(DA_u/DA_{REF})+a \qquad (2)$$

where a and b are the known constants; Q_{REF} and DA_{REF} are the daily discharge and drainage area for the reference gage, respectively; and Q_u and DA_u are the daily estimated discharge and the drainage area for the ungaged location of interest.

Next, equation (2) was transformed to solve for Q_u for each ungaged study site:

$$(Q_u/Q_{REF}) = e^{(b*Ln(DAU/DAREF)+a)} \quad (3)$$

where e is the base of natural logs. Utilizing equation (3), a daily discharge value for every day of recorded discharge data from the reference gage site (Bajo Pacuare) was estimated for each of the six ungaged field sites. An example of a year's worth (2012) of estimated daily discharge for a field site upstream (Arriba Pacuare) and downstream (Bajo Tigre) of the gaged site (Bajo Pacuare) is provided in Figure 0-10.

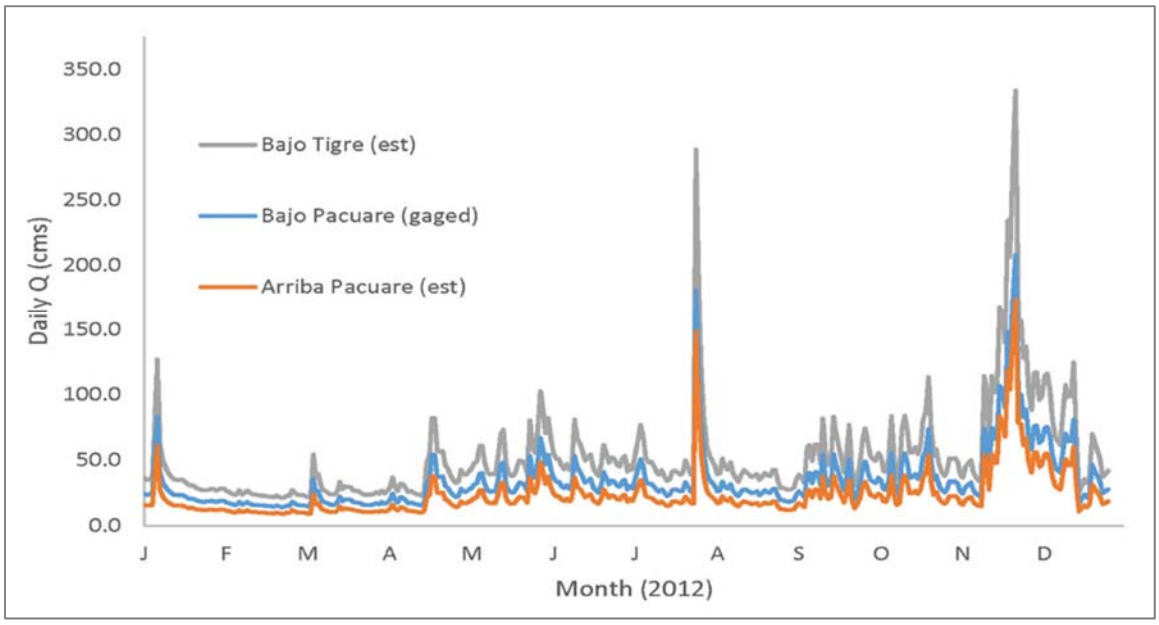

Figure 0-10. Estimated (est) daily discharge values for one year (2012) at two ungaged sites compared to the gaged reference site (Bajo Pacuare).

To validate this technique for generating daily discharges within the watershed, the estimated daily discharge for the other Rio Pacuare gage (ICE 8-03) at Dos Montañas was compared to the gaged discharge for 1971-1999, the available period of record at ICE 8-03 gage. The average difference between the gaged values and the estimated values is -2.1 cubic meters per second (cms) or just 3.8 percent of the median daily discharge reported at Dos Montañas (55.5 cms). Differences greater than 20 cms occurred

only 20% of the time. The difference between modeled and estimated daily discharge values partly results from R^2 values < 1 in the initial regression analysis (Table 0-3), and partly because flow lag time between sites is not considered in the estimated calculations. Notably, this technique also does not capture natural spatial variability of tropical storms within the Rio Pacuare watershed,

Synthesized Sub-Daily Hydrograph

Humid tropical mountain rivers often experience flashy high-magnitude flows (J.D. Restrepo, Lopez, & Restrepo, 2009; Wohl, 2005) driven by intense tropical precipitation events. On the Rio Pacuare, discharge in the channel was observed increasing or decreasing in a matter of hours in response to storm events. Thus, a single daily discharge value is expected to be smaller than the highest discharge value and larger than the lowest discharge value during that 24-hour period. The difference between actual and averaged discharge depends on how dynamic the fluctuations in flow are. However, only daily discharge values were available for this study. This is a note-worthy limitation considering bedload transport is often non-linear and the threshold to mobilize bedload usually occurs during the higher peaks of flow events.

An example that illustrates how a single daily discharge value mutes the flow fluctuations that can occur in these systems was observed in the field. On November 28, 2013 a high-flow event that inundated most of the bar surfaces in the system occurred after a few days of low-precipitation, low-flow days. The daily discharge value reported at the Bajo Pacuare gage for the high-flow day was only 47cms. This is the same daily discharge value reported for other moderate flow days that did not inundate bar-top surfaces. For the flood event day, because the previous day's discharge value, and likely the morning prior to the storm event, was very low, the reported daily average discharge value misrepresents and mutes the high-flow event that occurred later that day. The actual value and duration of the peak flow that inundated the surfaces during the high-flow event is unknown. For the moderate flow example, the previous and proceeding values were similar to the day's daily average, resulting in relatively no muting and a fairly representative daily discharge value for the entire 24-hour period. This shows that intense brief rain events can raise discharge, and presumably transport sediment capacity, yet not

be represented by the daily average discharge value. This then raises concern for accurately calculating sediment transport in such hydrologically dynamic systems using only a single daily discharge value, especially considering the often non-linearity of sediment transport.

To improve upon the limitation of only having access to a single daily discharge value for each day, a synthesized sub-daily hydrograph (8-hour average values) was created. This technique creates a sub-daily hydrograph that temporally downscales the daily data (24 hours) to capture some of the variability of flow that this system can experience in a single 24-hour period. First, each day of record was subdivided into three eight-hour periods (12am-8am; 8am-4pm; and 4pm-12am). The difference between the day's daily average and the daily average discharge from the previous day was determined. For the first period (12am-8am) half the difference was subtracted from the daily average value; for the third period (4pm-12pm) half the difference was added to the daily average. The second, or middle, period retained the original daily average value (Figure 0-11). Combined, the three discharge values average the reported daily discharge value. This is a new method presented here for improving the representation of a single daily discharge value in flashy systems that frequently (almost daily) experience rain events.

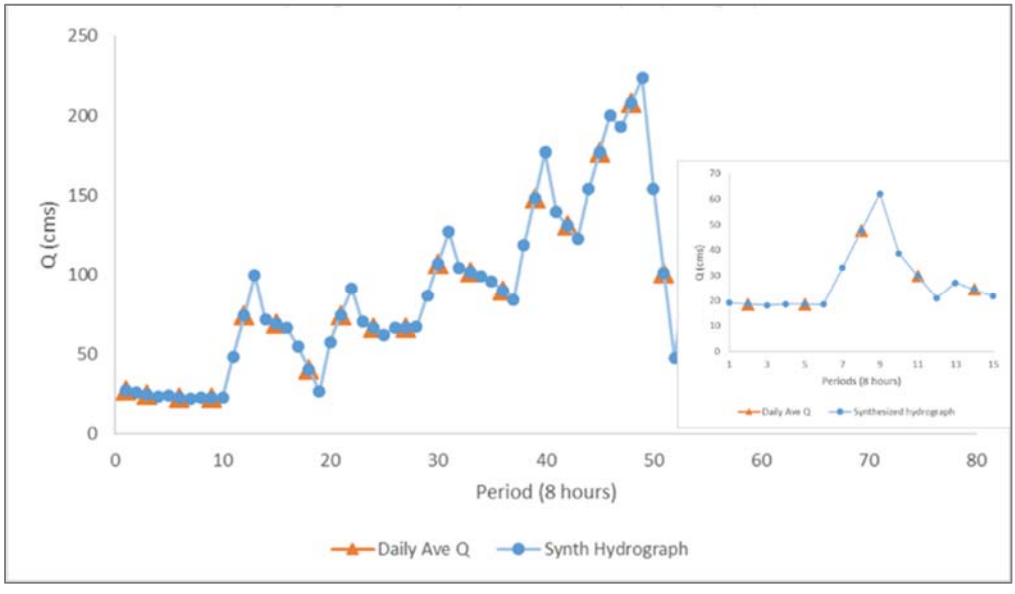

Figure 0-11. Examples of synthesized sub-daily (8 hour) hydrograph compared to original daily discharge value.

Significantly, the synthesized sub-daily hydrograph does not capture peak-flow values or duration. Instead, it likely still under-predicts the peak-flow discharge value by conservatively calculating for only three time periods per day. However, it assumes the synthesized discharge values last the full eight-hour duration. This conservative approach to creating a sub-daily hydrograph reduces the risk of over-estimating sediment transport values, while ensuring that dynamic flow events are not drastically under-estimated. For example, the difference in sediment transport for a representative year (2008), using one daily discharge value versus the synthesized sub-daily hydrograph, was calculated for a cross section at the Bajo Pacuare field site and gage location. The sub-daily hydrograph increased that year's annual sediment rates (tons/year) by 29%—supporting the need for a more detailed hydrograph than a single daily value in hydrologically dynamic river systems.

3.2.3 Modeling

Hydraulic and sediment transport modeling that integrates the collected and processed data was done sequentially to estimate sediment transport rates. Hydraulic modeling was undertaken to generate the flow parameters required for the sediment transport model (energy slope gradient, hydraulic radius, and width) and to predict grain mobilization (boundary shear stress).

Hydraulic Modeling

Hydraulic modeling of the cross sections from each field site was done in HEC-RAS 4.1.0 (1-D models) – see Figure 0-7 for maps of the distribution and number of cross sections surveyed at each site. The set of cross sections from each field site were modeled together. Critical flow boundary conditions were set for the upstream and downstream cross sections, allowing the model to adjust hydraulic parameters for the other cross sections as needed for the range of discharges used in the model. Twenty discharges that ranged from the maximum to the minimum sub-daily values were modeled in HEC-RAS for each site. Twelve of the modeled discharge values equally divided the 99.9-0.8% flow exceedance values and the other modeled discharge values equally divided the 0.8-0.004% flow exceedance values (Table 0-5). Flow exceedance

probabilities were derived with a flow duration curve created at each site based on the years of record with complete discharge data (51 years between1959-2012) using daily discharge.

Table 0-5. Discharge values (flow profiles) modeled in HEC-RAS at each field site and the general percent exceedance that flow represents. Flows ≤ 0.8% exceedance shaded in darker blue.

Modeled Flow Profile	% Exc	AP Q (cms)	PM Q (cms)	BP Q (cms)	BPSJ Q (cms)	MC Q (cms)	TE Q (cms)	BT Q (cms)
PF 1	0.004	2485.55	2872.81	1672	3180.1	3321.06	3455.31	3488.76
PF 2	0.0042	2186.33	2559.12	1477.62	2801.58	2926.69	3045.94	3075.66
PF 3	0.005	1887.11	2245.43	1283.24	2423.06	2532.32	2636.57	2662.56
PF 4	0.0053	1587.89	1931.74	1088.86	2044.54	2137.95	2227.2	2249.46
PF 5	0.006	1288.67	1618.05	894.48	1666.02	1743.58	1817.83	1836.36
PF 6	0.008	989.45	1304.36	700.1	1287.5	1349.21	1408.46	1423.26
PF 7	0.01	690.23	990.67	505.72	908.98	954.84	999.09	1010.16
PF 8	0.026	391.01	676.98	311.34	530.46	560.47	589.72	597.06
PF 9	0.8	91.82	123.3	117	151.9	166.12	180.32	183.96
PF 10	1.1	83.72	112.3	106.75	138.55	151.53	164.49	167.82
PF 11	1.5	75.62	101.6	96.5	125.2	136.94	148.66	151.68
PF 12	2.2	67.52	90.75	86.25	111.85	122.35	132.83	135.54
PF 13	3.6	59.42	79.9	76	98.5	107.76	117	119.4
PF 14	6.5	51.32	69.05	65.75	85.15	93.17	101.17	103.26
PF 15	11.6	43.22	58.2	55.5	71.8	78.58	85.34	87.12
PF 16	20.9	35.12	47.35	45.25	58.45	63.99	69.51	70.98
PF 17	37.2	27.02	36.5	35	45.1	49.4	53.68	54.84
PF 18	58.8	18.92	25.65	24.75	31.75	34.81	37.85	38.7
PF 19	82.4	10.82	14.8	14.5	18.4	20.22	22.02	22.56
PF 20	99.99	2.7	3.95	4.25	5.05	5.63	6.24	6.4

In natural high-energy fluvial systems flow tends toward critical (Grant, 1997) but, confinement and channel form may alter flow conditions (Montgomery & Buffington, 1997). Thus, both "Mixed" and "Critical" hydraulic conditions were modeled for each site to determine which produced the most representative flow conditions compared to observations and surveys. "Critical" flow conditions force the Froude number to or toward a value of 1 for all discharge profiles—producing relatively shallow fast-moving hydraulics. "Mixed" flow conditions in the model allowed hydraulics to

adjust between supercritical, critical, and non-critical flow based on site hydraulics and associated discharge (Brunner, 2010).

To validate the model results the water surface elevations produced in HEC-RAS were compared to field observations and SfM surveys of inundation after the T-day 2013 flood event. The inundation elevations visible in orthopohtos produced with the SfM surveys include high-water marks on the bars such as flotsam, vegetation removal, scour, and sand deposits. Thus, the SfM inundation elevations are considered the minimum flow stage. The "Mixed" HEC-RAS model results compared well to the SfM inundation elevations at all field sites, except at Mollejones Cañon. At Mollejones Cañon, the "Mixed" model produced flow elevations slightly higher than the surveyed T-day flood, and the "Critical" model produced flow elevations lower than the surveyed elevations. Based on best results, the "Mixed" model was used to represent the flow hydraulics at the cross sections at the field sites.

A single representative cross sections (XS_{rep}) from each field site was selected to simplify presentation and discussion of results. The representative cross section from each field was was selected by its relatively central location on the bar feature, inclusion in the gravel-count area, and a water surface slope most similar to the overall slope of the field site. In addition, the representative cross sections have a fairly regular topographic shape, meaning that, other than protruding boulders, it does not express split flow around mid-channel bars or contain multiple channel units in one cross section (i.e., a riffle on one side and a pool on the other).

Grain Mobilization

The discharge required to produce the necessary shear stress (Q_{cr}) to mobilize the D_{16}, D_{50}, D_{84} was calculated at each site to predict the frequency at which bedload is mobilized and bed forming flows occur. The total boundary shear stress (τ_o) at each cross section was predicted using the HEC-RAS model results of τ_o for the 20 modeled flows. A regression plot of the boundary shear (τ_o) vs. the flows' respective discharge values (Q_o) enabled estimating the discharge required to produce a boundary shear at the representative cross sections for predicting mobilization of specific grain sizes. Separate

models were created for the high flow (<0.8% exc.) and low-moderate flow (>0.8% exc.) $\tau_o \infty Q_o$ relationships (Table 0-6).

Table 0-6. Regression model results for discharge (Q_o) vs boundary shear (τ_o) at representative cross sections for each field site.

		<0.8% exc	$\tau_o=a(q_o)^b$		>0.8% exc.	$\tau_o=a(q_o)^b$	
Site	Cross Section	R^2	a	b	R^2	a	b
Arriba Pacuare	XS04	0.979	43.536	0.4864	0.952	190.87	0.1525
	XS07	0.994	0.0008	3.0182	0.998	36.911	0.6412
Paso Marcos	XS02	0.992	31.928	0.4979	0.987	215.52	0.3115
	XS03	0.995	230.41	0.295	0.919	249.9	0.2989
Bajo Pacuare	XS02	0.844	53.99	0.2728	0.978	35.772	0.395
	XS08	0.998	26.554	0.607	0.998	25.978	0.6279
Bajo Pacuare por San Juaquin	XS02	0.778	88.538	0.163	0.961	14.145	0.5752
	XS03	0.989	8.1334	0.5956	0.999	10.267	0.565
	XS04	0.923	34.112	0.6259	0.943	155.7	0.2929
Mollejones Cañon	XS03	0.997	2.4817	0.741	1	2.372	0.7478
	XS04	0.998	0.6178	1.1015	0.998	2.4378	0.7494
Tres Equis	XS02	0.951	24.351	0.6198	0.932	26.728	0.04232
	XS03	0.77	103.62	0.1948	0.951	22.862	0.4365
	XS04	0.974	17.855	0.6081	0.924	40.1	0.3882
Bajo Tigre	XS03	0.972	58.732	0.5067	0.493	683.91	0.0811
	XS04	0.991	1279.8	0.2652	0.877	21924	0.429

The ratio of boundary shear stress to critical shear stress (τ_{cr}) for a defined grain size can be used to determine when excess shear stress ($\tau^* = \tau_o/\tau_{cr}$) exists and mobilization of bed material is expected to occur (Petit et al., 2015; Van Oost et al., 2004; Yager et al., 2007). When τ^* values are <1, bed material is stable; and when τ^* values are >1, bed material mobilization is expected to occur. Similar to others' work in coarse bedded and/or mountain streams (Buffington & Montgomery, 1997; Lamb & Fonstad, 2010; Lenzi et al., 2006; Lenzi et al., 1999; Lisle et la., 2000; Prancevic et al., 2014; Wohl, 2005), the critical shear stress (τ_{cr}) necessary to mobilize fractions of the bed material (D_{16}, D_{50}, D_{84}) was determined at each site with selective grain-size entrainment equations:

$$\tau_{cr} = \theta_c \, gD_i(p_s-p) \quad \text{(Shields, 1936)}$$

$$\tau_{cr} = 0.045(\rho_s-\rho)gD_{50}^{0.6} \, D_i^{0.4} \quad \text{(Komar, 1987)}$$

where θ_c is the dimensionless Shield criterion for initiating motion, g is the acceleration due to gravity, D_i is the diameter of the grain size of interest, ρ_s is sediment density, and ρ is density of the fluid. It has been observed that an increase in critical stress for incipient motion occurs with increasing channel slope. This occurs because as channel slope increases flow velocity also increases. This usually leads to an increase in local grain size and thus increased grain protrusion which results in increased turbulence and thus an increased ratio of flow depth to bed-roughness. (Galia & Hradecký, 2012; Mueller et al., 2005; Pitlick et al., 2008). In this study θ_c was calculated by utilizing the equation derived by Lamb et al. (2008):

$$\theta_c = 0.15S^{0.25}$$

where S is slope. Site averaged slope was used to find θ_c. Then, the discharge required to produce the necessary shear stress (Q_{cr}) to mobilize the D_{16}, D_{50}, D_{84} was calculated with the relationships presented in Table 0-6, inserting the τ_{cr} for each grain-size. The results are presented in Table 0-7 for both the Shields (1936) and Komar (1987) derived τ_{cr}.

Table 0-7. Critical shear (τ_{cr}) for selected grain size fractions using Shields (1936) and Komar (1987); the required discharge (Q_{cr}) to create that boundary shear stress at a cross section; the flow exceedence (% exc.) of the Q_{cr}; and the number of days per year the flow exeedence equates to.

Shields (1936)	$\tau_{cr} = \theta_c g D_i(ps-p)$ - using Lamb et al. (2008) $\theta_c = 0.15S^{0.25}$											
	D_{16}			D_{50}				D_{84}				grain mobilization
Site and Cross Section	B-axis (m)	Q_{cr}	% exc	B-axis (m)	Q_{cr}	% exc	#day/yr	B-axis (m)	Q_{cr}	% exc	#days/yr	SfM validate
Arriba Pacuare XS04	0.017	0.15	100	0.014	11.58	74.75	272.8	0.59	222.81	0.12	0.4	na
Arriba Pacuare XS07	0.017	0.36	100	0.014	8.24	86.09	314.2	0.59	70.34	1.76	6.4	na
Paso Marcos XS02	0.0031	0.01	100	0.051	2.64	100	365.0	0.43	191.12	0.28	1.0	yes
Paso Marcos XS03	0.0031	0.00	100	0.051	0.01	100	365.0	0.43	8.75	94.25	344.0	no
Bajo Pacuare XS02	0.0031	0.00	100	0.15	36.06	35.23	128.6	0.53	671.27	0.01	0.0	na
Bajo Pacuare XS08	0.073	4.31	100	0.31	46.67	19.5	71.2	0.78	184.87	0.25	0.9	yes
Bajo Pacuare por San Juaquin XS02	0.048	0.01	100	0.13	4.24	100	365.0	0.36	214.61	0.34	1.2	yes
Bajo Pacuare por San Juaquin XS04	0.048	1.36	100	0.13	6.69	99.68	363.8	0.36	34.04	50.58	184.6	yes
Tres Equis XS03	0.0032	0.00	100	0.062	0.04	100	365.0	0.4	515.09	0.57	2.1	no
Tres Equis XS04	0.0032	0.05	100	0.062	6.19	100	365.0	0.4	132.85	2.15	7.8	yes
Bajo Tigre 03	0.068	1.03	100	0.19	7.82	99.85	364.5	0.45	42.88	50.04	182.6	yes
Bajo Tigre 04	0.068	0.00	100	0.19	0.00	100	365.0	0.45	0.01	100	365.0	yes

Komar (1987)	$\tau_{cr} = 0.045(ps-p)gD_{50}^{0.6}D_i^{0.4}$											
	D_{16}			D_{50}				D_{84}				grain mobilization
Site and Cross Section	B-axis (m)	Q_{cr}	% exc	B-axis (m)	Q_{cr}	% exc	#day/yr	B-axis (m)	Q_{cr}	% exc	#days/yr	SfM validate
Arriba Pacuare XS04	0.017	1.48	100	0.014	8.38	85.85	313.4	0.59	27.35	28	102.2	na
Arriba Pacuare XS07	0.017	1.86	100	0.014	6.52	92.45	337.4	0.59	15.37	61.75	225.4	na
Paso Marcos XS02	0.0031	0.70	100	0.051	6.60	98.76	360.5	0.43	36.59	30.92	112.9	no
Paso Marcos XS03	0.0031	0.00	100	0.051	0.03	100	365.0	0.43	0.54	100	365.0	no
Bajo Pacuare XS02	0.0031	0.72	100	0.15	31.86	43.12	157.4	0.53	109.39	1.04	3.8	na
Bajo Pacuare XS08	0.073	8.08	97.42	0.31	20.95	67.89	247.8	0.78	38.47	30.92	112.9	yes
Bajo Pacuare por San Juaquin XS02	0.048	0.53	100	0.13	40.48	39.68	144.8	0.36	82.19	6.41	23.4	yes
Bajo Pacuare por San Juaquin XS04	0.048	3.89	100	0.13	7.35	99.41	362.8	0.36	14.09	88.28	322.2	no
Tres Equis XS03	0.0032	0.00	100	0.062	0.44	100	365.0	0.4	20.34	83.8	305.9	yes
Tres Equis XS04	0.0032	1.98	100	0.062	13.88	94.27	344.1	0.4	47.31	42.36	154.6	yes
Bajo Tigre 03	0.068	2.41	100	0.19	5.42	100	365.0	0.45	10.71	98.8	360.6	yes
Bajo Tigre 04	0.068	0.00	100	0.19	0.00	100	365.0	0.45	0.00	100	365.0	yes

Grain mobilization was verified with the high-resolution repeat photogrammetric topographic SfM surveys described in Section 3.2.2. The high-resolution of the SfM DEMS and ortho-photos permitted identification of gain or loss of single-grains of gravel to boulder sized material (Figure 0-12). This was done by executing a change analysis in ArcMap (Grabowski et al. , 2014; James et al., 2012; Picco et al., 2013) conducted on the pre and post flood DEMs produced for the T-day Flood event. This technique also identifies areas of elevation loss (scour) and/or gain (deposition). The B-axis of the largest identified mobilized grain(s) was measured from the SfM orthophotos in GIS. Table 0-7 presents the results of the analysis of SfM identified max grain size mobilized. Both selective grain-size entrainment equations performed well. However, based on the SfM analysis results the Shield equation with the slope-derived Shield's parameter was accurate at seven of the nine sites analyzed and the Komar equation was accurate at six. Photo surveys were conducted pre and post the 2013 T-day Flood. Based on the flow duration curve, the T-day Flood has an 18% exceedance probability (~ 65 days/year).

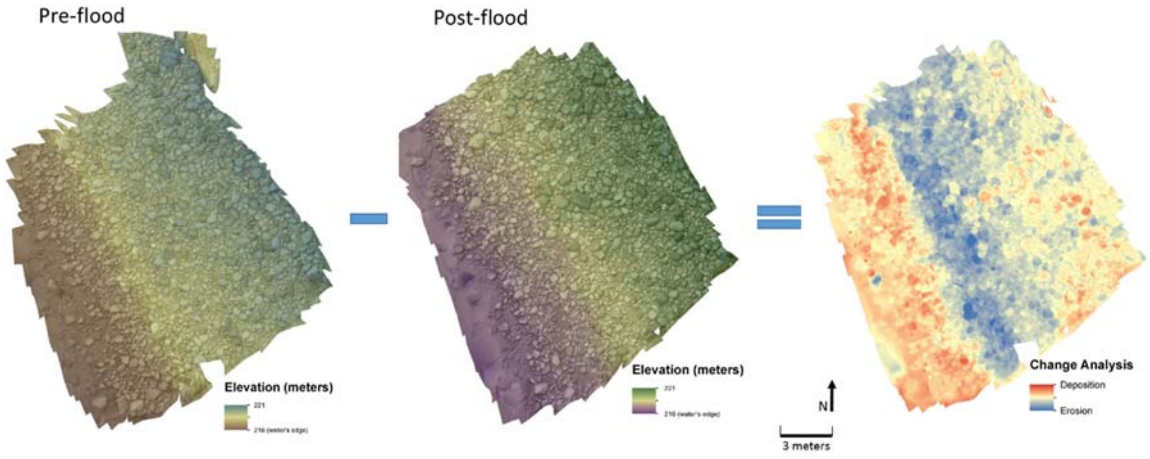

Figure 0-12. Example of GIS Change Analysis (DEM of difference) from SfM repeat photogrammetric survey pre and post the T-day flood. At field site Bajo Tigre – 12x18m survey unit.

3.2.4 Stream Power

Controlled by slope and discharge, stream power characterizes the energy a flow event has to perform work (sediment transport or erosion) on the channel bed it moves through (Knighton, 1998). Stream power, a function of discharge, slope, and channel

geometry, was calculated for each site to aid in characterizing the dominant hydraulic and/or geomorphic variables responsible for downstream patterns of sediment transport. The total cross sectional stream power (Watts/m (Ω)) and unit stream power (Watts/m^2 (ω)) (as defined by (Rhoads, 1987)) for the 0.2% (1 day/yr), 2.0% (7 days/yr), and 20% (73 days/yr) exceedance flows were calculated using the equations:

$$\Omega = \rho g Q S$$

$$\omega = \Omega / w$$

where ρ is density of fluid, g is acceleration due to gravity, Q is discharge, S is slope, and w is channel width. Site slope for each modeled flood was determined using the HEC-RAS produced energy gradient elevations of the upstream and downstream-most cross sections and the total length of the site between those cross sections. Site width was averaged from all cross sections surveyed at the field site for each modeled flow. These are presented along with the sediment transport rate (kg/sec) (method described below in Section 3.2.5) for those discharges at the representative cross sections (Table 0-8).

Table 0-8. Stream power at each field site for select flow events and the estimated sediment transport rate (kg/sec) at the best representative cross section for each site.

			0.2% exc. (~1 day/yr)			at	Sed Trans	2.0% exc. (~7 days/yr)			at	Sed Trans	20% exc. (~73 days/yr)			at	Sed Trans
Site	Rkm	Site Slope	Q (cms)	Ω (Watts/m)	ω (Watts/m^2)	XS	kg/sec	Q (cms)	Ω (Watts/m)	ω (Watts/m^2)	XS	kg/sec	Q (cms)	Ω (Watts/m)	ω (Watts/m^2)	XS	kg/sec
Arriba Pacuare	106.4	0.04	169	63784	1296	4	240	68	23752	627	4	97	32	11037	394	4	15
Paso Marcos	93.75	0.03	223	76808	1437	3	712	92	30206	659	3	20	44	13968	335	3	1
Bajo Pacuare	90.5	0.02	203	47653	1024	2	318	90	20136	515	2	69	46	9985	289	2	8
Bajo Pacuare	90.5	0.02	203	47653	1024	8	197	90	20136	515	8	15	46	9985	289	8	1
Bajo Pacuare por San Juaquin	82.6	0.01	272	28059	461	2	1093	114	11026	202	2	127	56	5700	140	2	23
Mollejones	74.9	0.01	296	26484	552	na	na	126	8675	199	na	na	62	3349	89	na	na
Tres Equis	66.25	0.02	319	50429	455	3	1414	137	25988	412	3	972	69	14208	371	3	249
Bajo Tigre	62.5	0.02	325	69362	1115	3	9283	140	32665	671	3	1450	70	16431	468	3	203

3.2.5 Sediment Transport Rating Curves

Sediment transport rating curves were created using the Recking (2013) transport model developed for coarse-bedded channels. The Recking model was selected for use because it requires surface, not sub-surface, grain-size fractions and it was developed for coarse bedload transport in steep mountain rivers. Although Recking's model is relatively new, it has been successfully implemented and evaluated in other studies (Anderson & Pitlick, 2014; Heimann et al., 2015; Kitsikoudis et al., 2014; Pourhoseinet al., 2015). In

addition, it has proven to be a good fit for modeling sediment transport in montane rivers of Costa Rica, compared to other methods (Arrieta, 2016).

Referred to as the "Simple Model," Recking's transport model is a non-threshold set of equations based on the surface grain sizes and slope. It uses dimensionless parameters for shear stress and bedload transport and assumes that sediment mobility is controlled by the D_{84}, integrating a ratio between the D_{50} and D_{84} into the equation. Similar to how Lamb et al. (2008) recognizes an increasing critical shear in increasing slope to identify initial motion, the Simple Model is designed to predict an increasing critical shear stress (based on the Shields parameter) with increasing slope to capture sediment flux. The Simple Model is constructed to represent two-phase transport and the transition between partial and full-bed mobilization. Rating curves were created with simple power functions rather than transport thresholds, as Barry (Barry et al., 2004) and Recking (2013) recommend for best results.

On the Rio Pacuare, for each modeled cross section, two transport rating curves were created using a power function. Example rating curves for field site Arriba Pacuare (AP) are provided in Figure 0-13 (See Appendix C for all sites). The two rating curves reflect the high-flow and low-moderate flow discharges modeled in HEC-RAS (> or < 0.8% exceedance flow). Hydraulic radius, channel width, and energy gradient slope are the hydraulic variables extracted from HEC-RAS model results and used in Recking's Simple Model. The Simple Model produces an instantaneous transport rate expressed in kg/sec. The sediment transport rate per 8-hour sub-daily period was calculated, and then the daily rate (tons/day) was computed by adding the transport for the three 8-hour sub-daily periods. This was done for six sites (AP, PM, BP, BPSJ, TE, and BT) for the 51 complete years of reported daily data (1959-1990, 1993-1994, 1996-2012).

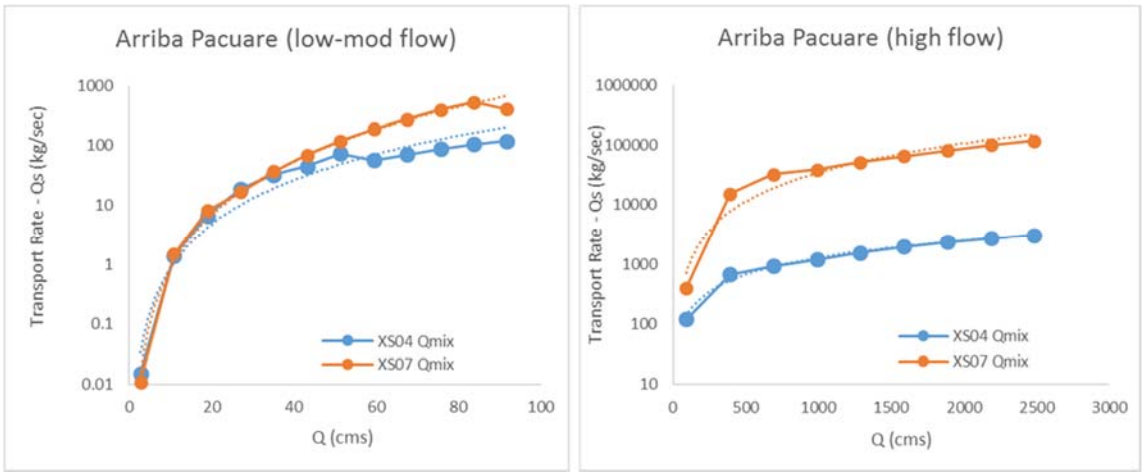

Figure 0-13. Example sediment transport rating curves for low-moderate flow and high flow at field site Arriba Pacuare (AP) located at Rkm 106.4.

The Recking Model is designed to produce a mean transport rate for each discharge input into the model. However, estimating a factor of uncertainty or potential range (maximum and minimum transported) is not possible without access to physically measured bedload transport for comparison. Pourhosein et al. (2015) report a standard deviation of variation coefficient for a ratio of calculated bedload transport to measured transport of only 1.18 using the Recking Model on the Babolroud River in Iran. When comparing the accuracy of transport models to observed bedload transport on the Tahoma Creek in Washington, Anderson and Pitlick (2014) report that Recking's Simple Model produced better results than the other models, but it still overestimated transport at low flows and underestimated transport at high flows. On the Rio Pacuare, cross sections located at the same field site can produce annual sediment transport capacity estimates that are notably different (Table 0-9).

Table 0-9. Resulting rating curve parameters using Recking's (2013) Simple Model. Average annual sediment transport capacity (million tons/year) for all of the modeled cross sections at all field site.

Cross Section	flow range	R^2	$q_s = aq^b$ (kg/sec)		Average Annual Sediment Transport Capacity 1959-2012 (million tons/year)	River km (from mouth)
			a	b		
AP-XS04*	high	0.991	1.8509	0.9481	0.40	106.47
	low-mod	0.963	2.90E-03	2.4728		
AP-XS05	high	0.990	1.47E+00	1.1386	0.50	106.44
	low-mod	0.983	1.70E-03	2.644		
AP-XS06	high	0.964	0.9553	1.2806	0.60	106.43
	low-mod	0.990	1.80E-03	2.6483		
AP-XS07	high	0.947	0.4777	1.6217	1.30	106.42
	low-mod	0.994	8.00E-04	3.0182		
PM-XS02	high	0.986	4.2976	1.1213	1.90	93.79
	low	0.998	2.00E-03	2.7311		
PM-XS03*	high	0.815	0.0023	2.3375	0.40	93.75
	low-mod	0.991	2.00E-06	3.5602		
BP-XS02*	high	0.987	6.10E-01	1.1776	0.30	90.53
	low-mod	0.999	5.00E-05	3.1417		
BP-XS04	high	0.968	4.00E-03	2.0507	0.10	90.47
	low-mod	0.987	4.00E-05	2.8627		
BP-XS05	high	0.976	3.00E-04	2.3854	0.05	90.44
	low-mod	0.990	4.00E-10	5.1893		
BP-XS08*	high	0.997	3.00E-04	2.5209	0.10	90.35
	low-mod	1.000	2.00E-06	3.5108		
BPSJ-XS02*	high	0.936	0.3191	1.4521	0.80	82.62
	low-mod	0.993	1.30E-03	2.4245		
BPSJ-XS03	high	0.997	4.57E-02	1.935	2.30	82.59
	low-mod	0.978	3.24E-02	1.9177		
BPSJ-XS04	high	0.943	9.9341	1.1181	6.80	82.55
	low-mod	0.904	8.60E-03	2.549		
MC-XS02 (shelf deposit)	high	0.987	3.00E-07	3.0358	0.01	74.94
	low-mod	0.995	2.00E-08	3.4005		
MC-XS03 (shelf deposit)	high	0.982	6.00E-11	4.6115	0.01	74.92
	low-mod	0.997	3.00E-07	3.0148		
MC-XS04 (shelf deposits)	high	0.976	2.00E-07	3.069	0.01	74.90
	low-mod	0.993	3.00E-14	6.1007		
TE-XS02	high	0.966	3.7718	1.107	11.80	66.31
	low-mod	0.935	0.1617	1.9077		
TE-XS03*	high	0.980	1.6298	1.1733	5.40	66.27
	low-mod	0.942	0.6110	1.9669		
TE-XS04	high	0.965	6.5094	1.0466	7.10	66.24
	low-mod	0.978	0.0244	2.2376		
BT-XS03*	high	0.840	40.7980	0.9382	5.00	62.55
	low-mod	0.996	0.0011	2.8529		
BT-XS04	high	0.653	203.43	0.5935	1.90	62.51
	low-mod	0.944	1.00E-06	3.7811		

* denotes the selected representative cross section (XS_{rep}).

Some of this range is assumed to result from hydraulic and topographic differences between the cross sections. However, some differences are expected to result from compiled model error. To normalize model uncertainty across the entire study area, the percent difference was calculated between the highest transport rate produced at a single cross section at each site and the rates calculated for the other cross sections at the same field site. The results vary among cross sections at a site by up to a factor of 5, fairly typical for coarse bedload modeling (Barry et al., 2004; Buffington & Montgomery, 1997; Vázquez-Tarrío & Menéndez-Duarte, 2015). When the percent differences for the cross sections at a site are combined with all other percent differences from the other sites, the combined average percent difference is 50% for the sites in the study area.

3.3 RESULTS

Table 0-9 above presents the average annual sediment transport capacity (million tons/year) calculated at all the modeled cross sections at all seven of the field sites established on the Rio Pacuare. The results of the gravel counts and grain size distribution for each site are presented in Table 0-10.

Table 0-10. Gravel Count grain-size fraction distribution at all field sites. Completed 2013.

		B-axis Diameter (mm)							
Site	River km	D16	D50	D84	% sand	% gravel	% cobble	% boulder	# of samples
Bajo Tigre	62.5	68	190	450	0	15	45	41	218
Tres Equis	66.25	3.2	62	400	0	51	27	23	229
Mollejones Cañon - *shelf deposit*	74.9	44	290	900	0	25	21	54	141
Bajo Pacuare por San Juaquin	82.6	48	130	360	0	23	49	28	205
Bajo Pacuare 01	90.35	73	310	780	0	13	32	56	183
Bajo Pacuare 02	90.5	3.1	150	530	0	34	23	43	136
Paso Marcos	93.75	3.1	51	430	0	55	25	19	251
Arriba Pacuare	106.4	17	140	590	0	32	33	35	222

The average annual sediment transport capacities (Table 0-9) combined with size-range of the active bedload (Table 0-10) indicate that the Rio Pacuare has relatively high bedload transport capacity (0.01 to 11.8 million tons/ year) of coarse-grained material throughout the study area. The results also show that sediment transport capacities do not follow a normal downstream trend of increasing sediment flux. The range of transport

capacities calculated at different cross sections located at the same field site is likely the result of variations in local channel hydraulics (i.e. slope for pool vs riffle), differences in cross section geometry, the sensitivity of the model to those variations, and inherent model inaccuracy described previously.

To evaluate the plausibility of the sediment transport capacity results (see Table 0-9) a very simplified sediment budget based on generalized assumptions regarding landscape denudation and sediment storage was constructed. First, assuming that the watershed maintains a general equilibrium between uplift rates and landscape denudation (Reneau & Dietrich, 1991), the potential hillslope inputs per year were calculated based on long-term uplift rates combined with upstream drainage area. Since no uplift or landscape denudation rate was found specifically for the Rio Pacuare, a 1mm/yr reported for the high central Talamanca Mountains is applied (Driese et al., 2007). The upstream drainage area for the downstream most field site at Bajo Tigre is used (575 km^2). The resulting potential volumetric output of 575,000 m^3 is converted to mass by multiplying with a general bulk density of 2500 kg/m^3 for a total of 1.4 billion kg, or 1.4 million metric tons of material potentially supplied to the stream per year.

Next, an in-channel sediment storage capacity for the length of the channel upstream of Bajo Tigre was estimated. Channel length (~70 Rkm) was multiplied by average channel width (50m) and an estimated depth of the available bedload of 5m and 3m for a resulting sediment mass of $17.5x10^6m^3$ and $10.5x10^6m^3$, respectively. The same bulk density was used and the results multiplied by 0.21 to adjust for porosity (Bunte & Abt, 2001) for a total of $5.5x10^9$kg and $9.2x10^9$kg respectively, or 5.5 and 9.2 million tons of sediment storage capacity within the active channel, assuming no net increase or decrease in sediment stored over time. The 1.4 million tons/yr potentially produced from the hillslopes is of the same magnitude but smaller than the transport capacities calculated at Bajo Tigre (1.9 and 5.0 million tons/yr). The estimated storage capacity (5.5 and 9.2 million tons) is also of the same magnitude as the calculated transport capacity at Bajo Tigre.

This general evaluation confirms the plausibility of the sediment transport capacity results by having inputs, storage and transport capacity values within the same order of magnitude, which is considered good for bedload transport modeling. However,

the small imbalances reveal potential uncertainties of either an over prediction in transport capacity by the Recking (2013) model, oversimplification in the assumptions used in developing the hillslope and storage components, or both. It is also important to note that sediment transport capacity is not necessarily equivalent to transport rates. Assuming inputs, storage, and transport capacity estimates are representative, sediment flux patterns would then likely result in periodic sediment accumulations where transport capacity is less than upstream, and periodical exposure of bedrock where inputs and storage are less than transport capacity. The similarity in storage and transport capacities suggests bedload replacement occurs relatively regularly. This also supports some degree of bedrock incision occurring during bed mobilizing discharge events. When combined, these variables explain the fairly linear longitudinal profile of the watershed which lacks obvious knickpoints regardless of active faulting and variability in bedrock resistance.

The sediment transport capacities estimated for the Rio Pacuare are generally higher than rates reported in non-tropical or arid mountain streams with coarse bedload (Lenzi et al., 1999; McLean et al., 1999; Rainato et al., 2016; Ryan et la., 2005; Wallick & O'Connor, 2011). The few available studies done on bedload transport in other humid tropical rivers such as the Ping, Wang, Yom, Nan rivers of the upper Chao Phraya basin in Thailand (Bidorn et al., 2015) and the Mae Sa River in northern Thailand (Ziegler et al., 2014) also report high bedload transport rates. Arrieta (2016) also communicated that the transport rates produced from this research are similar to unpublished results on other montane Costa Rican rivers. Thus the sediment transport capacities presented here are considered plausible values in which to characterize and discuss sediment flux in the Rio Pacuare.

The sediment transport capacity generated at the Mollejones Cañon (MC) field site are included in Table 0-9 but the results are considered greatly underestimated and thus unusable for evaluating downstream trends or flux through the site. The absence of exposed bars in Mollejones Cañon except at very low flow periods and the deep, confined channel shape in this segment where access was possible prevented collection of a gravel count from the channel bed during field work. The field site here includes a bedrock shelf topped with a single layer of coarse flood-wash deposits that, based on changes observed after a high flow, are likely armored by having the smaller grain

fractions plucked from the site. Therefore the grain-size distribution used in the transport model at MC is not representative of the plentiful bedload observed being flushed (auditory-saltation and visibly altered submerged bedforms) through the canyon at high flow. Accumulation of cobble-boulder bedload were observed at this site at or below the surface of the water at moderate and low flows.

To simplify the presentation and discussion of the magnitude variations in sediment transport capacities as well as the spatial and temporal variations through the study area, discussion will now focus on the results of the single representative cross section (XS_{rep}) from each field site. In addition to being included in the gravel-count area, and having a regular topographic shape, the water surface slope of the XS_{rep} is most similar to the site-averaged slope. Cross-section slope was determined by the field-surveyed difference in elevation of the cross section above and below the cross section of interest and the gain in elevation over that distance. Note that field site Bajo Pacuare has two XS_{rep}, because that site contains a depositional bar along river-right in the upstream section (BP-XS02) and another along river-left in the downstream section (BP-XS08).

Sections 3.3.1 presents the results related to the variations in the magnitude of sediment transport capacity over time. Section 3.3.2 presents the spatial variations in transport capacity through the study area. Section 3.3.3 presents temporal patterns focused on the seasonality (dry vs wet) of sediment transport capacity trends.

3.3.1 Magnitude

The magnitude of difference in annual sediment transport capacity characterizes the potential range in sediment flux that can occur at a cross section. **Error! Reference source not found.**Table 0-11 presents the two highest and two lowest calculated annual sediment transport rates at the XS_{rep} for each site, along with the average annual sediment transport capacity (tons/year). Since bedload transport directly correlates to discharge, the wide range of calculated annual sediment transport capacity demonstrates the variability in the precipitation-induced hydrologic regime of the Rio Pacuare. The sites with the greatest range reveal where sediment flux is more dependent on large flow events (PM, BP-XS08, and BPSJ).

Table 0-11. Average annual, highest, and lowest annual estimated sediment transport capacities (million tons/year) at the XS_{reps}.

			Annual Bedload Sediment Transport Capacity (million tons/year)							
Site	XS_{rep}	Avg Annual Sediment Transport (mil tons/year)	Highest	year	Next Highest	year	Lowest	year	Next Lowest	year
Arriba Pacuare (AP)	4	0.4	1.60	1970	0.70	1975	0.10	1985	0.20	2001
Paso Marcos (PM)	3	0.4	12.20	1970	0.80	1975	0.01	1985	0.02	1977
Bajo Pacuare (BP)	2	0.3	1.60	1970	0.60	1975	0.08	1985	0.10	1977
Bajo Pacuare (BP)	8	0.1	2.30	1970	0.30	1975	0.01	1985	0.02	1977
Bajo Pacuare por San Juaquin (BPSJ)	2	0.8	6.40	1970	1.60	1975	0.20	1985	0.30	1977
Tres Equis (TE)	3	5.4	14.00	1970	8.10	1968	2.80	1985	3.00	1977
Bajo Tigre (BT)	3	5.0	28.50	1970	10.40	1975	1.70	1985	1.80	1977

The highest annual transport capacity at all sites occurred in 1970. In 1970, several large flow events occurred, including the largest discharge event on record which occurred between April 8 and 17—during what is normally considered the dry season. Interestingly, record has yet been found that correlates The April 8th -17th discharge to a recorded tropical storm event. Historical records of tropical storms and hurricanes indicate that 1969-1970 was an active storm year (Longshore, 2010), listing Hurricane Martha making landfall as a tropical storm in late November 1969, and delivering large quantities of rain to Panama and Costa Rica that resulted in widespread landslides. In May 1970, Hurricane Alma formed in the southwestern Caribbean, spurring some precipitation events in Costa Rica. A signal from both of these storms is evident in the flow record by an increase in the reported daily discharge values. However, the April 1970 flow event is 4.5 times larger than what was produced as a result of the recorded hurricanes. Historical daily discharge data from two gages (Pascua and Angustora) on the neighboring Rio Reventazon also report the early April 1970 anomalously large flood event. This indicates that the flood was most likely generated by a locally formed weather system over the central Talamanca Mountains. This also represents the capacity of tropical climate patterns in this region to generate high-intensity localized events that can result in high-magnitude floods. Something of this scale likely required the combination of climate patterns—generated from weather conditions from the Pacific interacting with ITCZ weather patterns from the Atlantic (Enfield & Alfaro, 1999; Giannini et al., 2000)—converging over the high central ridges of the Talamanca Mountains.

Examples of the relationship between sediment rates and discharge at two different cross sections are provided in Figure 0-14 (see Appendices D for rating curves for all XS_{rep}). The pattern of transport rate to discharge varies at each cross section because site-specific components such as available sediment size, site slope, cross-section hydraulics, and channel geometry are integrated into Recking's (2013) Simple bedload transport model. Some cross sections express a non-linear pattern while others express an almost linear pattern in the relationship between sediment transport rates (kg/sec) and discharge.

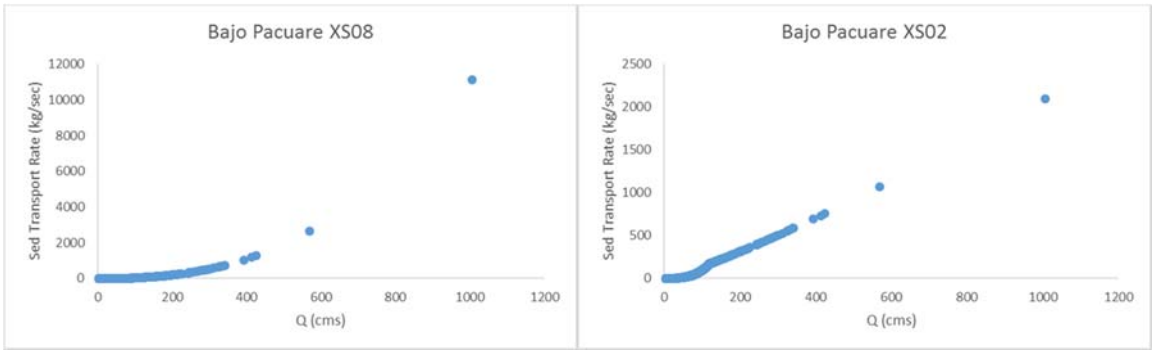

Figure 0-14. Examples of the sediment transport rate (kg/sec) vs discharge (cms) at two XS_{rep}.

Figure 0-15 provides an example of the potential cumulative total sediment transported (tons) over the period of record (51 years) for the same two XS_{rep} shown in Figure 0-14 (See Appendices E for cumulative plots for all XS_{rep}). The pattern of potential cumulative sediment flux is not the same among sites, again due to site-specific discharge, grain size, channel geometry, and hydraulic conditions. For example, at BP XS08 sediment transport is non-linear and a stair-step pattern is expressed in sediment transport capacity associated with large magnitude flood events, such as the 1970 flood. At TE XS03 less exaggerated increases in the relative sediment transport capacity occurs during large flood events than at BP XS08. At TE XS03 the general overall-trend in cumulative sediment flux has a more linear expression, indicating less dependence on large-magnitude flows to mobilize the available bedload. This also indicates potential for a more frequently active bedload at cross sections with a more linear sediment transport relationship to discharge.

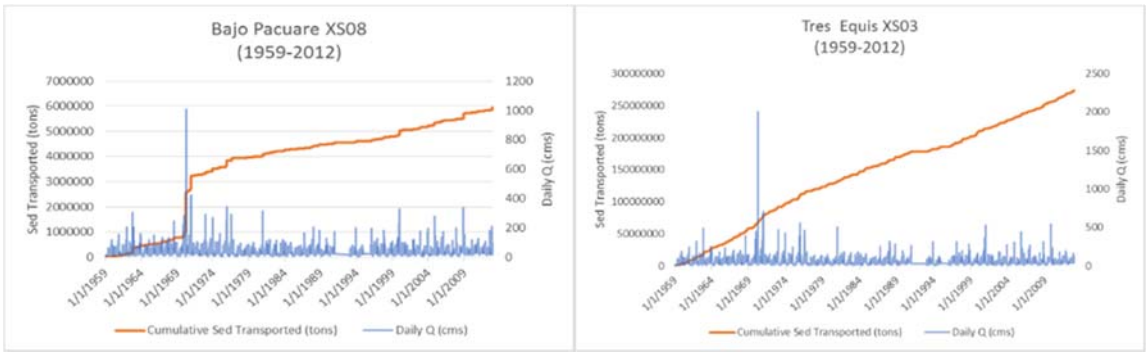

Figure 0-15. Examples (BP XS08 and TE XS03) of cumulative bedload sediment transported and daily discharge values over the period of record (1959-2012).

3.3.2 Spatial Variability

The average annual sediment transport capacity at the XS_{rep} from each field site on the Rio Pacuare do not increase in a normal downstream pattern with increasing discharge. And, the downstream pattern between the sites is inconsistent, depending on the magnitude of the flow event. For example, The XS_{rep} at the Paso Marcos (PM) site has a greater annual sediment transport capacity compared to the upstream XS_{rep} at the Arriba Pacuare (AP) site during high sediment flux (high discharge) years, but the results are reversed during low sediment flux years (See Table 0-11). Similarly, the XS_{rep} at the Bajo Tigre (BT) site has a greater annual sediment transport capacity compared to upstream at Tres Equis (TE) during high sediment flux (high discharge) years, but less during low sediment flux years. These variations are most likely related to site-specific slope and how site-averaged wetted channel width and depth relationships vary at each site. Table 0-12 presents the site-averaged wetted channel width and depth, as modeled in HEC-RAS, for three high flow events (0.2, 2.0, and 20% flow exceedance discharge) and the lowest flow (99.9% flow exceedance discharge) modeled. As expected, the XS_{rep} with the least amount of change in channel width from high flow and low flow events shows the greatest changes in flow depth.

Table 0-12. Site slope and site-averaged channel width and depth (meters) for selected flow exceedence discharges (modeled in HEC-RAS).

			0.2% Exc Q		2.0% Exc Q		20% Exc Q		99.9% Exc Q	
Site	Rkm	Site Avg Slope	Avg width (m)	Avg depth (m)	Avg width (m)	Avg depth (m)	Avg width (m)	Avg depth (m)	Avg width (m)	Avg depth (m)
AP	106.4	0.038	49.21	2.18	37.86	1.49	28.02	1.15	10.73	0.68
PM	93.7	0.034	53.44	1.65	45.85	1.06	41.68	0.74	11.8	0.23
BP	90.4	0.023	46.53	2.29	39.11	1.61	34.57	1.19	31.03	0.28
BPSJ	82.6	0.01	60.91	2.19	54.51	1.44	40.83	1.21	29.95	0.32
MC	74.9	0.01	47.99	3.69	43.49	2.45	37.44	1.85	23.5	1.09
TE	66.2	0.019	110.95	2.36	63.14	1.93	38.29	1.76	21.92	0.46
BT	62.5	0.023	62.22	3.38	48.70	2.42	35.07	2.00	12.62	0.79

As a function of slope, stream power expresses a similar non-normal downstream pattern between the study sites, as do sediment transport capacity. The total cross sectional stream power (Ω) and the unit stream (ω) for the three high-flow events (0.2%, 2.0% and 20% exceedance flows) at each field site are represented in Figure 0-16. The stream power values presented here, although high for non-tropical rivers, are comparable to values reported by Wohl (2005) on the Rio Changiunola, a montane tropical river located in the eastern Talamanca Mountains of Panama. Similarly, Fonstad (2003); mountains streams in the Sangre de Cristo Mountains, NM) and Knighton (1999); Trent River, UK) found that maximum stream power is not always attained at mid-basin, as expected.

At the field sites modeled on the Rio Pacuare, maximum unit stream power is found at the upstream sites where slope is greatest and channel width is narrow, and at the downstream-most site where slope is reduced but discharge is greatest and width is moderate. It should be noted that the pattern expressed by the seven field sites used for this study does not reflect the overall pattern in unit stream power for the study area presented in Chapter II (this dissertation), where mid-study river segment values are higher on average than downstream areas. This again confirms the dependence of site-specific hydraulics (including stream power) on sediment transport capacity through a specific site. And, it illustrates the potential spatial variability of sediment flux at and between the field sites – depending on the discharge that is occurring.

.

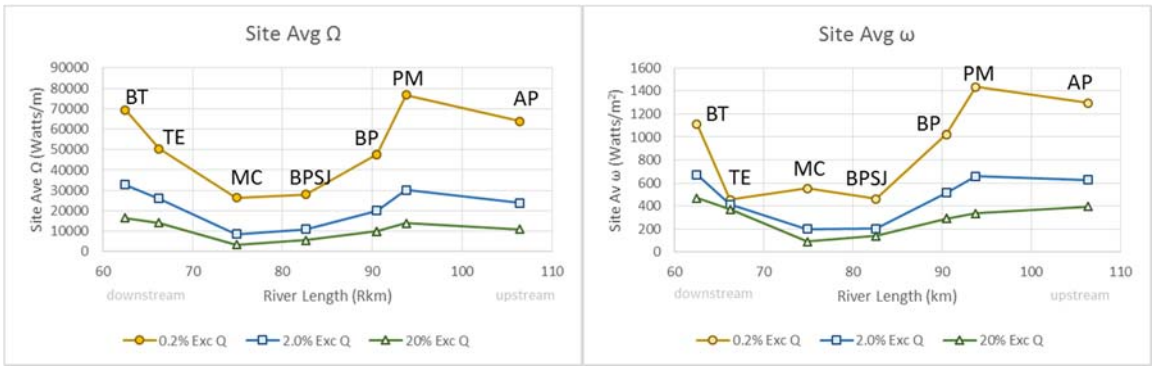

Figure 0-16. Total cross sectional stream power (Ω) and the unit stream (ω) for three high-flow events (0.2%, 2.0% and 20% exceedance flows) at each field site. See Table 0-8.

Stream power is used here to aid in characterizing the dominant hydraulic and/or geomorphic variables (discharge, slope, or site characteristics) responsible for the downstream patterns of sediment transport expressed at the representative cross section for each field site. When unit stream power (flow competence) and total stream power are plotted against the sediment transport capacity for each of the three flows at the XS_{rep} on a log-normal axis (Figure 0-17), a general expected pattern of increased bedload transport rate (kg/sec) with increased stream power emerges. However, the plots also show that sites with similar stream power can produce different transport capacities. This indicates that, although stream power and bedload transport are both a function of discharge and slope, variations in grain size also effect sediment transport capacity, as represented in the Recking (2013) model. For example, site-specific changes in flow stage and cross-section topography -– such as energy gradient and depth – effect a flow's shear stress and thus it's potential to mobilize the available bedload.

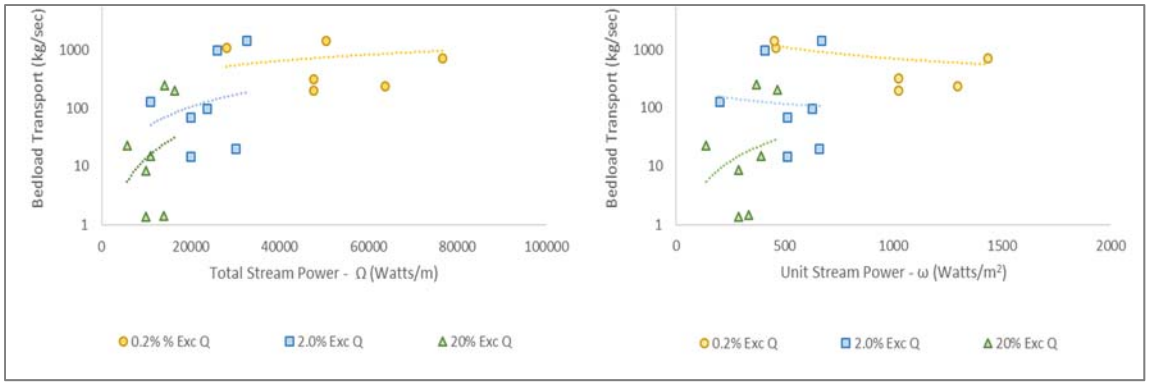

Figure 0-17. Bedload transport rate (kg/sec) vs total and unit stream power for the 0.2%, 2.0%, and 20% exceedance discharge values at the XS_{rep} for six field sites.

If the average annual sediment transport capacity for each site is normalized by upstream drainage area, a similar but slightly different spatial pattern is expressed. Table 0-13 offers the potential annual sediment yield for each site by using the upstream drainage area and the average annual sediment transport rate. The yields for the two downstream sites (BT and TE) are notably larger than the others. This supports transport capacity increasing with increasing downstream discharge as upstream drainage area increases. However, the upstream-most site (AP) is higher than the next three downstream sites. This supports an increased sediment transport capacity where unit stream power (higher slope and less channel width) increases. Thus, sediment transport through the system are spatially dependent on available discharge as well as unit stream power.

Table 0-13. Average annual sediment yield (tons per year/km^2) for the XS_{rep} for each site.

Site	Avg Annual Sed Transport Capacity (million tons/year)	Drainage Area (km2)	Potential Avg Annual Yield (tons km^{-2}y^{-1})
Arriba Pacuare	0.4	244	1639
Paso Marcos	0.4	351	1140
Bajo Pacuare upper	0.3	367	817
Bajo Pacuare lower	0.1	367	324
Bajo Pacuare por San Juaquin	0.8	454	1762
Tres Equis	5.4	561	9626
Bajo Tigre	5.0	575	8696

A comparison of the annual bedload yield estimates for the Rio Pacuare with other humid-region rivers is presented in (Table 0-14). The other rivers in the table were selected because they have some similar characteristics to the Rio Pacuare but none match the size, gradient, and vegetation cover. What is obvious from the table is that there is a wide variability in yield rates from tropical mountain rivers. Also, the Rio Pacuare, though in the higher yield values, is within the range of yields reported. However, the quality of the data used in this table is unknown. Several of the sources are from unreviewed reports and conference proceedings as compiled in (Ziegler et al., 2014), except for the cited source for the Marsyandi River in Nepal. The lack of published articles on bedload yields in humid tropical montane rivers requires the use of secondary sources at this point in time. This reveals the notable lack of information on bedload transport in humid topical montane systems and the great need for additional research of these systems.

Table 0-14. Annual bedload yields (tons $km^{-2}y^{-1}$) report for the Rio Pacuare and other rivers located in humid tropical montane regions of the world.

River and Location	Area (km^2)	Bedload yield (tons $km^{-2}y^{-1}$)	notes
Rio Pacuare, Costa Rica	244-575	324-8696	this study
Batangsi, Malaysia [1]	20	1264	steep, rainforest, sand-boulder bedload
Chongkak, Malaysia [1]	13	334-619	steep; sand-boulder bedload
Mae Thang, Thailand [2]	121	2013	mixed ag vegetation; bedrock is limestone & sedimentary
Huay Ma Feung, Thailand [3]	1.2	8395	road construction; bedrock is sandstone & gneis
Laclo & Caraulum, Timor Leste [4]	580-1386	360-3988	erosive landscape with landslides
Marsyandi, Nepal [5]	4800	1083	bedrock is meta-sedimentary and granite
Choshui, Taiwan [6]	3155	913-2107	steep gradient; tectonically active

NOTE: as listed in (Ziegler et al., 2014): 1) (Lai et al., 1995), 2) (Janeau et al.r, 2003), 3) (Henderson & Witthawatchutikul, 1984), 4) (Alongi et al., 2009), 5) (Pratt-Sitaula et al., 2007), 6) (Yeh et al., 2010).

3.3.3 Temporal Variability

Annual channel discharge in this region fluctuates due to annual variations in the hydrologic c regimes, or the amount of precipitation delivered to the watershed (J. D. Restrepo & Kjerfve, 2000). Variations in the hydrologic regime is reflected with variations in the potential annual sediment transported. he annual sediment transport capacity (tons/year) for the years of recorded discharge is provided in Figure 0-18 for the

XS_{rep} at field sites AP, PM, BP, BPSJ, TE, BT. An oscillating pattern of low-flux and high-flux years emerges from the graph. Not surprising, the year of greatest annual sediment transport capacity (1970) is associated with the year that generated the largest magnitude flow event on record plus a sequence of additional tropical storms in the same year.

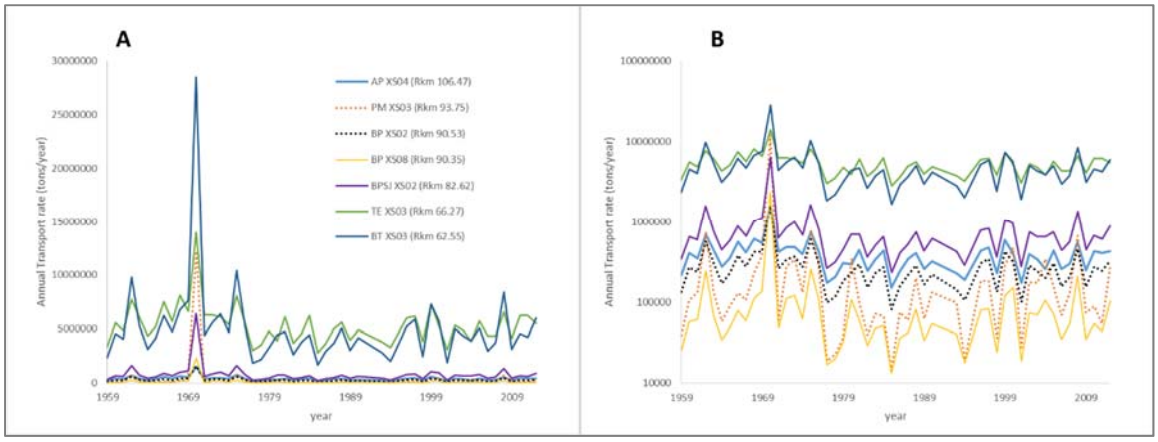

Figure 0-18. Annual bedload transport rate (tons/year) over the period of record for the XSrep. A = normal scale. B = log scale.

Seasonal variability of sediment flux is also related to inter-annual hydrologic cycles of the Rio Pacuare's wet and dry (less-wet) seasons. The percent of the total potential bedload transported during the normal dry and wet seasons of the Rio Pacuare is provided in Table 0-15. Approximately 10% of the cumulative potential sediment transported (tons) over the period of record (1959-2012) occurs during the dry season months (January – April) and the remaining approximately 90% occurs during the wet season months (May – December). However, approximately 40-75% of the total potential sediment transported occurs in the wettest months (October – December).

Table 0-15. Percent of total potential sediment transported per dry season (Jan-April) wet season (May-Dec), and wettest months (Oct-Dec) on the Rio Pacuare.

Site	XS_{rep}	% dry season	% wet season	% Oct-Dec
Arriba Pacuare	4	11	89	49
Paso Marcos	3	12	88	74
Bajo Pacuare	2	10	90	60
Bajo Pacuare	8	11	89	66
Bajo Pacuare por San Juaquin	2	11	89	56
Tres Equis	3	12	88	43
Bajo Tigre	3	11	89	55

The frequency at which the different grain-size fractions of the bedload are predicted to be mobilized and the frequency at which the bar feature at each site is inundated varies between field sites. The critical shear stress for grain-size fractions (D_{16}, D_{50}, and D_{84}) and the required discharge to mobilize them (Q_{cr}) is presented in Table 0-7. Table 0-16 shows the number of days select grain-size fractions are predicted to be mobilized at the XS_{rep}. Results indicate that bedload is expected to be mobilized multiple times a year, if not daily. Table 0-16 also includes the discharge required to inundate the bar surface (Q_{in}) and the number of days per year inundation is expected to occur on average. When compared to bedload mobilization, the results suggest that bar inundation is not required for bedload mobilization to occur at many of the sites, nor does inundation guarantee mobilization of the larger grain-size fractions at others.

Table 0-16. Number of days per year that grain-size fractions are predicted to mobilize and number of days per year that field-site bar surface is expected to be inundated, on average.

Site	XS_{rep}	Rkm	Grain Size		Tcr (N/m2)	Average days/year mobilized	Average days/year bar inundated	Q_{in} (cms)
Arriba Pacuare	4	106.47	D_{16}	17	17.59	365	42	39
			D_{50}	140	144.83	273		
			D_{84}	590	610.37	1		
Paso Marcos	3	93.75	D_{16}	3.1	3.87	365	10	58
			D_{50}	51	148.93	365		
			D_{84}	430	556.02	344		
Bajo Pacuare	2	90.53	D_{16}	3.1	2.49	365	24	66
			D_{50}	150	120.50	129		
			D_{84}	530	425.78	1		
Bajo Pacuare	8	90.35	D_{16}	73	58.64	365	14	76
			D_{50}	310	249.04	71		
			D_{84}	780	626.62	1		
Bajo Pacuare por San Juaquin	2	82.62	D_{16}	48	41.44	365	292	18
			D_{50}	130	112.22	365		
			D_{84}	360	310.77	2		
Tres Equis	3	66.27	D_{16}	3.2	2.57	365	5	164
			D_{50}	62	49.81	365		
			D_{84}	400	321.34	3		
Bajo Tigre	3	62.55	D_{16}	68	55.73	365	3	187
			D_{50}	190	155.72	364		
			D_{84}	450	368.82	183		

3.4 DISCUSSION

A river's geomorphic capabilities are characterized by the quantity and size of the sediment it manages and transports (Julien, 2015). Large active bars comprised of imbricated, well rounded, coarse material dominated by boulders (Figure 0-19), are distributed throughout much of the study area. These bedform feature are created and maintained during high-flow events and thus represent the material mobilized along the bed of the channel during those events. The transport capacity and frequency of bedload sediment flux that maintains these active bedforms provides insight into channel dynamics, probable geomorphic response, and channel stability.

Among the representative cross sections (XS_{rep}) at each field site the average annual sediment transport capacity ranges from 0.01 to 5.4 million tons per year. These rates may seem high when compared to bedload flux rates estimated for non-tropical humid montane rivers of a similar size such as rivers in western Oregon (0.01 to 0.4 million tons/year) (O'Connor et al., 2014) or even a high-bedload producing gravel and

cobble river from the Alborz Mountains in Iran (0.8 million tons/yr) (Kazemi et al., 2012) but, the Rio Pacuare is considered to have similar transport capacity as other humid tropical montane rivers. The bedload sediment transport capacity rates and observed plentiful bedload in the mainstem Pacuare confirm that regular bedload flux occurs throughout the montane portions of the Rio Pacuare on an annual basis.

Figure 0-19. Imbricated boulders on bar surface at field site Bajo Tigre. Photo by P.Lind.

The field sites dispersed through the study area offer examples of the variability of site-specific hydraulics, geometry, grain sizes, and stream power. Sediment transport capacity (tons/year) calculated at six of the field sites (AP, PM, BP, PBSJ, TE, and BT) show a wide range of transport rates—dependent on annual and seasonal discharge regimes, but also largely influenced by the site-specific characteristics mentioned above. In boulder-bed systems like the Rio Pacuare, a wide variability of transport capacities can occur due to flow variations as well as sediment packing, armoring, and availability (Rickenman, 2001; Bathurst, 1987). Interestingly, the average annual sediment transport capacities calculated at the selected XS_{rep} for each of the six sites on the Rio Pacuare do not increase in a normal downstream pattern with increasing discharge. Instead, in the mid-section of the study area at the Bajo Pacuare (BP) field site, transport capacities are smaller than at the upstream site at Paso Marcos (PM). River reaches with plentiful bedload, including side and mid-channel cobble-boulder bars, alternate with a few short

bedrock confined reaches with cobble-boulder lined channel beds occurring between site PM and site BP, but no dramatic aggradation in the channel was observed. This points to fairly regular bedload activation by flows capable of redistributing available/accumulated bedload downstream.

The frequency of bed material mobilization and bar inundation expresses interesting site-specific geomorphology. The mobilization of smaller grain-size fractions such as the D_{16} have been reported in other studies as signifying the early point at which bedload transport begins in mountain streams that have plentiful sediment supply (Ryan et al., 2005). Flows capable of mobilizing the D_{16} are predicted year-round at all field sites. The average number of days per year the D_{50} is likely mobilized ranges from 71-365 days a year and for the D_{84} it is 1- 183 days a year. Predicted mobilization of the D_{50} (median grain size) multiple times per year at all sites suggests regular active bedload sediment flux throughout the system. Flows capable of altering or replacing bedforms are expected when flows capable of mobilizing the D_{84} occur because non-uniformity of the bed grain size is negligible once the coarse material is mobilized (Lenzi et al., 2006; Lenzi et al., 1999; Schneider et al., 2015). Predicted mobilization of the D_{84} at least once per year, and often multiple times per year, suggests that bedform deformation or replacement occurs at least annually.

When compared with the frequency at which grain fractions are mobilized, bar inundation is clearly not required for the D_{50} and D_{84} grain size to be mobilized at field sites BT, TE, AP. Nor does bar inundation equate to a bed-forming flow event at field sites BPSJ, BP, PM. Bar inundation that does not mobilize the D_{84} has potential and was observed depositing and/or scouring smaller-sized grain fractions from bar surfaces. This appears to cause subtle bar surface armoring between bed-forming flow events by plucking and/or infilling surface voids between cobbles and boulder with smaller-sized bedload material. These observations support the theory of bedload transport at non-bed-forming discharges.

The subtle variability in linear or non-linear relationships between sediment transport rate and discharge at each site express variability in the timing of predicted mobilization of the coarser-grained (boulder) fraction of the bedload. Sites with a XS_{rep} that have non-linear relationships are generally more dependent on relatively large

magnitude flow events to deform or replace bedforms (See Appendix D and E for rating curves and cumulative sediment transport plots for all XS_{reps}). This suggest the potential for zones of bedload accumulation and channel aggradation to occur at or upstream of sites with non-linear sediment rating curves. When more linear transport occurs upstream, and vice-versa for bed degradation. However, as described above, flows capable of mobilizing the D_{84} are predicted at all sites on average at least once a year (Table 0-16). This suggests that the Rio Pacuare experiences flows capable of mobilizing its plentifully available or accumulated bedload material and likely rearranging annually. It is assumed that the massive boulders (approximately 1.5+ meters in diameter) that form steps or cascades in the higher gradient reaches where there is no or minimal bar accumulations are mobilized less frequently but, that the incoming bedload material of gravels to boulders are regularly flushed through—however a reach of this types was not modeled in this study.

Based on the stream power calculations for high flow events (0.2%, 2.0%, and 20% flow exceedance discharges), the maximum unit stream power is found at the upstream sites (AP and PM) where slope is greatest and channel width is narrow, and at the downstream-most site (BT) where slope is reduced but discharge is greatest and width is moderate (see Table 0-12 and Figure 0-16). When plotted, stream power vs sediment transport rate the overall trend in the relationship for the modeled sites is generally positive. However, site-specific hydraulic variables such as discharge-dependent energy gradient slope, depth, width, and velocity, as modeled in HEC-RAS, do not necessarily increase linearly with discharge. Combined with variations in grain size between sites, unit stream (as a proxy of flow competence) may not increase proportionately to increases in sediment transport capacity.

The temporal variations of annual and monthly sediment transport capacities at the modeled field sites are driven by the precipitation-induced hydrologic regimes of the Rio Pacuare. George et al. (1998) reported a direct correlation of monthly discharge runoff patterns on Rio Pacuare (using ICE gage 8-01 at Bajo Pacuare) compared to the recorded precipitation patterns received in the region. The oscillating sequences of high and less-high annual sediment transport capacities mimic the more-wet and less-wet precipitation years. This study shows that approximately 90 percent of the potential

annual sediment transported occurs during the wet-season months (May--December) and 43-74 percent occurring during the historically wettest three months of the year (November—December) (Table 0-15). The range between field sites in percent potentially transported during the wettest months indicates the dependence of the site on higher-magnitude flow events to mobilize the range of bed material at each site. The storm events on the Rio Pacuare produce flashy hydrographs with recorded discharge (cms) values that can increase by a factor of 10 or more in 24 hours. These types of storm events can result in a high variability of sediment transport over short temporal durations (hours or days) in the Rio Pacuare. This clearly suggests that changes in the hydrologic regime (quantity and timing) as a result of climate change or dam impoundment has the potential to change the current magnitude as well as spatial and temporal patterns of sediment flux throughout the study area. The quantity and frequency of current sediment flux also suggests that the channel would likely respond rapidly to such changes.

Since bedload transport increases, often non-linearly, in relation to discharge, it is assumed that periods of notable transport and bed-forming flows associated with peak discharge, though perhaps of short duration, are not represented in this study's results. This same issue also means that the number of days per year, in which the coarse grain size fractions are mobilized is likely under predicted. Thus, the Rio Pacuare is likely even more geomorphically and hydrologically dynamic than the bedload transport capacity results presented here suggest. Access to instantaneous discharge data would improve future estimates of sediment transport rates, thus more accurately capturing the range of dynamic processes (hydrologic and geomorphic) that occur in these systems. The sediment transport capacities calculated with the synthetized sub-daily discharge values generated for this study from the daily reported discharge do provide better representation than a single daily value.

Sediment transport capacity represents the maximum potential sediment flux through a site. However, pulses in bedload flux that naturally occur during flow events are not captured. Instead, bedload influx and transport are assumed to be constant throughout the duration of the bed-mobilizing flow. Also, the irregular temporal and spatial contributions of upstream sediment from the main channel, tributaries, debris flows, and landslides are not specifically characterized, but are simply considered a

combined source that maintains adequate sediment supply moving through the modeled field site**s.**

The technique of using high-resolution repeat photogrammetric surveys (Structure from Motion) proved successful at overcoming many of the challenges of validating bedload transport in high-energy mountain rivers. Although this study was able to capture only one bed-forming flood event—due to the uncommonly low occurrence of flood events that occurred during the field work (Nov-Dec 2012 and Oct-Dec 2013)—the SfM models were accurate enough to confirm grain mobilization and surface inundation of the hydraulic and sediment transport models used.

3.5 CONCLUSIONS

Bedload transport capacity has been calculated at six representative field sites distributed within 45 river kilometers of the montane portion of the Rio Pacuare. This research has been done to expand our understanding of the geomorphology and sediment dynamics of humid tropical montane rivers. Transport capacity at all six field sites is high (0.1 to 5.4 million tons per year on average) compared to non-tropical montane systems, but similar to other humid tropical montane rivers. The lack of peak discharge data has likely resulted in an underestimation of transport capacity because of the non-linear nature of sediment transport rates to discharge. Thus, the Rio Pacuare is probably more hydrologically and geomorphically dynamic than the results of this study conclude.

This research shows that the Rio Pacuare frequently experiences precipitation-generated high-magnitude flows that have the capacity to regularly mobilize its boulder-dominated bedload at all field sites modeled. Flows capable of mobilizing the D_{16} grain-size fraction at the field sites are expected to occur daily and for the D_{50} multiple times on average annually. Bed-forming flows capable of mobilizing the D_{84} occur at least once at all field sites modeled. Based on these results, bedload flux is expected to occur regularly throughout the study area. The capacity to regularly deform or maintain bedforms indicates that the Rio Pacuare frequently integrates and redistributes incoming upstream or lateral sediment inputs. This suggests that sediment distribution and storage as bars and other bedforms within the active channel is primarily controlled by flow hydraulics

(as a product of discharge, channel geometry, and slope) instead of point source input locations.

Magnitude (quantity) and temporal (annual and seasonal) variations in sediment flux are also controlled by the seasonal and annual discharge regimes. Highest annual sediment transport capacities are calculated for the years with the greatest discharge events. Likewise, approximately 50-75 percent of the potential annual sediment transported occurs during the wettest months of the year (Oct-Dec). Therefore, changes in the hydrologic regime (quantity and timing) as a result of climate change or dam impoundment has the potential to dramatically change the current magnitude as well as spatial and temporal patterns of sediment flux throughout the study area. The high quantity and frequency of current sediment flux also suggests that the channel will likely respond rapidly to such changes.

Limited anthropogenic impacts and the likeness of the Rio Pacuare, geologically and hydrologically, to other rivers in Central America make it a good analog for studying the geomorphology and sediment dynamics of humid tropical montane rivers in the region. This study provides some much needed information about transport capacity and potential sediment flux in these systems where climate change and human development is quickly impacting watersheds. However interesting and useful, the reality is that this study provides only a few small pieces to the gap of knowledge that exists on the geomorphology and sediment dynamics of humid tropical montane systems. Ideally future research will include peak discharge data and field surveys that capture the results of several high-magnitude flow events on the Rio Pacuare and in other tropical montane rivers across the world. For example, additional physical measurements of bedload mobilization should be a priority to confirm rates, pulses, and the influence of sediment inputs (i.e., influence on local slope and bed form).

CHAPTER IV

IMPACT OF CLIMATE CHANGE ON SEDIMENT TRANSPORT CAPACITY IN A MONTANE HUMID TROPICAL RIVER RIO PACUARE, COSTA RICA

4.1 INTRODUCTION

Climate change is a reality, and a major component of current and future hydrologic processes across the globe, including the rivers of Central America (Hidalgo et al., 2013; Magrin et al., 2014). Demands on the vital resources provided by these rivers (e.g. drinking water, hydroelectricity, ecology, and agriculture) continue to increase steadily (Johnston & Kummu, 2012; Kaygusuz, 2004). This trend is expected to continue into the future in response to quickly expanding populations and continued climate change (Jiménez et al., 2014; Schewe et al., 2013; Vorosmarty et al., 2000). In Central America, climate change is expected to generally produce more intense precipitation events and greater seasonality, especially drier dry seasons (Kamiguchi et al., 2005; Kitoh et al., 2013; McLean et al., 2015; Nakaegawa et al., 2014; Palomino-Lemus et al., 2015), which will inevitably alter the timing and quantity of discharge in the rivers (Hidalgo et al., 2013; Jiménez-Rodríguez et al., 2015; Maurer et al., 2008; Nohara et al., 2006).

A river's geomorphic capabilities, as a function of its discharge regime, are characterized by the quantity and size of the sediment it manages and transports (Julien, 2015). Suspended sediment and bedload sediment transport reveal information about sediment sources and flow competence of a river, but bedload often defines channel type, form, and stability (Knighton, 1998). Because precipitation patterns and related discharge regimes are predicted to continue to change, sometimes severely, across the globe as a result of climate change, research on how changes in precipitation and/or discharge may alter geomorphic processes such as bedload sediment transport has recently been undertaken in a few regions. For example, Pralong et al. (2015) modeled decreased bedload sediment yields due to reduced predicted runoff and a temporal shift in seasonal transport in rivers located in the Swiss Alps for 2070-2099. Praskievicz (2015) developed

a set of models to examine the impact of downscaled climate-change projections on small gravel-bedded channels in the mountains of Washington and Idaho where increased seasonality (increased winter rain and discharge and decreased spring and summer discharge) shifted the timing of bedload transport. Coulthard et al. (2012) implemented a probabilistic modeling approach on the Swale River in the UK where winter rainfall is projected to increase with exaggerated storm events. A 100% increase in catchment sediment yield resulted on the Swale for the 2070-2099 scenario modeled. These and other studies (Lu et al., 2013; Nishimune et al., 2003; Turowksi et al., 2009) clearly show that bedload sediment transport is linked to an area's precipitation patterns. Thus, future changes in climate are expected to alter bedload transport. This is particularly probable in the humid tropics where the difference in dry and wet season precipitation patterns are predicted to increase, as well as the intensity of storm events. However, no studies were found on the potential changes to bedload transport in humid tropical montane rivers. This is a major gap in knowledge considering the growing demand and related infrastructure development occurring on humid tropical montane rivers and how geomorphic responses are faster in these systems compared to other river systems in the world (Garcin et al., 2005; Latrubesse et al., 2005; Scatena & Gupta, 2013; Wohl et al., 2012).

This study examines changes to bedload transport capacity in response to future climate predictions. The analysis is done at two surveyed cross sections on the Rio Pacuare in Costa Rica. Though relatively close together (175 m), they represent two different kinds of discharge-sediment transport relationships identified at other sites along the Rio Pacuare (see Chapter III, this dissertation). The geomorphic responses to the changes in transport capacity at each site are discussed based on the previously provided detailed geomorphic assessment in Chapter II (this dissertation). The goal of this work is to not only examine how sediment transport capacity may change in response to changes in this river's seasonal discharge regime, but also to establish a foundation and expose the need for more thorough climate change and dam impoundment-related research on this and other humid tropical montane rivers.

Fifty-one years of observed daily discharge data from a gage on the Rio Pacuare is statistically decomposed to create a time-series hydrological model comprised of trend,

seasonal, and irregular components. The model is then used to simulate twenty years of daily discharge representative of modern observed discharge and, through manipulation of the components, future climate scenarios. Two regional climate change models that predict future precipitation changes specific to the region and one global model that predicts changes in extreme events for the time period 2070-2100 were used to develop the eight discharge scenarios for this study. The regional climate models for southern Central America generally predict exaggerated seasonality with drier and extended dry periods and wetter wet periods (Enquist, 2002; Hidalgo et al. , 2013; Maldonado et al., 2013; Maurer et al., 2008). However, various climate change projections for Costa Rica show divergent (both positive and negative) changes in precipitation through the twenty-first century with averaged precipitation change of $\pm$10 percent for 2080-2100 (Magrin et al., 2014). First, a no-change control simulation is ran with the model to establish a control and then seven other change simulations are ran. The simulated discharge for each scenario is then input into a bedload transport model designed for steep mountain rivers to estimate annual and seasonal changes in bedload transport. Changes in transport capacity for each scenario are compared and potential geomorphic response to those changes are discussed.

4.1.1 Regional Setting

The Rio Pacuare is located in Costa Rica's Talamanca Mountains in the central portion of the Chorotega volcanic front of Central America (Figure 0-1). In total, the channel is approximately 132 river kilometers (Rkm) long from headwaters to sea: flowing north-northeast through the Talamanca Mountains (Rkm 44-132), across the Caribbean plane, and eventually into the Caribbean Sea. The entire watershed is 890 km^2, and the mainstem channel falls approximately 3018 meters in elevation with almost the entire fall (2068m) occurring in the upper 88 Rkm contained within the mountains. In the mountains, vegetation cover is dominated by dense tropical mid-elevation forests. Small-scale farming plots, a few unincorporated villages, bio and cultural reserves, and a handful of rafting camps accessed by dirt roads, trails, or river also exist.

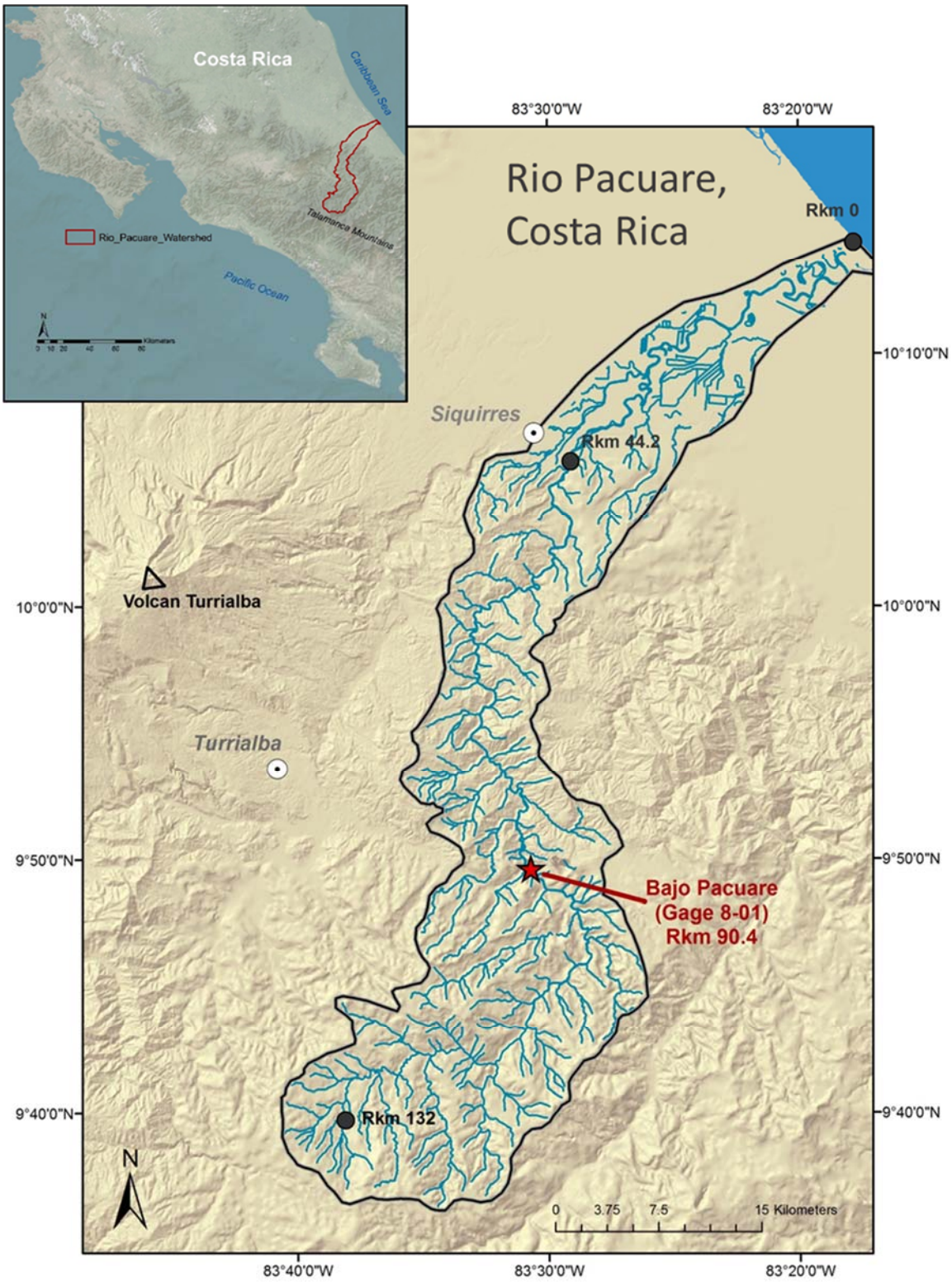

Figure 0-1. Study area with Bajo Pacuare site identified. Basemap: 30m DEM (ASTER 1999) and ESRI GeoEye.

Hillslope, tributary, and channel slopes are relatively high and lateral contributions from landslides and debris torrents periodically deliver sediment and other materials to the main channel. Plentiful, frequently-mobilized bedload exists throughout the montane reaches. Bedforms, including large cobble-boulder bars and boulder steps, influence channel form and type at low to normal flows. The distribution of bedload material and the stored grain-size fractions in the bedforms were correlated to the site and reach-scale hydraulic processes. In Chapter III (this dissertation) sediment transport capacity estimates confirm that current discharge regimes are expected to mobilize available bedload multiple times a year—the D_{84} grain size fraction was predicted to be mobilized at least once a year at all sites modeled. Thus, the montane portion of the Rio Pacuare is currently considered a geomorphically and hydrologically dynamic system, similar to other humid tropical rivers that transport relatively high quantities of bedload compared to other types of mountain systems (Bidorn et al., 2015; Juan D. Restrepo et al., 2006; Ziegler et al., 2014).

4.1.2 Site Description

This study focusses on simulating potential future sediment transport capacity in response to potential future changes in the discharge regime due to climate change. The two cross sections used in this analysis are located near the Bajo Pacuare discharge gage (8-01). The gage is located at Rkm 90.4 in the mid-section of the montane portion of the watershed at 582m elevation. The contributing watershed upstream of the Bajo Pacuare site is approximately 367 km^2. One cross section (BP XS02) is located 150 meters upstream from the gage and the other (BP XS08) is 25 meters downstream from it (Figure 0-2). At both cross sections, bedload material, dominated by cobbles and boulders, cover the underlying confining bedrock. Thickness of the bedload material atop the bedrock channel bed is unknown. However, a scour hole located 60 meters downstream from BP XS02 along the bedrock wall on river-left is lined with boulders and measured 2.7 meters below the surface elevation of the depositional bar on river left.

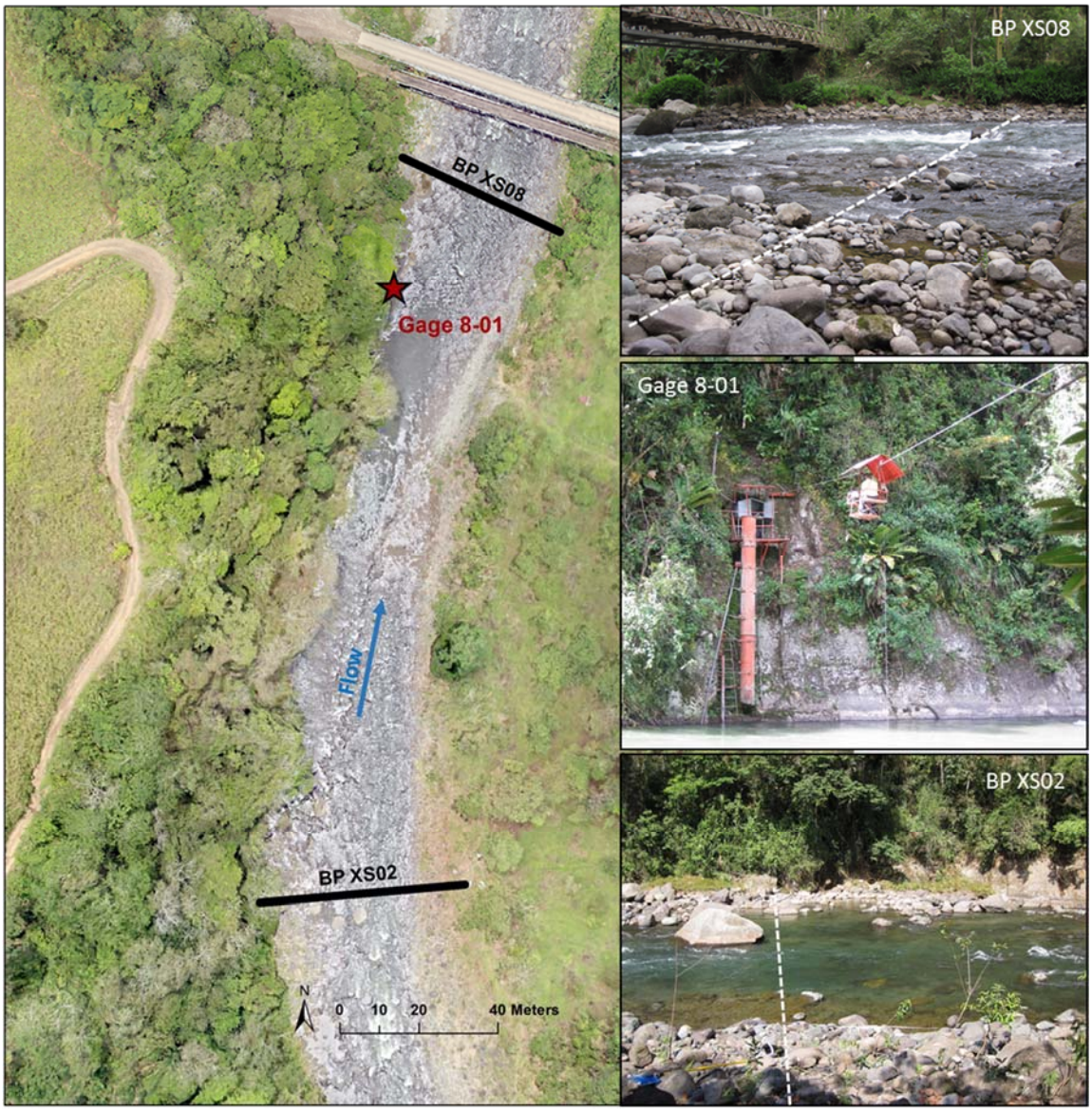

Figure 0-2. Study site at Bajo Pacuare (Rkm 90.4). Inset photos of both cross sections (BP XS02 and BP XS08) and the Bajo Pacuare discharge gage (8-01).

The two cross section are geomorphically different though they receive generally the same daily discharge. This is the result of site-specific topography, cross section geometry, and the resulting hydraulics. A steeper slope and narrower channel at BP XS08 results in higher boundary shear stress and for the same discharge values. The topography of each cross section is provided in (Figure 0-3). This results in a coarser grain size fraction at BP XS08.

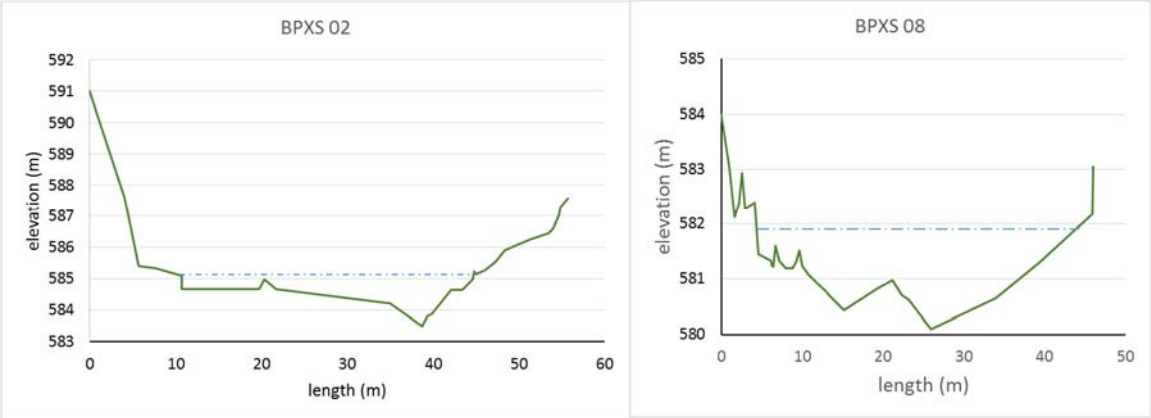

Figure 0-3. Cross section topography for BPXS02 and BPXS 08. Dashed blue line indicates bar inundation discharge (Q_{in}).

Table 0-1 provides the modern grain size distribution and the required discharge to inundated (Q_{in}) the depositional boulder bars at both cross section locations. In addition, the channel width, slope, and depth at Q_{in} are also included in the table to provide context to the geomorphic differences between the cross sections and the potential for BP XS02 to be inundated more frequently than BP XS08. BP XS02 is located at the tail of a riffle that includes large boulders. BP XS08 is in the middle of a riffle composed primarily of very large boulders. Downstream of BP XS02 approximately 40 meters the channel is confined on river-left by a vertical bedrock wall for 154 meters. The Bajo Pacuare gage 8-01 is attached to that bedrock wall.

Table 0-1. Grain size distribution and channel metrics for the bar inundating discharge (Q_{in}) at both cross sections (BP XS02 and BP XS08).

Site	Grain Size (mm)			Q_{in} (cms)	Q_{in} Slope (m/m)	Q_{in} Chan width (m)	Q_{in} Chan depth (m)
	D_{16}	D_{50}	D_{84}				
BP XS02	3.1	150	530	66	0.013	48.53	1.63
BP XS08	73	310	780	76	0.024	44.4	1.65

As expected, the shape and slope of channel and grain size variations at each site produce a slightly different modern bedload transport to discharge relationship when modeled in a sediment transport model with the observed data (Figure 0-4). The wider cross section at BP XS02 produced a slightly non-linear relationship for the lower discharge values but overall it has a fairly linear transport to discharge relationship,

where bedload mobilization increases relative to increasing discharge. In contrast, the narrower cross section at BP XS08 produced a non-linear relationship where less transport is expected to occur at lower discharges. As a result, observed and simulated average annual transport rates are lower at BP XS08 than at BP XS02.

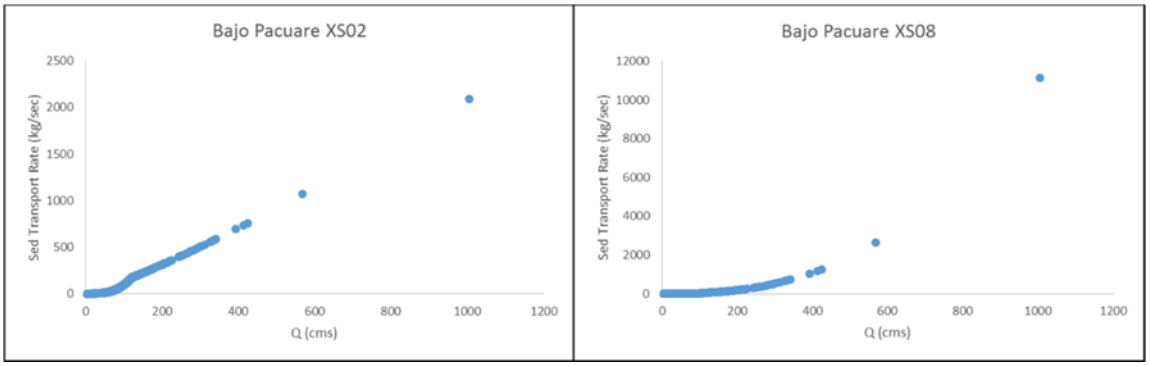

Figure 0-4. Sediment transport to discharge relationship for BP XS02 and BP XS08. Modeled and presented in Chapter III (this dissertation) – Appendix C.

4.1.3 Climate

Both regional and localized precipitation patterns govern the Rio Pacuare's hydrologic flow regime. Although the river's headwaters are at relatively high elevations, precipitation neither falls nor is stored as snow due to its tropical location. The central mountains of Costa Rica are expected to receive two rainy and two dry seasons annually. However, given the combination of local orographic uplift and climate patterns primarily generated from the Caribbean, the Rio Pacuare watershed is typically wet all year with a drier season (less wet) that occurs January to April, and a wetter period from May to December. Figure 0-5 presents the average monthly precipitation values (1959-2012) recorded at the research station Centro Agronómico Tropical de Investigación y Enseñanza (CATIE) in the community of Turrialba (see Figure 0-1 for relative location to the study area). CATIE maintains the closest and most reliable long-term weather station to the Bajo Pacuare gage site but, it is located in the adjacent watershed 20 kilometers to the west where local precipitation may occasionally be more influenced by Volcan Turrialba (storm generation and/or rain shadowing). Nevertheless, The CATIE weather

station provides a good representation for the area's monthly average precipitation pattern over the last several decades.

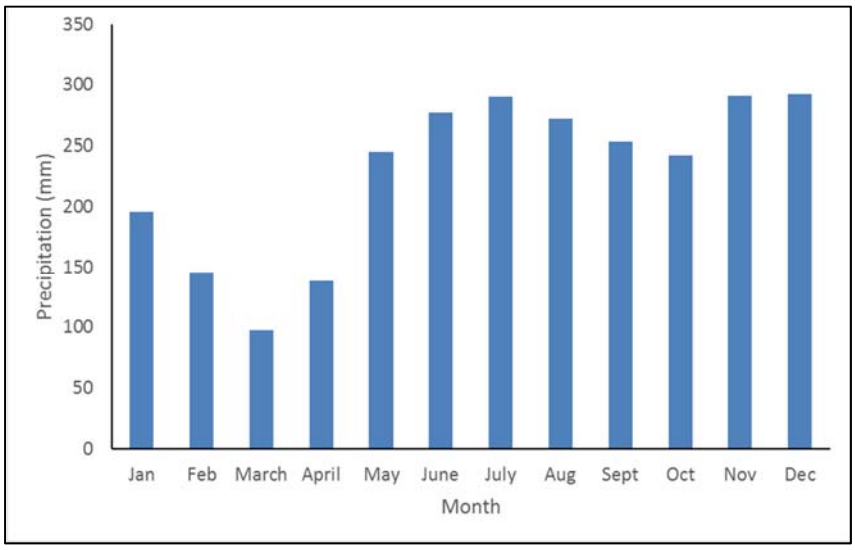

Figure 0-5. Average monthly precipitation (mm) at Turrialba, Costa Rica (1959-2012)(CATIE - Centro Agronómico Tropical de Investigación y Enseñanza, 2016).

On average the trend for the wet season expresses a bi-modal distribution of precipitation June to August and then November to December. During intense precipitation events, the Rio Pacuare can experience rapid increases in discharge. Daily discharge data acquired from the Instituto Costarricense de Electricidad (ICE) for gage 8-01 (Bajo Pacuare) at Rkm 90.4 [1958-2013] indicates that high magnitude flow events most commonly occur in October, November, and early December, when the watershed seasonally receives the greatest amounts of precipitation. The seasonal pattern reflected in the long-term average monthly precipitation in this region is thought to be the result of the north-south shift of the Inter-Tropical Convergence Zone (ITCZ) and sea surface temperatures of the Caribbean. Interannual variability in climate is likely governed by El Nino Southern Oscillation (ENSO) and its related sea surface temperatures of the Pacific combining with the western Atlantic warm pool to create storms over the high central ridge of the Talamanca Mountains (Enfield & Alfaro, 1999; Giannini et al., 2001a; Giannini et al., 2001b; Giannini et al., 2000; Poveda et al., 2006; Quesada & Waylen, 2004; Waylen et al., 1998).

4.2 MATERIAL AND METHODS

To examine how changes in discharge may influence the sediment transport capacity on the Rio Pacuare we developed eight different discharge based on regional climate-change projections for the area for 2070-2100. The discharge scenarios were input into a sediment transport model for steep mountain rivers and the results compared.

A few assumptions that likely add uncertainty to the results have been made. The first assumption is that site-specific characteristics surveyed in the field, such as modern grain size and channel topography, will remain the same in the future. Detailed modeling and speculation of changes to these site-specific characteristics are not included in the scope of this study. This technique has been applied by others that have estimated sediment transport for projected future climate scenarios (Pralong et al., 2015; Praskievicz, 2015).

The second assumption is that discharge and precipitation are well correlated in this river system. This is based on reported correlations of discharge and precipitation for rivers in the region, including in Costa Rica (Marsik & Waylen, 2006; Maurer et al., 2008; Restrepo & Kjerfve, 2000) and on the Rio Pacuare specifically (George et al., 1998). Figure 0-6 shows one year (2012) of the daily discharge data reported at the Bajo Pacuare gage (8-01) along with the daily precipitation reported at the CATIE weather station in Turrialba, located approximately 20 kilometers away from the gage site. Although the gage and weather station are not in the same watershed, the data expresses a clear correlation between large precipitation events (i.e. July 27, 2012) and flashy discharge events, as well as seasonally wet periods (November) and higher discharge values. The few days when high discharge events occur on the Rio Pacuare without a recorded precipitation event at CATIE likely represent localized storm events in the watershed of the Rio Pacuare. Localized storm events that deliver highly varied quantities of precipitation in the same watershed are not uncommon in the mountains of Costa Rica (Maldonado et al., 2013).

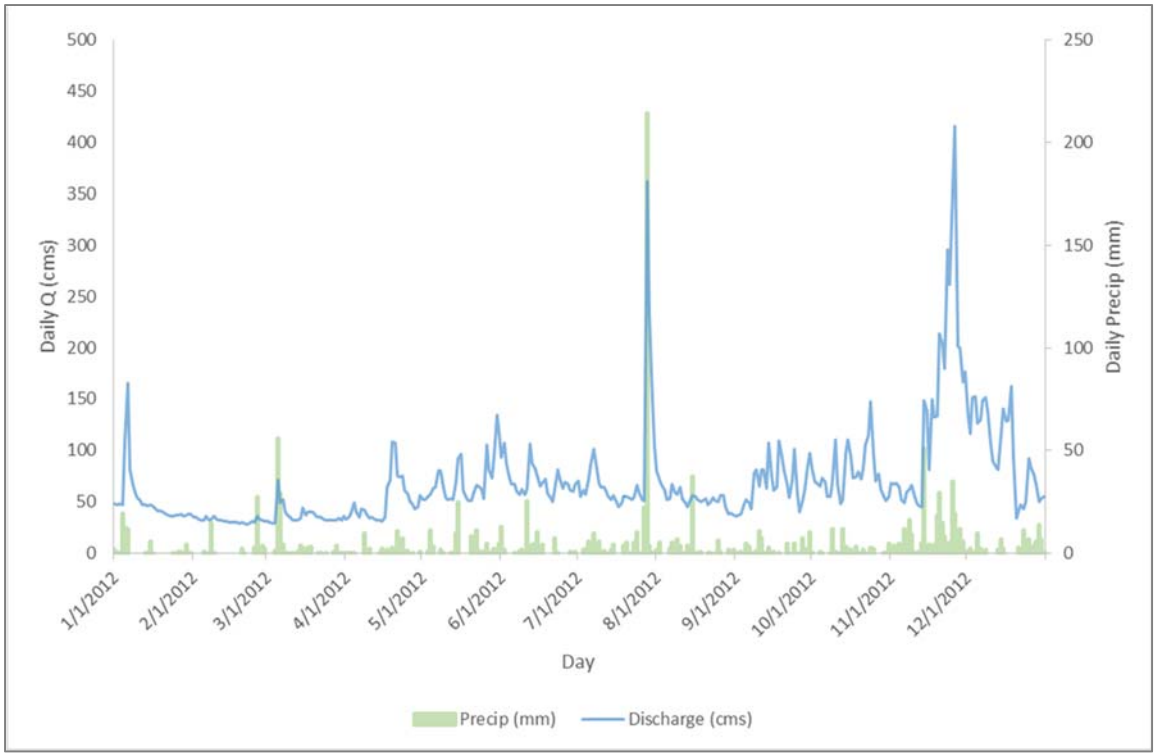

Figure 0-6. Daily precipitation (mm) at Turrialba and daily discharge (cms) for one year (2012) at Bajo Pacuare gage (8-01) on the Rio Pacuare.

Development of a site-specific runoff model representing the site-specific river discharge to rainfall relationship was not undertaken as part of this study due to a lack of available rainfall data for the watershed. Instead, the projected future discharge changes are assumed to be correlated with the future precipitation changes. Observed and simulated precipitation and runoff for rivers in the Bocas del Toro area (located in southern Talamanca Mountains along the northern-most Caribbean coast of Panama with relatively similar climate patterns to the Rio Pacuare) confirm that this assumption is acceptable, though uncertainty is of course implied (Fabrega et al., 2013). In Bocas del Toro the simulated future changes in precipitation are similar to or slightly less than the simulated changes in runoff, with only small reported changes in evaporation. Thus, using the range of projected precipitation changes as guideposts should establish plausible, and perhaps even conservative, changes for developing hypothetical future discharge regime scenarios on rivers in this region. Fabrega et al. (2013) also concluded that using seasonally or monthly specific percent changes for simulating both

precipitation and discharge are more reliable for these systems than temporally constant rates of change (a single rate change per year) applied in past studies.

The third assumption is that land-use change will be minimal in the upper Rio Pacuare in 2070-2100 compared to today. This assumption is based on the fact that currently over ninety percent of the watershed upstream from the study sites is contained within the Talamanca Cabecar Indigenous Reserve which borders the Amistad National Park. Based on Costa Rica's current commitment to conserving both its ecological and cultural heritage in this section of the country, it is assumed that the reserve will be intact in 2070-2100, and that anthropogenic impacts from the indigenous communities will likely neither decrease or increase. Included in this assumption is that dense tropical forests will remain the dominant vegetation type.

4.2.1 Modeling Discharge Scenarios

Observed daily discharge data was acquired from the Instituto Costarricense de Electricidad (ICE) for the Bajo Pacuare Gage (8-01). Only the years with data reported for each day were included in the modeling process (1959-1990, 1993-1994, and 1996-2012). A statistical model developed in R 3.2.5 was developed and applied to decompose the 51 years of observed daily discharge data on the Rio Pacuare into trend, seasonal, and irregular components. The components can then be individually modified to reflect the particular nature of a future-climate scenario, and then recombined to produce a synthetic time series of daily discharge consistent with that scenario. In practice, projected changes in long-term mean discharge can be represented by adjusting the trend and seasonal components, while changes in variability of daily discharge can be represented by changes in the shape of the statistical distribution of the irregular component.

Data Decomposition and Time-Series Analysis

The observed daily discharge data was transformed into $\log_{10}Q$ values and then sine and cosine terms were generated to represent the average mid-month values of discharge by a Fourier series:, or

$$log_{10}Q_t = T_t + S_t + I_t$$

where T_t, S_t, and I_t are the *trend*, *seasonal* and *irregular* components, respectively, and *t* is time (days). The *trend* component (T_t) is simply a constant value for the $\log_{10}Q$, derived from the long-term mean for the data used.

The *seasonal* component is represented by a Fourier series:

$$S_t = \sum_{j=1}^{nh} a_j \cos(2\pi(j/N)t) + b_j \sin(2\pi(j/N)t)$$

where a_j and b_j are Fourier or harmonic-regression coefficients for *nh* harmonic or sine-cosine terms, and *N* is the fundamental frequency (or 365 days). In application, we chose nh = 6 to represent exactly the mid-month values, while also adequately representing the seasonal cycle of the daily values.

Daily discharge is highly temporally correlated and so we represented the *irregular* component by an ARMA(*p,q*) "Box-Jenkins"-type time-series model (Box et al., 1994; Hipel & McLeod, 1994). The particular model that was identified and fit here was an ARMA(2,2) model:

$$I_t = z_t = \phi_1 z_{t-1} + \phi_2 z_{t-2} - \theta_1 a_{t-1} - \theta_2 a_{t-2} + a_t$$

where the ϕ's and θ's are autoregressive and moving-average coefficients, and a_t is the time series of residuals or "noise". In the application here, the a_t's for generating new data are based on suitably transformed normally distributed random numbers, $e_t \sim N[0,1]$.

The various coefficients were estimated using the arima() function in R, with the seasonal components as "ARMAX" regressors. This was done iteratively, adjusting the order of the autoregressive and moving-average operators, and then examining residuals for autocorrelation. The final iteration shows that the autocorrelation or persistence in the irregular component has been removed (Box-Ljung statistic = 48.407, p=0.376). Figure 0-7 provides the series residuals (acf) and the cumulative periodogram for the model, showing that the standard errors provide no evidence of autocorrelation.

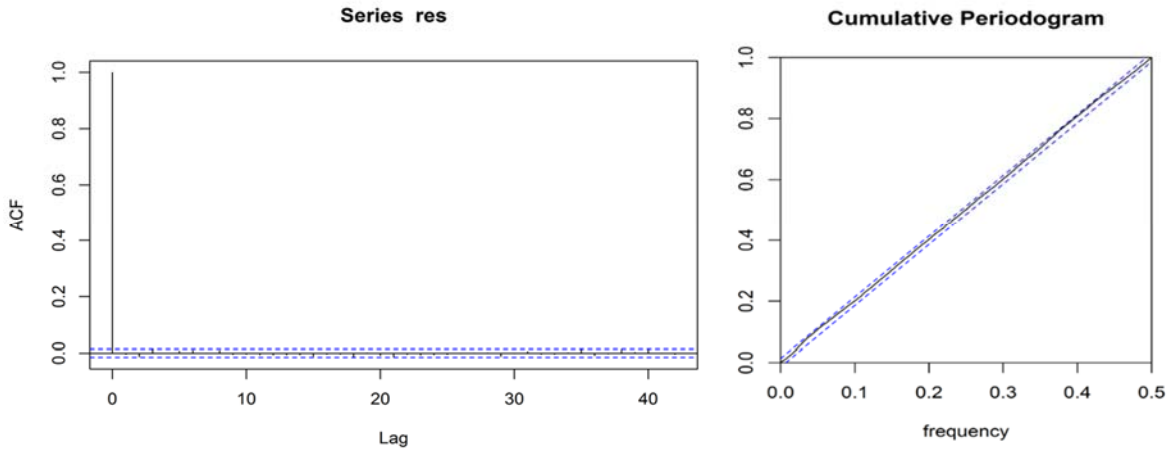

Figure 0-7. Residual autocorrelation and cumulative periodogram of the final iteration of the model.

The resulting seasonal component of the observed daily discharge data generated with the sine and cosine series and the Fourier coefficients calculated by the fitted ARMAX model are plotted for the first 365 days in Figure 0-8.

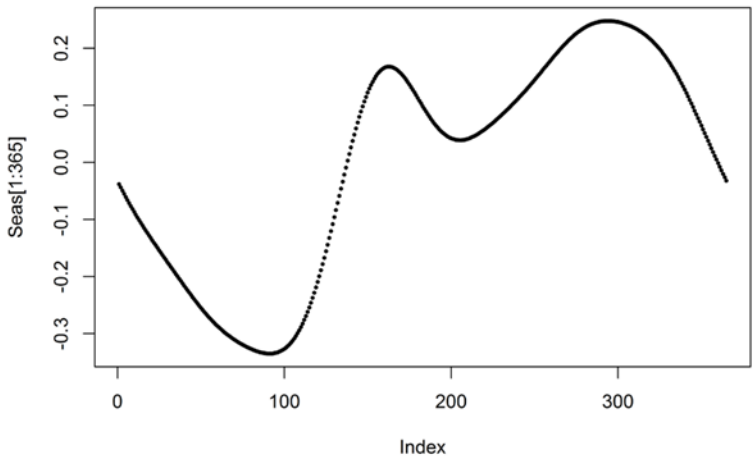

Figure 0-8. Modeled seasonal component (365 days with Jan 1 as day 1) of the observed decomposed daily discharge data from Bajo Pacuare (gage 8-01)

The irregular component, z_t, of the observed $\log_{10}Q$ daily discharge data is presented in Figure 0-9.

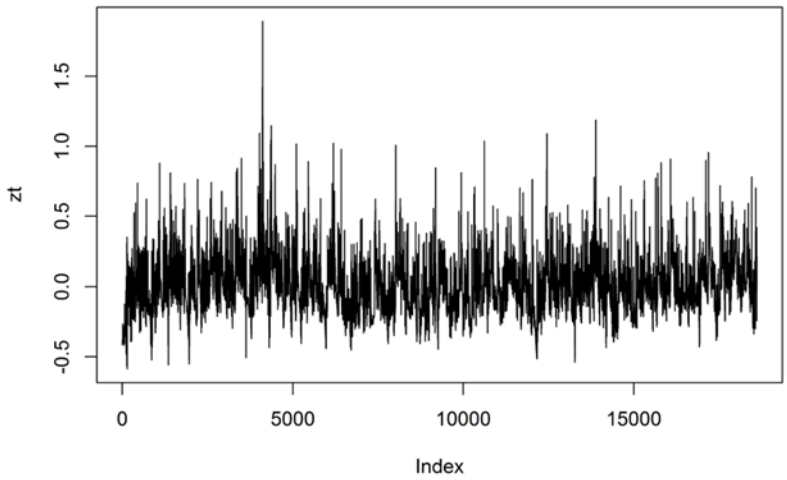

Figure 0-9. Modeled irregular component of the observed decomposed daily discharge data from Bajo Pacuare.

Finally, the trend component here was represented by the simple long-term mean of the log10 discharge data, 1.4360.

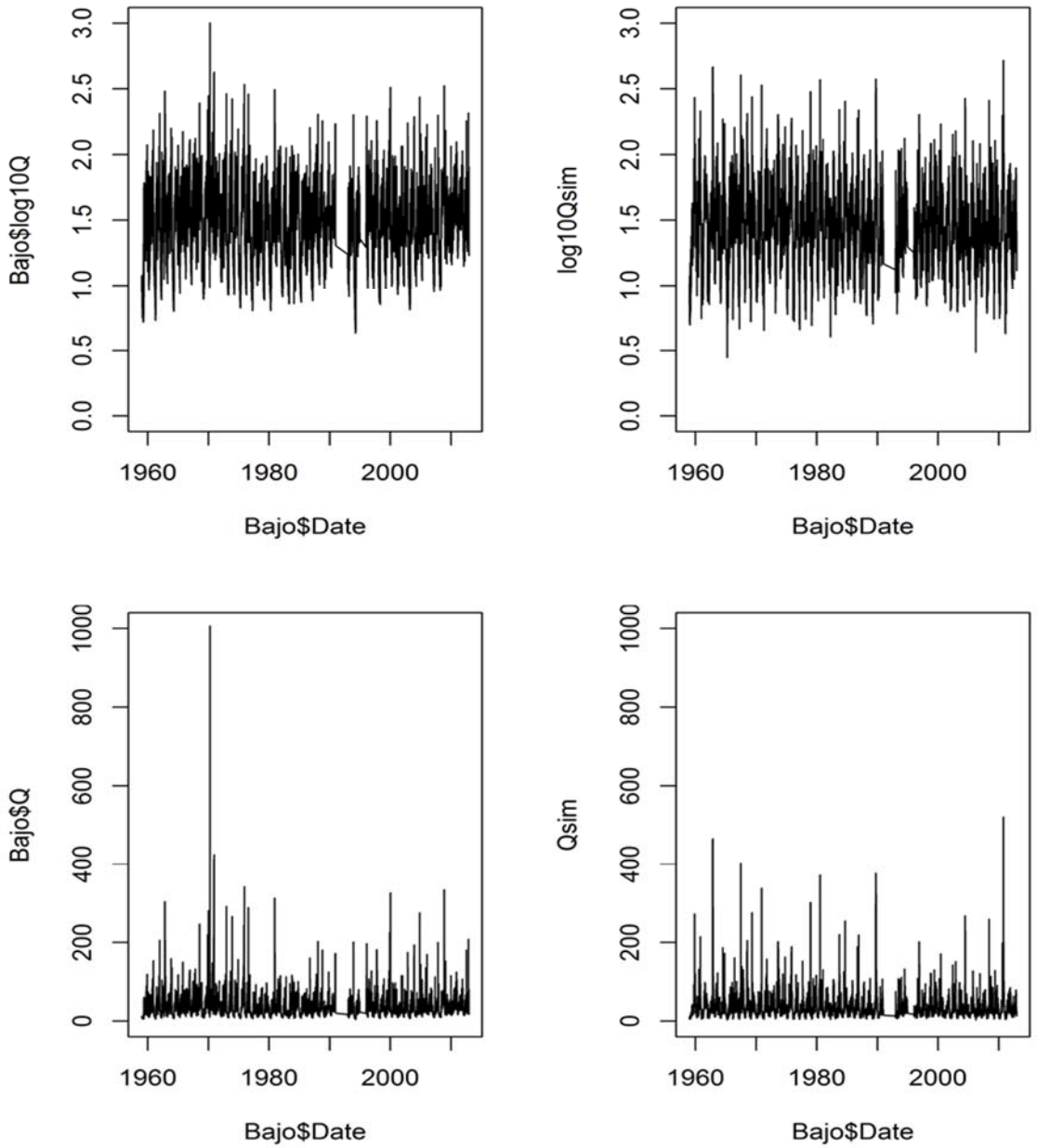

Figure 0-10. Modeled $log_{10}Q$ (observed daily discharge data) and $log_{10}Q_{sim}$ (synthesized daily discharge data) – top two graphs. Bottom two graphs – observed Q(cms) and synthesized Q_{sim} at Bajo Pacuare for 1959-1990, 1993, 1994, 1996-2012.

Model Evaluation

To evaluate the model, a synthesized times series of data ($log_{10}Q_{sim}$) was generated with the model and compared to the observed $log_{10}Q$. The analog values of these data were also calculated to compare observed daily discharge data (Q) from the Bajo Pacuare gage site and the synthetically generated daily discharge data (Q_{sim}). Figure 0-10 presents both. Although the synthetic and observed are not exactly alike, they are

similar. There is a tendency to under-estimate the magnitude of very large infrequent discharge events, which are admittedly important for sediment transport, but otherwise the ability of the model to synthesize new data that represents the trends and seasonality of the observed is considered very good.

The residuals for this model are not distributed normally. When fitting ARMAX models it is assumed that the residuals are independent, identically normally distributed random variables (iid Normal). However, the histogram for the reported data is leptokurtic (peaky) and skewed (asymmetric). As a result, the quantiles plot does not produce a straight line. Figure 0-11 presents the histogram of the residuals and the QQ (quantiles) plot.

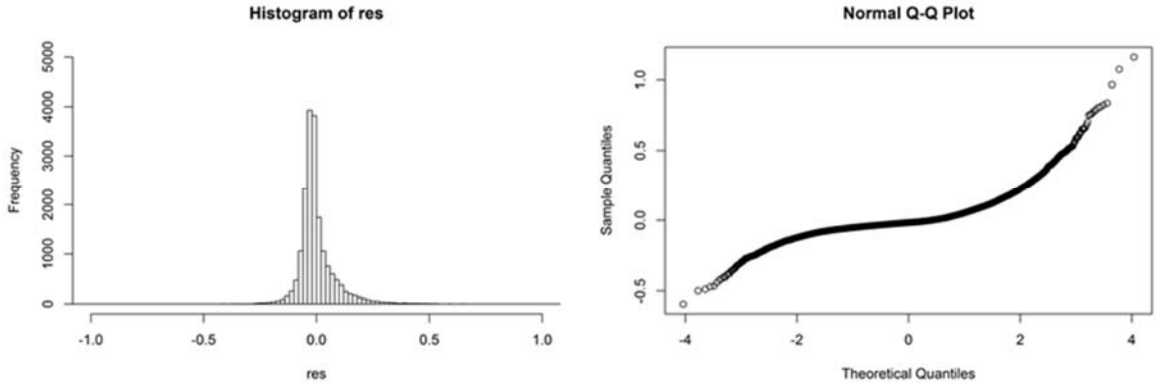

Figure 0-11. Histogram of residuals and plot of quantiles (sample vs theoretical).

With respect to this assumption violation, the actual fit is considered robust but it did pose a challenge in generating new data. To adjust for this, we developed an empirical cumulative density function which translates normally distributed random values to have the same (empirical) distribution as the observed residuals (the a_t's). This technique is acceptable for the purposes of this study.

Synthesizing New Discharge Data

Synthesizing new data for a specific future climate scenario requires generating new series of T_t, S_t, or I_t -- the *trend*, *seasonal* and *irregular* components. For synthesizing new daily time-step data the seasonal cycle was approximated by sampling at twelve mid-month points, a Fourier series is fit to those points, and then used to

produce daily time steps. Figure 0-12 presents the daily time-step of the seasonal component (presented above in Figure 0-8), overlain by the mid-month time-step values using a harmonic regression fit. The fit is quite good.

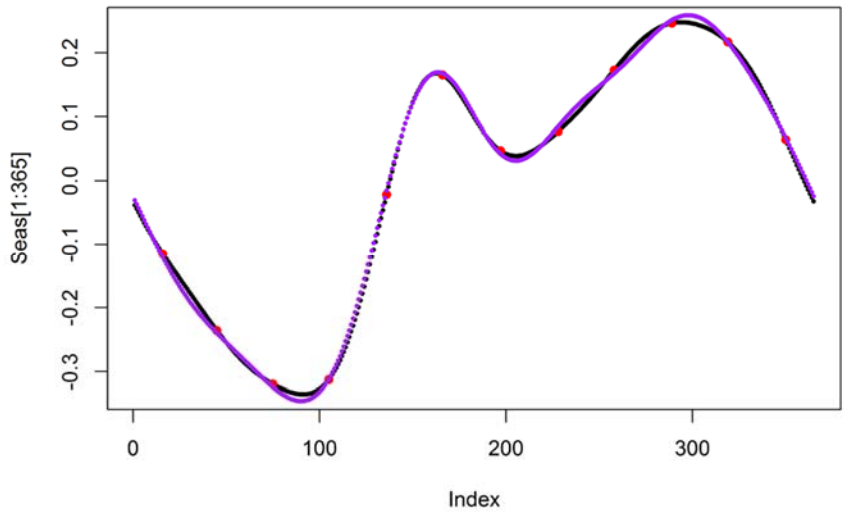

Figure 0-12. Modeled seasonal component as mid-month time-step (purple line with pink points) regression fit and daily time-step (black line) of decomposed observed data.

To synthesize new discharge data consistent with future climate projections, the twelve mid-month values are manipulated or perturbed. The model then fits and evaluates a periodic regression to produce new $\log_{10}Q_{sim}$ and Q_{sim} values for twenty years' worth of daily time-step data. To alter the irregular component, or distribution of flows, to represent future climate scenarios with changes in the distribution of precipitation events (e.g. more high-precipitation and low-precipitation events, and fewer intermediate events), the variability of the standard-normal equivalents of the residuals can be manipulated.

4.2.2. Future Climate Scenarios

The regional climate models for southern Central America generally predict exaggerated seasonality with drier and extended dry periods and wetter wet periods (Enquist, 2002; Hidalgo et al. , 2013; Maldonado et al., 2013; Maurer et al., 2008). To reflect the more extreme high-precipitation events, and more extreme low-precipitation intervals, the residuals of the fitted model (seasonal and irregular components) were

perturbed accordingly. Climate change projections for Costa Rica show divergent (both positive and negative) changes in annual precipitation through the twenty-first century with averaged precipitation change of ±10 percent for 2080-2100 (Magrin et al., 2014). This divergence is due to the ensemble of climate models producing inconsistent predictions because of the difficulty of modeling for atmospheric features such as shift in the ITZ, but also the major influence that mountainous topography, land use, and east-side versus/combined with west-side climate have on localized precipitation and discharge regimes across this small country (Enquist, 2002; Quesada & Waylen, 2012).

This study uses three climate model predictions of future precipitation change for 2070-2100. Two regional models that integrate local climate station data and predicted changes specific for the eastern Talamanca Mountains were used, though they produce divergent seasonal predictions (Campbell et la., 2011; Karmalkar et al., 2011). The third model is a high-resolution global model that predicts changes in extreme events such as the percent of annual total precipitation due to extreme wet days (Kamiguchi et al., 2006). Utilizing the projected changes presented in these three studies, we derived eight hypothetical discharge scenarios. The first scenario represents no-change from the observed modern discharge and acts as a control for comparing the other seven simulation results. Climate Simulation Family 1 (ClimSim 1) modify the seasonal component of the model to reflect the change predictions of the two regional climate models separately and then combined. Climate Simulation Family 2 (ClimSim 2) adds a change in discharge variability to the simulations in ClimSim 1 by manipulating the irregular component. Since none of the models focus on changes in the overall long-term mean precipitation, no perturbation was applied to the trend component of the model.

A brief description of each simulation and their discharge regime scenarios are provided here. The changes applied are summarized below in Table 0-2.

Climate Simulation Family 1 (ClimSim 1)

No-Change Scenario (the control) is the simulated daily discharge with no change in seasonal components or irregular component applied. This is considered the control discharge scenario that simulates the seasonal trends and variability in the observed daily discharge data from the Bajo Pacuare gage (8-01).

Wetter Scenario is the simulated daily discharge with changes applied to the mid-month seasonal components to reflect projected precipitation percent change as simulated by Campbell et al. (2011):

November to January = 0 to +25

February to April = 0 to -25

March to July = 0 to -25

August to October = +25 to +50

Although decreases are predicted for February to July, the increases predicted for the seasonally wetter months of the year make the overall annual change for this scenario "wetter" than the No Change scenario. Perturbation in our model to the residuals of the mid-month seasonal component was applied to reflect the predicted monthly changes and then simulated daily discharge data was generated. Although no perturbation to the trend component of our model was applied, perturbing the seasonal cycle in this manner does indirectly perturb the trend of the original model.

For the *Wetter* scenario, the range in the predicted percent change per month was distributed across three-month periods to encompass the reported projections in Campbell et al (2011). As a result, each mid-month seasonal component was perturbed by a different percent change value, but the average applied changes to the three-month periods equaled the median of the projected percent range. For example, a 0-25% precipitation change (positive or negative) over a three-month period resulted in changes to the mid-monthly components for those three months of 1%, 12%, and 25% (positive or negative). A 25-50% change resulted in mid-monthly component changes for those three months of 25%, 37.5%, and 50%. The distribution of the percent change across the three months was done to reflect existing seasonal discharge and precipitation patterns of the area. The transition months between wet and dry seasons were assigned the smallest percent change.

Drier Scenario is the simulated daily discharge with changes applied to the mid-month seasonal residual components to reflect projected precipitation changes as simulated by Karmalkar et al. (2011). Perturbation in our model to the residuals of the mid-month seasonal component was applied to reflect the predicted monthly changes and then simulated daily discharge data was generated. Although no perturbation to the trend

component of our model was applied, perturbing the seasonal cycle in this manner does indirectly perturb the trend of the original model. The projected precipitation change (expressed as percentages) from this model are:

November to April = -23.8

May to October = -8.4

All months are projected to have a decrease in precipitation, resulting in drier conditions overall. To establish the change applied to the mid-month seasonal components, the projected changes in Karmalkar et al (2011) were treated as an average for the six month periods. Then, the range in percent change across the six-month period was defined as fifty percent greater-than and less-than the projected percent change, so that the average of the six months reflects the value reported for that time period in Karmalkar et al (2011). As a result, the change to mid-monthly seasonal components for November to April ranges from -35.7% to -11.9% and for May to October the range is -12.6% to -4.2%. The monthly percent change values were assigned so as to maintain existing seasonal discharge and precipitation patterns of the area. To reflect the Karmalkar et al (2011) results, the largest percent change was assigned to the currently dry months and the smallest change was assigned to the currently wet months.

Combined Scenario is the simulated daily discharge with changes applied to the mid-month residual seasonal components to reflect projected change as modeled by Campbell et al (2011) for the wet season months and by Karmalkar et al (2011) for the dry season months. Dry season months are January to May and wet season months are June to December. This scenario exaggerates the seasonality of dry and wet periods.

Climate Simulation Family 2 (ClimSim 2)

In the ClimSim 2 simulations, all of the ClimSim 1 scenarios were redesigned to, in addition to the seasonal component changes, also simulate an increase in the variance between the low and high discharge events by perturbing the irregular component in the model, or variability of the standard-normal equivalents of the residuals (mean of the $\log_{10}Q_{ratio}$). For the *No Change* scenario only the irregular component was perturbed. The perturbation of the irregular component was done to reflect the prediction that precipitation, due to extreme wet days (storm events), will increase by 2-6% in the latter

half of the twenty-first century (Kamiguchi et al., 2006). The four simulations in ClimSim 2 apply the same perturbation of the irregular component to the *No Change, Wetter, Drier*, and *Combined* scenarios for comparison within each simulation. Through iterative processes it was determined that a perturbation of the irregular component of 0.05 was necessary to increase the variance between high and low discharge in the *No Change* control scenario by 4%. Thus, the irregular component was increased by 0.05 in all ClimSim 2 simulations.

Table 0-2 lists the percent changes applied to the mid-month residual seasonal component for the scenarios in ClimSim 1 and ClimSim 2.

Table 0-2. Percent change applied to seasonal mid-month residual in the simulated potential future discharge scenarios.

	percent change		
Month	**Wetter**	**Drier**	**Combined**
Jan	1	-35.7	-35.7
Feb	-1	-35.7	-35.7
March	-12	-23.8	-23.8
April	-25	-11.9	-11.9
May	-25	-12.6	-12.6
June	-12	-4.2	-12
July	-1	-12.6	-1
Aug	25	-8.4	25
Sept	37.5	-8.4	37.5
Oct	50	-4.2	50
Nov	25	-11.9	25
Dec	12	-23.8	-23.8
Avg Annual Change	6.208	-16.100	-1.583

Figure 0-13 presents the resulting monthly average of the synthesized discharge (Qsim) for the simulated discharge scenarios in ClimSim 1. The discharge scenarios alter, yet maintain, the general shape of the observed seasonal trend with a relatively dry season January—April and a wet season May—December. The wet season has two precipitation maxima with one generally occurring May—August and then a wetter phase from September—December, while the dry season shows less month-to-month variability.

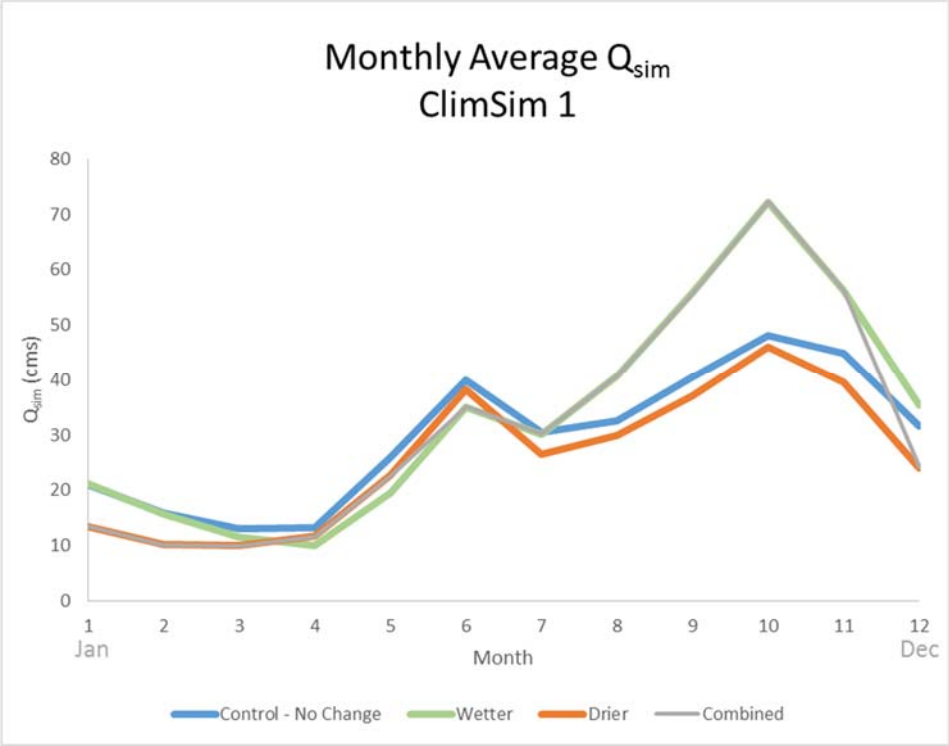

Figure 0-13. Monthly average synthesized discharge for the potential future discharge scenarios in ClimSim 1.

Figure 0-14 and Figure 0-15 show the histograms of the simulated discharge (Qsim) for the ClimSim 1 scenarios and ClimSim 2 scenarios respectively. These graphs illustrate the different distribution of discharge values within each simulated discharge scenario. Note the axis values on each graph are different. The *No Change – Control* shows a more regular bell shape to the spread of discharge values over the time period with a relatively fat tail. The *Wetter* scenario has a fatter tail to the spread, indicating an increase in larger discharge values. This scenario also has more frequent lower discharge values because, although it is a wetter scenario overall compared to the *No Change* scenario, it includes a decrease in discharge during the dry season months. The *Drier* scenario has a diminished tail (reduced large discharge values) and an increased frequency of low discharge values. The *Combined* scenario has both the fatter tail and an increased frequency of low discharge values. The general shape of each scenarios' histogram is similar between the ClimSim1 and ClimSim 2 graphs but, the tails are all slightly fattened as a result of increased storm intensity in ClimSim 2.

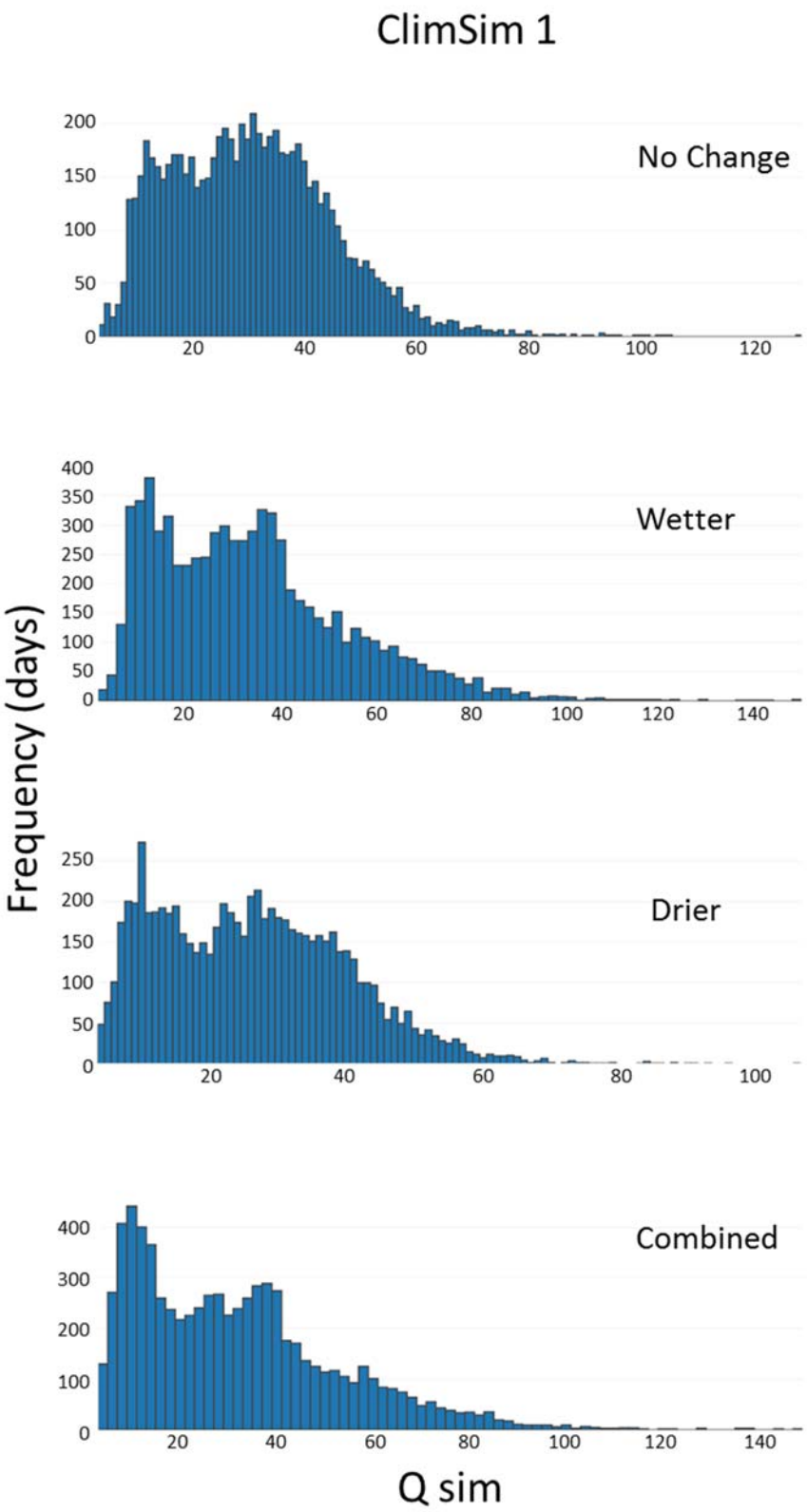

Figure 0-14. Histograms of ClimSim 1 simulated daily discharge (Qsim) in cms. 20 years of simulated data (7300 days).

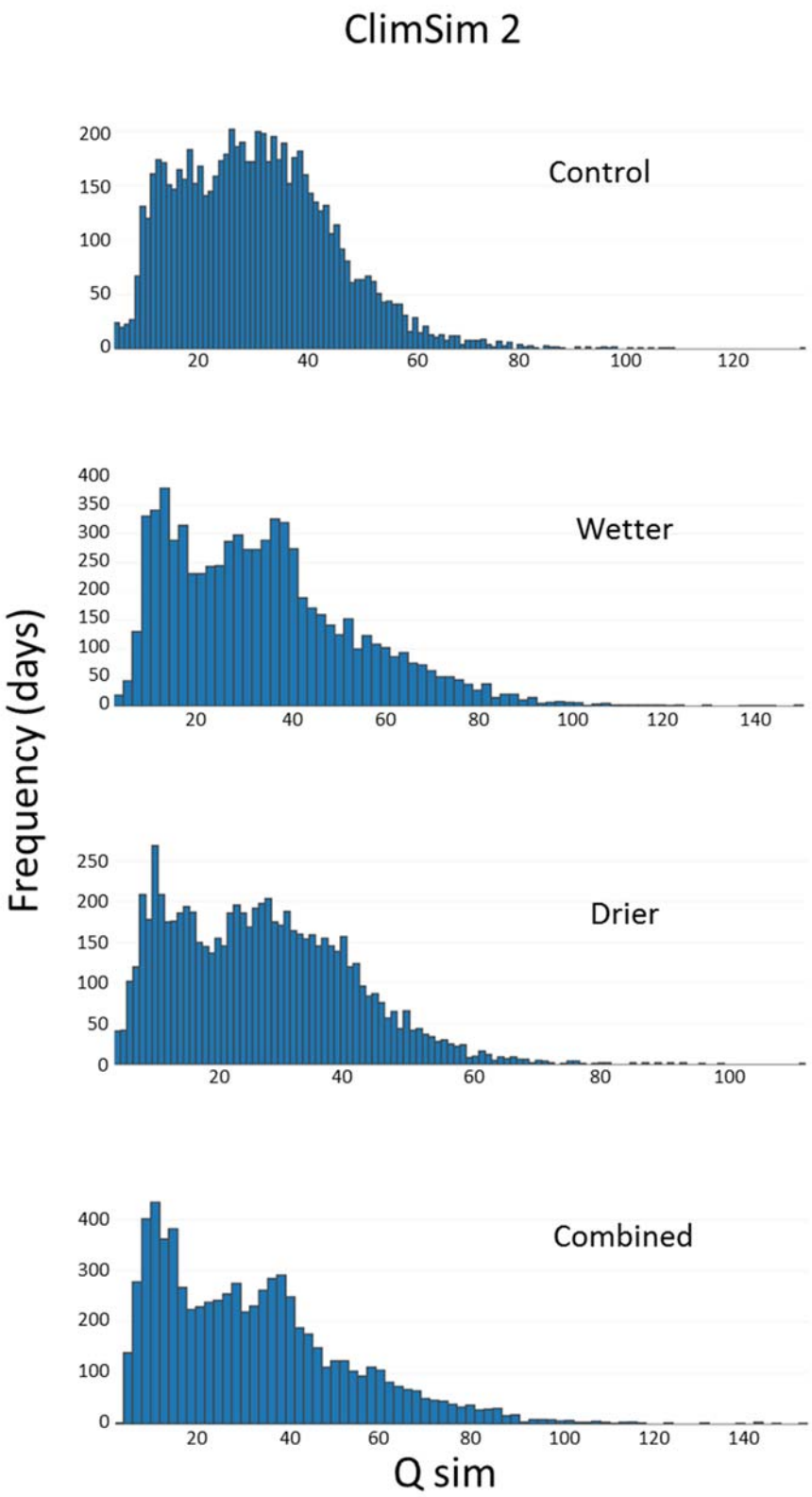

Figure 0-15. Histogram of ClimSim 2 simulated daily discharge (Qsim)in cms. 20 years of simulated data (7300 days).

Appendix F provides the seasonal component regression variations of the mid-month values for the desired percent change for each potential discharge scenario. Note that the seasonal component is manipulated for ClimSim1 scenarios and that since this component is not manipulated for ClimSim2, no change occurs for the *Wetter, Drier,* or *Combined* scenarios in ClimSim2. Appendix G provides time series plots of the simulated daily discharge for each of the eight scenarios. Note that all scenarios in ClimSim2 result in increased magnitudes between the high and low flow daily values.

4.2.2 Calculating Sediment Transport Capacity

The synthesized daily discharge data for the eight future scenarios were combined with field survey channel characteristics to calculate the potential future sediment transport capacity at two cross sections located at Bajo Pacuare in the mid-upper portion of the Rio Pacuare (see Section 4.1.2 and Figure 0-2). However, prior to calculating sediment transport, the synthesized new discharge data was downscaled from daily discharge values to 8-hour discharge values. Then, the previously developed sediment rating curves for the site (Chapter III, this dissertation) were used to calculate transport capacity for the modeled future discharge regimes.

Site Survey and Hydraulic Modeling

Grain size and channel topography, required to run the Recking (2013) bedload transport model, were surveyed in the field in 2013. Grain size fractions across the surface of the exposed bar at each cross section were determined by gridded sampling laid out with 100m tapes (Bunte & Abt, 2001) to eliminate bias of grain selection. Grain size was measured with a gravelometer and boulder calipers. The field surveys completed at each cross section captured channel topography as well as Manning's roughness estimates. The cross section topography was surveyed with a Laser Technologies laser range finder (LRF) (Impulse-Series) with a typical range accuracy of 0.01meters and inclination accuracy of 0.1 degree attached to a stabilizing pole (Figure 0-16). The survey data was then input into HEC-RAS 4.1.0 for 1-D hydraulic modeling with a range of discharges that included the maximum to the minimum discharge values reported for the

site. The HEC-RAS modeling generated the other necessary variables used in the Recking transport model (channel width, hydraulic radius, and energy slope gradient).

Figure 0-16. A) Laser Range Finder used for cross-section surveys. B) Grain size surveys with calipers and gravelometer. Photos by P.Lind – 2013.

Synthesized Sub-Daily Hydrograph

Humid tropical montane rivers often experience flashy high-magnitude flows (Restrepo et al., 2009; Wohl, 2005) driven by intense tropical precipitation events. Thus, a single daily discharge value can be smaller than the highest discharge value and larger than the lowest discharge value during a 24-hour period. The difference between actual and averaged discharge depends on how dynamic the fluctuations in flow are. This can result in an under prediction of bedload transport because transport rates are nonlinear as discharge increases.

To represent the flashiness of the system, a synthesized sub-daily hydrograph (8-hour average values) was created, following the procedure described in Chapter III (this dissertation). The sub-daily hydrograph temporally downscales the daily data from 24 hours to three eight-hour periods. Combined, the three discharge values average the reported daily discharge value (Figure 0-17). The synthesized sub-daily hydrograph does not capture peak-flow values or duration. However, this conservative approach to

creating a sub-daily hydrograph reduces the risk of over-estimating sediment transport values, while ensuring that dynamic flow events are not drastically under-estimated.

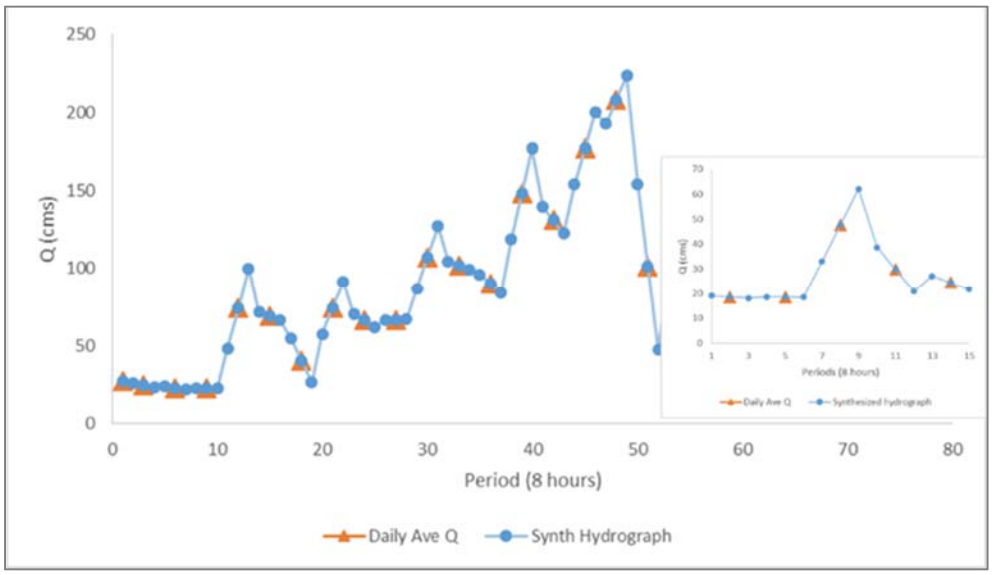

Figure 0-17. Examples of synthesized sub-daily (8 hour) hydrograph plotted with daily discharge value.

Bedload Transport Model

Sediment transport rating curves developed in Chapter III (this dissertation) were used to calculate the transport capacity at both cross sections. The transport model developed by Recking (2013) for coarse-bedded, steep mountain channels was used. This is the same model previously used to estimate bedload transport capacity for modern discharge regimes at Bajo Pacuare and six other sites on the Rio Pacuare (Chapter III, this dissertation). Although Recking's model is relatively new, it has been successfully implemented and evaluated in other studies (Anderson & Pitlick, 2014; Heimann et al., 2015; Kitsikoudis et al., 2014; Pourhosein et al., 2015). In addition, it has currently proven to be a good fit for modeling sediment transport in montane rivers of Costa Rica, compared to other methods (Arrieta, 2016). Recking's transport model is a non-threshold set of equations based on the surface grain sizes and slope. It assumes that sediment mobility is controlled by the D_{84}, integrating a ratio between the D_{50} and D_{84} into the equations. It is designed to predict an increasing critical shear stress with increasing

slope. This model is constructed to estimate non-linear or linear transport, as well as the transition between partial and full-bed mobilization.

The transport rating curves for BP XS02 and BP XS08 are developed as two-phase to best represent the high-flow and low to moderate-flow relationships (Figure 0-18). The results of the high-flow rating curve are used for calculating transport rates for discharges greater than the 0.8% exceedance flow (117 cms at Bajo Pacuare) and the other rating curve is used for discharges less than the 0.8% exceedance flow. The flow duration curve was developed from the daily discharge data reported at the Bajo Pacuare gage.

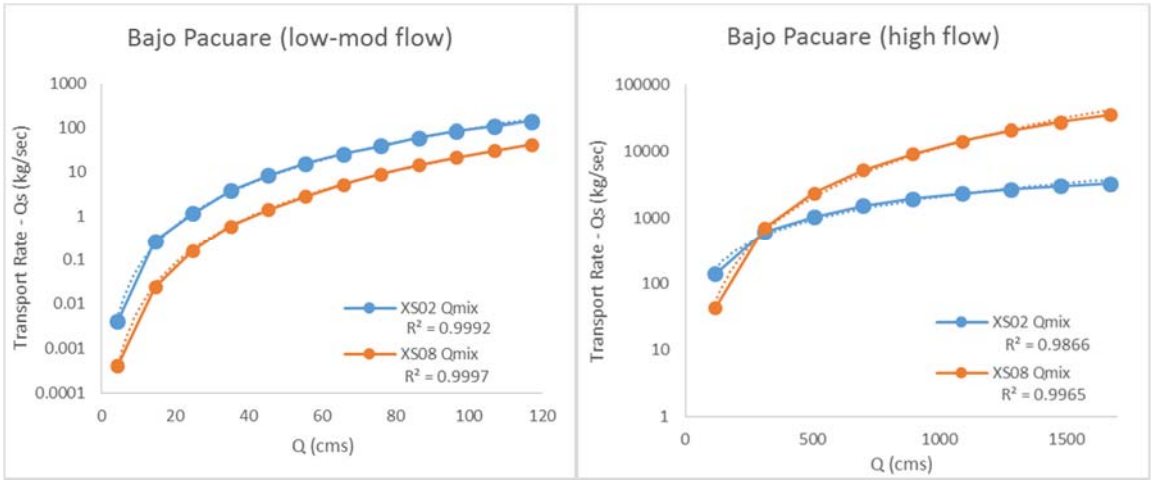

Figure 0-18. Sediment transport rating curves for low-moderate flow and high-flow at BP XS02 and BP XS08.

The Recking (2013) model produces an instantaneous transport rate expressed in kg/sec. From that the sediment transport rate per 8-hour sub-daily period was calculated, and then the daily rate (tons/day) was computed by adding the transport for the three 8-hour sub-daily periods. This was done for both of the cross sections for the twenty years of simulated discharge data created for each of the seven climate scenarios. An evaluation of the Recking model in Chapter III (this dissertation) found that the result can vary among cross sections at a site by up to a factor of 5. This apparently is fairly typical for coarse bedload modeling (Barry et al., 2004; Buffington & Montgomery, 1997; Vázquez-Tarrío & Menéndez-Duarte, 2015).

4.3 RESULTS

The results of the bedload transport estimates presented here for potential future discharge scenarios are discussed as transport capacity, instead of transport rate. Transport capacity is used because it is unknown from this analysis at what point in time the available sediment will match transport capacity or oversupply the system. Sediment transport capacity is equivalent to the actual sediment transport rate only when a river is transport-limited (Wallick & O'Connor, 2011). . The results of the bedload transport modeling for each of the potential future discharge scenarios at cross sections BP XS02 and BP XS08 are provided below.

4.3.1 Annual Bedload Transport Capacity

The average annual sediment transport capacity (tons/year) over the twenty modeled years for the eight potential future discharge scenarios are provided in Table 0-3 for both cross sections. Differences in the annual transport capacity results between the two sites for each discharge scenario is the result of site-specific characteristics (grain size, slope, channel geometry, and hydraulics) and likely some potential sediment transport model error reported in Chapter III (this dissertation). Table 0-3 also includes the difference between the average annual sediment transport capacity of the *No Change* control scenario and the other seven simulations, as well as the percent change those differences represent. As a reminder, Climate Simulation Family 1 (ClimSim 1) includes the *No Change (control), Wetter, Drier*, and *Combination* scenarios, while Climate Simulation Family 2 (ClimSim 2) includes these same simulations with an additional variance increase between the high and low discharge events.

Table 0-3. Average annual bedload transport capacity (tons/year) for twenty years of simulated discharge data, and the resulting percent change for each simulated discharge scenario.

BP XS02							
Model	ClimSim1 Avg Ann Sed Trans (tons/yr)	Difference	% change	Model	ClimSim2 Avg Ann Sed Trans (tons/yr)	Difference	% change
No Change - Control	**140,840**			No Change	146,679	5,839	4
Wetter	263,741	122,901	87	Wetter	271,401	130,560	93
Drier	98,443	-42,398	-30	Drier	102,014	-38,827	-15
Combination	244,692	103,851	74	Combination	250,953	110,113	112

BP XS08							
Model	ClimSim1 Avg Ann Sed Trans (tons/yr)	Difference	% change	Model	ClimSim2 Avg Ann Sed Trans (tons/yr)	Difference	% change
No Change - Control	**23,717**			No Change	29,807	6,090	26
Wetter	50,972	27,254	115	Wetter	53,200	29,482	124
Drier	15,985	-7,732	-33	Drier	16,734	-6,983	-29
Combination	46,987	23,270	98	Combination	48,835	25,117	106

As expected, a positive change (percent increase) in the average annual sediment transport capacity (tons/year) resulted from the *Wetter* scenario at both cross section locations and a negative change (percent decrease) resulted from the *Drier* scenario in both ClimSim 1 and ClimSim 2. At both cross section locations, the *Combination* scenario also result in a positive difference (percent increase) in average annual sediment transport capacity. The difference between the *No Change* and the *Combination* scenario is less than that of the *Wetter* scenario, but only slightly less at BP XS02. Since the *Combination* scenario includes a dry scenario for the relatively drier - months (Jan-May) and the wet scenario for the wetter months (June-December), this indicates that, while decreases in discharge during the drier months can impact annual sediment transport capacity, positive change to the wet-season months exert more control on the resulting annual transport capacity. This is further illustrated in Figure 0-19 where the annual transport capacity of the twenty years of simulated discharge for *Wetter, Drier*, and *Combination* scenarios that include seasonal change are presented with the *No Change* control scenario. The largest difference in annual transport (tons/year) between these scenarios occurs when the *No Change* scenario produces a relatively high annual transport rate.

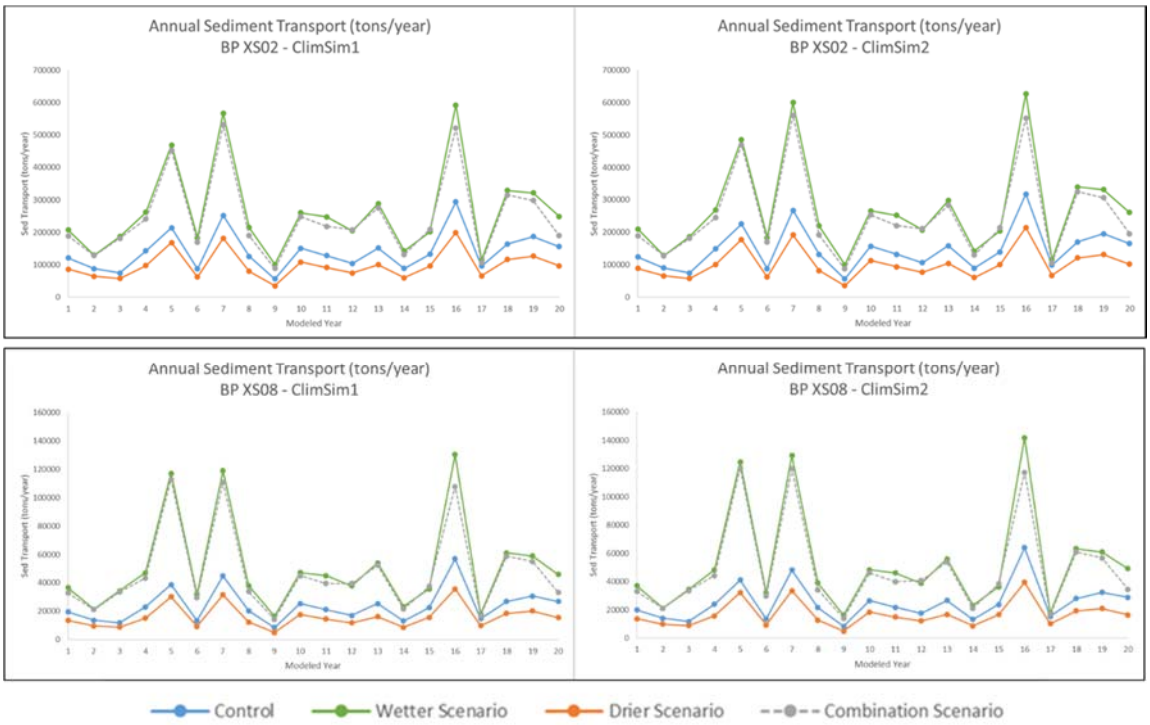

Figure 0-19. Twenty years of modeled annual sediment transport capacity at both cross section locations for the four climate change scenarios (Control = no change) for both climate simulations.

Since the same simulated twenty years' worth of discharge values was modeled at both cross sections, the differences in the average and annual sediment transport capacity (tons/year) at the two cross section locations are the result of the other variables input into the transport model (Recking 2013), site-specific differences in hydraulics, channel width, depth and slope, and grain size distribution. As depicted in Figure 0-4 bedload transport at BP XS02 has a linear relationship with discharge while a non-linear relationship occurs at BP XS08. Thus, a greater increase in discharge at BP XS08 is required to mobilize the coarser bedload fractions. This explains why percent changes in both ClimSim 1 and ClimSim 2 are greater at BP XS08 than BP XS02 for the *No Change, Wetter* and *Combination* scenarios when the relatively high discharge values are further increased. For example, the linear discharge to transport capacity relationship at BP XS02 resulted in a 4% increase in the average annual transport capacity between the *No Change* control scenario of ClimSim 1 and the ClimSim 2 *No Change* scenario with

the 4% increase in variance, while the non-linear relationship at BP XS08 resulted in a 26% increase for the same scenario (Table 0-3). This illustrates the importance of high-flow events for mobilizing bedload at BP XS08. It also suggests that a mere 4% increase in discharge variation (low to high) can result in a large enough increase in discharge during an event to mobilize the coarse-grained bedload material more frequently at BP XS08.

For both cross sections the ClimSim 2, with increased event variability, results in higher average annual transport capacity for all simulated discharge scenarios. Interestingly, the increased variance appears to at least partially offset the reduced overall annual discharge simulated for the *Drier* scenario at both cross section locations. This offset is most prominent at BP XS02 where the negative percent change of the *Drier* scenario was reduced by half in ClimSim 2 compared to ClimSim 1. As expected, the percent change for the *W*etter and *Combination* scenarios increased by 6-38% for ClimSim 2 compared to ClimSim 1.

4.3.2. Seasonal Bedload Transport

The percent of the bedload transported during different periods of the year was examined to determine the temporal variation in sediment transport annually and how that may change as a result of the simulated discharge scenarios. Table 0-4 provides the total sediment transported (cumulative load in metric tons) over the simulated twenty-year period and the percent of that load transported during four-month seasonal periods. The four-month periods are defined by the seasonal trends displayed in the monthly averages of the discharges (see Figure 0-13). The dry season is defined as January to April, the wet season is May to August, and the wettest season is September to December. For all discharge scenarios, the smallest percent of the total bedload transported occurs during the drier months of January to April. But, over half (61-83.9%) of the average bedload transported per year generally occurs during the wettest months of September to December. This illustrates the high degree of variability in sediment transported during a year and the significance of the wet season discharge and high flow event transport capacity on channel geomorphology in the Rio Pacuare.

Table 0-4. Seasonal distribution in cumulative load and percent of total sediment load transported (metric tons) at both modeled cross sections over the duration of the simulations (20yrs).

BP XS02	ClimSim1						
Model	**Total Cumulative Load (tons)**	**Load (Jan-April)**	**% dry (Jan-April)**	**Load (May-Aug)**	**% wet (May-Aug)**	**Load (Sept-Dec)**	**% wettest (Sept-Dec)**
No Change - Control	2,816,804	183,735	6.5	915,390.1	32.5	1,717,678.7	61.0
Wetter Scenario	5,274,823	163,307	3.1	873,347.4	16.6	4,238,169.0	80.3
Drier Scenario	1,968,851	59,104	3.0	698,495.5	35.5	1,211,251.0	61.5
Combination Scenario	4,893,833	59,003	1.2	925,375.1	18.9	3,909,454.6	79.9
	ClimSim2						
Model	**Total Cumulative Load (tons)**	**Load (Jan-April)**	**% dry (Jan-April)**	**Load (May-Aug)**	**% wet (May-Aug)**	**Load (Sept-Dec)**	**% wettest (Sept-Dec)**
No Change	2,933,573	199,483	6.8	950,477.7	32.4	1,788,884.0	61.0
Wetter Scenario	5,428,013	179,188	3.3	899,199.1	16.6	4,349,626.7	80.1
Drier Scenario	2,040,274	64,353	3.2	723,152.8	35.4	1,252,768.7	61.4
Combination Scenario	5,019,059	64,288	1.3	955,564.1	19.0	3,999,207.6	79.7

BP XS08	ClimSim1						
Model	**Total Cumulative Load (tons)**	**Load (Jan-April)**	**% dry (Jan-April)**	**Load (May-Aug)**	**% wet (May-Aug)**	**Load (Sept-Dec)**	**% wettest (Sept-Dec)**
No Change - Control	474,347	26,472	5.6	146,407.0	30.9	301,467.3	63.6
Wetter Scenario	1,019,436	23,718	2.3	140,327.1	13.8	855,390.6	83.9
Drier Scenario	319,702	7,303	2.3	108,596.6	34.0	203,802.6	63.7
Combination Scenario	939,744	7,304	0.8	149,246.9	15.9	783,193.1	83.3
	ClimSim2						
Model	**Total Cumulative Load (tons)**	**Load (Jan-April)**	**% dry (Jan-April)**	**Load (May-Aug)**	**% wet (May-Aug)**	**Load (Sept-Dec)**	**% wettest (Sept-Dec)**
No Change	500,503	29,530	5.9	153,154.0	30.6	317,819.6	63.5
Wetter Scenario	1,063,994	26,609	2.5	145,470.9	13.7	891,914.3	83.8
Drier Scenario	334,681	8,116	2.4	113,307.0	33.9	213,258.3	63.7
Combination Scenario	976,693	8,126	0.8	155,274.8	15.9	813,292.2	83.3

The simulated discharge scenarios modeled in this study maintain the general pattern of seasonal wet and dry periods but the seasonal variance is exaggerated or diminished compared to the observed seasonal trend. However, the *Wetter, Drier*, and *Combination* scenarios all result in a smaller percent of the annual sediment transported during the dry season, while having an equal or larger percent of annual sediment transported during the wettest months (Sept-Dec) compared to the *No Change* control scenarios in both ClimSim1 and ClimSim 2. Interestingly, the percent of sediment transported during the wet months (May-August) for both the *Wetter* and *Combined*

scenarios is smaller than the *No Change* scenario, but the total load transported is greater for the *Combination* scenarios. This reflects the increased discharge simulated during these months in combination with decreased discharge during the dry season months. Also, the *Drier* scenario produces larger percent of the load during the wet months (May-August) but a smaller quantity of the cumulative load compared to the *No Change* control scenario. This is interesting since the largest percent change applied to the monthly seasonal component was for the *Drier* scenario (-23.8 and -37.7%) for the months of December through March (Table 0-3). As expected, the *Wetter* and *Combined* scenario produce both an increase in the percent and load of the potential total sediment transported during the wettest months of the year (Sept-Dec). Only very minor change in the seasonal distribution and loads (0.1-0.4% change) occurred between the *No Change* control scenario of ClimSim 1 and the *No Change* scenario of ClimSim 2 at both cross sections modeled.

4.4 DISCUSSION

The results show that all of the simulated future discharge scenarios, when compared to the No Change control scenario, will alter the average annual sediment transport capacity at both modeled cross sections (BP XS02 and BP XS08) on the Rio Pacuare. The percent and quantity of potential sediment transported seasonally is also altered for all simulations except the *No Change* scenario of ClimSim 2, because only the variance was perturbed, without change in seasonal mean discharge. Changes to the quantity and timing of flow alters when and if sediment is mobilized. Therefore, on the Rio Pacuare and in other humid tropical montane systems, even subtle changes in discharge regimes and seasonality will have geomorphic consequences. For example, it will change how and when the river integrates lateral and upstream contributions of sediment. It could also change vegetation establishment patterns (spatial and temporal) and density along the river because vegetation growth on inactive bars is very rapid (weeks) in humid tropical regions.

At both cross sections, decreased discharge during the dry months (Jan-April) produces less change to sediment transport capacity than decreases in the wet season months (May-Dec). Increased discharge during the wet months produced the largest

percent change at both cross sections, with the greatest percent change occurring at BP XS08. In addition, increased discharge variability as simulated in ClimSim 2 scenarios increased sediment transport capacity at both sites for all of the scenarios. This supports the hypothesis that the timing and size of higher magnitude flow events is an important component of sediment flux in these systems.

Of interest is that increased variation between high and low flow events (ClimSim 2) during the *Drier* scenario partially off-set the percent decrease in average annual sediment transport for this scenario as modeled in ClimSim 1. This was most notable at BP XS02 where percent decrease in average annual transport capacity was reduced by half in ClimSim 1 compared to ClimSim 2, further supporting the idea that large-flow events are and will continue to be an important component of sediment flux and channel morphology on the Rio Pacuare.

The variability in changes between the two cross section locations are attributed to site-specific characteristic (grain size, slope, channel geometry, and hydraulics) that produce a non-linear discharge to transport relationship at one cross section (BP XS08) and a linear relationship at the other (BP XS02). Thus, although the sediment transport capacity (tons/year) is smaller at BP XS08, an increase in wet season discharge produces a larger percent change there than at BP XS02. This illustrates the requirement for higher discharges at BP XS08 than at BP XS02 to initiate mobilization of its coarser grain-size fraction and provides an example of how different locations on the Rio Pacuare may respond differently to changes in its flow regime. For example, bedload accumulations would be expected upstream of BP XS08 between high-flow events or floods, while some quantity of material is mobilized through BP XS02 during lower flows. This process is especially inferred and likely exaggerated for the *Drier* scenario where discharge is reduced for both the dry and wet seasons, even with the increased intensity of ClimSim 2 applied.

The results of this study clearly show that the ClimSim 1 and ClimSim 2 discharge scenarios simulated in this study are expected to shift the quantity, timing, and distribution of sediment transported during a year compared to the *No Change* control scenario. This is caused by the exaggerated seasonality that was simulated for the *Wetter, Drier,* and *Combination* scenarios in ClimSim 1 and Clim Sim 2. Interestingly, increased

variation in high and low discharge events, as simulated in ClimSim 2, only minimally influences the how sediment transport is distributed throughout the year. This may be a product of the climate model, which increased relative discharge variation throughout the year instead of only increasing the high-magnitude events which normally occur in the wet season months.

Geomorphic change in response to changes in the magnitude and timing of bedload sediment transport can be inferred based on basic morphodynamics (Church & Ferguson, 2015; Fryirs, 2016; Ziliani & Surian, 2012). However, there are challenges and limitations involved when inferring geomorphic change as a result of future climate scenarios such as predicting external forcing conditions, accounting for changes in lateral and upstream inputs, changing channel characteristics (grain size, geometry, etc.), validation of the models used (Lotsari et al., 2015), and the non-linearity of evolving natural systems that imply additional changes in climate, and thus discharge, may occur during the period of modeled sediment transport.

Lateral contributions of sediment and nutrients are important components of sediment production and thus channel geomorphology on the Rio Pacuare and other humid tropical montane systems (Pike et al., 2010; Rengers & Wohl, 2007; Wohl & Merritt, 2005). On the Rio Pacuare lateral contributions occur throughout the system via landslides off the steep adjacent hillslopes or as debris torrents and fluvial material delivered by a dense network of tributaries. Gravity, earthquakes, and soil saturation from heavy precipitation are all considered triggers for activating landslides and/or debris torrents in geologically active humid tropical mountain environments such as the Rio Pacuare (Ahmad et al., 1993; Dadson et al., 2004; Fuller et al., 2003; Hovius et al., 2000). Future climate scenarios that predict more or less precipitation and/or altered storm intensities have the potential to influence the frequency of lateral contributions to a channel by changing the amount of water delivered to the watershed for effective weathering processes. But, precipitation does not control tectonic uplift on the Rio Pacuare (Chapter II, this dissertation). Therefore, even if precipitation-induced mass wasting is reduced due to climate change (e.g. Drier scenario), lateral contributions triggered by tectonic processes or gravity will continue unencumbered by climate change.

Integration and redistribution of the material supplied to the channel from those contributions will depend on the competence of future discharge regimes.

The montane reaches of the Rio Pacuare currently flow through steep confining bedrock walls and hillslopes with small pockets of floodplain or terrace surfaces. The modern channel bed contains plentiful coarse (cobble-boulder dominated) bedload material of unknown depths. The bedload has been arranged into prominent bedforms (riffles, pools, steps, cascading riffles) that reflect the stream power of each reach (Chapter II, this dissertation). Increased annual sediment transport capacity, as simulated for the *Wetter* and *Combination* scenarios (ClimSim1 and ClimSim 2), would likely result in seasonal bedload scour at points along the channel as a result of increased discharge. If sediment availability does not match an increased bedload transport capacity, the system will be a sediment-limited system and bedload depletion and incision will occur. This would likely instigate upstream migration of channel bed lowering, where bedrock controls allowed, and downstream pulses or flushes of the mobilized sediment. Bedload material would likely be redistributed and the small floodplain pockets of stored material would be more readily activated and perhaps converted to active channel material through channel enlargement. If upstream and lateral contributions matched the channel's increased transport capacity, a transport-limited system status would occur. This will result in very little change to channel form or sediment distribution but sediment flux and bedform replacement would be more rapid. If upstream and lateral contributions exceed the channel's transport capacity, the system will be transport-limited and bedload accumulations will occur and aggradation will result.

For both the *Wetter* and *Combination* scenarios, the reduced bedload transport capacity simulated for the dry season months could result in channel accumulations of lateral or upstream inputs – assuming lateral contributions continue. The accumulations could act as a temporary buffer or delay-mechanism to incision processes, while the channel works through the added load during the wet season months with increased transport capacity. Under the ClimSim 2 simulations, where increased discharge variation further increases sediment transport capacity for the *Wetter* and *Combination* discharge scenarios, the flushing of accumulated sediment and/or incision processes would likely be

more rapid, perhaps even accomplished in a single event, depending on discharge magnitude.

Decreased annual bedload transport capacity, as modeled for the *Drier* scenario, would inevitably result in channel shrinkage and vegetation encroachment on abandoned currently-active surfaces. The channel would likely become transport limited due to the quantity of material already available in the system. Aggradation will occur in reaches with relatively lower transport capacity than upstream reaches, especially at points or reaches where bedload transport is non-linear. Accumulation of material at points of lateral contribution may impose local restrictions, grade changes, or push the channel to the opposite side of an already confined valley. Sediment accumulation locations, such as alluvial fans at tributary mouths, could create grade changes in the channel bed that result in an increased downstream gradient off the toe of the fan. This grade change would instigate upstream migrating incision and downstream pulses and accumulations of sediment during bedload-mobilizing flows.

4.5 CONCLUSIONS

The Rio Pacuare is a hydrologically dynamic and geomorphically responsive river system, similar to other tropical humid montane rivers. Results from this study conclude that even minor changes to the simulated modern discharge regime have the ability to notably alter the sediment transport capacity of the river. Linear and non-linear relationships between discharge and bedload transport also influence sediment flux through a site. These results have very real implications associated with the river's geomorphology and the freshwater resources and habitat that it supplies now and in the face of future climate change.

In this study, at two cross section locations, eight potential future discharge scenarios were simulated, based on the most current and regionally-specific climate projections (2070-2100) for the area. The first scenario modeled no-change based on modern observed discharge and seasonal trends. The other potential future discharge regimes resulted in significant changes (-33 to +124%) in the average annual sediment transport capacity. For these same future discharge scenarios, the quantity of material potentially transported during each seasonal was also altered. Changing the timing of

sediment transport is the result of simulating changes in seasonal discharge. Exaggerated seasonality further limits freshwater resources during the dry season and increases the risk of flooding and channel-changing events in the wet season. Exaggerated seasonality in bedload transport translates to less stable geomorphology, altered habitat, and potentially increased risks to anthropogenic infrastructures.

In conclusion, the potential future discharge regime scenarios simulated in this study have probable geomorphic responses that will alter the ecologic and freshwater resources of the river. From these results it is apparent that even relatively minor changes in monthly discharge values can alter sediment transport capacity and flux patterns on the Rio Pacuare. Predictions of increased storm intensity and thus the flashiness or intensity of discharge events have also been shown to increase sediment transport capacity. Intense discharge events may help off-set sediment accumulation patterns in the *Drier* future discharge scenarios but they could represent channel-changing flood events with potentially hazardous outcomes to anthropogenic infrastructures. This supports the idea that the Rio Pacuare is geomorphically responsive to projected future climate scenarios and most likely other anthropogenic impacts that alter discharge regimes, such as dam development.

Currently, massive gaps in humid tropical montane river research exist, yet these rivers are being developed across the world for irrigation, hydro-electricity, flood-control, etc. at an astounding rate. This study provides a basic foundation for understanding the potential impacts that future climate changes may have on sediment transport capacity, and thus the geomorphology, of the Rio Pacuare and other humid tropical montane rivers in the area. Ideally these results will instigate further research on the current and potential impacts of climate change and other activities that impact discharge regimes. Future research should be designed so that it is useful for both the scientific community as well as for resource managers and decision makers.

CHAPTER V

CONCLUSIONS AND SUMMARY

5.1 SUMMARY

This body of work uses traditional field survey methods combined with new applications of remote sensing techniques to examine the geomorphology and sediment dynamics of the montane portions of the Rio Pacuare in Costa Rica. In Chapter II, a suite of geomorphic components is examined and a model presented that illustrates how those components are interconnected and how the distribution of alluvial sediment varies in relation to geology (tectonics and lithology) and flow hydraulics. Chapter III, presents annual bedload sediment transport capacity at six field sites within the study area. Variability in the spatial and temporal distribution of sediment flux is discussed. In Chapter IV, a time-step hydraulic model is used to simulate eight potential future discharge scenarios based on climate change predictions. The simulated discharge data for two field sites is then integrated into the sediment transport model to examine how sediment flux, and thus channel geomorphology, is likely to change. Several conclusions based on the results of this research are presented in each chapter. Here, a summary of the most significant findings is provided for review.

The distribution of plentiful alluvial sediment as active bedload or stored in small pockets of floodplain or low terraces is dependent on the long-term watershed-scale influence of geology (tectonics and lithology) combined with the watershed's hydrologically dynamic flow regime. Geologic influences control valley width, channel width, and landscape erosion patterns that supply sediment to the river. Lateral contributions of sediment via landslides, debris torrents, and fluvial tributary inputs are distributed relatively evenly along the mainstem channel. Flows capable of mobilizing the lateral contributions occur frequently, and no or minimal accumulations of sediment occur at lateral contribution locations. These processes mobilize and redistributes available sediment downstream where valley and channel width accommodates, while the channel continues to incise into the tectonically uplifting landscape. The watershed is

composed of mixed lithilogies of differing resistance, but long-term incision has produced a channel with a bedrock confined meander planform and a linear longitudinal profile with no obvious geologic knickpoints.

Active bedload material was observed throughout the study area as either a veneer over bedrock or, more commonly, as alluvial deposits and bedforms of unknown depths, including large cobble and boulder bars that influence channel form at low flows. Active bedload and floodplain or low-terraces surface occur more frequently where channel slope is reduced and where valley widths are greater, including immediately upstream from fault intersections. At the reach and channel-unit scale, flow competence, represented by unit stream power, redistributes and organizes the bed material into channel units (pools, riffles, cascades, steps). The type and length of the channel unit is dependent on the slope of the channel. Analysis revealed that unit stream power is more directly controlled by slope than it is by width on the Rio Pacuare.

The high sediment transport capacity estimates for six field sites combined with coarse grain size fraction (D_{50}: 51-310mm and D_{84}: 360-900mm) reveals a highly competent system capable of transporting large quantities of sediment. Sediment transport capacity estimates generated for the representative cross sections from each field site range from 0.1 to 5.4 million tons per year. The tropical precipitation events that generate the channel's discharge produce high-magnitude flows capable of mobilizing the coarsest grain fraction (D_{84}) at least once but usually several times a year and the median grain fraction (D_{50}) multiple times a year at all field sites modeled. Approximately 50 to 75 percent of the annual potential sediment transported happens during the wet-season months of October to December when the channel's discharge rapidly fluctuates in response to seasonal storm events.

Changes to the discharge regime of the Rio Pacuare, even minor changes, can notably change the river's sediment transport capacity. Based on modeled climate change predictions, eight different potential future discharge scenarios were developed to modeled sediment transport capacity at two different cross section locations. Changes of -33 to +124 percent in the average annual transport capacity were found. The greatest changes occurred when changes to the wet-season months were applied (positively or negatively). Though small compared to the seasonal changes, increased variability in

discharge events – storm intensity – also increased transport capacity for all scenarios modeled, further elucidating the importance of high-flow events to sediment transport capacity.

Changing the timing and quantity of bedload flux through the system will result geomorphic changes in the system. Probable geomorphic responses include sediment accumulations as a result of reduced discharge, especially with drier dry season scenarios, and increased sediment flux or flushing in response to increased discharge, especially with wetter wet season scenarios. Increased sediment transport capacity may lead to localized scour into stored bedload material and eventually increased incision into the underlying bedrock. However, lateral contributions are expected to continue supplying material to the channel (perhaps at increased rates with increased storm intensity). Based on these results the Rio Pacuare will likely respond geomorphically to changes in its discharge regime.

5.2 CONTRIBUTIONS OF RESEARCH

This body of work contributes information on the processes that influence and control the Rio Pacuare's main stem geomorphology and sediment flux patterns. Bedload transport capacity estimates show the spatial and temporal patterns of sediment flux in these systems and reveal that the coarsest grain size fraction are mobilized, on average, at least one a year or more. And, time-series hydraulic models coupled with bedload transport modeling reveals the sensitivity of the river's transport capacity to change in its discharge regime. Though only small pieces to the many existing gaps in our knowledge regarding the geomorphology of humid tropical rivers, this research also provides a foundation from which to build further work on the Rio Pacuare and other tropical montane rivers.

Specifically, this research provides a conceptual model that identifies select geomorphic components and illustrates their complex interactions and relative influence on alluvial sediment distribution throughout the study area. This model is a tool for illustrating the complex geomorphology of the Rio Pacuare and predicting probable geomorphic responses to change in different geomorphic components included in the model. If this model is tested on other rivers, a better understanding of the processes and

controls could be developed. This could expand our knowledge of the specifics and generalizations that exist regarding geomorphic processes of humid tropical montane rivers, as well as rivers across the world.

Another tool created and provided by this research is the regional discharge to upstream drainage area relationship model (see Chapter III). This tool can reasonably be used to generate daily discharge estimates for additional ungaged sites on the Rio Pacuare. Additionally, with slight modifications to fit a specific river, it could be used to generate daily discharge for other ungaged rivers located on the eastern slopes of the Talamanca Mountains.

The use of Structure from Motion (SfM) to identify single-grain mobilization after a flood event was successfully applied, for the first time, in this research to confirm grain mobilization after a flood event. This was used to validate hydraulic model results. This technique proved useful and viable for this purposes in an region that poses many challenges to bedload transport data collection, including likely destruction to traditional sediment traps.

This work also reveals how subtle changes in the system's discharge regime will likely notably change sediment transport capacity and thus channel geomorphology of the Rio Pacuare. This is an important contribution to consider in the face of climate change and potential dam development on this, other rivers in the Talamanca Mountains, and humid tropical montane watersheds across the world. Ideally, this work will expose the need for more thorough climate change and impoundment related research on humid tropical montane rivers. Hopefully it will also contribute to the discussion of local resource management and development in the region and elsewhere.

5.3 RETROSPECTION

A myriad of methods and techniques were utilized to complete this research. As is usually the situation, through the process of data collection, processing, and analysis, lessons were learned on how to improve the methods and techniques for future similar research applications. The main things I would do differently are:

1. Conduct gravel counts during a year with a drier dry season so that the counts would include more of the bedload than was exposed during this study. This

would have been particularly useful in Mollejones Cañon (River Segment 3) where bedload is mobilized frequently but covered by flow during anything but very low-flow periods. As it so happened, the year of data collection for this study had the driest wet season on record and a moderately wet dry season. This made capturing multiple flood events and a true low-flow period difficult.

2. Conduct the pre and post flood photogrammetric surveys during more than one wet season to improve grain-mobilization validation and the understanding of sediment transport relative to flow events--preferably a year or years with wet season(s) that produce more flood events (>1) than the wet seasons surveyed during this study.
3. Conduct cross section surveys during a year with a drier dry season so that more detailed topography of the bed of the channel can be captured. Perhaps use bathometry at the cross section to better capture channel geometry.
4. Conduct more detailed geologic surveys of the exposed bedrock along the channel banks to correlate source areas to alluvial sediment downstream for an analysis of attrition rates and clast residency times. .Although geology was noted, the complexity of different bedrock stratigraphy were not captured. Instead, it was generalized in the field notes to the dominant lithology. This level of detail proved more than adequate for this study, but future studies on connectivity, attrition, or the influence of lithology on channel form, etc. would benefit from more detailed survey work.
5. Establish precipitation and/or climate stations within the watershed of interest to better correlate climate patterns to discharge patterns. This would improve model results of simulated discharge as a result of predicted climate change scenarios.
6. Establish a discharge gage with the capacity to capture instantaneous discharge data. This would provide information on peak flow events that are muted by daily discharge data. It is predicted that access to instantaneous discharge data would produce more accurate and higher sediment transport capacity estimates.

5.4 FUTURE WORK

The body of work presented here provides a foundation for future work on the Rio Pacuare and other humid tropical montane rivers. Considering the increased development pressures that these rivers are faced with, I recommend that future research be designed so that it is useful and accessible for both the scientific community and for resource managers and decision makers.

On the Rio Pacuare, development of a sediment budget for each river segment would be beneficial for better understanding sediment flux and connectivity from upstream to downstream. The budget should include quantitative data on sediment inputs, storage, and outputs. This would also improve modeling and predictions of the impacts of future development (impoundment, etc.) and climate change on the geomorphology of the river.

Lateral contributions have proven to be primary sources of the high quantity of available sediment in these systems. Future study on the frequency and distribution of lateral contributions from landslides, debris torrents, and tributaries would be highly useful in understanding sediment distribution and landscape evolution of humid tropical montane rivers.

Future sediment transport research on the Rio Pacuare and other humid tropical montane river needs to include peak discharge data. These systems are hydrologically flashy and as a result a single daily discharge value likely underestimate the systems actual capacity to transport sediment. This will aid in better understanding long and short term transport rates, the character of sediment pulses in these dynamic systems, and how different ranges in grain size influence mobilization at different sites in steep systems with active bedload.

It would be interesting to integrate some type of grain tracing (via radio tagging or otherwise) with future sediment transport studies to determine residence time of bedload material in humid tropical montane rivers. Tracing would also reveal flux patterns as well as upstream to downstream connectivity.

Of the utmost importance is future research specifically on the geomorphic impact of dam impoundment on humid tropical montane rivers, including the rivers of the Talamanca Mountains. Hydro-electric development is on a rapid uphill trajectory in many

humid tropical regions. Understanding the potential impacts before damage is done could influence both development design (to minimize negative impacts) and resource conservation. Knowledge on how these systems work prior to them being altered by anthropogenic influences will also be important for the remediation efforts that will likely follow development, as we have learned in North America river development and restoration.

APPENDICES

A. GEOMORPHIC SUMMARY OF RIVER SEGMENTS

This appendix examines how the evaluated components combine to produce the geomorphology of each river segment. A map is provided for each river segment that includes the major identified faults that intersect the channel, as well as the digitized channel, bars, floodplain and low terrace surfaces, plus the locations of modern landslides and debris torrents either identified in the field and/or in the high resolution aerial imagery collected April 2014. In addition, channel slope and estimated unit stream power (for the 0.2% exceedance flow) at 100m increments along the channel pathway are represented as parallel maps. These combined variables intend to illustrate the primary sediment sources (upstream and lateral) and alluvial sediment distribution (stored during low-flow periods), plus how alluvial sediment distribution correlates to measurements of flow competence.

R-Seg 1 (Rkm 44.2-54.9), Figure A-1: Large cobble-boulder bars are plentiful from Rkm 44.2-54, except where the channel cuts through the confined Dos Montañas Canyon. At Dos Montañas (Rkm 46.5-47), the channel is deep, low gradient, and completely confined within shear rock walls. In contrast Rkm 44.5-46.5 and 47.5-52, the channel is it's widest as it crosses the footwall valleys of the Siquirres-Matina thrust fault. These reaches also have a relatively slow slope and low unit stream power. The large alluvial fan, sourced from the unstable fault ridge on river left, pushes the channel to the valley's west side, from Rkm 47.5-52 into a high (~20m) eroding sandstone cutbank topped with unstable soil and colluvium. Upstream of Rkm 52, bar area gradually reduces as both channel confinement and bedrock controlled meandering increase. A bedrock unit boundary also exists at approximately Rkm 52 (see Figure 0-7), likely controlling the change in channel form that occurs as the channel shifts from more resistant bedrock upstream to less resistant material downstream of Rkm 52. Multiple geologic controls force channel geomorphology in this short river segment. However, no notable changes in channel slope pattern occur, because the plentiful bedload is arranged fluvially to minimize flow gradient. This indicates that reduced stream power in this river segment

(relative to upstream segments) is still plenty competent to mobilize available and incoming alluvial material composed of cobbles and boulders.

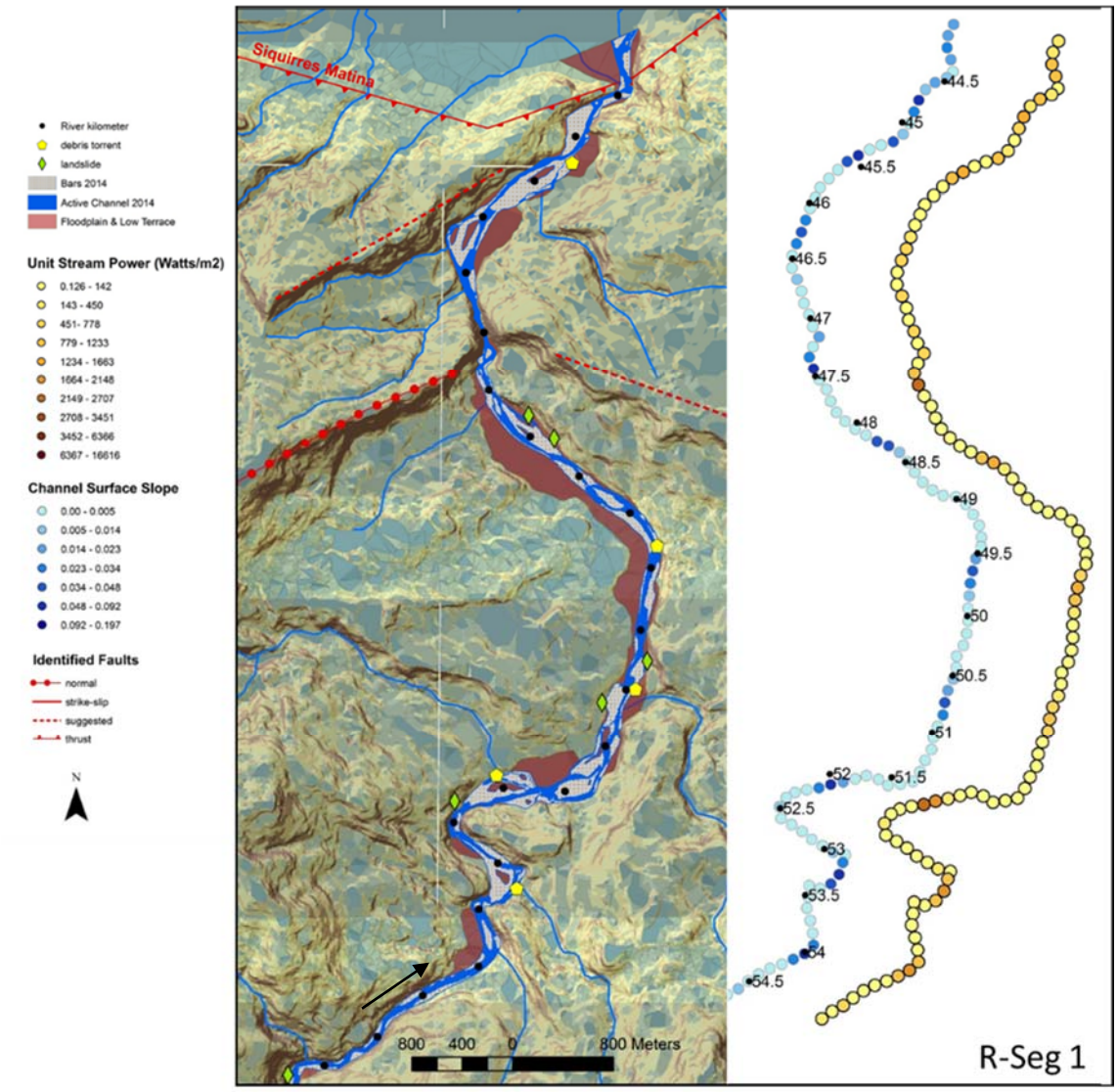

Figure A-1. R-Seg 1. Alluvial sediment distribution, channel surface slope, and unit stream power.

R-Seg 2 (Rkm 54.9-70), Figure A-2: A few small pockets of floodplain or low terrace surfaces are irregularly scattered throughout R-Seg 2 where lateral valley space allows, but most R-Seg 2 stored alluvium is found in large, active boulder bars. The large bars accentuate the channel's otherwise bedrock-confined meandering pattern during normal or low-flow periods. The greatest accumulations of exposed bar material occur upstream

of fault intersections at approximately Rkm 59.5 and 65, which is interesting considering the uplifting normal fault that runs parallel to the river upstream of Rkm 65 is presumed to influence incision rates in the R-Seg 2 upper reaches. Downstream of the normal fault at Rkm 59.5, channel slope remains about the same as upstream by increasing the frequency of cascading-riffle features—most likely to accommodate a slight uplift-induced grade increase at the fault face. However, unit stream power does increase here due to channel narrowing. An additional geologic control on channel form and reach-scale geomorphology is the prominent confined bedrock meanders at Rkm 56-57 (Juacas Cañon) where bar and floodplain features are minimal.

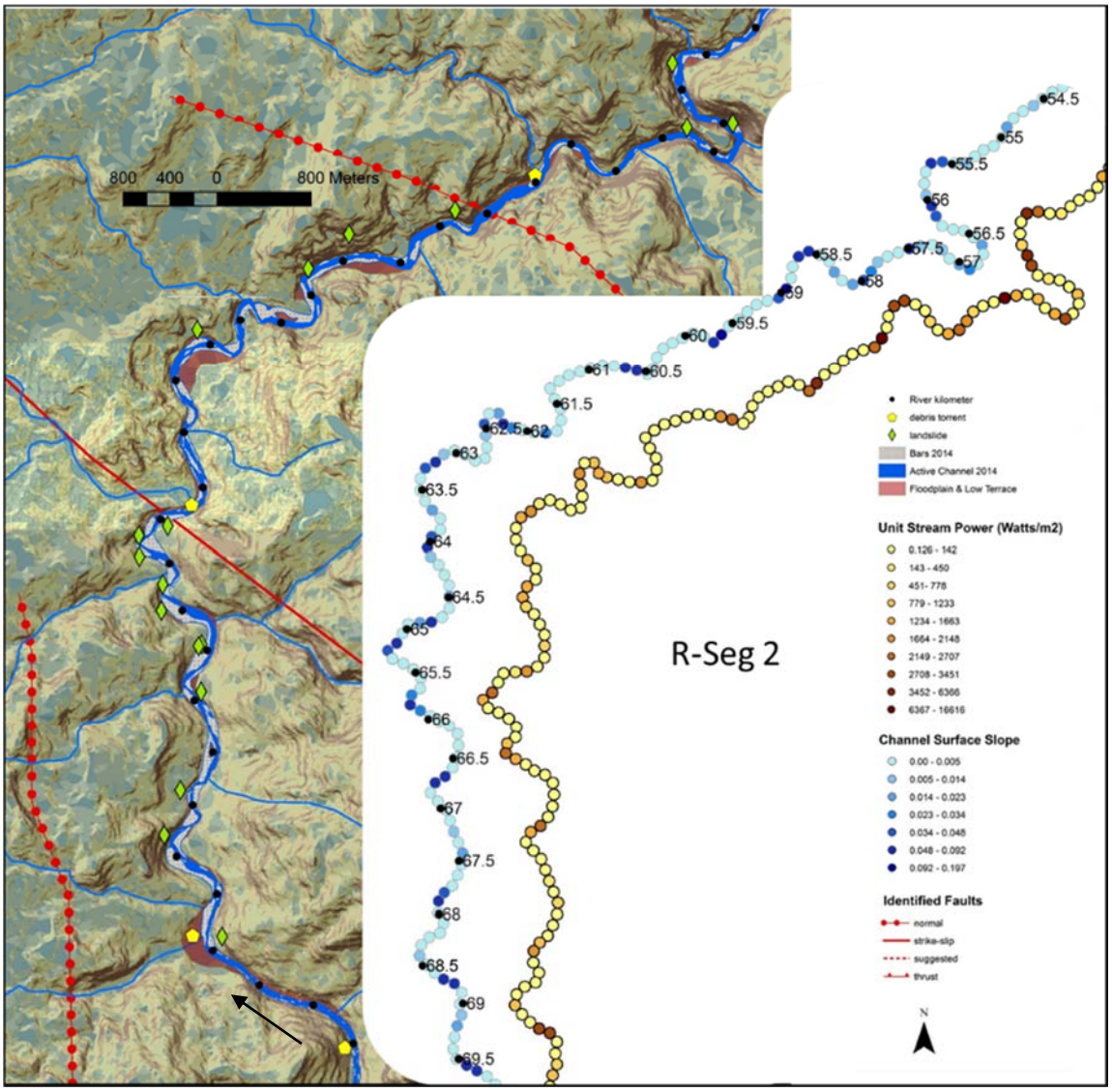

Figure A-2. R-Seg 2. Alluvial sediment distribution, channel surface slope, and unit stream power.

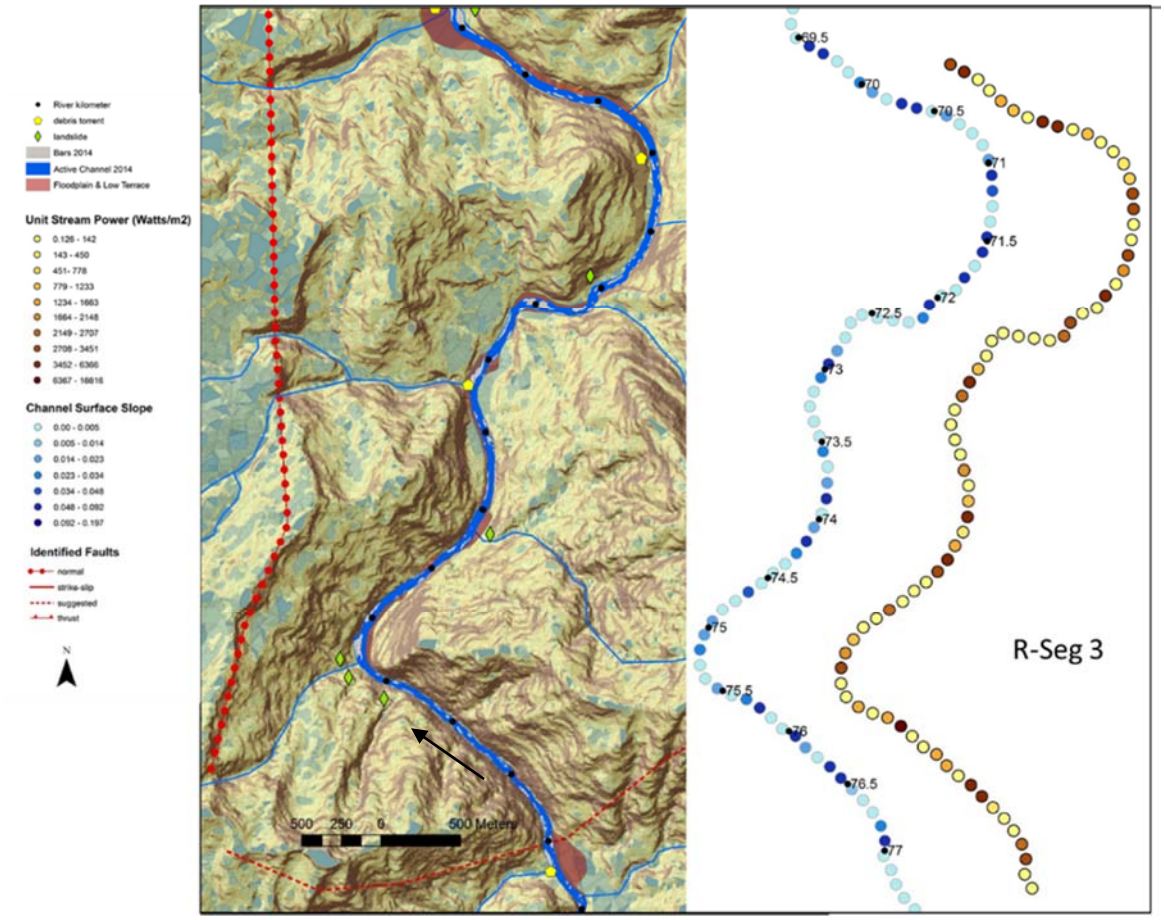

Figure A-3. R-Seg 3. Alluvial sediment distribution, channel surface slope, and unit stream power.

R-Seg 3 (Rkm 70-76.9), Figure A-3: Small side bars and a few point bars are located throughout this confined river segment known as Mollejones Cañon. Most bar area exists below Rkm 75, where narrow bedrock shelves and thin floodplain pockets are also found. The channel greatly narrows upstream of Rkm 75, and large boulders, likely originally sourced from the steep adjoining hillslopes, serve as the foundation for sets of boulder steps and pools. R-Seg 3, in contrast to upstream and downstream, has a notably narrower channel width, which requires increased flow velocity and/or channel depth through this segment. Consequently, mean unit stream power is higher in this segment compared to downstream, but is, except at steps and cascading riffles, slightly lower than upstream R-Seg 4. Imbricated large boulder deposits observed on bedrock shelves above normal flow stage, as well asregularly deformed cobble-boulder bedforms visible below the water's

surface, indicate that this segment mobilizes its available alluvial sediment. A suggested secondary fault intersects the channel at the upstream end of the segment. This secondary fault associates with the stair-step set of normal faults that run parallel to the channel on the west side (river-left). Uplift rates are not available for this set of faults, but the active processes undoubtedly influence channel incision rates into the R-Seg 3 resistant calcareous limestone bedrock.

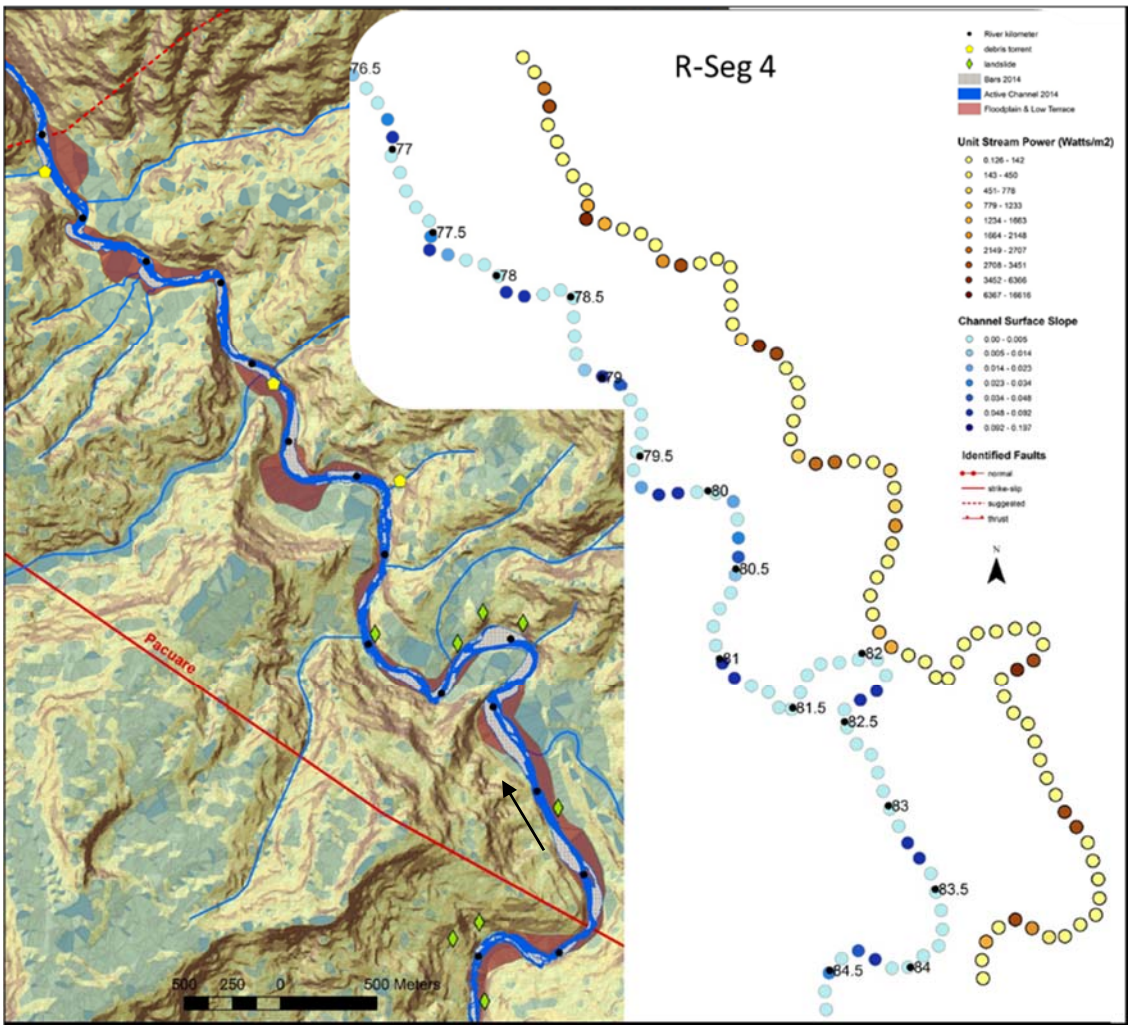

Figure A-4. R-Seg 4. Alluvial sediment distribution, channel surface slope, and unit stream power.

R-Seg 4 (Rkm 76.9-84.1), Figure A-4: Large cobble-boulder bars upstream of Rkm 81 are elongate side-channel bars that alternate from one side of the channel to the other, and mid-channel transverse bars. Here, thin pockets of floodplain or low terrace surfaces

border sections of the channel. Between Rkm 79.8 and 81.5, the channel narrows, bar size and prevalence decrease greatly, and very few floodplain surfaces exist. Massive boulders in the channel here split the flow in what is otherwise a straight confined reach which has the highest slope and unit stream power of the segment. Large cobble-boulder bars and pockets of floodplain or low terrace surfaces occupy the R-Seg 4 downstream reaches from Rkm 76.8 to 79.8—though channel width does decrease and bar size diminishes in a downstream trend. The highest peaks in slope and unit stream power occur between Rkm 79 and 81, but fluctuations in both, related to cascade-riffle locations, occur throughout. R-Seg 4 is located between the Pacuare strike-slip fault at the upstream boundary and the suggested secondary normal fault at the downstream boundary. Bedrock-forced meander form is exaggerated at visible bedrock deflection points from river-left at Rkm 79.5 and 82.5.

R-Seg 5 (Rkm 84.1-95.25), Figure A-5: This river segment contains semi-confined reaches with pockets of floodplain and low terraces surfaces that alternate with bedrock confined reaches. Bar distribution is more prominent in the semi-confined reaches (Rkm 84-84.5, Rkm 87.5-90.7, Rkm 93-95.25). Channel planform is bedrock controlled. Between Rkm 84.5 and 86.5, the channel is relatively straight and narrow. Upstream of Rkm 90, the channel type is predominantly riffle-pool, and downstream is cascading riffle-pool. In R-Seg 5, the cascading riffles are longer and the pools are shorter than the upstream riffle-pool sequence, indicating bedform adjustment to compensate for a higher underlying gradient. At Rkm 87, a set of cascading step-pools formed from massive boulders, likely supplied from the steep adjacent hillslope, in a bedrock confined section that produces the R-Seg 5 highest unit stream power estimates. This variability in channel types and widths results in a wide range of both slope and unit stream power in R-Seg 5.

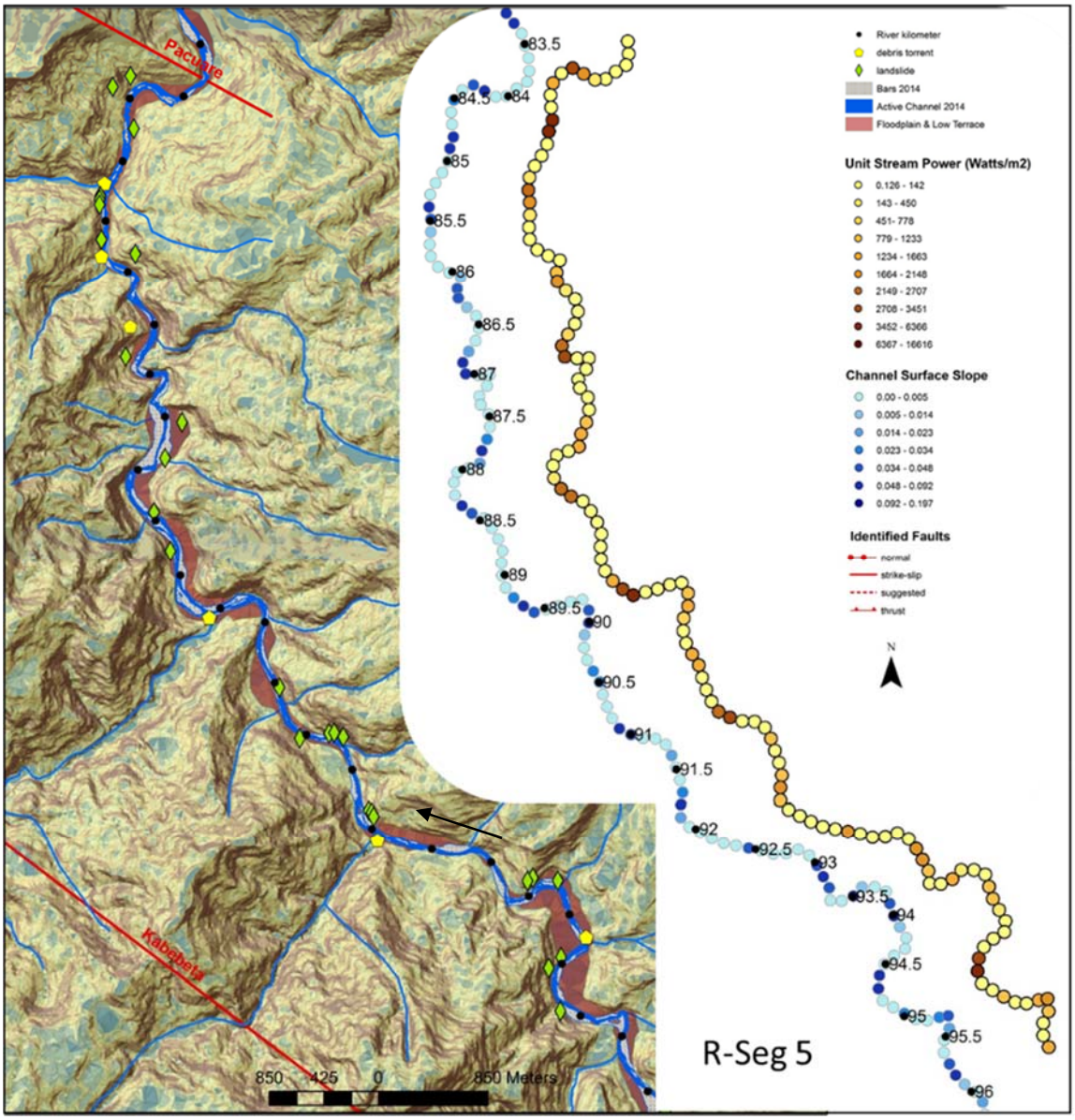

Figure A-5. R-Seg 5. Alluvial sediment distribution, channel surface slope, and unit stream power.

R-Seg 6 (Rkm 95.25-108.3), Figure A-6: Narrow floodplain and low terrace surfaces are relatively continuous and border at least one side of the channel throughout most of this semi-confined river segment. The only reaches with no or minimal floodplain and low terrace surface are downstream of the channel intersection of the Kabebeta strike-slip fault (Rkm 98.5-100), a 500m hillslope confined section at Rkm 103, and a few short (100-200m) sections in the R-Seg 6 upper reach. Upstream of the Kabebeta fault and Rkm 103, the cobble-boulder bars are most prevalent, and the channel is braided during

normal and low-flow river stages. Mean channel slope is similar to R-Seg 5, but mean unit stream power is less, except at the aforementioned confined sections, where some cascading-riffles and a few step-pools exist. Overall, gradient is managed by adjusting the plentiful bedload material into long extended riffles and relatively short pool units. Upstream of Rkm 105, the dominant channel type shifts to cascading riffle-pool, with the length of the cascading riffle increasing with an upstream trend as slope increases, valley width narrows, and unit stream power increases.

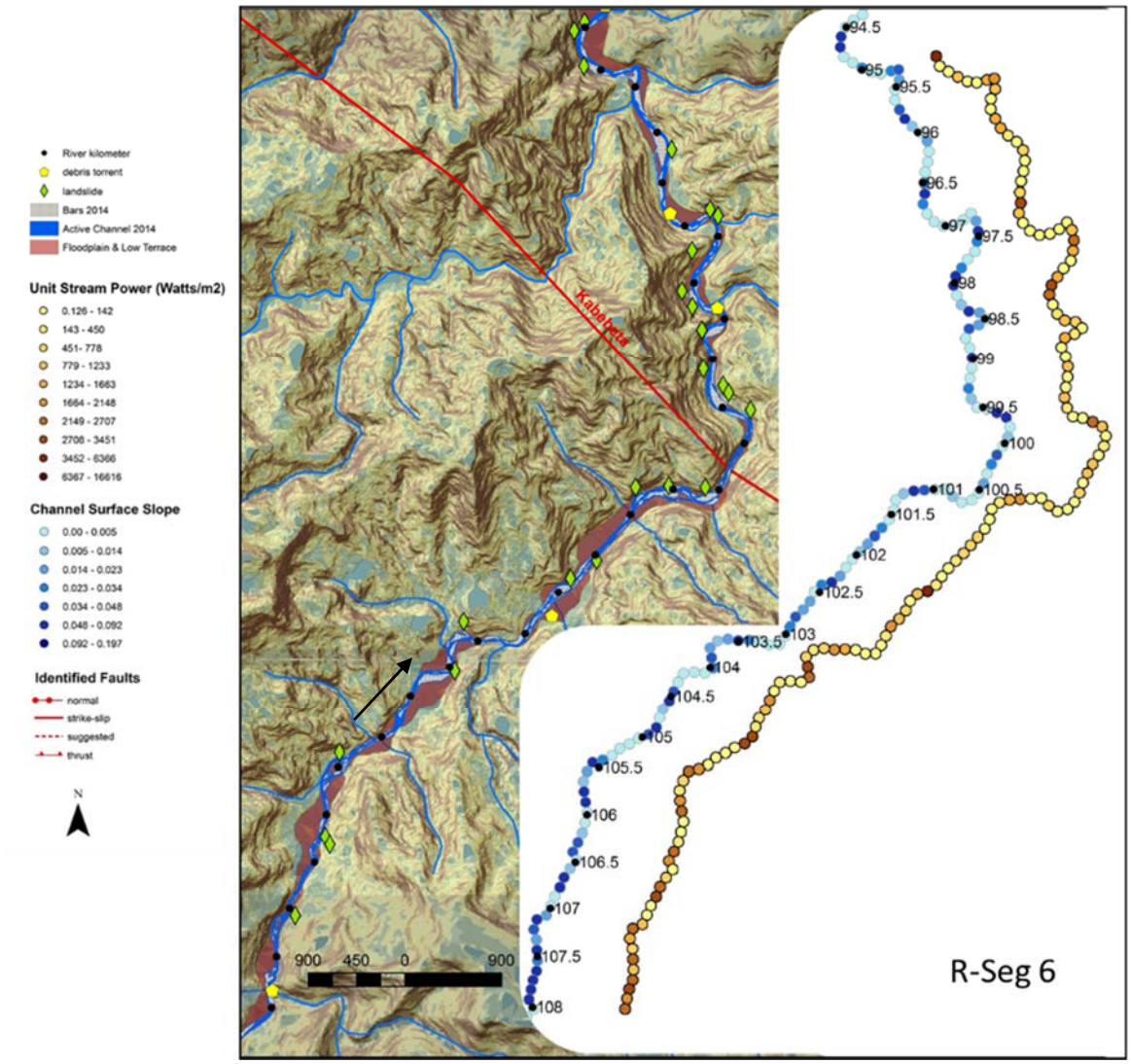

Figure A-6. R-Seg 6. Alluvial sediment distribution, channel surface slope, and unit stream power.

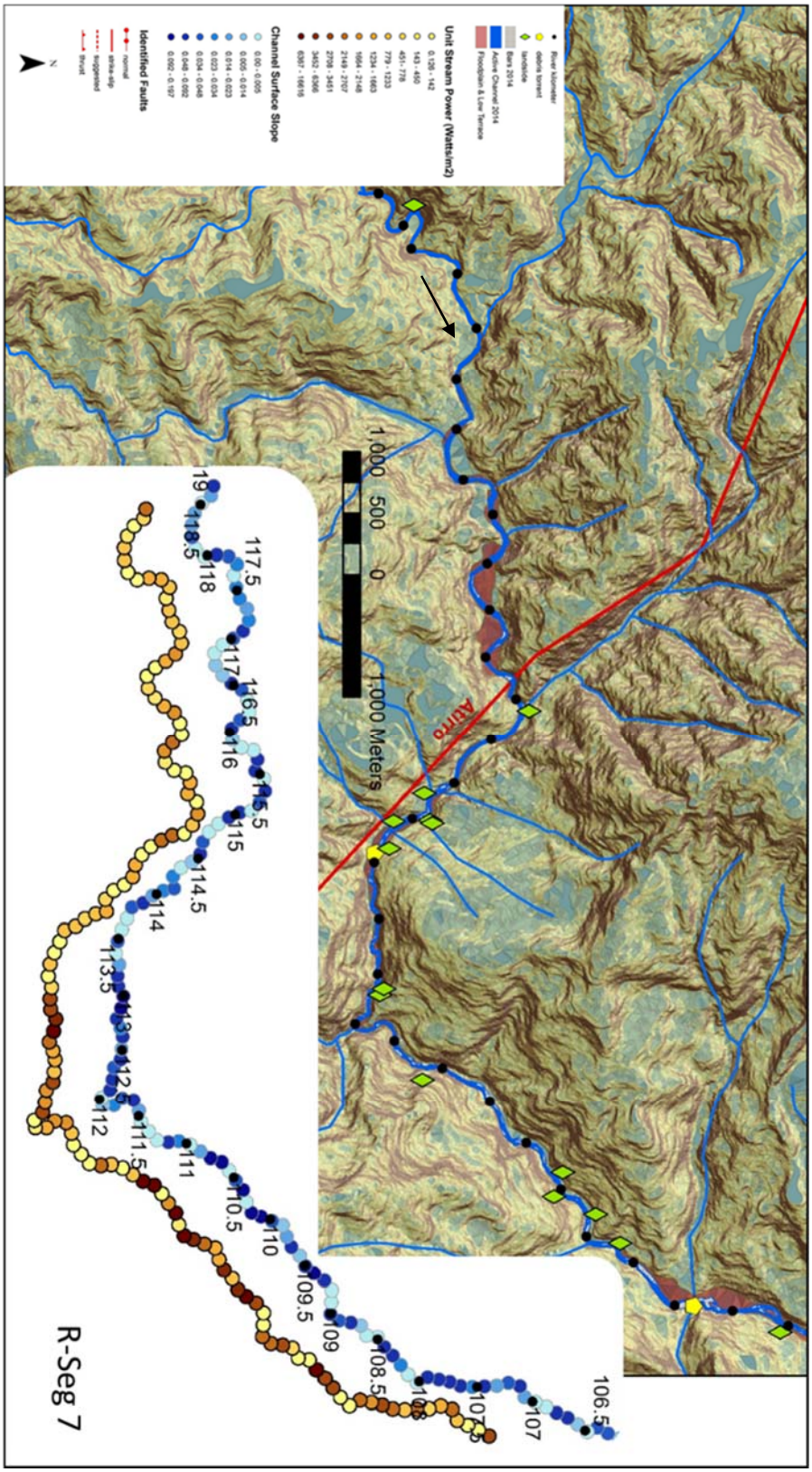

Figure A-7. R-Seg 7. Alluvial sediment distribution, channel surface slope, and unit stream power.

R-Seg 7 (Rkm 108.3-132), Figure A-7: Minimal bar development and sliver-pocket floodplain and low terrace surface areas exist between Rkm 113.5 and120. Upstream of Rkm 122, the channel is a steep, completely confined single-thread, cascading to step-pool channel with large-to-massive boulders lining the bed. The channel intersects and travels along the Atirro strike-slip fault from Rkm 113.5 to 115.5. Along the fault zone, the channel type is cascading riffle-pool. Downstream of Rkm 113.5 to 112, the channel is hillslope/bedrock confined and relatively steep, with cascading to step-pool channel geomorphology. Downstream of Rkm 112, gradient decreases slightly and channel type shifts to a cascading riffle reach with a few step-pool units. Upstream of Rkm 115.5 to approximately Rkm 117, floodplain and low-terrace surfaces, up to four times wider than the active channel, fill the valley floor. Bar surface area increases only slightly, however, within this reach, but some riffle-pool sequences occur. This perhaps indicates that periodic or episodic valley infilling and aggradation is a response to seismic activity that constricts the channel at the upstream fault intersection at Rkm 115.5. After the constriction is fluvially processed, the channel incises into the alluvium in an attempt to readjust channel slope to downstream bed-elevations. Evolution and sequencing of these processes would be/is related to frequency and magnitude of tectonic shift or seismically-induced landslide colluvium inputs and frequency and magnitude of competent flow events.

B. PHOTOS OF FIELD SITES

Photos by P.Lind or O.A. Nunez (2013-2014)

Arriba Pacuare (AP) – Rkm 106.4

Bajo Pacuare (BP) – Rkm 90.4

Tres Equis (TE) – Rkm 66.2

Bajo Pacuare por San Juaquin (BPSJ) – Rkm 82.6

Paso Marcos (PM) – Rkm 93.7

Bajo Tigre (BT) – Rkm 62.5

Mollejones Canon (MC) – Rkm 74.9

Arriba Pacuare – Rkm 106.4

Paso Marcos – Rkm 93.7

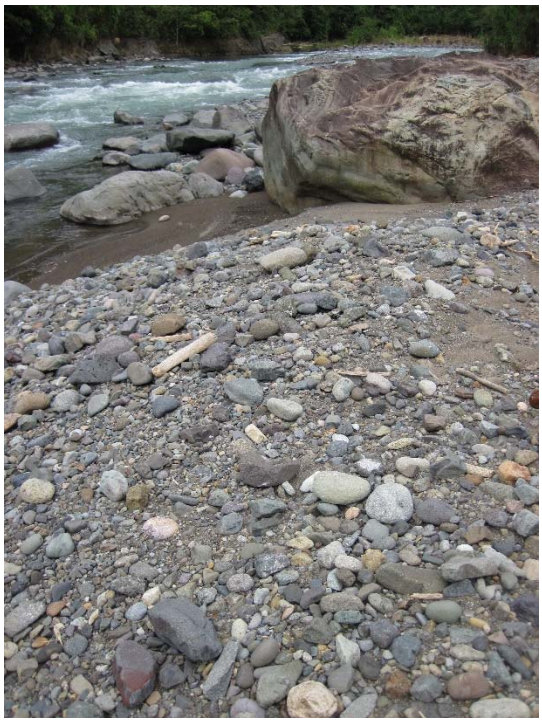

Bajo Pacuare – Rkm 90.4
Upstream bar on river right:

Downstream bar on river left:

Bajo Pacuare por San Juaquin – Rkm 82.6

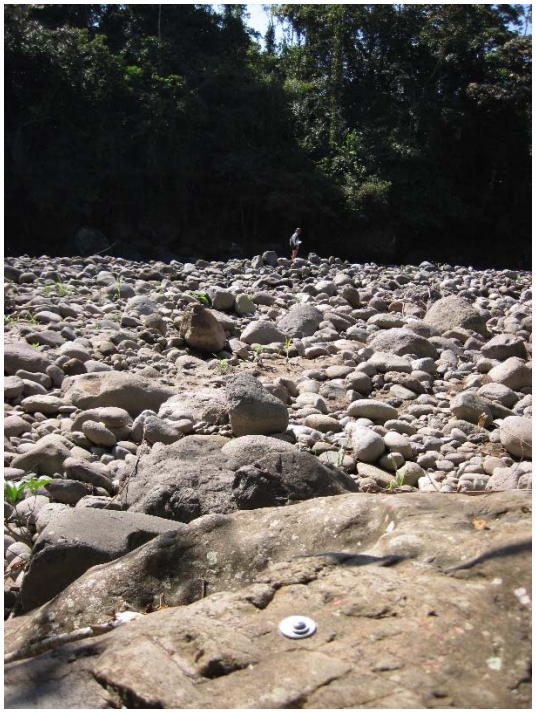

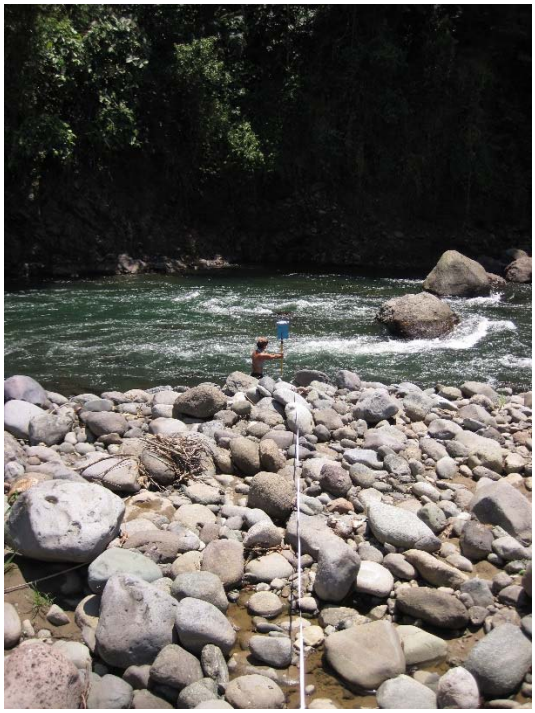

Mollejones Canon – Rkm 74.9

Tres Equis – Rkm 66.2

Bajo Tigre – Rkm 62.5

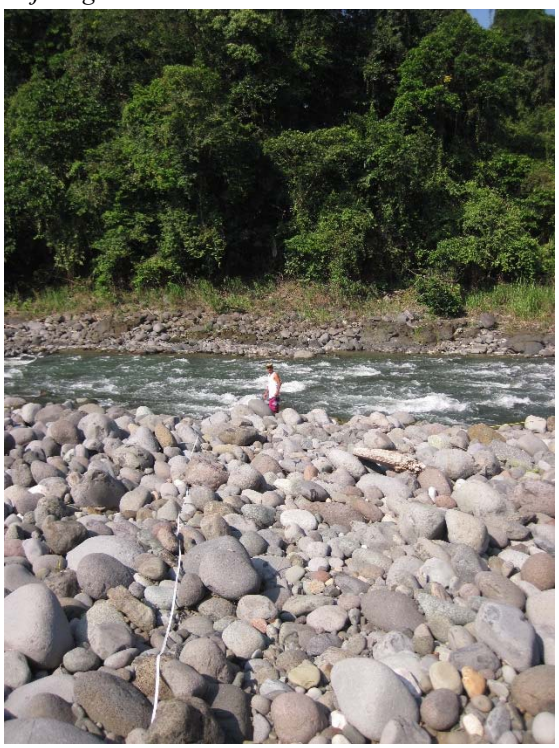

C. SEDIMENT TRANSPORT RATING CURVES

Low-moderate flow and high flow (transport rate vs discharge).

Arriba Pacuare – Rkm 106.4

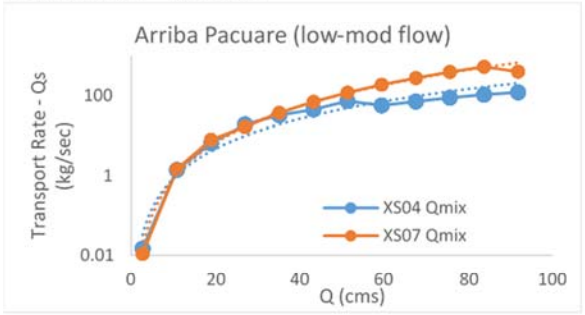

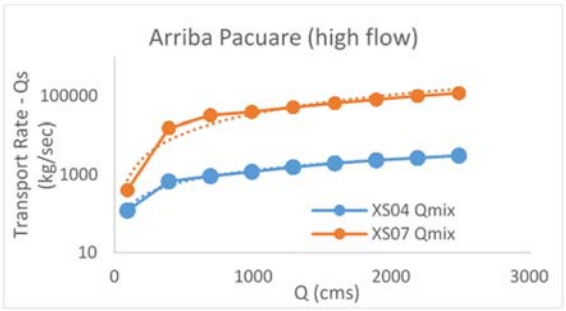

Paso Marcos – RKm 94.8

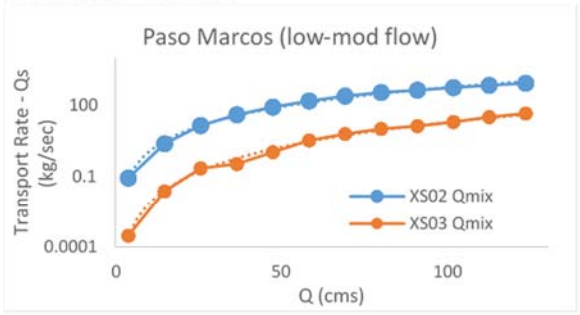

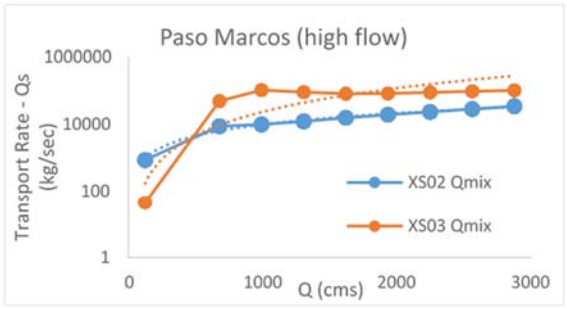

Bajo Pacuare – Rkm 90.4

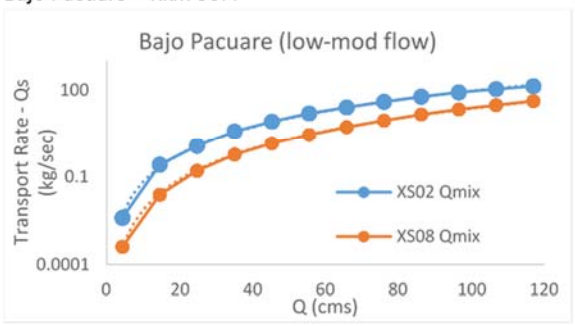

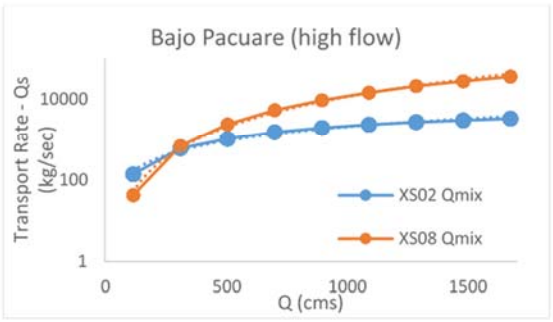

Bajo Pacuare for San Juaquin – Rkm 82.6

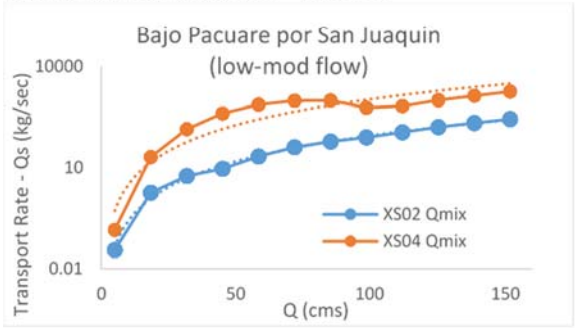

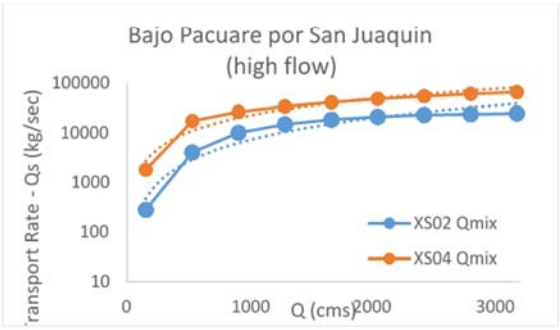

Mollejones Cañon – Rkm 74.9

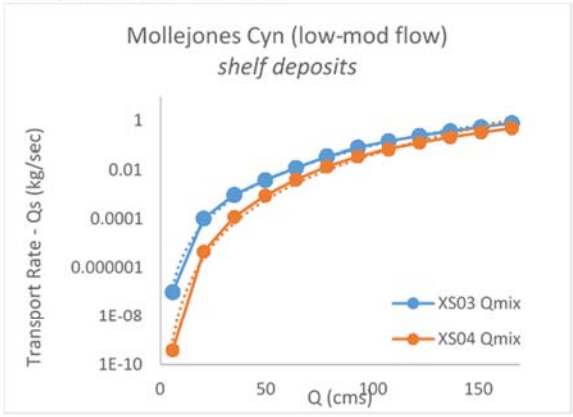

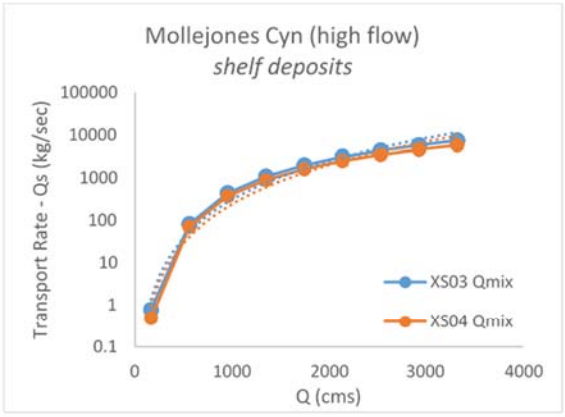

Tres Equis – Rkm 66.2

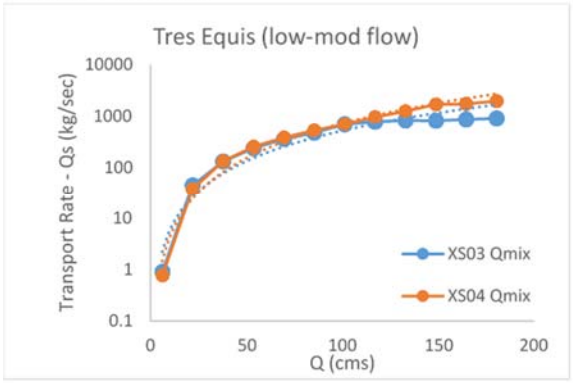

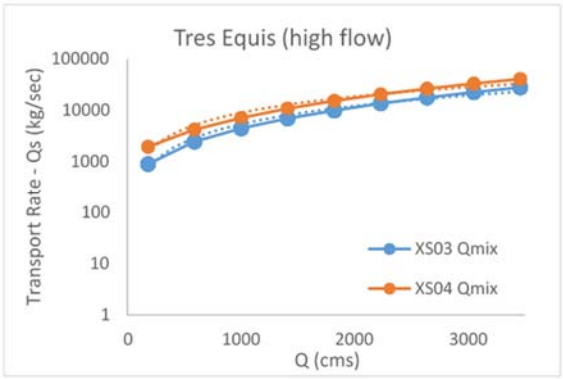

Bajo Tigre – Rkm 62.5

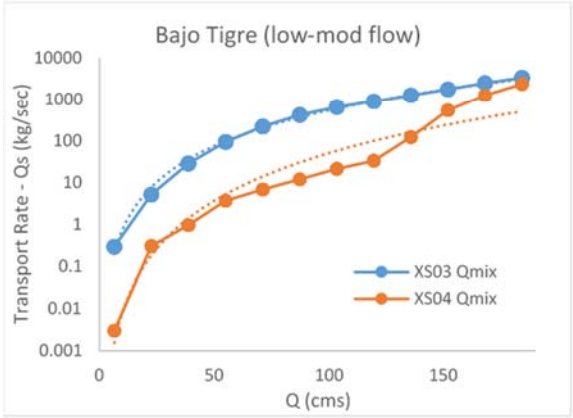

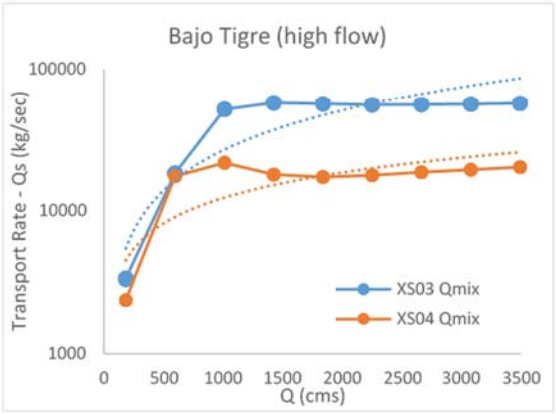

D. SEDIMENT TRANSPORT RATE (kg/sec) vs DISCHARGE (cms) FOR ALL XSrep.

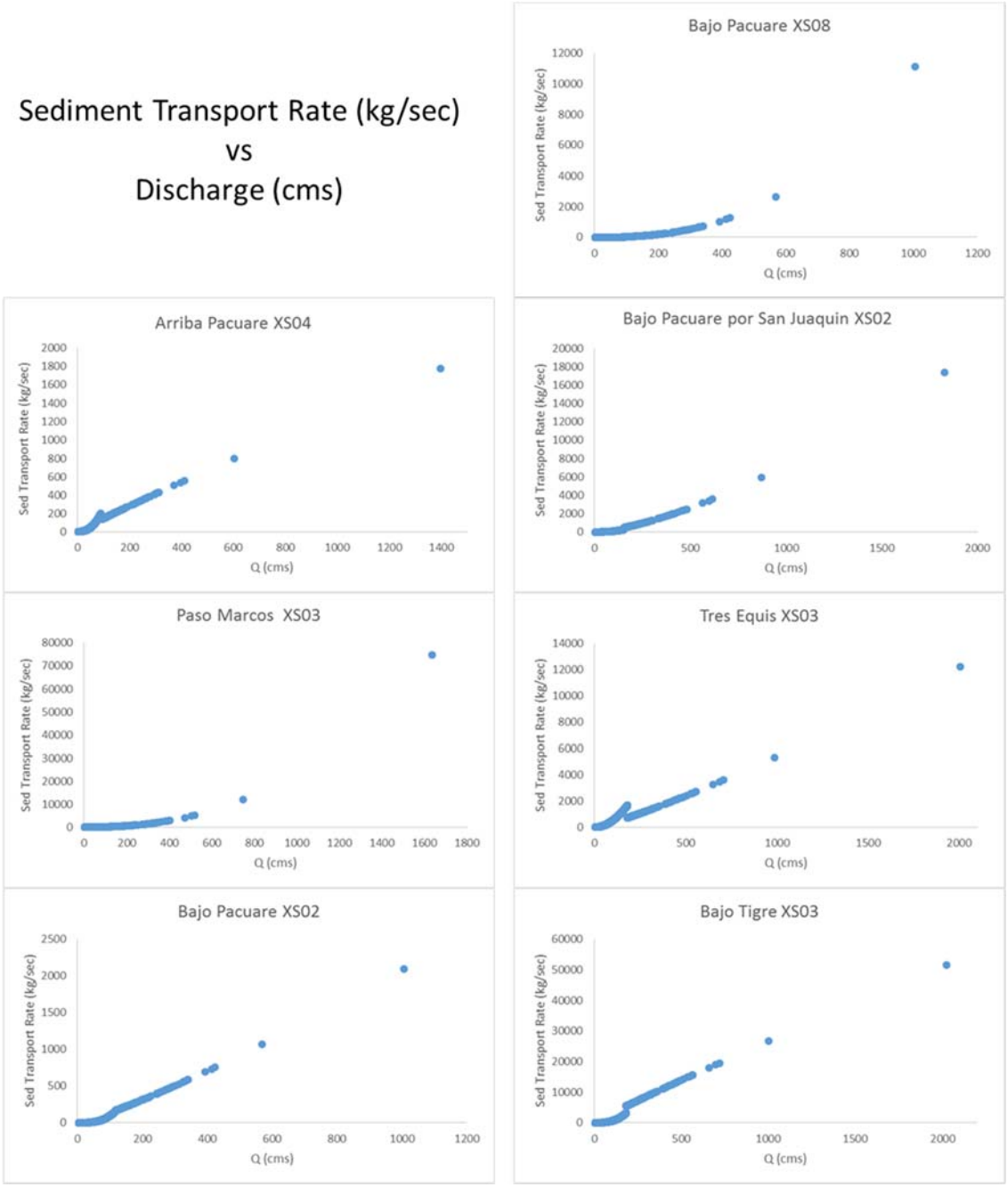

E. CUMULATIVE BEDLOAD TRANSPORT AND DISCHARGE FOR ALL XS_{rep}.

Cumulative bedload transported (tons) and daily discharge (cms) – per day, for the period of record (1959-2012)

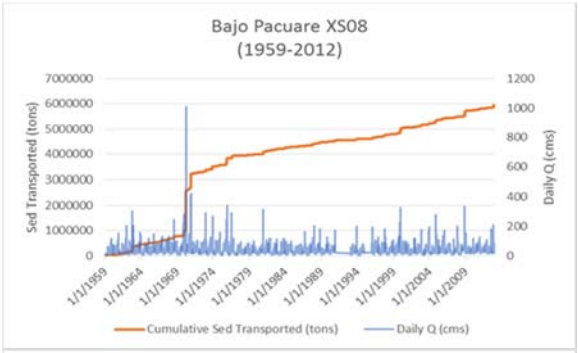

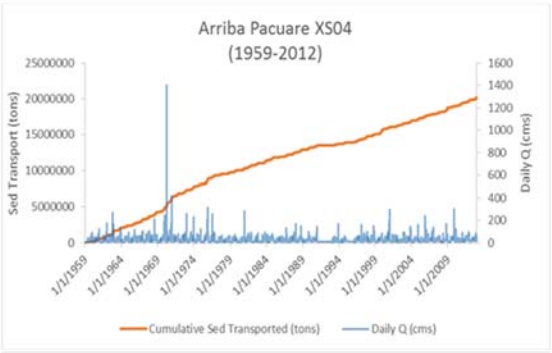

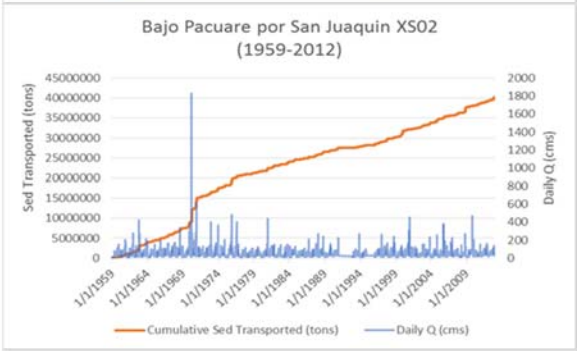

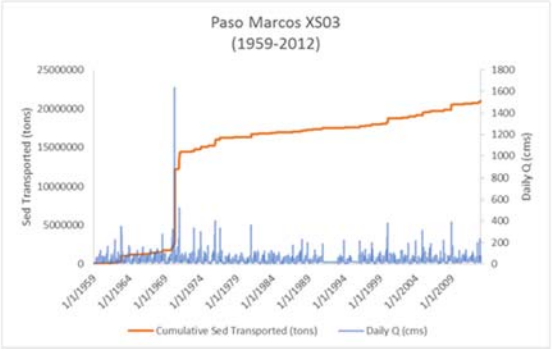

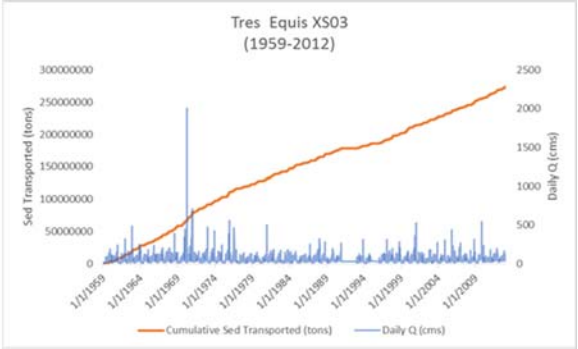

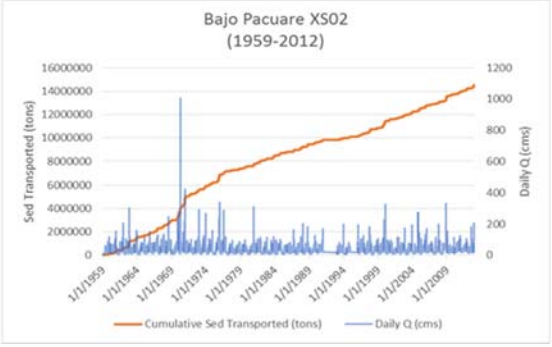

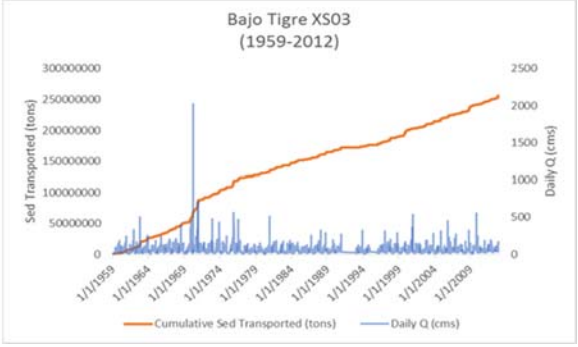

F. SEASONAL REGRESSION VARIATIONS FOR THE MODELED DISCHARGE SECNARIOS.

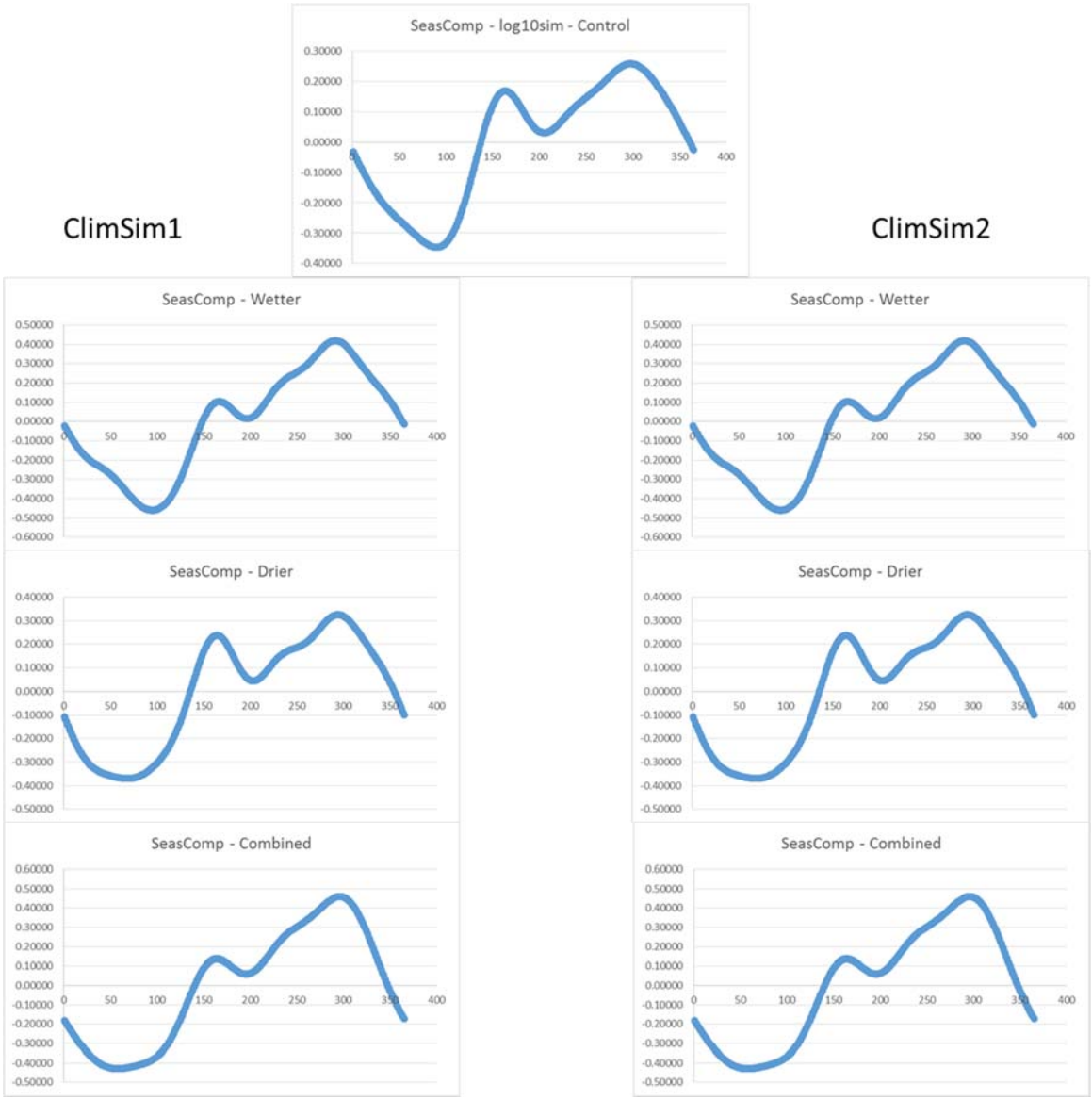

G. 20 YEARS OF SIMULATED DAILY DISCHARGE (Qsim) FOR POTENTIAL FUTURE DISCHARGE SCENARIOS

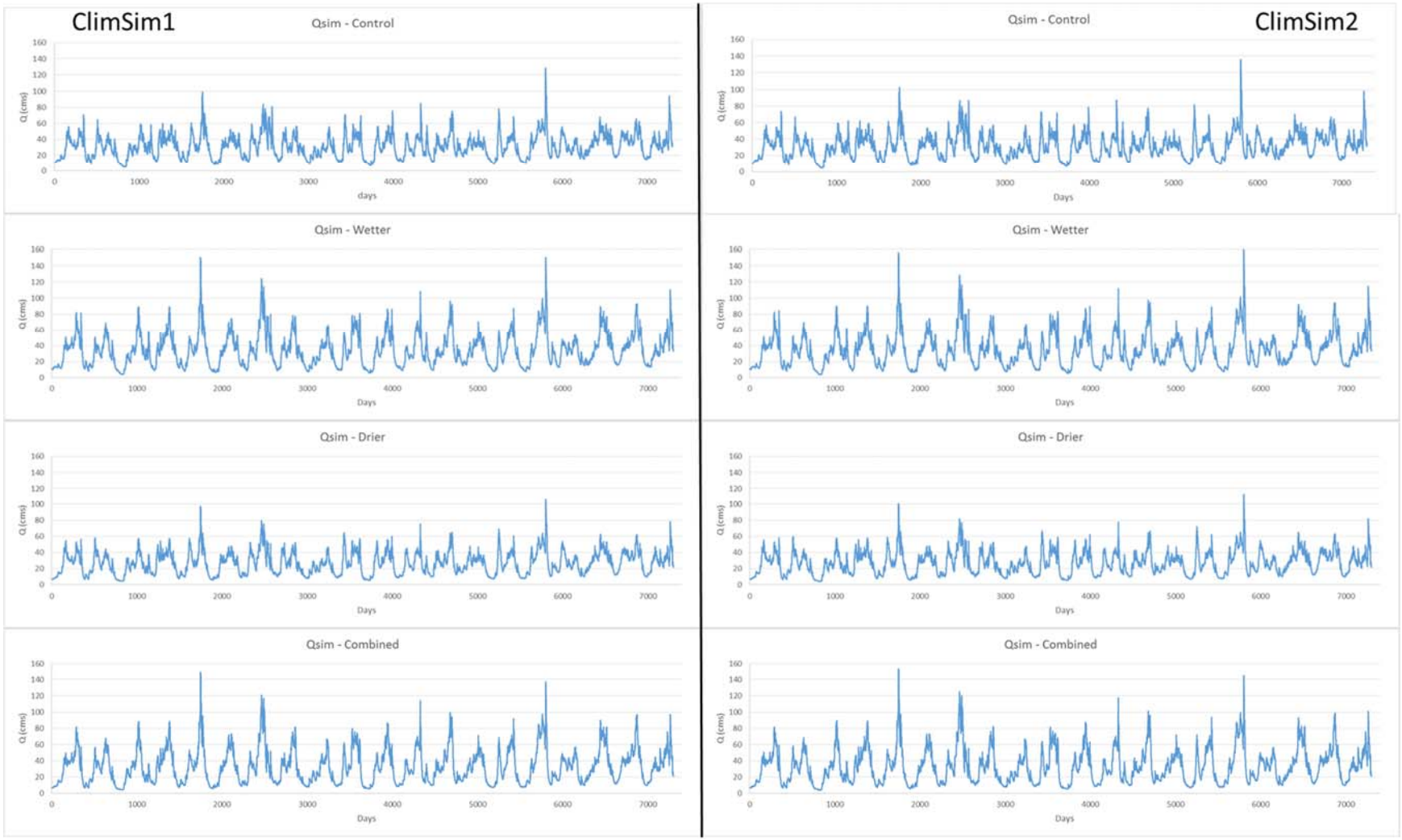

REFERENCES CITED

Aalto, R., Dunne, T., & Guyot, J. L. (2006). Geomorphic controls on Andean denudation rates. *The Journal of Geology*, *114*(1), 85–99. http://doi.org/10.1086/498101

Abratis, M., & Wörner, G. (2001). Ridge collision, slab-window formation, and the flux of Pacific asthenosphere into the Caribbean realm. *Geology*, *29*(2), 127–130. http://doi.org/10.1130/0091-7613(2001)029<0127:RCSWFA>2.0.CO;2

Ahmad, R., Scatena, F. N., & Gupta, A. (1993). Morphology and sedimentation in Caribbean montane streams: examples from Jamaica and Puerto Rico. *Sedimentary Geology*, *85*(1-4), 157–169. http://doi.org/10.1016/0037-0738(93)90080-O

Alongi, D., Amaral, A., Carvalho, D., McWilliam, A., Rouwenhorst, J., Tirendi, F., … Wasson, R. J. (2009). *The Timor-Leste coastal / marine habitat mapping for tourism and fisheries development project. Project No. 6. River catchments and marine productivity in Timor Lest: Caraulun and Laclo catchments*. Retrieved from http://riel.cdu.edu.au/sites/default/files/managed/downloads/Timor-Leste Coastal Marine Habitat Mapping for Tourism and Fisheries Development Project No_6_0.pdf

Anderson, S., & Pitlick, J. (2014). Using repeat lidar to estimate sediment transport in a steep stream. *Journal of Geophysical Research: Earth Surface*, *119*(3), 621–643. http://doi.org/10.1002/2013JF002933

Arcement, G. J., & Schneider, V. R. (1989). *Guide for selecting Manning's roughness coefficients for natural channels and floodplains.* (Water Supply Paper No. 2339). U.S. Geological Survey.

Arrieta, R. F. (2016). Evaluation of bedload transport models for Costa Rican rivers. University of Illinois at Urbana, Chicago, IL: Personal Communications.

Asfaha, T. G., Frankl, A., Haile, M., Zenebe, A., & Nyssen, J. (2015). Sediment flux dynamics as fingerprints of catchment rehabilitation: The case of western Rift Valley escarpment of northern Ethiopia. *Geomorphology*, *250*, 220–235. http://doi.org/10.1016/j.geomorph.2015.09.004

ASTER. (1999). 30m Digital Elevation Model - Costa Rica. provided by Instituto Geográfico Nacional of Costa Rica.

Barry, J. J., Buffington, J. M., & King, J. G. (2004). A general power equation for predicting bed load transport rates in gravel bed rivers. *Water Resources Research*, *40*(10), 1–22. http://doi.org/10.1029/2004WR003190

Benda, L., & Bigelow, P. (2014). On the patterns and processes of wood in northern California streams. *Geomorphology*, *209*, 79–97. http://doi.org/10.1016/j.geomorph.2013.11.028

Benda, L., & Dunne, T. (1997). Stochastic forcing of sediment supply to channel networks from landsliding and debris flow. *Water Resources Research*, *33*(12), 2849–2863.

Benda, L., Hassan, M. A., Church, M., & May, C. L. (2005). Geomorphology of steepland headwaters: the transition from hillslopes to channels. *Journal of the American Water Resources Association*, *41*(4), 835–851. http://doi.org/10.1111/j.1752-1688.2005.tb03773.x

Bertoldi, W., Zanoni, L., & Tubino, M. (2010). Assessment of morphological changes induced by flow and flood pulses in a gravel bed braided river: The Tagliamento

River (Italy). *Geomorphology*, *114*(3), 348–360. http://doi.org/10.1016/j.geomorph.2009.07.017

Bidorn, B., Chanyotha, S., Kish, S. A., Donoghue, J. F., Bidorn, K., & Mama, R. (2015). The effects of Thailand′s Great Flood of 2011 on river sediment discharge in the upper Chao Phraya River basin, Thailand. *International Journal of Sediment Research*, *30*(4), 328–337. http://doi.org/10.1016/j.ijsrc.2015.10.001

Box, G. E. P., Jenkins, G. M., & Reinsel, G. C. (1994). *Time Series Analysis, Forecasting and Control* (Vol. 3rd Editio). Englewood Cliffs, New Jersey: Prentice Hall. http://doi.org/10.1002/9781118619193

Brandt, S. A., & Swenning, J. (1999). Sedimentological and geomorphological effects of reservoir flushing: The Cachí Reservoir, Costa Rica, 1996. *Geografiska Annaler: Series A, Physical Geography*, *81*(3), 391–407. http://doi.org/10.1111/j.0435-3676.1999.00069.x

Bravard, J.-P., Landon, N., Peiry, J.-L., & Piégay, H. (1999). Principles of engineering geomorphology for managing channel erosion and bedload transport, examples from French rivers. *Geomorphology*, *31*(1–4), 291–311. http://doi.org/10.1016/S0169-555X(99)00091-4

Brunner, G. W. (2010). *HEC-RAS River Analysis System: User's Manual (4.1)*. Davis, CA: US Army Corps of Engineers, Institute for Water Resources, Hydrologic Engineering Center.

Buffington, J. M., & Montgomery, D. R. (1997). A systematic analysis of eight decades of incipient motion studies, with special reference to gravel bed rivers. *Water Resources Research*, *33*(8), 1993–2029.

Bundesanstalt fur Gewasserkunde. River Discharge Time Series, Gobal Runoff Database (2014).

Bunte, K., & Abt, S. R. (2001). *Sampling surface and subsurface particle-size distributions in wadable gravel-and cobble-bed streams for analysis in sediment transport, hydraulics, and streambed monitoring.* U.S. Department of Agriculture, Forest Service. Fort Collins, CO. Retrieved from http://www.stream.fs.fed.us/publications/PDFs/rmrs_gtr74.pdf

Burton, G. A., & Pitt, R. E. (2002). *Stormwater Effects Handbook*. Boca Raton, Florida: Lewis Publishers, CRC Press Company.

Cadol, D., & Wohl, E. (2010). Wood retention and transport in tropical, headwater streams, La Selva Biological Station, Costa Rica. *Geomorphology*, *123*(1-2), 61–73. http://doi.org/10.1016/j.geomorph.2010.06.015

Cadol, D., & Wohl, E. (2013). Variable contribution of wood to the hydraulic resistance of headwater tropical streams. *Water Resources Research*, *49*(8), 4711–4723. http://doi.org/10.1002/wrcr.20362

Campbell, J. D., Taylor, M. A., Stephenson, T. S., Watson, R. A., & Whyte, F. S. (2011). Future climate of the Caribbean from a regional climate model. *International Journal of Climatology*, *31*(12), 1866–1878. http://doi.org/10.1002/joc.2200

Carbonneau, P., Fonstad, M. A., Marcus, W. A., & Dugdale, S. J. (2012). Making riverscapes real. *Geomorphology*, *137*(1), 74–86. http://doi.org/10.1016/j.geomorph.2010.09.030

Carey, D. (1994). Erosion and sediment transport monitoring programmes in river basins. *Soil Science*, *158*, 303. http://doi.org/10.1097/00010694-199410000-00012

Castellarin, A., Galeati, G., Brandimarte, L., Montanari, A., & Brath, A. (2004). Regional flow-duration curves: reliability for ungauged basins. *Advances in Water Resources*, *27*(10), 953–965. http://doi.org/10.1016/j.advwatres.2004.08.005

CATIE - Centro Agronómico Tropical de Investigación y Enseñanza. (2016). Turrialba daily precipitation data. Retrieved May 1, 2016, from https://www.catie.ac.cr/en/products-and-services/catie-weather-station/catie-weather-station.html

Church, M., & Ferguson, R. I. (2015). Morphodynamics: Rivers beyond steady state. *Water Resources Research*, *51*, 1883–1897. http://doi.org/10.1002/ 2014WR016862

Conyers, M. M., Fonstad, M. A., Lovell, M., & Marcos, S. (2005). The unusual channel resistance of the Texas Hill Country and its effect on flood flow predictions. *Physical Geography*, *26*(5), 379–395.

Coulthard, T. J., Ramirez, J., Fowler, H. J., & Glenis, V. (2012). Using the UKCP09 probabilistic scenarios to model the amplified impact of climate change on drainage basin sediment yield. *Hydrology and Earth System Sciences*, *16*(11), 4401–4416. http://doi.org/10.5194/hess-16-4401-2012

Dadson, S. J., Hovius, N., Chen, H., Dade, W. B., Lin, J. C., Hsu, M. L., … Stark, C. P. (2004). Earthquake-triggered increase in sediment delivery from an active mountain belt. *Geology*, *32*(8), 733–736. http://doi.org/10.1130/G20639.1

de Boer, J. Z., Drummond, M. S., Bordelon, M. J., Defant, M. J., Bellon, H., & Moury, R. C. (1995). Cenozoic magmatic phases of the Costa Rican island arc (Cordillera de Talamanca). In P. Mann (Ed.), *Geologic and tectonic development of the Caribbean Plate boundary in southern Central America* (Special Pa, pp. 35–56). Boulder, CO: Geologic Society of America, Inc.

Dietrich, E. (1999). The Fly River, Papua New Guinea: Inferences about river dyamics, floodplain sedimentation and fate of sediment. In A. J. Miller & A. Gupta (Eds.), *Varieties of Fluvial Forms* (p. 538). Hoboken, N.J.: John Wiley & Sons Ltd.

Dietrich, J., & Lind, P. (2013). The use of Structure from Motion for repeat topographic surveys of active boulder bars on a hydrologically dynamic tropical river (poster). In *International Geomorphology Association Meeting*. Paris, France., France.

Dietrich, J. T. (2016). Geomorphology Riverscape mapping with helicopter-based Structure-from-Motion photogrammetry. *Geomorphology*, *252*, 144–157. http://doi.org/10.1016/j.geomorph.2015.05.008

Dietrich, J. T., Fonstad, M., & Marcus, W. A. (2012). Three-dimensional field mapping of the Granite Boulder Creek restoration project, Oregon. In *Binghamton Geomorphology Symposium*. Poster, Jackson Hole, WY.

Dodson, S. J. (2003). *Erosion of an active mountain belt, PhD Thesis.* Cambridge, UK.

Driese, S. G., Orvis, K. H., Horn, S. P., Li, Z. H., & Jennings, D. S. (2007). Paleosol evidence for Quaternary uplift and for climate and ecosystem changes in the Cordillera de Talamanca, Costa Rica. *Palaeogeography, Palaeoclimatology, Palaeoecology*, *248*(1-2), 1–23. http://doi.org/10.1016/j.palaeo.2006.11.013

Emmett, W. W., & Wolman, M. G. (2001). Effective discharge and gravel-bed rivers.

Earth Surface Processes and Landforms, *26*(13), 1369–1380. http://doi.org/10.1002/esp.303

Enfield, D. B., & Alfaro, E. J. (1999). The dependence of Caribbean rainfall on the interaction of the tropical Atlantic and Pacific Oceans. *Journal of Climate*, *12*(7), 2093–2103. http://doi.org/10.1175/1520-0442(1999)012<2093:TDOCRO>2.0.CO;2

Enquist, C. (2002). Predicted regional impacts of climate change on the geographical distribution and diversity of tropical forests in Costa Rica. *Journal of Biogeography*, 519–534. Retrieved from http://onlinelibrary.wiley.com/doi/10.1046/j.1365-2699.2002.00695.x/abstract

Escalante, G., & Astorga, A. (1994). Geologia del este de Costa Rica y el norte de Panama. *Revista Geologica de America Central*, *Especial*(Terremoto de Limon), 1–14. Retrieved from http://dx.doi.org/10.15517/rgac.v0i0.13388

Fabrega, J., Nakaegawa, T., Pinzón, R., Nakayama, K., & Arakawa, O. (2013). Hydroclimate projections for Panama in the late 21st Century. *Hydrological Research Letters*, *7*(2), 23–29. http://doi.org/10.3178/HRL.7.23

Fernandez, J. A., Bottazzi, G., Barboza, G., & Astorga, A. (1994). Tectonica y estratigrafia de la cuence Limon Sur. *Revista Geologica de America Central*, *especial*(Terremoto de Limon), 15–28. Retrieved from http://dx.doi.org/10.15517/rgac.v0i0.13391

Fernandez, M., Camacho, E., Molina, E., Marroquin, G., & Strauch, W. (2007). Siesmicity and neotectonic. In J. Bundschuh & G. Alvarado (Eds.), *Central America geology resources hazards - volume I* (pp. 323–344). London, UK: Taylor and Francis.

Fernández-Arce, M. (2009). Sesimicity of the Pejibaye-Matina, Costa Rica, region: A strike-slip tectonic boundary. *Geofisica Internacional*, *48*(4), 361–374.

Fernández-Arce, M. (2013). Seismotectonic and the hipothetical strike-slip tectonic boundary of Central Costa Rica. *Earthquake Research and Analysis - New Advances in Seismology*, (1999). http://doi.org/10.5772/54989.

Flint, J. J. (1974). Stream gradient as a function of order, magnitude, and discharge. *Water Resources Research*, *10*(5), 969–973. http://doi.org/10.1029/WR010i005p00969

Fonstad, M. A. (2003). Spatial variation in the power of mountain streams in the Sangre de Cristo Mountains, New Mexico. *Geomorphology*, *55*(1-4), 75–96. http://doi.org/10.1016/S0169-555X(03)00133-8

Fonstad, M. A., Dietrich, J. T., Courville, B. C., Jensen, J. L., & Carbonneau, P. E. (2013). Topographic structure from motion: a new development in photogrammetric measurement. *Earth Surface Processes and Landforms*, *38*(4), 421–430. http://doi.org/10.1002/esp.3366

Fryirs, K. A. (2016). River sensitivity: A lost foundation concept in fluvial geomorphology. *Earth Surface Processes and Landforms*. http://doi.org/10.1002/esp.3940

Fuller, C. W., Willett, S. D., Hovius, N., & Slingerland, R. (2003). Erosion rates for Taiwan Mountain basins: New determinations for suspended sediment records and a stochastic model of their temporal variations. *The Journal of Geology*, *111*(1), 71–

87. http://doi.org/10.1086/344665
Galia, T., & Hradecký, J. (2012). Critical conditions for the beginning of coarse sediment transport in the torrents of the Moravaskoslezske Beskydy Mountains (Western Carpathians). *Carpathian Journal of Earth and Enivronmental Sciences*, *7*(4), 5–14. Retrieved from https://www.researchgate.net/profile/Tomas_Galia/publication/251238115_Critical_conditions_for_the_beginning_of_coarse_sediment_transport_in_the_torrents_of_the_moravskoslezsk_beskydy_mts_(western_carpathians)/links/004635370d019290bd000000.pdf
García-Martinó, A. R., Warner, G. S., Scatena, F. N., & Civco, D. L. (1996). Rainfall, runoff and elevation relationships in the Luquillo Mountains of Puerto Rico. *Caribbean Journal of Science*, *32*(4), 413–424.
Garcin, M., Poisson, B., & Pouget, R. (2005). High rates of geomorphological processes in a tropical area: the Remparts River case study (Réunion Island, Indian Ocean). *Geomorphology*, *67*(3-4), 335–350. http://doi.org/10.1016/j.geomorph.2004.11.002
George, R., Waylen, P., & Laporte, S. (1998). Interannual variability of annual streamflow and the Southern Oscillation in Costa Rica. *Hydrological Sciences Journal*. http://doi.org/10.1080/02626669809492135
Giannini, A., Cane, M. A., & Kushnir, Y. (2001). Interdecadal changes in the ENSO Teleconnection to the Caribbean Region and the North Atlantic Oscillation. *Journal of Climate*, *14*(13), 2867–2879. http://doi.org/10.1175/1520-0442(2001)014<2867:ICITET>2.0.CO;2
Giannini, A., Chiang, J., Cane, M. A., Kushnir, Y., & Seager, R. (2001). The ENSO teleconnection to the Tropical Atlantic Ocean: Contributions of the remote and local SSTs to rainfall variability in the Tropical Americas. *Journal of Climate*, *14*(24), 4530–4544. http://doi.org/10.1175/1520-0442(2001)014<4530:tetttt>2.0.co;2
Giannini, A., Kushnir, Y., & Cane, M. A. (2000). Interannual variability of Caribbean rainfall, ENSO, and the Atlantic Ocean. *Journal of Climate*, *13*(2), 297–311. http://doi.org/10.1175/1520-0442(2000)013<0297:IVOCRE>2.0.CO;2
Gilvear, D., & Bryant, R. (2003). Analysis of aerial photography and other remotely sensed data. *Red*, *600*(5.8), 23.
Golden, L. A., & Springer, G. S. (2006). Channel geometry, median grain size, and stream power in small mountain streams. *Geomorphology*, *78*(1-2), 64–76. http://doi.org/10.1016/j.geomorph.2006.01.031
Goldsworthy, M., & Jackson, J. (2000). Active normal fault evolution in Greece revealed by geomorphology and drainage patterns. *Journal of the Geological Society*, *157*, 967–981. http://doi.org/10.1144/jgs.157.5.967
Gonzalez, V. S., Bierman, P. R., Nichols, K. K., & Rood, D. H. (2016). Long-term erosion rates of Panamanian drainage basins determined using in situ 10Be. *Geomorphology*. http://doi.org/10.1016/j.geomorph.2016.04.025
Grabowski, R. C., Surian, N., & Gurnell, A. M. (2014). Characterizing geomorphological change to support sustainable river restoration and management. *Wiley Interdisciplinary Reviews: Water*, *1*(5), 483–512. http://doi.org/10.1002/wat2.1037
Grant, G. E. (1997). Critical flow constrains flow hydraulics in mobile-bed streams: A

new hypothesis. *Water Resources Research*, *33*(2), 349–358. http://doi.org/10.1029/96WR03134
Gupta, A. (1995). Magnitude, frequency, and special factors affecting channel form and rocesses in the seasonal tropics. *Natural and Anthropogenic Influences in Fluvial Geomorphology*, (1), 125–136. http://doi.org/10.1029/GM089p0125
Gupta, A. (2011). *Tropical Geomorphology*. Cambridge, UK: Cambridge University Press.
Gurnell, A. M., Piegay, H., Swanson, F. J., & Gregorys, S. V. (2002). Large wood and fluvial processes. *Freshwater Biology*, (47), 601–619. http://doi.org/10.1046/j.1365-2427.2002.00916.x
Habersack, H. M. (2000). The river-scaling concept (RSC): a basis for ecological assessments. In M. Jungwirth, S. Muhar, & S. Schmutz (Eds.), *Assessing the Ecological Integrity of Running Waters* (pp. 49–60). Dordrecht: Springer Netherlands.
Hamilton, S. K., Kellndorfer, J., Lehner, B., & Tobler, M. (2007). Remote sensing of floodplain geomorphology as a surrogate for biodiversity in a tropical river system (Madre de Dios, Peru). *Geomorphology*, *89*(1-2 SPEC. ISS.), 23–38. http://doi.org/10.1016/j.geomorph.2006.07.024
Hassan, M. A., Gottesfeld, A. S., Montgomery, D. R., Tunnicliffe, J. F., Clarke, G. K. C., Wynn, G., … Macdonald, S. J. (2008). Salmon-driven bed load transport and bed morphology in mountain streams. *Geophysical Research Letters*, *35*(4), L04405. http://doi.org/10.1029/2007GL032997
Heimann, F. U. M., Rickenmann, D., Bockli, M., Badoux, A., Turowski, J. M., & Kirchner, J. W. (2015). Calculation of bedload transport in Swiss mountain rivers using the model sedFlow: Proof of concept. *Earth Surface Dynamics*, *3*(1), 35–54. http://doi.org/10.5194/esurf-3-35-2015
Henderson, G. S., & Witthawatchutikul, P. (1984). The effect of road construction on sedimentation in a forested catchment at Rayong, Thailand. In *Symposium on effects of forest land use on erosion and slope stability.* Honolulu, HI: IOUFO/NZFS/USDA University of Hawaii. Retrieved from https://www.researchgate.net/publication/294200951_The_effect_of_road_construction_on_sedimentation_in_a_forested_catchment_at_Rayong_Thailand
Hicks, D. M., & Gomez, B. (2003). Sediment Transport. In G. Kondolf & H. Piégay (Eds.), *Tools in Fluvial Geomorphology* (pp. 425–461). John Wiley & Sons, Ltd.
Hicks, D. M., & Mason, P. D. (1998). *Roughness Characteristics of New Zealand Rivers*. Christchurch, New Zealand: National Institute of Water and Atmospheric Research, Water Resources Publication.
Hidalgo, H. G., Amador, J. A., Alfaro, E. J., & Quesada, B. (2013). Hydrological climate change projections for Central America. *Journal of Hydrology*, *495*, 94–112. http://doi.org/10.1016/j.jhydrol.2013.05.004
Hipel, K. W., & McLeod, A. I. (1994). *Time Series Modelling of Water Resources and Environmental Systems.* Amersterdam New York: Elsevier. Retrieved from http://www.stats.uwo.ca/faculty/aim/1994Book/
Holbrook, J., & Schumm, S. A. (1999). Geomorphic and sedimentary response of rivers

to tectonic deformation: A brief review and critique of a tool for recognizing subtle epeirogenic deformation in modern and ancient settings. *Tectonophysics*, *305*(1-3), 287–306. http://doi.org/10.1016/S0040-1951(99)00011-6

Hovius, N., Stark, C. P., Hao-Tsu, C., & Jiun-Chuan, L. (2000). Supply and removal of sediment in a landslide dominated mountain belt: Central Range, Taiwan. *The Journal of Geology*, *108*(1), 73–89. http://doi.org/10.1086/314387

Humphrey, N. F., & Konrad, S. K. (2000). River incision or diversion in response to bedrock uplift. *Geology*, *28*(1), 43–46. http://doi.org/10.1130/0091-7613(2000)28<43:RIODIR>2.0.CO

James, L. A., Hodgson, M. E., Ghoshal, S., & Latiolais, M. M. (2012). Geomorphic change detection using historic maps and DEM differencing: The temporal dimension of geospatial analysis. *Geomorphology*, *137*(1), 181–198. http://doi.org/10.1016/j.geomorph.2010.10.039

James, M. R., & Robson, S. (2012). Straightforward reconstruction of 3D surfaces and topography with a camera: Accuracy and geoscience application: 3D SURFACES AND TOPOGRAPHY WITH A CAMERA. *Journal of Geophysical Research: Earth Surface*, *117*(F3), n/a–n/a. http://doi.org/10.1029/2011JF002289

Janeau, J. L., Maglinao, A. R., Lorent, C., Briquent, J. P., & Boonsaner, A. (2003). The off-site effect of soil erosion: a case study of the Mae Thang Reservoir in Northern Thailand. *Internaitonal Water Management Institute*, 191–202.

Jansson, M. B. (1996). Estimating a sediment rating curve of the Reventazon River at Palomo using logged mean loads within discharge classes. *Journal of Hydrology*, *183*(3-4), 227–241. http://doi.org/10.1016/0022-1694(95)02988-5

Jansson, M. B. (2002). Determining sediment source areas in a tropical river basin, Costa Rica. *Catena*, *47*(1), 63–84. http://doi.org/10.1016/S0341-8162(01)00173-4

Jarrett, R. D. (1984). Hydraulics of high gradient streams. *Journal of Hydraulic Engineering*, *110*(11), 1519–1539. http://doi.org/10.1061/(ASCE)0733-9429(1984)110:11(1519)

Javernick, L., Brasington, J., & Caruso, B. (2014). Modeling the topography of shallow braided rivers using Structure-from-Motion photogrammetry. *Geomorphology*, *213*, 166–182. http://doi.org/10.1016/j.geomorph.2014.01.006

Javernick, L., Hicks, D. M., Measures, R., Caruso, B., & Brasington, J. (2015). Numerical modelling of braided rivers with Structure-from-Motion-derived terrain models. *River Research and Applications*, n/a–n/a. http://doi.org/10.1002/rra.2918

Jiménez, B. E., Oki, T., Arnell, N. W., Benito, G., Cogley, G. J., Doll, P., … Mwakalila, S. S. (2014). Freshwater Resources. In C. B. Field, V. R. Barros, D. J. Dokken, K. J. Mach, M. D. Mastrandrea, T. E. Bilir, … L. L. White (Eds.), *Climate Change 2014: Impacts, Adaptation, and Vulnerability. Part A. Global and Sectoral Aspects. Contribution of Working Group II to the Fifth Assessment Report of the Intergovernmental Panel on Climate Change.* (pp. 229–269). New York, NY. http://doi.org/10.2134/jeq2008.0015br

Jiménez-Rodríguez, C. D., Calvo-Alvarado, J. C., & Jackson, J. K. (2015). Performance of two hydrological models in predicting daily flow under a climate change scenario for mountainous catchments in northwestern Costa Rica. *Mountain Research and*

Development, *35*(3), 240–253. http://doi.org/10.1659/MRD-JOURNAL-D-14-00109.1

Johnston, R., & Kummu, M. (2012). Water resource models in the Mekong Basin: A review. *Water Resources Management*, *26*(2), 429–455. http://doi.org/10.1007/s11269-011-9925-8

Julien, P. Y. (2010). *Erosion and Sedimentation* (Second). Cambridge, UK: Cambridge University Press.

Julien, P. Y. (2015). Downstream hydraulic geometry of alluvial rivers. *Proceedings of the Interational Association of Hydrological Sciences*, *367*, 3–11. Retrieved from http://www.proc-iahs.net/367/3/2015/

Kamiguchi, K., Kitho, A., Uchiyama, T., Mizuta, R., & Noda, A. (2006). Changes in precipitation-based extreme indices due to global warming projected by a global 20-km-mesh atmospheric model. *Sola*, *2*, 64–67. http://doi.org/10.2151/sola.2005-040

Kao, S. J., & Milliman, J. D. (2008). Water and sediment discharge from small mountainous rivers, Taiwan: The roles of lithology, episodic events, and human activities. *The Journal of Geology*, *116*(5), 431–448. http://doi.org/10.1086/590921

Karmalkar, A. V., Bradley, R. S., & Diaz, H. F. (2008). Climate change scenario for Costa Rican montane forests. *Geophysical Research Letters*, *35*(11), 1–5. http://doi.org/10.1029/2008GL033940

Karmalkar, A. V., Bradley, R. S., & Diaz, H. F. (2011). Climate change in Central America and Mexico: Regional climate model validation and climate change projections. *Climate Dynamics*, *37*(3), 605–629. http://doi.org/10.1007/s00382-011-1099-9

Kaygusuz, K. (2004). Hydropower and the world's energy future. *Energy Sources*, *26*(3), 215–224. Retrieved from http://www.tandfonline.com/doi/abs/10.1080/00908310490256572

Kazemi, Y., Salajegheh, A., Mahdavi, M., Rostami, N., & Abbassi, M. (2012). The relation of bed and suspended loads in central Alborz Rivers , Iran. *Agriculture*, *42*, 6120–6123.

Kesel, R.H. and Lowe, D. R. (2016). Geomorphology and sedimentology of the Toro Amarillo alluvial fan in a humid tropical environment , Costa Rica. *Geografiska Annaler . Series A , Physical Geography*, *69*(1), 85–99.

Kirby, E., & Whipple, K. X. (2012). Expression of active tectonics in erosional landscapes. *Journal of Structural Geology*, *44*, 54–75. http://doi.org/10.1016/j.jsg.2012.07.009

Kitoh, A., Endo, H., Krishna Kumar, K., Cavalcanti, I. F. A., Goswami, P., & Zhou, T. (2013). Monsoons in a changing world: A regional perspective in a global context. *Journal of Geophysical Research Atmospheres*, *118*(8), 3053–3065. http://doi.org/10.1002/jgrd.50258

Kitsikoudis, V., Sidiropoulos, E., & Hrissanthou, V. (2014). Machine learning utilization for bed load transport in gravel-bed rivers. *Water Resources Management*, *28*, 3727–3743. http://doi.org/10.1007/s11269-014-0706-z

Knighton, A. D. (1999). Downstream variation in stream power. *Geomorphology*, *29*(3-4), 293–306. http://doi.org/10.1016/S0169-555X(99)00015-X

Knighton, D. (1998). *Fluvial forms and processes: a new perspective*. New York, NY: Oxford University Press.
Koch, R. (2003). 3D-Scene modeling From image sequences. *Camera*, *XXXIV*, 3–9. Retrieved from http://www.isprs.org/proceedings/XXXIV/3-W8/papers/pia03_inv1.pdf
Kolarsky, R. A., Mann, P., & Montero, W. (1995). Island arc response to shallow subduction of the Cocos Ridge, Costa Rica. In P. Mann (Ed.), *Geologic and tectonic development of the Caribbean Plate boundary in southern Central America* (Special Re, pp. 235–262). Boulder, CO: Geologic Society of America, Inc.
Komar, P. D. (1987). Selective gravel entrainment and the empirical evaluation of flow competence. *Sedimentology*, *34*. http://doi.org/10.1111/j.1365-3091.1987.tb00599.x
Kra, E. Y., & Merkley, G. P. (2004). Mathematical modeling of open-channel velocity profiles for float method calibration. *Agricultural Water Management*, *70*(3), 229–244. http://doi.org/10.1016/j.agwat.2004.06.008
Krishnaswamy, J., Richter, D. D., Halpin, P. N., & Hofmockel, M. S. (2001). Spatial patterns of suspended sediment yields in a humid tropical watershed in Costa Rica. *Hydrological Processes*, *15*(12), 2237–2257. http://doi.org/10.1002/hyp.230
Kuo, C. W., & Brierley, G. (2014). The influence of landscape connectivity and landslide dynamics upon channel adjustments and sediment flux in the Liwu Basin, Taiwan. *Earth Surface Processes and Landforms*, *39*(15), 2038–2055. http://doi.org/10.1002/esp.3598
Lai, F. S., Lee, M. J., & Rizal, S. M. (1995). Changes in sediment discharge resulting from commercial logging in the Sungai Lawing basin , Selangor , Malaysia. In *Effects of scale on interpretation and management of sediment and water quality* (pp. 55–62). Boulder, CO: IAHS International Symposium. Retrieved from http://agris.fao.org/agris-search/search.do?recordID=GB9618333
Lamb, M. P., & Fonstad, M. A. (2010). Rapid formation of a modern bedrock canyon by a single flood event. *Nature Geoscience*, *3*(7), 477–481. http://doi.org/10.1038/ngeo894
Latrubesse, E. M., Stevaux, J. C., & Sinha, R. (2005). Tropical rivers. *Geomorphology*, *70*(3-4), 187–206. http://doi.org/10.1016/j.geomorph.2005.02.005
Lenzi, M. A., D'Agostino, V., & Billi, P. (1999). Bedload transport in the instrumented catchment of the Rio Cordon: Part I: Analysis of bedload records, conditions and threshold of bedload entrainment. *Catena*, *36*(3), 171–190.
Lenzi, M. A., Mao, L., & Comiti, F. (2006). Effective discharge for sediment transport in a mountain river: Computational approaches and geomorphic effectiveness. *Journal of Hydrology*, *326*(1-4), 257–276. http://doi.org/10.1016/j.jhydrol.2005.10.031
Leopold, L. B., & Maddock, T. J. (1953). *The hydraulic geometry of stream channels and some physiographic implications*. Washington, DC. Retrieved from http://pubs.usgs.gov/pp/0252/report.pdf
Lindholm, C. D., Climent, A., Camacho, E., Strauch, W., Cepeda, J., Caceres, D., … Bungum, H. (2007). Seismic hazards and monitoring. In J. Bundschuh & G. E. Alvarado (Eds.), *Central America geology resources hazards - volume II* (pp. 1099–1118). England, UK: Taylor and Francis.

Lisenby, P. E., Slattery, M. C., & Wasklewicz, T. A. (2014). Morphological organization of a steep, tropical headwater stream: The aspect of channel bifurcation. *Geomorphology*, *214*, 245–260. http://doi.org/10.1016/j.geomorph.2014.02.009

Lisle, T. E., Nelson, J. M., Pitlick, J., Madej, M. A., & Barkett, B. L. (2000). Variability of bed mobility in natural, gravel-bed channels and adjustments to sediment load at local and reach scales. *Water Resources Research*, *36*(12), 3743–3755. http://doi.org/10.1029/2000WR900238

Longshore, D. (2010). *Encyclopedia of Hurricanes, Typhoons, and Cyclones, New Edition*. Infobase Publishing.

Lotsari, E., Thorndycraft, V., & Alho, P. (2015). Prospects and challenges of simulating river channel response to future climate change. *Progress in Physical Geography*, *39*(4), 483–513. http://doi.org/10.1177/0309133315578944

Lu, X. X., Ran, L. S., Liu, S., Jiang, T., Zhang, S. R., & Wang, J. J. (2013). Sediment loads response to climate change: A preliminary study of eight large Chinese rivers. *International Journal of Sediment Research*, *28*(1), 1–14. http://doi.org/10.1016/S1001-6279(13)60013-X

MacMillan, I., Gans, P. B., & Alvarado, G. (2004). Middle Miocene to present plate tectonic history of the southern Central American Volcanic Arc. *Tectonophysics*, *392*(1-4), 325–348. http://doi.org/10.1016/j.tecto.2004.04.014

Magrin, G. O., Marengo, J. A., Boulanger, J.-P., Buckeridge, M. S., Castellanos, E., Poveda, G., … Vicuña, S. (2014). Central and South America. In V. R. Barros, C. B. Field, D. J. Dokken, M. D. Mastrandrea, K. J. Mach, T. E. Bilir, … L. L. White (Eds.), *Climate Change 2014: Impacts, Adaptation, and Vulnerability. Part B: Regional Aspects. Contribution of Working Group II to the Fifth Assessment Report of the Intergovernmental Panel on Climate Change [Barros, V.R., C.B. Field, D.J. Dokken, M.D. Mastrandre* (pp. 1499–1566). New York, NY: Cambridge University Press.

Maldonado, T., Alfaro, E., Fallas-Lopez, B., & Alvarado, L. (2013). Seasonal prediction of extreme precipitation events and frequency of rainy days over Costa Rica, Central America, using Canonical Correlation Analysis. *Advances in Geosciences*, *33*, 41–52. http://doi.org/10.5194/adgeo-33-41-2013

Mao, L., Andreoli, A., Iroume, A., Comiti, F., & Lenzi, M. A. (2013). Dynamics and management alternatives of in-channel large wood in mountain basins of the southern Andes. *Bosque*, *34*(3), 319–330. http://doi.org/10.4067/S0717-92002013000300008

Marshall, J. S. (2007). Geomorphology and physiographic provinces. In J. Bundschuh & G. E. Alvarado (Eds.), *Central America geology resources hazards - volume I* (pp. 75–122). London, UK: Taylor and Francis.

Marshall, J. S., Fisher, D. M., & Gardner, T. W. (2000). Central Costa Rica deformed belt: Kinematics of diffuse faulting across the western Panama block. *Tectonics*, *19*(3), 468–492. http://doi.org/10.1029/1999TC001136

Marshall, J. S., Idleman, B. D., Gardner, T. W., & Fisher, D. M. (2003). Landscape evolution within a retreating volcanic arc, Costa Rica,Central America. *Geology*, *31*(5), 419–422. http://doi.org/Doi 10.1130/0091-

7613(2003)031<0419:Lewarv>2.0.Co;2
Marsik, M., & Waylen, P. (2006). An application of the distributed hydrologic model CASC2D to a tropical montane watershed. *Journal of Hydrology*, *330*(3-4), 481–495. http://doi.org/10.1016/j.jhydrol.2006.04.003
Maurer, E. P., Adam, J. C., & Wood, a. W. (2008). Climate model based consensus on the hydrologic impacts of climate change to the Rio Lempa basin of Central America. *Hydrology and Earth System Sciences Discussions*, *5*(6), 3099–3128. http://doi.org/10.5194/hessd-5-3099-2008
McLean, D. G., Church, M., & Tassone, B. (1999). Sediment transport along lower Fraser River: Measurements and hydraulic computations. *Water Resources Research*, *35*(8), 2533–2548. http://doi.org/10.1029/1999WR900101
McLean, N. M., Stephenson, T. S., Taylor, M. A., & Campbell, J. D. (2015). Characterization of future Caribbean rainfall and temperature extremes across rainfall zones. *Advances in Meteorology*, *2015*. http://doi.org/10.1155/2015/425987
Micheletti, N., Chandler, J. H., & Lane, S. N. (2015). Structure from motion (SFM) photogrammetry. *Geomorphological Techniques*, 2047–0371.
Milliman, J. D., & Farnsworth, K. L. (2013). *River Discharge to the Coastal Ocean: A Global Synthesis*. Cambridge University Press.
Milliman, J. D., & Syvitski, J. P. M. (1992). Geomorphic/Tectonic control of sediment discharge to the ocean: The importance of small mountainous rivers. *The Journal of Geology*, *100*(5), 525–544.
Montero, W., & Linkimer, L. (2005). The Central Costa Rica Deformed Belt: Neotectonics of the eastern segment. In *American Geophysical Union, Fall Meeting*. San Francisco, CA.
Montero, W. P., Lewis, J. C., Marshall, J. S., Kruse, S., & Wetmore, P. (2013). Neotectonic faulting and forearc sliver motion along the atirro-Rio Sucio fault system, Costa Rica, Central America. *Bulletin of the Geological Society of America*, *125*(5-6), 857–876. http://doi.org/10.1130/B30471.1
Montgomery, D. ., & Brandon, M. . (2002). Topographic controls on erosion rates in tectonically-active mountain ranges. *Earth and Planetary Science Letters*, *201*(3-4), 481–489.
Montgomery, D. R., & Buffington, J. M. (1997). Channel-reach morphology in mountain basins. *Geological Society of America Bulletin*, *109*(5), 596–611.
Montgomery, D. R., & Gran, K. B. (2001). Downstream variations in the width of bedrock channels. *Water Resources Research*, *37*(6), 1841–1846. http://doi.org/10.1029/2000WR900393
Mueller, E. R., Pitlick, J., & Nelson, J. M. (2005). Variation in the reference Shields stress for bed load transport in gravel-bed streams and rivers. *Water Resources Research*, *41*(4), 1–10. http://doi.org/10.1029/2004WR003692
Nagle, G. N., Fahey, T. J., & Lassoie, J. P. (1999). Management of sedimentation in tropical watersheds. *Environmental Management*, *23*(4), 441–452. http://doi.org/10.1007/s002679900199
Nakaegawa, T., Kitoh, A., Ishizaki, Y., Kusunoki, S., & Murakami, H. (2014). Caribbean low-level jets and accompanying moisture fluxes in a global warming climate

projected with CMIP3 multi-model ensemble and fine-mesh atmospheric general circulation models. *International Journal of Climatology*, *34*(4), 964–977. http://doi.org/10.1002/joc.3733

Nishimune, N., Onodera, S. I., Naruoka, T., & Birmano, M. D. (2003). Comparative study of bedload sediment yield processes in small mountainous catchments covered by secondary and disturbed forests, western Japan. *Hydrobiologia*, *494*, 265–270. http://doi.org/10.1023/A:1025491005408

Nohara, D., Kitoh, A., & Hosaka, M. (2006). Impact of climate change on river discharge projected by multimodel ensemble. *Journal of Hydrometeorology*, *7*(2002), 1076–1089.

O'Connor, J. E., Mangano, J. F., Anderson, S. W., Wallick, J. R., Jones, K. L., & Keith, M. K. (2014). Geologic and physiographic controls on bed-material yield, transport, and channel morphology for alluvial and bedrock rivers, western Oregon. *Bulletin of the Geological Society of America*, *126*(3-4), 377–397. http://doi.org/10.1130/B30831.1

Ohl, C., & Bussmann, R. (2004). Recolonisation of natural landslides in tropical mountain forests of Southern Ecuador. *Feddes Repertorium*, *115*(34), 248–264. http://doi.org/10.1002/fedr.200311041

Ouchi, S. (1985). Response of alluvial rivers to slow active tectonic movement. *Geological Society of America Bulletin*, *96*(4), 504–515. http://doi.org/10.1130/0016-7606(1985)96<504:ROARTS>2.0.CO;2

Palomino-Lemus, R., Cordoba-Machado, S., Gamiz-Fortis, S. R., Castro-Diez, Y., & Esteban-Parra, M. J. (2015). Summer precipitation projections over northwestern South America from CMIP5 models. *Global and Planetary Change*, *131*, 11–23. http://doi.org/10.1016/j.gloplacha.2015.05.004

Petit, F., Houbrechts, G., Peeters, A., Hallot, E., Van Campenhout, J., & Denis, A. C. (2015). Dimensionless critical shear stress in gravel-bed rivers. *Geomorphology*, *250*, 308–320. http://doi.org/10.1016/j.geomorph.2015.09.008

Picco, L., Mao, L., Cavalli, M., Buzzi, E., Rainato, R., & Lenzi, M. A. (2013). Evaluating short-term morphological changes in a gravel-bed braided river using terrestrial laser scanner. *Geomorphology*, *201*, 323–334. http://doi.org/10.1016/j.geomorph.2013.07.007

Pike, A. S., Scatena, F. N., & Wohl, E. E. (2010). Lithological and fluvial controls on the geomorphology of tropical montane stream channels in Puerto Rico. *Earth Surface Processes and Landforms*, *35*(12), 1402–1417. http://doi.org/10.1002/esp.1978

Pitlick, J., Mueller, E. R., Segura, C., Cress, R., & Torizzo, M. (2008). Relation between flow, surface-layer armoring and sediment transport in gravel-bed rivers. *Earth Surface Processes and Landforms*, *33*(8), 1192–1209. http://doi.org/10.1002/esp.1607

Plink-Björklund, P. (2015). Morphodynamics of rivers strongly affected by monsoon precipitation: Review of depositional style and forcing factors. *Sedimentary Geology*, *323*, 110–147. http://doi.org/10.1016/j.sedgeo.2015.04.004

Pourhosein, M., Afzalimehr, H., Singh, V. P., & Dehghani, A. A. (2015). Evaluation of bed load in a gravel-bed river, *4*(3), 70–79.

http://doi.org/10.5923/j.ijhe.20150403.03
Poveda, G., Waylen, P. R., & Pulwarty, R. S. (2006). Annual and inter-annual variability of the present climate in northern South America and southern Mesoamerica. *Palaeogeography, Palaeoclimatology, Palaeoecology*, *234*(1), 3–27. http://doi.org/10.1016/j.palaeo.2005.10.031
Pralong, R. M., Turowski, J. M., Rickenmann, D., & Zappa, M. (2015). Climate change impacts on bedload transport in alpine drainage basins with hydropower exploitation. *Earth Surface Processes and Landforms*, *40*(12), 1587–1599. http://doi.org/10.1002/esp.3737
Prancevic, J. P., Lamb, M. P., & Fuller, B. M. (2014). Incipient sediment motion across the river to debris-flow transition. *Geology*, *42*(3), 191–194. http://doi.org/10.1130/G34927.1
Praskievicz, S. (2015). A coupled hierarchical modeling approach to simulating the geomorphic response of river systems to anthropogenic climate change. *Earth Surface Processes and Landforms*, *40*(12), 1616–1630. http://doi.org/10.1002/esp.3740
Pratt-Sitaula, B., Garde, M., Burbank, D. W., Oskin, M., Heimsath, A., & Gabet, E. (2007). Bedload-to-suspended load ratio and rapid bedrock incision from Himalayan landslide-dam lake record. *Quaternary Research*, *68*(1), 111–120. http://doi.org/10.1016/j.yqres.2007.03.005
Quesada, M. E., & Waylen, P. R. (2004). Occurrencia de crecidas en dos cuencas hidrograficas ubicadas en vertientes opuestas en Costa Rica. *Ingenieria Hidraulica En Mexico*, *19*(3), 129–138.
Quesada, M. R., & Waylen, P. R. (2012). Diferencias hidrologicas anuales y estacionales en regiones adyacentes: estudio de las subcuencas de los rios Virilla y Grande de San Ramon, Costa Rica. *Cuadernos de Geografia, Revista Colombiana de Geografia*, *21*(2), 167–175.
Rainato, R., Mao, L., García-Rama, A., Picco, L., Cesca, M., Vianello, A., … Lenzi, M. A. (2016). Three decades of monitoring in the Rio Cordon instrumented basin: Sediment budget and temporal trend of sediment yield. *Geomorphology*. http://doi.org/10.1016/j.geomorph.2016.03.012
Recking, A. (2013). Simple method for calculating reach-averaged bed-load transport. *Journal of Hydraulic Engineering*, *139*(1), 70–75. http://doi.org/10.1061/(ASCE)HY.1943-7900.0000653.
Recking, A., Piton, G., Vasquez, D., & Parker, G. (2015). Quantifying the morphological print of bedload transport. *Earth Surface Processes and Landforms*, *3869*, n/a–n/a. http://doi.org/10.1002/esp.3869
Rengers, F., & Wohl, E. (2007). Trends of grain sizes on gravel bars in the Rio Chagres, Panama. *Geomorphology*, *83*(3-4), 282–293. http://doi.org/10.1016/j.geomorph.2006.02.019
Restrepo, C., Alvarez, N., Box, P. O., Piedras, P. R., Juan, S., & Rico, P. (2006). Landslides and their contribution to land-cover change in the mountains of Mexico and Central America. *Biotropica*, *38*(4), 446–457.
Restrepo, J. D., & Kjerfve, B. (2000). Magdalena river: Interannual variability (1975-

1995) and revised water discharge and sediment load estimates. *Journal of Hydrology*, *235*(1-2), 137–149. http://doi.org/10.1016/S0022-1694(00)00269-9

Restrepo, J. D., Kjerfve, B., Hermelin, M., & Restrepo, J. C. (2006). Factors controlling sediment yield in a major South American drainage basin: The Magdalena River, Colombia. *Journal of Hydrology*, *316*(1-4), 213–232. http://doi.org/10.1016/j.jhydrol.2005.05.002

Restrepo, J. D., Lopez, S. A., & Restrepo, J. C. (2009). The effects of geomorphic controls on sediment yield in the Andean rivers of Colombia. *Latin American Journal of Sedimentology and Basin Analysis*, *16*(2), 79–92.

Rhoads, B. L. (1987). Stream power terminology. *Professional Geographer*, *39*(2), 189–195.

Rickenmann, D. (2001). Comparison of bed load transport in torrents and gravel bed streams. *Water Resources Research*, *37*(12), 3295–3305. http://doi.org/10.1029/2001WR000319

Roering, J. (2012). Tectonic geomorphology: Landslides limit mountain relief. *Nature Geoscience*, *5*(7), 446–447. http://doi.org/10.1038/ngeo1511

Roering, J. J., Perron, J. T., & Kirchner, J. W. (2007). Functional relationships between denudation and hillslope form and relief. *Earth and Planetary Science Letters*, *264*(1-2), 245–258. http://doi.org/10.1016/j.epsl.2007.09.035

Ryan, S. E., Bishop, E. L., & Daniels, J. M. (2014). Influence of large wood on channel morphology and sediment storage in headwater mountain streams, Fraser Experimental Forest, Colorado. *Geomorphology*, *217*, 73–88. http://doi.org/10.1016/j.geomorph.2014.03.046

Ryan, S. E., Porth, L. S., & Troendle, C. A. (2005). Coarse sediment transport in mountain streams in Colorado and Wyoming, USA. *Earth Surface Processes and Landforms*, *30*(3), 269–288. http://doi.org/10.1002/esp.1128

Sandoval, L. F. (1982). Mapa geologico de Costa Rica - Limon Prov (1:200000). San Jose, Costa Rica: Ministerio de Industria, Energia y Minas and Direccion de Geologia, Minas Y Petroleo and Nacional de Investigaciones Cinetificas y Tecnologicas.

Scatena, F. N., & Gupta, A. (2013). Streams of the montane humid tropics. *Treatise on Geomorphology*, *9*, 595–611. http://doi.org/10.1016/B978-0-12-374739-6.00256-6

Schewe, J., Heinke, J., Gerten, D., Haddeland, I., Arnell, N. W. N. W., Clark, D. B. D. B., … Kabat, P. (2013). Multimodel assessment of water scarcity under climate change. *Proceedings of the National Academy of Sciences of the United States of America*, *111*(9), 1222460110–. http://doi.org/10.1073/pnas.0709640104

Schlunegger, F., Melzer, J., & Tucker, G. (2001). Climate, exposed source-rock lithologies, crustal uplift and surface erosion: A theoretical analysis calibrated with data from the Alps/North Alpine foreland basin system. *International Journal of Earth Sciences*, *90*(3), 484–499. http://doi.org/10.1007/s005310100174

Schneider, J. M., Rickenmann, D., Turowski, J. M., Bunte, K., & Kirchner, J. W. (2015). Applicability of bed load transport models for mixed-size sediments in steep streams considering macro-roughness. *Water Resources Research*, *51*(7), 5260–5283. http://doi.org/10.1002/2014WR016417

Schumm, S. A. (2005). *River variability and complexity*. New York, NY: Cambridge University Press.
Schumm, S. A., Dumont, J. F., & Holbrook, J. M. (2000). *Active tectonics and alluvial rivers*. Cambridge, UK: Cambridge University Press.
Schumm, S. a., & Lichty, R. W. (1965). Time, space, and causality in geomorphology. *American Journal of Science*, *263*(2), 110–119. http://doi.org/10.2475/ajs.263.2.110
Shields, A. (1936). Application of Similarity Principles and Turbulence Research to Bed-Load Movement Report. *Translated from Anwendung Der Ähnlichkietsmechanic Und Turbulenzforschung Auf Die Geshiebebwegung. Mitteilungen Der Preussischen Versuchsanstalt Fur Wasserbau Und Schiffbau*, *Report 26*.
SIGMA. (1998). 5m DEM of Costa Rica - from topographic maps. provided for this research by the Ministerio de Ambiente y Energia of Costa Rica.
Sitchler, J. C., Fisher, D. M., Gardner, T. W., & Protti, M. (2007). Constraints on inner forearc deformation from balanced cross sections, Fila Costena thrust belt, Costa Rica. *Tectonics*, *26*(6), 1–11. http://doi.org/10.1029/2006TC001949
Sklar, L. S., & Dietrich, W. E. (2012). A mechanistic model for river incision into bedrock by saltating bed load. *Water Resources Research*, *48*(6), 1–22. http://doi.org/10.1029/2003WR002496
Slaymaker, O. (1988). The distinctive attributes of debris torrents. *Hydrological Sciences Journal*, *6667*(May), 567–574. http://doi.org/10.1080/02626668809491290
Sterling, S., & Slaymaker, O. (2007). Lithologic control of debris torrent occurrence. *Geomorphology*, *86*(3-4), 307–319. http://doi.org/10.1016/j.geomorph.2006.09.002
Stock, J. D., & Dietrich, W. E. (2006). Erosion of steepland valleys by debris flows. *Bulletin of the Geological Society of America*, *118*(9-10), 1125–1148. http://doi.org/10.1130/B25902.1
Studt, K. (2014). Rafting guide. Personal Conversation. Turrialba, Costa Rica.
SWAP. (2011). Guidance compendium for watershed monitoring and assessment. Clean Water Team Citizen Monitoring Program: State Water Resources Control Board, California Environmental Protection Agency.
Tajima, F., & Kikuchi, M. (1995). Tectonic implications of the seismic rupture associated with the 1983 and 1991 Costa Rica Earthquakes. In P. Mann (Ed.), *Geologic and tectonic development of the Caribbean Plate boundary in southern Central America* (Special Re, pp. 327–340). Boulder, CO: Geologic Society of America, Inc.
Thomas, M. F. (1996). *Geomorphology in the tropics: A study of weathering and denudation in the low latitutdes*. West Sussex, UK: John Wiley & Sons Ltd.
Trimble. (2009). GeoExplorer 2008 Series GeoXH Handheld: FAQs for Customers. Trimble. Retrieved from https://solutions.seilerinst.com/Portals/1/Catalog Items/Mapping/2-9-10 FAQ_GeoXH.pdf
Turowksi, J. M., Yager, E. M., Badoux, A., Rickenmann, D., & Molnar, P. (2009). The impact of exceptional events on erosion, bedload transport and channel stability in a step-pool channel. *Earth Surface Processes and Landforms*, *34*, 1661–1673. http://doi.org/10.1002/esp
Turowski, J. M., Rickenmann, D., & Dadson, S. J. (2010). The partitioning of the total sediment load of a river into suspended load and bedload: A review of empirical

data. *Sedimentology*, *57*(4), 1126–1146. http://doi.org/10.1111/j.1365-3091.2009.01140.x
USBR, U. S. B. of R. (1997). Water measurement manual. Water Resources Publications, LLC, Highlands Ranch, CO.
Van Oost, K., Beuselinck, L., Hairsine, P. B., & Govers, G. (2004). Spatial evaluation of a multi-class sediment transport and deposition model. *Earth Surface Processes and Landforms*, *29*(8), 1027–1044. http://doi.org/10.1002/esp.1089
Vargas, A. B., & Trejos, V. R. S. (1994). Changes in the General Circulation and its influence on precipitation trends in Central America: Costa Rica. *Ambio*, *23*(1), 87–90. http://doi.org/10.5363/tits.6.3_37
Vargas, I. O. (2007). Estudio hidraulico de la explotacion de sedimento en el Rio Reventazon. Instituto Costarricense de Electricidad. San Jose, Costa Rica.
Vázquez-Tarrío, D., & Menéndez-Duarte, R. (2015). Assessment of bedload equations using data obtained with tracers in two coarse-bed mountain streams (Narcea River basin, NW Spain). *Geomorphology*, *238*, 78–93. http://doi.org/10.1016/j.geomorph.2015.02.032
Vázquez-Tarrío, D., & Menéndez-Duarte, R. (2015). Assessment of bedload equations using data obtained with tracers in two coarse-bed mountain streams (Narcea River basin, NW Spain). *Geomorphology*, *238*, 78–93. Retrieved from http://www.sciencedirect.com/science/article/pii/S0169555X15001312
Vera, M., Jara, C., Iroume, A., Ulloa, H., Andreoli, A., & Barrientos, S. (2014). Reach scale ecologic influence of in-stream large wood in a Coastal Mountain range channel, Southern Chile. *Gayana*, *78*(2), 85–97. http://doi.org/10.4067/S0717-65382014000200002
von Blanckenburg, F. (2005). The control mechanisms of erosion and weathering at basin scale from cosmogenic nuclides in river sediment. *Earth and Planetary Science Letters*, *237*(3-4), 462–479. http://doi.org/10.1016/j.epsl.2005.06.030
Vorosmarty, C. J., Green, P., Salisbury, J., & Lammers, R. B. (2000). Global water resources: vulnerability from climate change and population growth. *Science*, *289*, 284–288.
Wallick, J. R., Anderson, S. W., Cannon, C., & O'Connor, J. E. (2012). *Channel change and bed-material transport in the lower Chetco River, Oregon* (Scientific). US Geological Survey, US Department of the Interior. Retrieved from http://pubs.usgs.gov/sir/2010/5065/pdf/sir20105065.pdf
Wallick, J. R., & O'Connor, J. E. (2011). *Estimation of bed-material transport in the lower Chetco River, Oregon, Water Years 2009 – 2010*. US Geological Survey, Open File Report 2011-1123. Retrieved from https://pubs.usgs.gov/of/2011/1123/pdf/ofr20111123.pdf
Wang, Z. ., Lee, J. H. W., & Melching, C. S. (2015). Mountain rivers and incised channels. In *River Dynamics and Integrated River Management* (pp. 123–191). Beijing: Tsinghua University Press.
Warrick, J. A., Milliman, J. D., Walling, D. E., Wasson, R. J., Syvitski, J. P. M., & Aalto, R. E. (2013). Earth is (mostly) flat: Apportionment of the flux of continental sediment over millennial time scales. *Geology*, *41*(3), 343–346.

http://doi.org/10.1130/G33918.1
Waylen, P.R., Quesada, M.E., Caviedes, C. N. (1996). Temporal and spatial variability of annual precipitation in Costa Rica and the Southern Oscillation. *International Journal of Climatology*, *16*, 173–193.
Waylen, P., Caviedes, C., Poveda, G., Mesa, O., & Quesada, M. (1998). Rainfall distribution and regime in Costa Rica and its response to the El Nino-Southern Oscillation. *Conference of Latin Americanist Geographers*.
Waylen, P. R., Caviedes, C. N., & Quesada, M. E. (1996). Interannual variability of monthly precipitaton in Costa Rica. *Journal of Climate*, *9*, 2606–2613. Retrieved from http://journals.ametsoc.org/doi/abs/10.1175/1520-0442(1996)009<2606:IVOMPI>2.0.CO;2
Wheaton, J. M., Brasington, J., Darby, S. E., & Sear, D. A. (2010). Accounting for uncertainty in DEMs from repeat topographic surveys: improved sediment budgets. *Earth Surface Processes and Landforms*, *35*(2), 136–156. http://doi.org/10.1002/esp.1886
Whipple, K. X. (2004). Bedrock rivers and the geomorphology of active orogens. *Annual Review of Earth and Planetary Sciences*, *32*(1), 151–185. http://doi.org/10.1146/annurev.earth.32.101802.120356
Wohl, E. (2005). Downstream hydraulic geometry along a tropical mountain river. In R. S. Harmon (Ed.), *The Rio Chagres, Panama* (pp. 169–188). Netherlands: Springer.
Wohl, E. (2010). *Mountain Rivers Revisted*. Washington, DC: American Geophycial Union.
Wohl, E., Barros, A., Brunsell, N., Chappell, N. A., Coe, M., Giambelluca, T., … Ogden, F. (2012). The hydrology of the humid tropics. *Nature - Climate Change*, *2*(9), 655–662. http://doi.org/10.1038/nclimate1556
Wohl, E., & Merritt, D. (2001). Bedrock channel morphology. *GSA Bulletin*, *113*(9), 1205–1212. http://doi.org/10.1130/0016-7606(2001)113<1205
Wohl, E., & Merritt, D. (2005). Prediction of mountain stream morphology. *Water Resources Research*, *41*(8), 1–10. http://doi.org/10.1029/2004WR003779
Yager, E. M., Kirchner, J. W., & Dietrich, W. E. (2007). Calculating bed load transport in steep boulder bed channels. *Water Resources Research*, *43*(7), 1–24. http://doi.org/10.1029/2006WR005432
Yanites, B. J., & Tucker, G. E. (2010). Controls and limits on bedrock channel geometry. *Journal of Geophysical Research: Earth Surface*, *115*(4). http://doi.org/10.1029/2009JF001601
Yeh, K. C., Wang, S. S. Y., Chen, H., Liao, C. T., Jia, Y., & Zhang, Y. (2010). Numerical Simulation of Sediment Transport and Morphological Change of Upstream and Downstream Reach of Chi-Chi Weir. *Numerical Simulations - Examples and Applications in Computational Fluid Dynamics*. Retrieved from http://cdn.intechopen.com/pdfs-wm/12623.pdf
Ziegler, A. D., Sidle, R. C., Phang, V. X. H., Wood, S. H., & Tantasirin, C. (2014). Bedload transport in SE Asian streams-Uncertainties and implications for reservoir management. *Geomorphology*, *227*, 31–48. http://doi.org/10.1016/j.geomorph.2014.01.015

Ziliani, L., & Surian, N. (2012). Evolutionary trajectory of channel morphology and controlling factors in a large gravel-bed river. *Geomorphology*, *173-174*, 104–117. http://doi.org/10.1016/j.geomorph.2012.06.001